Power Loss Reduction in Distribution Network with Electric Vehicles by Using Energy Storage System

Wang, Cheng

Award date:
2017

Awarding institution:
University of Bath

Power Loss Reduction in Distribution Network with Electric Vehicles by Using Energy Storage System

Cheng Wang

A thesis submitted for the degree of Doctor of Philosophy (PhD)

University of Bath

Department of Electronic and Electrical Engineering

July 2016

Signature:…… Date:……

Abstract

The main focus of this thesis is to minimise power loss in the Distribution Network (DN) caused by Electric Vehicle (EV) penetration. When large numbers of EVs are connected to the DN, the power loss in the DN increases dramatically. In order to reduce this power loss, optimal active and reactive power dispatch methods of Energy Storage System (ESS) and charging stations are proposed in this study.

This study develops a new active and reactive optimal power dispatch method using ESS to reduce the power loss caused by EV penetration. A power flow analysis model of two ESSs was built in order to minimise the power loss. Two sub-methods based on this optimal power dispatch method are presented. These are uncoordinated optimal active-reactive power flow of the ESS and coordinated optimal active-reactive power flow of ESS. These two methods were tested in an IEEE 33-bus DN. The power loss was compared with and without optimisation methods: meanwhile, the power loss caused by the EVs was quantified. The simulation results show that by using the proposed method in this study, 1.43 MW of total power loss can be reduced and 1.64 MW of active power does not need to be imported from the DN.

This study also develops a novel analytical location choosing method based on optimal active and reactive power dispatch and power flow analysis for optimal placement of charging stations. A concept of charging stations combined with Battery Energy Storage Systems (BESSs) is given. The analytical method is compared with the current density method used in other papers. The results show the analytical location method was more accurate than the current density method for finding the optimal location of charging station two's location. This analytical method was tested in an 11-bus distribution line, the IEEE 33-bus DN and a 36-bus DN. The simulation results proved the accuracy of analytical method used in this study. Moreover, 27% of the average active power loss was saved by installing two charging stations rather than no charging stations in the test-line. It is also shown that a 2.6% annual yield above inflation can be obtained by investing in installing and running such charging stations.

In order to analyse how the optimal location of charging station two changes with different impact factors, such as different EV charging locations, line resistance, reactance and different loads, a quantitative analysis was carried out by using the proposed active and reactive method. The 36-bus DN was used as the test network. The results showed that the optimal location only changed when all the impact factors were changed simultaneously.

In addition, to reduce the calculation time and find more optimal charging station locations, a Genetic Algorithm (GA) was developed to find multiple (>2) charging stations' optimal locations for power loss minimisation. The GA was tested in the 36-bus DN, which found that 6 charging stations were optimised. Meanwhile, the GA's different settings, such as population size, cross over probability, mutation probability and the stopping criteria were changed in order to analyse how these settings influenced the GA's performance. Moreover, the calculation time of traditional quadratic optimisation method and GA calculation time was compared. From the comparison, the GA was 22 times faster than the quadratic optimisation method for finding the six charging stations' optimal locations in the 36-bus DN case.

Acknowledgements

Firstly, I would like to thanks to my supervisor Dr Rod Dunn, for his kindness help, gentle encouragement and patience to keep me on the right research direction through three and half years.

I am grateful to thanks my colleagues Mr Puxi Huang, Ms Siqi Li, Mr Bo Lian, Mr Da Huo, Mr Yang Yao, Mr Jianwei Li , Miss Qing qing Yang, and Dr Anthony M. Gee for providing the helps not only in academic, but also in social life.

I am grateful to thank my previous colleagues Dr Hazem M. Zubi, Dr Chenchen Yuan, Dr Kapildev Lout, Dr Newman Malcolm, Dr Sun Jin and Dr Min Wang for giving me useful advices through out of my research.

I would thank to Dr Simon Le Blond, Dr Rohit Bhakar for their constructive suggestions in my first year's transfer report.

And I would like also thanks to the IT support team in our department for providing simulation and office software.

In addition, I would like to thanks to Prof Furong Li, Dr Francis Robinson, Prof Raj Aggarwal, Dr Simon Le Blond, Dr Chenghong Gu for kindly answering my questions throughout my study.

Last not the least, I would like to thanks to my greatest parents. It would not have been possible to complete my study and research in the UK without their financial support and enormous encouragements as well as supports in my life.

CONTENTS

List of Abbreviations

AF	Activation Function
ARPD	Active and Reactive Power Dispatch
APL	Active Power Loss
AI	Artificial Intelligence
ANN	Artificial Neural Network
BEV	Battery Electric Vehicles
BESS	Battery Energy Storage System
BSS	Battery Storage Systems
CO_2	Carbon Dioxide
CCP	Centralized Charging Pattern
CCCA	Committee on Climate Change Analysis
CAES	Compressed Air Energy Storage
CA-RPF	Coordinated Optimal Active-reactive Power Flow
DCP	Decentralized Charging Pattern
DSR	Demand Side Response
DSM	Demand-side Management
DECC	Department of Energy and Climate Change
DG	Distribution Generation
DMS	Distribution Management System
DN	Distribution Network
DT	Distribution Transformers
EV	Electric Vehicle
EVI	Electric Vehicle Initiative
ENSG	Electricity Network Strategy Group
ESS	Energy Storage System
GA	Genetic Algorithm
HEV	Hybrid Electric Vehicles
ICE	Internal Combustion Engine
LP	Linear Programming
Li-ion	Lithium ion
LCTP	Low Carbon Transition Plan
MOT	Mathematical Optimization Technique
MVAr	Mega volt-ampere Reactive
NREL	National Renewable Energy Laboratory
NPV	Net Present Value
NA	Network Architecture

NIMH	Nickel Metal Hydride
NP	Nonlinear Programming
PV	Photovoltaic
PHEV	Plug-in Hybrid Electric Vehicle
PCS	Power Conditioning System
PD	Power Demand
PHES	Pumped Hydro Energy Storage
QFQC	Quadratic Function with Quadratic Constraints
QP	Quadratic Programming
RPL	Reactive Power Loss
SW	Setting Weights
NaS	Sodium-sulphur battery
SOC	State of Charge
SMS	Storage Management System
SMES	Superconducting Magnetic Energy Storage
TAP	Total Active Power
TPD	Total Power Demand
TPL	Total Power Loss
TN	Transmission Network
UA-RPF	Uncoordinated Optimal Active-reactive Power Flow

List of Symbols

A	Effective cross-sectional area of cable
a	Inequality constant function coefficient
c	Objective function linear coefficient
C_{Bsi}^{I}	Capacity per-unit investment cost of battery
$C_{Bsi}^{O}(t)$	Operation cost of battery per unit
$C_{BSi}^{M}(t)$	Battery per-unit capacity maintenance cost
$C_{CBi}^{O}(t)$	Battery operation cost
C_{CHi}^{I}	Capacity per-unit investment cost of charging devices
$C_{CHi}^{O}(t)$	Charging cost
$C_{CHi}^{M}(t)$	Charging devices
C_{DEi}^{I}	Capacity per-unit investment cost of other devices
$C_{DEi}^{M}(t)$	Other devices
C_{EAi}^{I}	Land utilization cost
$C_{EEi}^{O}(t)$	Power consumption cost
C_{ETi}^{I}	Capacity per-unit investment cost of transformers
$C_{ETi}^{M}(t)$	Transformers
$C_{EVCSi}^{I}(t)$	Investment cost
$C_{EVCSi}^{O}(t)$,	Operation cost
$C_{EVCSi}^{M}(t)$	Maintenance cost
$C_{HRi}(t)$	Human resources cost
$C_{PS}^{L}(t)$	Network loss cost
$C_{VCi}^{O}(t)$	Active power filtering and reactive power compensation cost
E_B	Capacity of battery
E_{EV}	Energy demand of EVs
E_h	Energy level in ESS during the hour h
E_{max}	Upper bound of the storage capacity
E_{Re}	Energy demand of residents
F_{EAi}	The area of ith charge station
H	Hessian symmetric matrix
I	Current
i	Discount rate
$I(x, T_i)$	Feeder current through that test line
$I_d(x, T_i)$	Load current density
K_i	Simultaneity coefficient of charging

	devices
L	Length of the line
L_{EVCSi}^{max}	Daily maximal load rate of the ith EV charging station
n_i	The number of charging devices
N_t	Number of time durations in the time period T
P	Power Losses
P_{CHij}	output active power
P_{chi}^{N}	Rated power of charging devices
P_{EEi}^{max}	Maximal power consumed of the electric devices respectively
P_{ES}	Capacity of battery
$P_{EVCSi}(t)$	Annual profit of charge station
P_i	Sending active through the branch i between node k and m
P_L	Power loss of distribution line model
P_{mDG}	Active power injected by the distribution generation
P_{mL}	Total active power loads at bus m
P_{mF}	Sum of active power flows through all the downstream branches connected to bus m
P_{mcharE}	Active power charging of ESS at bus m
P_{mdiscE}	Active power discharging of ESS at bus m
P_{NPV}	Net present value
P_{Rt}	Net cash flow
$Q_{dis\ (k,h)}$	Reactive power for Discharging
Q_i	Sending reactive through the branch i between node k and m
Q_{mDG}	Reactive power injected by the distribution generation
Q_{mL}	Total reactive power loads at bus m
Q_{mF}	Sum of reactive power flows through all the downstream branches connected to bus m
R	Resistance
R_{AC}	AC resistance
R_{DC}	DC resistance
$R_{EVCSi}^{T}(t)$	Revenue of charge station
S_{CHi}	Total capacity of the charging devices
S_{DEi}	The total capacity of other devices except transformers and charging devices

S_{ESS}	Apparent power of ESS
S_{ESSMAX}	Maximum apparent power of ESS
S_{ETi}	Transformers' capacities
T_{EEi}	Annual utilization hours of the electric devices
V_k	Voltage at bus k
V_m	Voltage at bus m
V_{s2}	Voltage at bus S_2
x	Decision variable
x_0	The optimal location of charing station
$Y_{EVCSi}(t)$	Yield per year for charge station
y_p	Correction factor for the proximity effects
y_s	Correction factor for skin effect
Z	Constant value
α_{20}	Temperature coefficient of resistance
η_{char}	Charge efficiency
$\eta CHij$	Charging efficiency
η_{disc}	Discharge efficiency
θ_m	Maximum permissible conductor operating temperature
ρ	Resistivity

List of Figures

List of Tables

Chapter 1 The introduction

This chapter briefly describes the background, motivation, challenges, objectives, and contributions of this thesis.

1.1 Overview

Electricity a modern essential: plays a significant role for economy, national security, public health and safety. Global demand for electricity is continually and dramatically increasing. Unless changes are made, by 2030 global electricity consumption will have reached approximately 30,000 terawatt hours a year，the figure 1.1 represents an increase of 76% from 2007 figures [1].

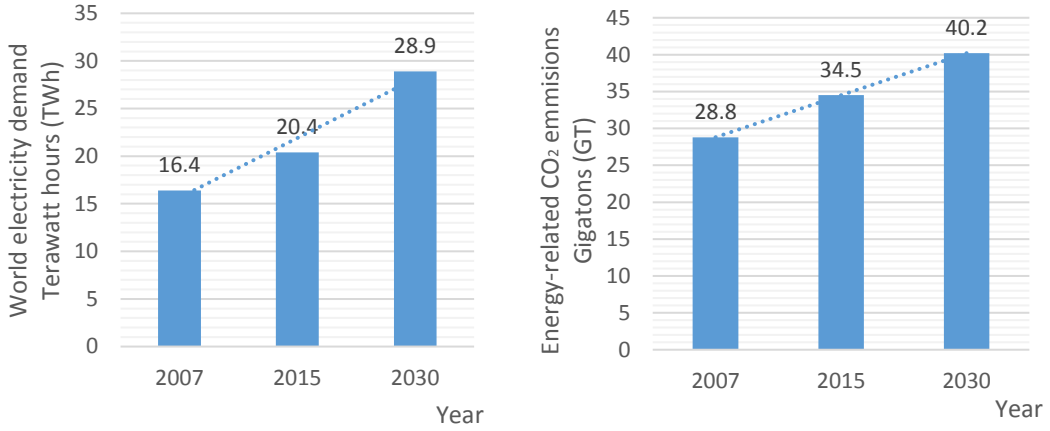

Figure 1.1 World electricity demand and energy-related carbon dioxide emission[1]

In order to supply that amount of electricity, increased power generation will be needed during the next 20 years, and this requires examination of how such power will be generated. Over 65% of the world's electricity used today is generated by steam turbine generators burning fossil fuels as their source of raw energy [2]. This large consumption of fossil fuel has given rise to a significant amount of carbon dioxide (CO_2) emissions. Figure 1.1 shows that these CO_2 emissions are predicted to rise to 40.2 Gt by 2030. This rapid growth has already impacted upon our living environment in areas such as air quality and global warming. In order to mitigate these impacts, more than 180 countries, including the United

Kingdom signed the United Nations' Kyoto Protocol agreement to limit CO_2 emission in their countries.

In the UK, the government has published a Low Carbon Transition Plan (LCTP), which aims to achieve the target of 80% reduction in all carbon emissions by 2050 [3]. Currently, three quarters of UK electricity is generated by coal and gas, and by 2050, there will be a need for a greater supply of power. To achieve the low carbon target, electricity needs to be generated from low carbon sources, such as renewables, nuclear, and fossil fuel plants fitted with carbon capture and storage. As a passive energy delivery platform, the traditional power grid cannot meet this target; therefore the more advanced grid needs to be built.

1.1.1 Today's Grid

Today's grid is very reliable, and can cope with normal fluctuations in demand for electricity. However to satisfy the requirements of low carbon generation, we still need a fully modernised electricity grid with larger capacity and ability to manage greater fluctuations and challenges in supply and demand, while maintaining the system's stability and security.

Applying information and communication technologies to the grid can make it smarter, which offers possibilities for the current grid to transform into a larger, lower carbon and more cost-effective grid. By applying these technologies, the system operators are able to monitor the network better, manage more smoothly the fluctuation in demand. Thus the smart grid will play a leading role in terms of meeting the lower carbon emission target.

In practical terms, the smart grid can help network operators identify problems more swiftly and to re-distribute power, helping to ensure a more reliable and secure supply. It can also support renewable generation, storage through a wider, more sophisticated range of smart methods to manage the supply, and demand at a more local level. Moreover, smart grids facilitate the electricity system to perform better by offering a proactive electricity management service: for example, through demand side response, electricity consumers are incentivised to use energy away from peak-time. By doing so, peak-time demand can be decreased, and this will reduce risk levels for system security. Meanwhile, it also benefits the

electricity consumers: for example, electricity bills can be reduced by using off-peak electricity. Thus although smart grids do not remove the need for the conventional reinforcement of networks, they can minimise or defer the need for investment through more efficient use of the current infrastructures.

The development of smart grids needs cooperation between government, the system regulator, the energy industry and consumers. In 2009 and 2010, the Electricity Network Strategy Group (ENSG) in the UK published a smart grid vision and route map to guide the transmission and DN operators in developing a smart grid. Since that time, significant progress and important developments have been made. In 2011, the UK Carbon Plan and renewable energy roadmap were released to help the conventional grid transfer to a smart grid. Future of Heating, a strategic framework for low carbon heating in the UK, set out in the same year to deliver a step-change in heating to meet the 2050 carbon emission target. In 2014, the community energy strategy was developed: this strategy engages with participating communities to balance supply and demand locally. Independent modelling has shown that by 2020, community electricity could provide between 0.5 MW to 3GW of installed capacity through solar PV, onshore and hydro projects [4][5][6]. This large amount of renewable energy integration not only facilitates smart grid development, but also accelerates the pace for reaching the carbon emission target.

1.1.2 Renewable Generation

In order to meet the challenge of climate change, renewable generation technologies are being encouraged for integration into power systems. In the UK, the government has committed to sourcing 15% of its energy from renewable sources by 2020. There are several different types of renewable electricity available for this sourcing: the main ones being wind, hydro, wave and tidal. A comparison between 2008 and the projected 2020 renewable electricity generation can be seen in figure 1.2 below [7]. This figure shows that total renewable electricity generation in 2020 will be almost 8 times that of 2008.

Among these renewable generation technologies, onshore and offshore wind energy are making significant contributions to electricity supplies, providing 11% of the UK's electricity in 2015: enough electricity was generated to meet 8 million homes' annual needs. Onshore

wind supply works well in the UK because of its excellent wind resource: it is currently providing over 5,000 MW of capacity. One commercial scale (2.5MW) turbine on a reasonable location can generate approximately 6.5 million units of electricity each year—enough to make 230 million cups of tea. The total offshore wind capacity in the UK can provide around 15 TWh of electricity annually, equivalent to 3 and half million home's electricity consumption. Industry projections show that by 2016, 6GW capacity can be installed, and around 10GW by 2020. Thus by 2020, offshore wind will potentially supply 8 to 10 percent of the UK's electricity annually [8].

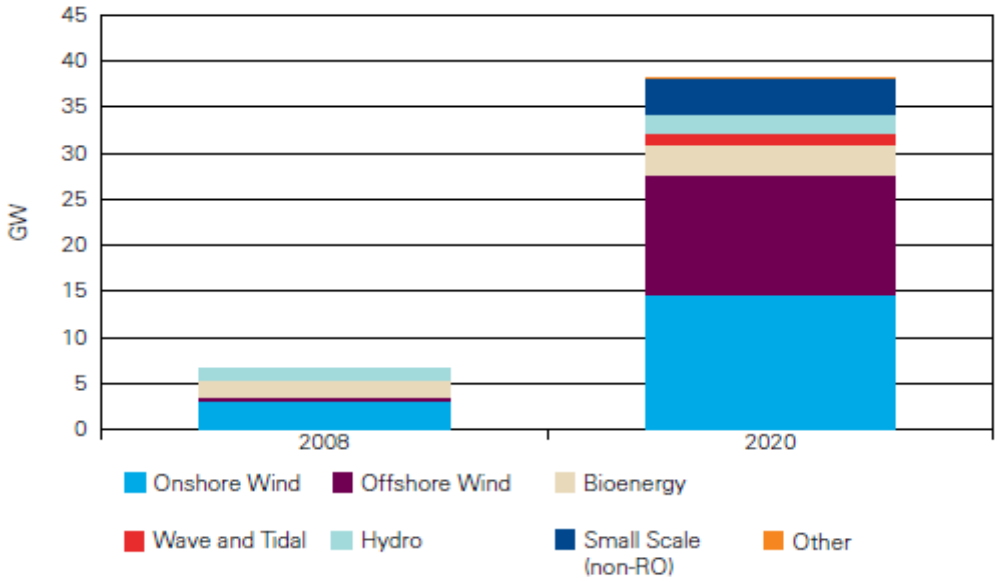

Figure 1.2 Renewable electricity technologies comparison between 2008 and projected to 2020[9]

The other major renewable energy sources also have a significant role to play in the development of low-carbon energy production. Hydropower has been benefitting the UK for over a century. The current installed capacity is 1676 MW, generating 5885 GWh/year [10]. Conventional hydroelectric power and run-of-the-river stations occupied 1.3% of the UK's total electricity production in the year 2012 [11]. Wave and tidal energy could be a very useful source for decarbonising the energy supply. Around 10MW of wave and tidal stream devices are being tested in the UK waters, and the Department of Energy and Climate Change (DECC) estimates that combined wave and tidal stream energy has the potential to deliver around 20 percent of the UK's current electricity needs.

However, when large scale renewable generation is connected to the grid, problems in terms of thermal limit, voltage, and stability constraints may arise as the result of intermittency.

Therefore, the integration of renewable energy can result in more pressure on the grid. Demand side response is one practical way to relieve this pressure.

1.1.3 Demand Side Response

Demand Side Response (DSR) refers to when electricity consumers (the demand sides) sign up to special tariffs and schemes, which reward them for changing their electricity using habits. DSR aims at delivering a reduction in electricity use at peak times. It can save generation costs and emissions by reducing the demand for use of more costly and emissions-intensive plants. If 10% of on-peak hour's demand in the UK is shifted to the off-peak hour's demand, the 2,550t CO_2 emission can be reduced, the annual network investment cost can be saved £ 28m. In addition, the maximum daily benefit from energy cost reduction can be £ 1.7m. Figure 1.3 shows the use of DSR across the electricity system.

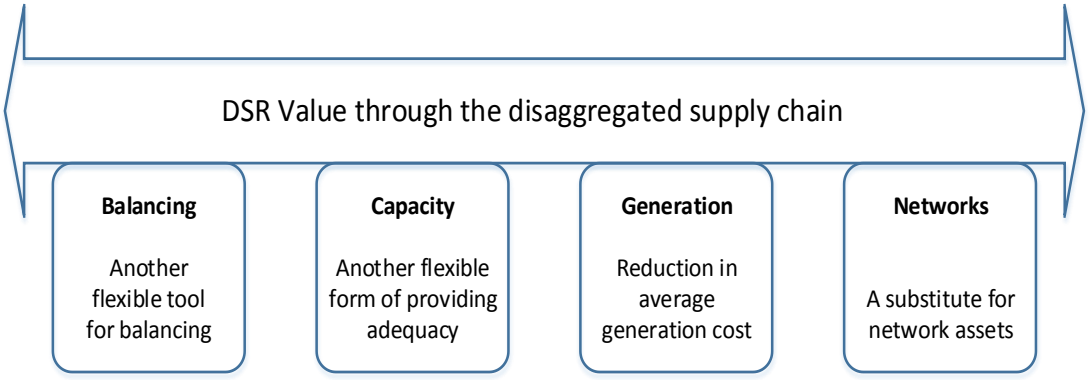

Figure 1.3 Different uses of DSR in power system

DSR has several potential benefits for power provision, which are discussed below. One major issue with power supply is that electricity cannot be stored economically. Therefore, at any moment in time, the power demand and supply must be equal. With too much electricity, the equipment could fail: too little, and there is a risk of blackout. DSR can help system operators to balance peak period electricity demand and supply by providing additional power to grid.

A second benefit of DSR is that it can reduce the average generation cost. The need for higher cost on-peak generation can be reduced by shifting demand from higher demand periods to lower demand periods. Moreover, by flattening the electricity usage pattern over

time, the system operating efficiency of existing generation plants can potentially be increased.

As a substitute for network assets, DSR can avoid or delay additional investment in Transmission Network (TN) and DN by balancing supply and demand. With the increasing demand for EVs and other forms of technology, DSR provides the DN operators with an alternative solution for managing increases in demand on the network and could, therefore, reduce or defer the need for network investment in reinforcement.

DSR is also significant to business: for example, the northern power grid in the UK has 3.9 million customers; 3.6 million of which are domestic households. As more renewable sources such as wind and solar generation, and low carbon demand, such as EV, are connected to grid, the local grids could need to carry twice as much load as today by 2050 [12]. Therefore, DSR will have to take more responsibility for balancing demand and supply and meeting the emission reduction target [13] .

1.1.4 Electric Vehicle

The Committee on Climate Change Analysis (CCCA) in the 4^{th} carbon budget conference concluded that EVs will play a key role in decarbonising transport throughout the 2020s [14]. Based on research [15][16][17], it has been shown that EVs should be cost effective against carbon price. Compared with conventional vehicles, the capital cost of EVs is a little higher, but this is expected to be offset by significantly lower running costs [18].

In order to reduce CO_2 emissions from transportation, a multi-government policy forum has been established called the Electric Vehicle Initiative (EVI). EVI members include Canada, China, the United Kingdom, the United States, Japan, Italy, and Korea. EVI member governments have announced that the cumulative national targets for EV and Plug-in Hybrid Electric Vehicle (PHEV) sales are estimated to add up to almost 6 million by 2020. If this is achieved, it would constitute approximately 6 percent of total vehicle sales by 2020 [10].

Evidence of the actual increase in EV numbers in the UK has been clear in the last three years, which have seen a surprising surge in demand for EV. New registrations of PHEV increased from 3,500 in 2013 to almost 61,000 toward the start of May 2016 [19]. The top four selling models are Mitsubishi Outlander P-HEV, Nissan Leaf, BMW i3, and Renault Zoe. The increased sales have resulted in a significant penetration of EVs to the grid, and this is challenging the grid in terms of managing EV charging, whilst maintaining system stability and security.

1.2 The challenges for power systems operation

With increasing power demands and environmental awareness, more power needs to be generated with less environmental damage. However, conventional power generation cannot meet emission reduction targets. This situation brings opportunities for the development of renewable generation. However, with the penetration of these renewable energies, such as wind, solar and hydro, power system security and reliability can be adversely influenced, especially the TN and DN. Conventional DN is unidirectional in nature. It not only has low energy efficiency, but also lacks self-monitoring and self-healing. Therefore, it can easily suffer from domino-effect failures connected to increased penetration of new types of energy.

Traditional power grids convert only one-third of fuel energy into electricity, without recovering waste heat. Usually, the normal losses of TN and DN are between 6% and 8%. The figures taken from 2005 seven year statement shows total electric power transmission and distribution losses in the UK are 1423.5MW [20]. Furthermore, increasing loads in the DN can also increase power loss, because loading of a distribution feeder is inherently unbalanced. These unbalanced loads such as EVs, could result in degradation of power quality, and increase harmonics and voltage problems. In additional, dramatic changes in the load pattern can impact line voltage, especially over long feeders [21].

Wind and solar generators are becoming more widespread in use. However, these intermittent renewable resources pose many uncertainties to the current grid. Due to the random nature of wind and solar power, and the characteristics of wind and solar generation, switching off these generators could cause the power system to lose transient stability and result in a voltage dip. Additionally, without accurate forecasting for these natural sources, and effective

scheduling of daily operations, large penetration of wind and solar generation may lead to over-generation conditions.

1.3 Response to challenges

As mentioned above, old power systems have experienced significant challenges caused by emerging renewable generators and new types of load. In order to cope with these challenges and reduce CO_2 emissions, system operators need to build next generation electricity grids: known as smart grids. In essence, a smart grid is required to accommodate a wide variety of generation options, including central, distributed, intermittent as well as mobile options. It needs the potential to empower consumers to manage the system to adjust their energy use and reduce electricity bills [22]. It should also have a self-healing, self-monitory ability, as well as the ability to coexist with the current grid.

As a major factor in a smart grid, DSR provides several solutions to these issues. The distributed ESS is usually used for DSR, and this system is also one of the components in a smart micro-grid that integrates several components, such as distributed generation, home area network, PHEV, Volt-VAr optimization application and energy storage [23].

ESS has many merits: the central ones being voltage support, power quality and reliability increase, transmission congestion relief and power loss reduction. This is especially significant for the power loss caused by unbalanced DN. By installing ESS into DN, network performance can be dramatically improved. More specifically, ESS could be used to reduce the impacts caused by EVs, and that is the focus of this research work.

1.4 Research Objectives

The major objective of this work is to develop an active and reactive power dispatch method for ESS to reduce the power loss caused by EV penetration. Additional objectives are to choose the optimum location for charging stations in terms of power loss minimisation, and to analyse how impact factors influence optimum charging station locations. The research attempts to achieve the following targets.

- To develop a new power dispatch strategy for ESS to reduce the power loss caused by EV penetration in DN.

- To investigate the current location choosing methods and develop a new method for choosing ESS locations.

- To choose optimum charging station locations for EV and to analyse how the impact factors influence the location.

- To extend and strengthen the active and reactive power dispatch method by using Genetic Algorithm (GA) for choosing charging station location to achieve power loss reduction.

1.5 Contribution

The main contributions for this work are as follows:

- Develop active and reactive power dispatch strategies for ESS to reduce the power loss caused by EV penetration.

- Analyse and compare the current density method which has been used in other journal papers with the proposed method in this thesis and test them in the same and different DN tests.

- Extend the active and reactive power dispatch method for choosing ESS location for power loss minimisation.

- The influence of the impact factors on choosing charging station location in terms of power loss minimisation are analysed by using the active and reactive power dispatch method. Moreover, annual yield of the charging stations is also considered.

- Extend and strengthen the active and reactive power dispatch method by using GA for choosing charging station location in the more complex test DN.

1.6 Thesis Layout

The Rest of the thesis is organised as follows:

Chapter two presents impacts of EVs on DN. In this chapter, the specifications of the most popular EVs are listed, and the impacts of the large number of EVs connections to DN in terms of voltage drop, transformer overloading and power loss are shown.

Chapter three provides a literature review of the history of ESS, the specifications of ESS, and the benefits of using ESS in DN. Moreover, in this chapter, the model of battery ESS is briefly introduced, and its function is explained.

Chapter four presents several optimisation technologies; these technologies are widely used in power system analysis and include economic dispatch, optimal power flow analysis, unit commitment, multi-area systems economic dispatch, and active and reactive power optimisations. Moreover, one artificial intelligences: GA is listed as having potential for solving problems.

Chapter five proposes a novel active and reactive power dispatch of the ESS approach. System operators can use this approach to reduce the power loss caused by EVs. The impact of power loss is quantified. Based on the dispatch approach, two optimisation methods are developed by considering the peak and off-peak time electricity price. Furthermore, the results, in terms of active power loss, reactive power loss and total active power from TN, are compared by using these two different optimisation methods. The proposed approach is tested on the IEEE 33-bus DN.

Chapter six extends the method used in chapter five and uses it for choosing charging station location problems. In this chapter, the stations' cooperation is considered and applied through the active and reactive power dispatch location choosing method. By using this method, the power loss is significantly reduced. Meanwhile, the current density method, which has been used in the other research papers, is compared with the method used in this chapter. Moreover, the location choosing results show that the method used in this chapter is more accurate than the current density method. In addition, the annual yield of the charging stations

is calculated by considering the inflation in 15 years of station operation. The proposed method is tested in 11-bus, IEEE 33-bus DN and 36-bus DN.

Chapter seven uses the method proposed in chapter six to analyse how impact factors, such as network topology, load patterns and distribution line parameters, influence optimum charging station location. It is shown that optimum locations are not affected by a single change in these impact facts, but by the changes of all these factors.

Chapter eight extends and strengthens the method used in chapter six by using the new GA. This GA is more robust than the mathematical optimiser, so charging station locations and charging station numbers are optimised. The method is tested in the 36-bus DN.

Chapter nine summarizes the main findings from research and major contributions to this study and provides the suggestions for potential future researchers.

Chapter 2 The Impacts of EVs on Distribution Networks

This chapter covers the characteristics of EVs, EV impacts on the DN in terms of voltage drop, distortion, transformer overloading and power loss. In addition, this chapter also shows the ways to reduce power loss in a power system.

2.1 The Overview

With modern technological development and rising awareness of the need for environmental protection, EVs are becoming cheaper and are regarded as less environmentally damaging alternatives to traditional vehicles. Customers can charge their EVs using electric outlets in their homes, work places or at public charging stations. One issue with EVs is that they can only be driven over a limited range: some EVs do have larger batteries and better drive systems, but their range is still limited [24][25].

According to National Renewable Energy Laboratory (NREL) reports [26][27], high penetration of EVs can cause impacts on power generation requirements. If EVs were to constitute 50% of total vehicles, the generation capacity would need to increase by 4% and electricity generation by 8%. Meanwhile, large-scale development of EVs would result in power loads increasing. These unpredictable loads would lead to a potential power supply shortage if too many EVs were charged at the same peak period [28].

The charging process can significantly affect the DN, especially when large numbers of EVs are connected to the DN at the same time. Since these vehicles use considerable amounts of energy, if this scenario happens at peak time, it will worsen the insecurity level of the DN, and cause a great deal of active power loss. This would also put great pressure on the system operators in terms of keeping the system secure. It has been shown that if EV penetration increases by 10% between 18:00-21:00 hours, energy losses will rise by almost 3.7% [29]. Moreover, by connecting with large numbers of EVs, the DN also encounters the risks of voltage drop and distortion, as well as transformer overloading [30].

2.2 EV Introduction

This section covers the merits of EV, different EV types. EV’s charging patterns and market

share.

2.2.1 Merits of EV's

Traditional transport vehicles have been extensively observed to be the most culpable in terms of greenhouse gas emissions, through their heavy reliance on fossil fuels. Globally, the emissions caused by light-duty vehicles account for 44% of total CO_2 emissions [31]. Furthermore, private transport relies heavily on fossil fuels for 95% of its fuel supply, and this occupies over 50% of world oil consumption [32]. With world population increasing, this non-renewable energy will eventually run out. Therefore, actions need to be taken to reduce CO_2 emissions and the amount of non-renewable energy exploitation.

There are two ways to solve this problem; on the one hand, automakers must significantly improve vehicle fuel efficiency. On the other hand, novel technologies for new vehicles that use other forms of energy instead of conventional ones must be developed. The EV is one such vehicle that exploits new technology [33].

The adoption of high numbers of EVs has several merits:

- A cleaner environment. Compared with traditional vehicles, EVs have zero tail-pile emissions and their energy demands can be supplied by various sources. Therefore, these vehicles make contributions to a cleaner environment.

- Alternative type of energy consumption. Traditional vehicles rely on oil. However, some countries do not have rich oil resources, so they depend on oil imports from other countries. Electricity, however, can be derived from domestic resources. Thus developing EVs contributes to balanced energy consumption and improves energy security.

- Cheaper topping up. Topping up EVs is much cheaper than conventional vehicles, especially when charging vehicles at off peak times.

2.2.2 EV Type and Market Share

EV is the general term for a vehicle which can be powered by electricity, or partly by electricity. This term includes Hybrid Electric Vehicles (HEV), Plug-in Hybrid Electric Vehicles (PHEV) and Battery Electric Vehicles (BEV). The first EV on the road was in the late 1800s [34], with the invention of rechargeable lead–acid batteries. The early 1900s, the golden period for the EV, saw its widespread emergence. However, by 1920, it had almost vanished, with the whole market being taken by Internal Combustion Engine (ICE) cars. The main reason for this decline were the limitations of heavy weight, short trip range, long charging time and the poor durability of batteries.

The current need for low-carbon transport has led to a renewed interest in the development of effective EVs. As mentioned above, there are various types of EV to consider. HEV refers to a vehicle with an electric motor, an internal combustion engine, and limited on-board energy storage that can improve engine efficiency. There are several typical HEV models, such as the Toyota Prius, and the GM Chevy Volt. With battery technology development, more attention is being paid to PHEVs and BEVs. When compared with other EVs, PHEVs and BEVs have larger on-board energy storage, and this increases the range limit and thus driving flexibility. A PHEV also contains an internal combustion engine, which makes the drive model and engine efficiency more diverse. A BEV has an electric motor, without a combustion engine, and the battery requires higher power levels and higher energy capacities within a limited space. The weight and affordability of this type of EV also needs to be considered.

Efficient batteries are naturally key to the successful development of EVS. Nickel metal hydride (NIMH) and lithium ion (Li-ion) are the two major battery technologies used in current EVs. Nearly 90% of HEVs in the market use NIMH due to its mature technology, whereas BEVs and PHEVs have largely adopted the Li-ion battery because it has the higher energy density. The batteries specifications for EVs can be seen from table 2.1 below.

Table 2.1 Batteries used in the EVs

Company	Country	Vehicle Model	Battery Technology
BYD	China	E 6	Li-ion
Think	Norway	Think EV	Li-ion, Sodium/Metal Chloride
Hyundai	South Korean	Sonata	Lithium polymer
BMW	Germany	X 6	NiMH
Daimler Benz	Germany	ML450,S400	NiMH
Chrysler	USA	Chrysler 200C	Li-ion
Tesla	USA	Roadster	Li-ion
Ford	USA	Escape	Li-ion
Toyota	Japan	Prius, Lexus	NiMH
Nissan	Japan	Leaf EV	Li-ion

The benefits of EVs have caused many countries and entrepreneurial firms to invest in them and in relevant charging facilities: for example, EDF has a joint venture with Electromotive Limited based in Brighton, UK, and installed new charging points in London and elsewhere in the UK in 2015 [35]. Table 2.2 shows European countries occupy the majority of the EV market [36][37].

Table 2.2 The top ten EV countries in 2013 and 2014[36][37]

Country	PHEV market share (%)	Country	BEV market share (%)	Country	HEV market share (%)
Switzerland	0.05	United States	0.28	Denmark	0.29
France	0.05	Denmark	0.28	Switzerland	0.44
United Kingdom	0.05	Sweden	0.30	United States	0.60
Finland	0.13	Switzerland	0.39	Sweden	0.71
Iceland	0.25	Japan	0.51	Estonia	0.73
United States	0.31	Iceland	0.69	France	0.83
Norway	0.34	Estonia	0.73	Japan	0.91
Japan	0.40	France	0.79	Iceland	0.94
Sweden	0.41	Netherlands	0.83	Netherlands	5.55
Netherlands	4.72	Norway	5.75	Norway	6.10

2.2.3 EV Charging Patterns

In general, EV charging can be divided into two categories. The first is called Centralized Charging Pattern (CCP) and the second Decentralized Charging Pattern (DCP). For the CCP, all EV owners are coordinated by centre operators. The central operator collects all the needed information, such as State of Charge (SOC), permissible charging interval and charging cost, while leveraging the renewable energy or extra sources to charge each EV by using various charging scheduling algorithms [38]. For the DCP, the charging behaviours are manged by EV owners themselves, depending on each one's preferences, and on electricity prices. Normally, the individual owner sends a load request to a charging station. Then each EV defines its own charging schedule according to the different charging requirements, SOC and electricity tariffs. These charging features reduce the communication requirements between individual EVs and centre operators.

Both CCP and DCP need to be well-coordinated in order to guarantee appropriate control without violating any given limits or constraints. Figure 2.1 shows the charging coordination between CCP and DCP [28]. This cooperation ensures a stable charging process by reducing any potential violations. The first stage of the charging process is the Distribution Management System (DMS). This is the information collecting and processing system, and it consists of different algorithms which control the network and all its elements. It collects all the EV's information, such as SOC, plug-in and plug-out time and battery capacity. Then, the DMS use dynamic programming optimization techniques to dispatch an optimized charging schedule if no feeder's current carrying capacity or voltage limitation violations occur. For effective decentralised local control to occur, the voltage limitation should be controlled within permissible values. If the voltage limitation is exceeded, the connections between EVs and DN will be turned off. If the voltage limitation is not exceeded, the operating state will be updated dynamically.

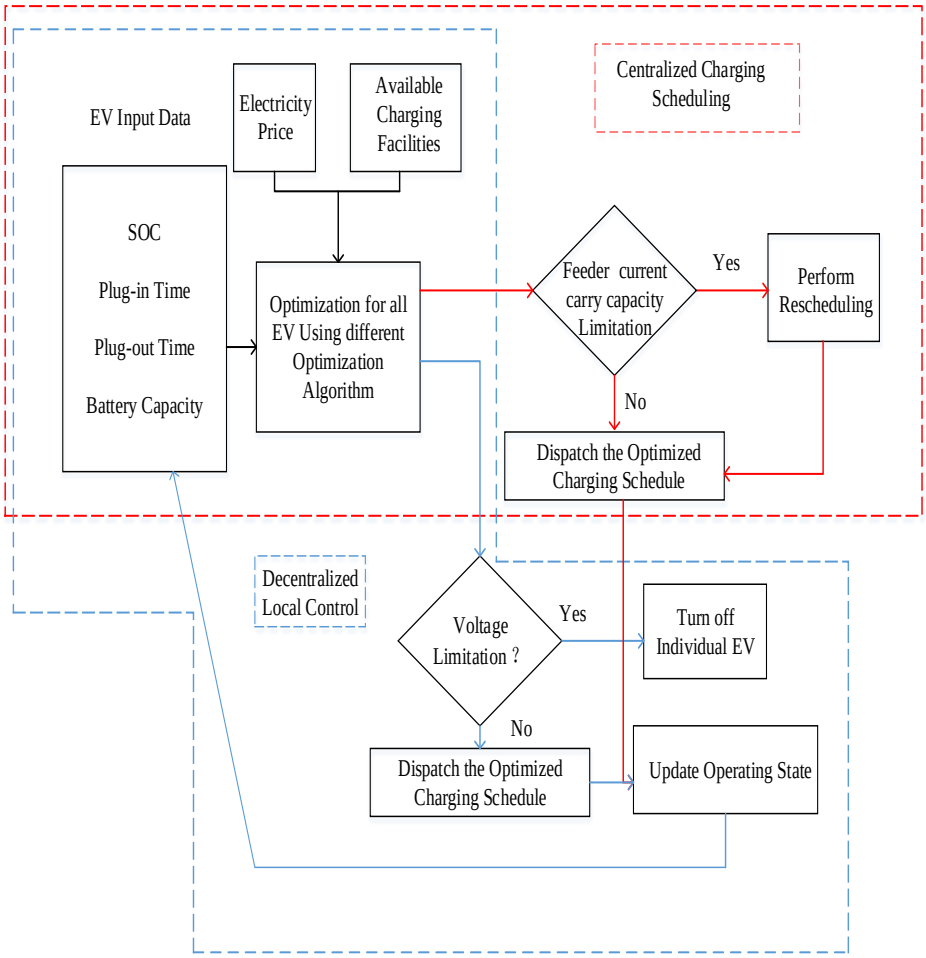

Figure 2.1 Charging Coordination between CC and DC

The Charging Level can also be divided into three types, Level 1 Charging, Level 2 Charging and DC fast Charging. Level 1 Charging is the slowest charging level. It provides a single phase 120V/15A AC plug. This charging level is suitable for home charging as no additional infrastructure is necessary [39]. Level 2 Charging is the primary option for public or commercial charging stations. This charge option can operate at up to 80A and 19.2 kW. It is much faster compared with Level 1 charging. This charging is not suitable for home and private use, but is suitable for CCP charging [39][40]. DC Fast Charging is much faster than the other methods and it is also suitable for charging stations. It provides up to 40 miles of range for around 10 minutes of charging. Its installation in charging stations requires a 480V AC input and other relevant devices, such as power electronics to convert AC to DC [40].

The tremendous developments in EVs have created massive benefits for the automotive industries, but has also brought some concerns which cannot be ignored: for example, is there a sufficient charging infrastructure? Can charging time be reduced? How should the range

limitations of the EV be expanded? And what are the impacts when a large number of EVs are connected to the DN?

2.3 Impacts of EV Penetration on Distribution Networks

The EVs' impacts can be divided into two areas, which are EV to grid and grid to EV. This thesis will only consider the impacts caused by EV to grid. When a large number of EVs are connected to the DN, the system's stability and security are dramatically influenced [41].

Figure 2.2 below shows the daily electricity (excluding electric heating) using profile of a typical resident in the UK.

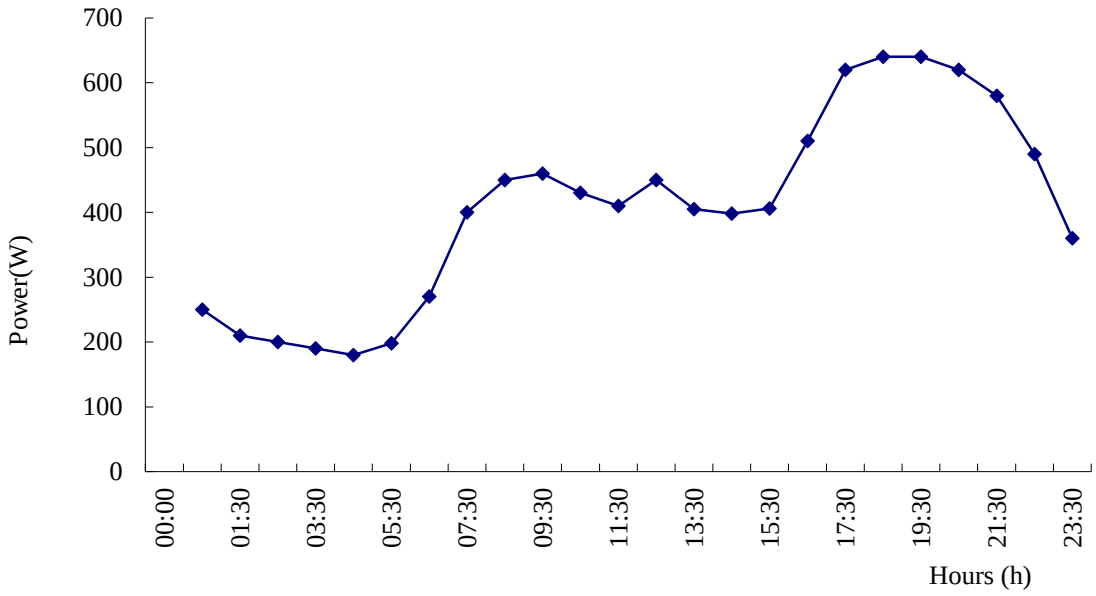

Figure 2.2 Daily profile for electricity use [42]

From figure 2.2 we can see the period between 8:30-14:30 people start using electricity. From 14:30 to 19:30 the demand of electricity increased significantly. Whereas, after 19:30 till 20:30, that demand reduced largely. During the time between 9:00- 17:00, people usually arrive their working places (except weekends) and charge their EVs. After 17:00 they leave office and arrive home, EVs can be charged after that time. It is worth to be noticed if they charge their vehicle during 9:00-21:00, they have to pay a higher bills because the peak period. Therefore, from a customers' view, charging EVs directly to DN can raise their electricity bill.

From the system operator's viewpoint, an EV is regarded as a non-linear load when it connects to the DN. Such a load draws a non-sinusoidal current from inverter and converter inside the charger. This current can cause voltage drop and distortion. Distorted voltage consists of several harmonic waves and these waves have adverse effects upon other components in the DN, such as transformers, when they are connected to the EV. High levels of harmonic distortion can cause effects such as increasing transformer, capacitor, or generator heating, and incorrect meter readings. It follows that these negative effects will increase dramatically, if and when large numbers of EVs connect to the network [41].

A single EV charging may not cause many problems. Compared with other household appliances, such as clothes dryers (0.7kW), oven (3kW), and an electric kettle (1.8kW) [43], an EV needs more power for charging. However, it will not damage any relevant charging facilities: for example, a Toyota Prius needs 3.3kW to be fully charged, or around that power level, depending on specific types, and a 15kVA transformer is capable of coping with this load, which is unlikely to pose any real challenges for that transformer. Moreover, the fuses in local houses or flats will not trip because the current of the EV charger (for 3.3kW EV the current is 14.35A) will not exceed the tolerant fuse current, which is 50A. Therefore, a single EV charging will not cause uncertainties in the DN.

However, a large number of EVs charging simultaneously on the same DN will influence the grid significantly: for example, in real life, residential area a uses phase A, residential area b uses phase B, and residential area c uses phase C. When EVs connect to area a, an unbalanced load will occur because compared with the other residential area loads. The EVs need much more power, and this will result in a greater power loss [44]: for instance, 20 Nissan Leaf needs 1.2 MW, and this figure is almost 600 times that required for a 1.8 kW electric kettle [43].

In this situation, the designed limitation of the transformer could be exceeded. For example a 10kVA distribution transformer, which power factor is 0.8 can provide 8kW to the main bus, is able to handle any single charger of 1.4kW, 3.3kW, or 6.6 kW [45]. However, more than two 3.3kW or one 6.6 kW will exceed the 10KVA transformers designed limitations. Table 2.3 shows the safe limit for numbers of EVs for two different transformer ratings. This shows that transformers could be overloaded with a low number of EVs. Although currently no report indicates that a normal residential transformer has been over loaded by EVs, for EVs

such as the Tesla Roadster 16.8 kW, overload is likely to occur and this could damage large residential transformers.

Table 2.3 Transformer class for EV load

Transformer kVA	1.4 kW EV charger	3.3 kW EV charger	6.6 kW EV charger
10	1	1	0
20	2	2	1

As mentioned above, connecting large numbers of EVs to the DN brings harmonic impacts such as voltage drop and voltage distortion. A large number of EVs charging at the same time can cause damage to local transformers, causing residents' relays to trip, and such uncertainties will increase the probabilities of blackouts. Moreover, unbalanced loading in the DN caused by the EVs can also lead to a large amount of power loss. The authors [46]compares with different power loss in terms of different penetration levels of EVs. With every 10% increase in EVs being charged, the power loss is 3.7%. For the system operators, this loss needs to be reduced, and the methods for mitigating this loss need to be considered.

2.4 Power Loss

After electric power is generated, it transfers through the transmission and distribution lines to customers. During transmission, a significant portion of power loss happens. This loss occurs in numbers of components in the transmission and distribution system. In the DN, two major sources, transformers and distribution lines, can cause system losses and need to be considered [47].

There are several types of line loss, such as core loss, copper loss, and magnetic hysteresis losses in steel armouring or pipe work, and dielectric losses occurring in the main body of cable insulations. In addition, the time-varying electromagnetic field of the main current also causes the induction of currents in any metallic sheathing, cable armouring or steel pipes [48].

The majority of power losses in the distribution line can be considered as copper losses [49] and can be calculated by:

$$P = I^2R \tag{2-1}$$

They are determined by either current or resistance. The current is affected by external factors such as loads changing. The resistance varies with the internal factors of the cable according to the equation 2-2 below:

$$R_{DC} = \rho \, /A \tag{2-2}$$

where R is the DC resistance, ρ is the resistivity, L is the length of the line, and A is the effective cross-sectional area of cable.

In practical terms, the value of the DC resistance is influenced by factors such as environment and structure; therefore, two additional effects are added into the equation 2-2 the first effect is

$$Effect\ 1 \ = \ 1 + \alpha_{20}(\theta_m - 20) \tag{2-3}$$

where α_{20} is the temperature coefficient of resistance per 1 °C at the reference temperature of 20 °C. θ_m is the maximum permissible conductor operating temperature in °C. The second effect is:

$$Effect\ 2 \ = \ 1 + Z \tag{2-4}$$

where Z is a constant value between 0.03 (for single core cables of cross section equal to or less than 500mm^2). The value of Z depends on the structure of the cables.

The final DC resistance is multiplied by these two factors:

$$R_{DC} = \ \rho \, \mathrm{L/A} \ \times \ [\ 1 + \alpha_{20}(\theta \mathrm{m} \ - 20) \ ] \ (1 + \mathrm{Z}) \ \ \Omega/\mathrm{m} \tag{2-5}$$

The skin and proximity effects take into consideration the AC resistance, which can be seen from equation 2-6 below:

$$R_{AC} = R_{DC}(1 + y_s + y_p) \quad (2\text{-}6)$$

where y_s is the correction factor for skin effect, and y_p is the correction factor for the proximity effects.

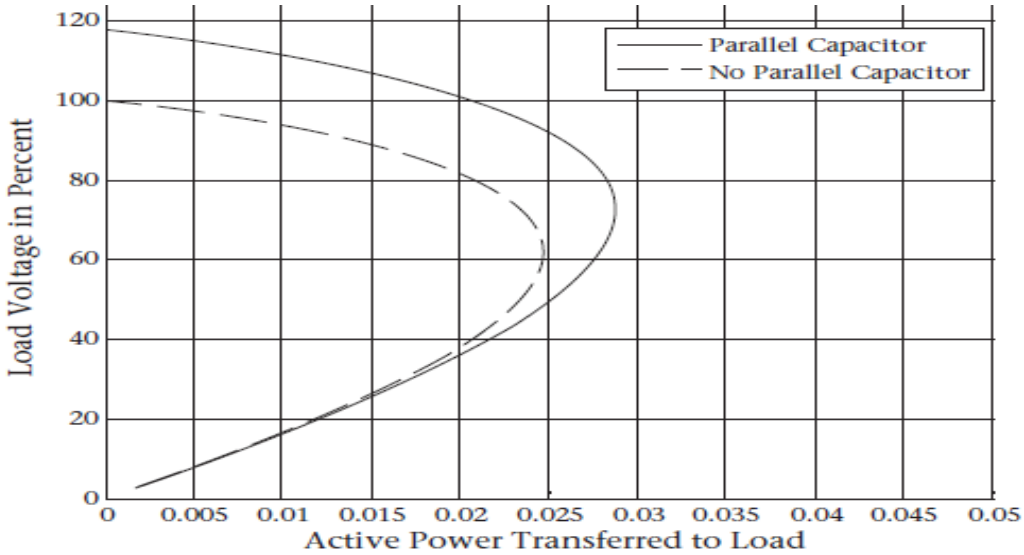

Figure 2.3 P-V curve for delivery of power [44]

Increasing the load levels can also increase the power loss. The reason for this is that when the load grows, the resulting total power generation raises more power which is delivered to load, and the voltage at the node drops. When the demand reaches the point where the voltage is approximately 60% of the supply voltage, voltage collapse occurs. This drop can be seen from figure 2.3.

In that situation, with increased EV penetration, more power is generated and transferred to local communities, and the voltage of loads drops. From equation 2-7 below, it can be deduced that the current of the distribution system increases. This results in more I^2R losses rises in the DN:

$$P = UI \quad (2\text{-}7)$$

Generally speaking, there are two types of losses in the distribution transformers (DT), these losses occur both as copper and core losses [50]. The copper losses in the DT are the same as those in the distribution lines. However, the core losses are different: they consist of eddy current and hysteresis losses. The copper loss can be calculated using $P=I^2R$, which is

illustrated in the equation 2-1, but its magnitude is smaller than the core loss. This loss occurs in the form of the heat caused by the current in both the primary and secondary windings of transformers. In addition, the winding resistance will also affect copper losses.

The core loss of the DT can cause eddy current and hysteresis losses. The former is due to the magnetically induced current in the core, and the latter is caused by the less than perfect permeability of the core material. Hysteresis loss happens in the process of magnetization of the ferromagnetic material caused by magnetic hysteresis. This loss can be reduced by using better quality materials in the core, which have high magnetic permeability [51][52]. The core loss is relatively constant for an energized transformer, and can be considered as the transformer load [52][53] .

Additionally, the presence of harmonics in the system also increases losses in DT. Harmonic current only causes a small amount of copper losses. However, harmonic voltage can cause large transformer core losses.

2.5 Methods of Reducing the Power Losses in the Distribution Network

A wide variety of solutions have been proposed in the area of power loss reduction, and these are shown below.

- Feeder reconfiguration
- Adding distribution generators
- Installing high efficiency DT
- Demand-side Management (DSM)
- Embedding capacitors
- Re-conducting in primary and secondary feeder
- Re-locating the DT by using the optimal method in DN.
- Voltage upgrading

Network reconfiguration is the process of changing the topological structure of networks by using different status of tie switches. The re-configured network can reduce power loss and relieve overload in the network. However, unlike TNs, more uncertainties occur in the DN, in terms of control and operation: especially for areas where the load density is high [54]. This

increases the difficulties for the operators in relieving the loads on the feeders. Moreover, the voltage profile of the system will be hard to improve to the required level. Overall, the main drawback of the network reconfiguration is it cannot provide more power to customers.

In order to meet the required demands, some researchers integrated Distribution Generation (DG) in the network to improve the performance of the voltage profile, provide more power to the DN, and reduce power loss while increasing energy efficiency. Normally, researchers use methods such as varying the optimal size and location of DGs, but these DGs are usually considered and developed by entrepreneurs, and in practice, utilities will not implement and plan such optimal solutions [55]. In addition, the location and rating of generators are limited by a variety of factors, such as land, environment, and residents' attitudes to these DGs: for instance, the location of wind power generation needs to consider wind resource, frequencies of lightning in the area, and local residents' opinions. This latter would include whether they are willing to accept wind turbines near their homes or not. An additional factor is that wind turbines can influence air flow, so may change the local climate: what people think about this issue still remains to be seen.

Some researchers have considered optimizing the location and size of DT. Using this method, the total power loss can be reduced to some degree, but installing the DT itself brings two main losses: no-load loss and load loss of the DT. No-load loss appears from the energy required to retain the continuously varying magnetic flux in the core. Load loss arises mainly from resistance losses in the conducting material of the windings. Moreover, with the nonlinear load increases (such as the battery charger in the EVs, fax machines and photocopiers) especially in DN, power loss of DT becomes great. The eddy current caused by harmonic loads also affects the operating temperatures and lifespan of the DT [56]; therefore, it forces the operators to reconsider use of the DT.

Another approach has been to concentrate on installing the shunt capacitors of reactive power optimization to reduce power loss. However, for light loads, which do need more reactive power, the power loss does not reduce significantly. For the feeders away from capacitors, this has less effect on power loss reduction. Additionally, only reactive power is considered in the optimization process and installed capacitors cannot supply any active power to the grid.

Compared with the above options, the ESS is a good alternative. It not only can provide

active and reactive power to the DN, but also is not limited by constraints such as natural resources, such as wind or solar power, and it will not alter the local climate. In addition, the installation fee is much cheaper than for distribution generation. Over all, ESS has notable merits, and needs to be installed into the DN to improve performance.

Together with the increasing deployment of renewable generators, the intensive power demand, the high capital cost of managing grid peak demands, as well as large capital investments in grid infrastructure, more attention is being paid to ESS. As with the TN and DN transfer, from power to demand sides, the ESS is able to provide power when and where it is needed, and from the power supply side, installing ESS can dramatically reduce power loss. Generally, there are several main applications for ESS which can support the whole chain of electrical systems. Included are: renewables integrations, TN and DN support, commercial and industrial power quality and reliability, home energy management, and home back-up storage. These applications are discussed in Chapter three.

2.6 Chapter Summary

By way of summary, in Chapter two, the main research aim has been given, which is to reduce the power loss caused by the large number of EV's penetration. Around this research aim, the introduction of EV in terms of its specification, market share, charging process and merits has been shown. Following this, the impacts of EV were given. Connecting a large number of these vehicles to DN can influence the network significantly in terms of power loss, voltage drop, distortion, harmonic current, and unbalanced loading. In addition, if customers charge EVs directly during peak time, electricity bills will rise significantly. Several methods have been introduced for mitigating these impacts. One of them is to install the ESS in DN. The introduction of ESS and the benefits of using ESS as an application will be shown in Chapter three.

Chapter 3 Energy Storage System Overview

This chapter covers the introduction and history of ESSs, different storage options, and the technical benefits of ESS.

3.1 Overview

The power network is facing great challenges in generation, transmission and distribution to meet all types of requirements: for example, reduction of CO_2 emissions, accommodation of renewable energy, and mitigation of the negative impacts caused by new loads such as EVs. These requirements can result in a need for the restructuring of electric utilities, and the upgrading of grids. However, adding new components into pre-existing systems will cause problems: for instance, connecting large number of EVs to local DN causes voltage drop and power loss. ESS could be a solution to such problems and be used to reduce such negative impacts which are emerging in the evolving grid.

ESSs have long been in use. They were built from the 1920s to 1980s, but with environmental opposition and changes in deregulation, and the restructuring of electric utility, the number of ESSs, especially pumped hydro plants, decreased [57]. By the mid-1980s, the ESS was only used for charging from coal off-peak to replace natural gas on-peak, to make sure the coal units remained at optimal output as the system load varied. However, in the early 1990s, emerging storage technologies could provide more than 10 services, according to the SNL report [58][59], and during the last ten years, the range of grid services has been expanded, and more detailed applications, guidance and benefits have been established [60].

3.2 Energy Storage System

A complete ESS consists of three major subcomponents: storage, a Storage Management System (SMS) and a Power Conditioning System (PCS) [61][62]. The storage can be of various types, such as Pumped Hydro Energy Storage (PHES), battery, flywheel, and Compressed Air Energy Storage (CAES). The SMS consists of the battery monitors and computers and controls the ESS's daily operations: for example, how to dispatch the active and reactive power of ESS for different purposes. A simple PCS consists of a capacitor, diode

and a transformer. In the battery and flywheel storage systems, when the ESS discharges to the network, the PCS can be seen as the inverter; whereas when it charges from the system, it can be regarded as the rectifier.

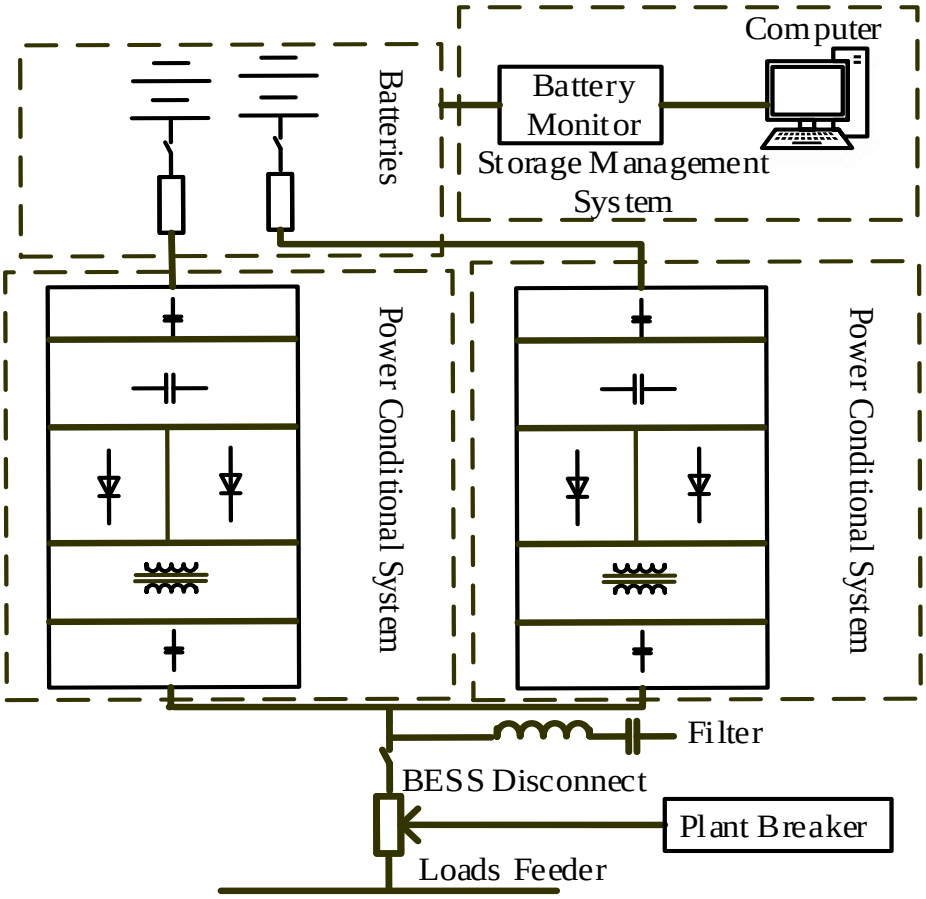

Figure 3.1 An ESS Structure

For most operation conditions, the ESS can be regarded as the voltage source. The PCS generated voltage is completely controllable within the current rating of the converter equipment. The ESS power generating capacity is limited by the available battery voltage. ESS can generate both active and reactive power in all four quadrants as indicated in figure 3.2. At operation point 1, active and reactive power is being discharged to the system. At operation point 2, the system is being charged, absorbing both active and reactive power from the TN.

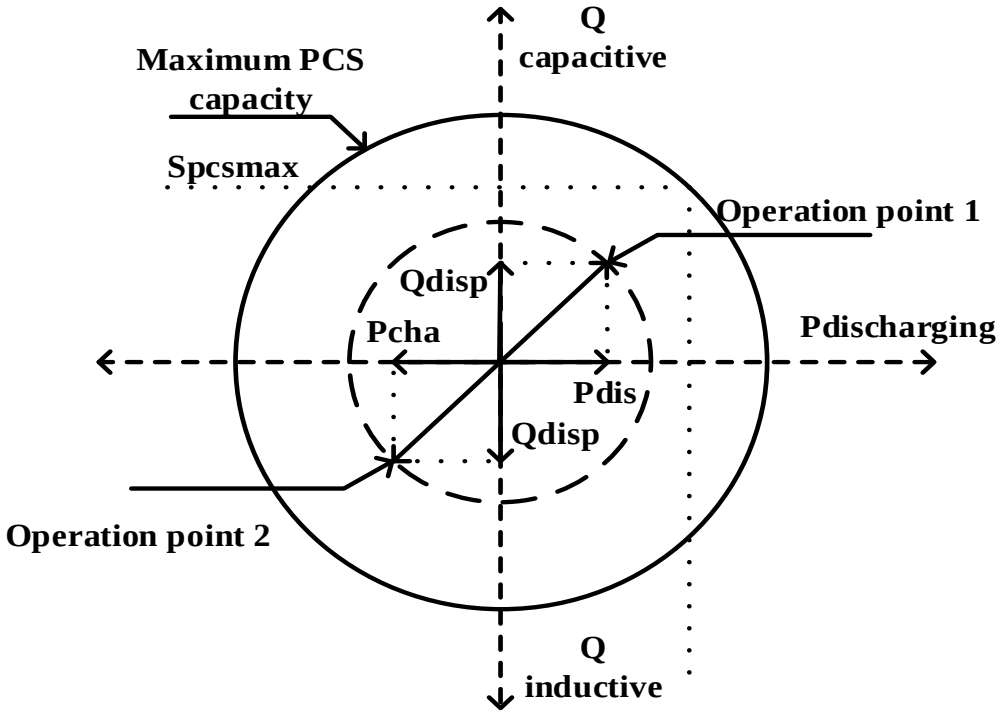

Figure 3.2 Active and reactive power capability [63]

The apparent power of ESS can be represented by

$$S_{ESS(k,h)} = \begin{cases} \sqrt{P_{char(k,h)}^2 + Q_{disp(k,h)}^2} \\ \sqrt{P_{dis(k,h)}^2 + Q_{disc(k,h)}^2} \end{cases} \quad (3-1)$$

The active and reactive power discharge of ESS should not exceed the maximum apparent power $S_{BESSMAX}$ of the BESS [64].

$$P_{dis}^2 + Q_{disp}^2 \leq S_{BESSmax}^2 \quad (3-2)$$
$$P_{char}^2 + Q_{disc}^2 \leq S_{BESSmax}^2 \quad (3-3)$$

The active power for charging and discharging must be positive values

$$P_{char(k,h)} \geq 0, \qquad P_{dis(k,h)} \geq 0 \quad (3-4)$$
$$-S_{ESSmax(k,h)}^2 \leq Q_{dis\,(k,h)} \quad (3-5)$$

Moreover the upper and lower bound of the storage capacity should satisfy.

$$E_{min} \leq E_{Low}, \qquad E_{Up} \leq E_{max} \qquad (3-6)$$

Usually the control variables can be defined as any of the variables for different operation purposes.

3.3 Energy Storage Options

Energy storage can be different types: it can be batteries, flywheels, or superconducting magnetic energy storage. They all store energy and release it at the appropriate time. They have different capacity and physical size depending on different applications. Their current battery types and technologies are shown below.

3.3.1 Lithium-ion Battery

The Lithium-ion battery is becoming the most common battery used in ESSs, as well as being positioned as the leading technology platform for the plug-in EV and all other EVs. Compared with other batteries, such as lead-acid batteries, the lithium and lithium-ion battery is relatively new. It has salient energy densities and a reasonable cycle life. The majority of Lithium-ion battery cells contain two reactive materials capable of undergoing an electron transfer chemical reaction. Normally, cylindrical and prismatic cells are the most common cells in liquid Lithium-ion batteries. The creation of a satisfactory large-format Lithium-ion prismatic cell currently lacks intense research and development, scale-up, and durability evaluation for EV use [65].

3.3.2 Sodium-sulphur (NaS) Battery

An NaS battery uses molten sodium as its anode, sulphur and ceramic as its cathode. NaS batteries are the most common commercial technology used in ESS, and this technology is widely used in electric utility distribution grid support, wind power integration, and high-value grid services. The operation temperature for this battery is between 300-500 °C. Figures from [65], shows the normal NaS battery ESS has 4500 life cycles for rated discharge capacity of 6 MW per installation MW.

3.3.3 Flywheels

Flywheel systems are regarded as kinetic or mechanical batteries. These systems transfer kinetic energy into AC power by using control and power conversion systems. From [56] a single flywheel, an energy storage unit can deliver 100kW power and store 25kWh. This means this battery can deliver 100kW power at around 0.25 hour. In its first implementation, it was designed for system frequency regulation with output energy of 5MW at a power of 20MW [66]. The size and speed of rotor decide the energy sizing for the flywheel system, and the power rating depends on the motor generator. Power and energy can be sized independently. The main drawbacks of flywheels are their relatively poor energy density and large standby losses.

3.3.4 Superconducting Magnetic Energy Storage (SMES)

SMES is a relatively new technology, which stores electricity from TN or DN within a magnetic field by creating current flow in a superconducting inductor. A SMES can charge and discharge large quantities of power instantaneously. It consists of a cryogenically cooled superconducting coil and power conditioning systems, which are motionless, and can result in higher reliability than many other storage types. It has almost infinite cycling capability, rapid response and a salient energy recovering rate close to 100%. In addition, it is more environmentally friendly compared with other batteries. SMES is still under development, so currently, there is no large-scale grid usage [67][68].

3.3.5 Pumped Hydro Energy Storage (PHES)

PHES is almost the oldest type of large-scale energy storage; it pumps water from a low reservoir to a high reservoir. Energy is utilised by the down flow, through a turbine and a generator, to create electricity. The capacity of PHES is sized up to 4000MW and operating efficiency is around 75%-85%. The main disadvantage of this method is it is geographically constrained [69].

3.3.6 Zebra Battery and Compressed Air Energy Storage (CAES)

A Zebra battery utilizes a molten sodium as anode, a solid separator and a solid metal

chloride cathode. The principle of CAES storage is it uses electricity to compress air and store it in an over or underground reservoir. When the compressed air is expanded through a turbine, electricity is produced. The capacity of an underground CAES is 10GWh: for an over ground one, it is 60MWh: the underground version is bigger and cheaper than the over ground. Germany and Alabama have installed first generation CAES, and the second generation has been defined and is currently being developed [70]. Compared with other batteries, the zebra battery offers a very low level of self-discharging, similar to the NaS battery. However, it has longer life cycles. It has also been developed for EV applications. The application for the grid is limited to date; a 400kW unit is still under development [71].

3.4 Technical benefits of ESS

This section discusses the technical benefits of ESS: how it can provide energy to customers, support system voltage, and relieve transmission congestion [65]. These benefits enable system operators to install ESS in power systems to provide better electricity services.

3.4.1 Electric Supply Capacity

Depending on different situations in given electricity supply systems, ESS can be used to reduce total power import from TN, or to defer the need to buy new generators. The technical specifications are shown below:

Storage System Size Range: 1 – 500 MW
Target Discharge Duration Range: 1 – 6 hours
Minimum Cycles/Year: 5 – 100

Using the ESS as supply capacity may require consideration of issues such as annual hours of operation, and frequency of operation. Additionally, the price of generation capacity may influence the discharging of ESS for this service. Thus if capacity is priced per hour, the storage duration is more flexible, or if price requires the capacity be available for some specific periods, (for example 11:00pm-6:00pm), or some specific time (for example 4:00am), the ESS has to accommodate these requirements.

3.4.2 Electric Energy Time Shift

ESS for electric energy time shift can be used by customers to purchase cheaper electricity during the periods when electricity prices and the system's marginal costs are low to charge the ESS, and then use or sell the electricity at a later time when the price or cost is high. In addition, similar duty (time –shift) can be provided by storage for excess energy production from renewable sources, such as wind or PV cells. The technical specifications are given below:

Storage System Size Range: 1 – 500 MW
Target Discharge Duration Range: <1 hour
Minimum Cycles/Year: 250 +

Storage for small scale wind farms would be in the lower end of the storage system size, whereas for a large wind farm or a group of wind farms or PV plants, the upper end of the size range should be chosen. Additionally, seasonal and diurnal impacts can also affect this service, especially from wind and PV plants.

3.4.3 Voltage Support

ESS can be used to maintain voltage within specified limits in DN and TN. In most cases, ESS needs to offset the reactive effects caused by the grid connected equipment through the whole process of electricity generation, transmission and distribution.

One method to offset reactance is by using designated power plants. However, maintenance and capital costs for these power plants are higher than for ESS. It is quite possible for strategically placed ESS to be used instead of these plants as voltage support when considering the economic aspect of system operation. ESS can be installed at a central location or near a large load in the network to provide this service. The technical specifications are given below:
Storage System Size Range: 1 – 10 mega volt-ampere reactive (MVAr)
Target Discharge Duration Range: Not Applicable
Minimum Cycles/Year: Not Applicable
The nominal time for voltage support is assumed to be 30 minutes: time for system

stabilization and also for operators to arrange available generation for load shedding.

3.4.4 Transmission Congestion Relief

With the high growth of electric demands, transmission capacity does usually not keep pace with this growth: for example, transmission facilities are not adequate or lack maintenance, and available energy cannot be delivered to some or all down streams. This situation may cause transmission congestion, and this leads to increased congestion costs or marginal pricing. ESS can provide a service to reduce transmission congestion. It would be installed downstream from the congested portion of TN. The specification is shown below:

Storage System Size Range: 1 – 100 MW
Target Discharge Duration Range: 1 – 4 hours
Minimum Cycles/Year: 50 - 100

3.4.5 Distribution Infrastructure Service

Distribution infrastructure service includes delaying, or avoiding investment, in terms of replacing old existing DTs, or re-conducting distribution lines with heavier wire. An installed ESS can aid this service and manage grid peak demands, and reduce the negative impacts caused by EVs.

Usually, a replaced transformer is selected to be of a size which can accommodate future load growth over the next 15 to 20 years. However, before loads increase to that level, a large number of transformers may be underutilized in most new equipment. Installed storage can defer the upgrade of transformers, and thus extend the currently in-use transformer’s potential life.

Installing storage can also reduce power system investigation and planning risk if planned load growth does not occur: for instance, a supermarket or a cinema is not built because of investigator delay or project cancellation. This strategy would save the investment required to upgrade transformers or replace lines.

3.4.6 Customer Energy Management Services for Power Quality

The customer energy management service involves using ESS to protect loads side against short-duration events that affect quality of power delivery to customers. Poor power quality includes the following:

- Harmonic
- Variation in voltage magnitude
- Interruptions in service
- Variations in primary frequency during power delivery

The specifications can be seen below:

Storage System Size Range: 100 kW – 10 MW
Target Discharge Duration Range: 10 seconds – 15 minutes
Minimum Cycles/Year: 10 – 200

Typically, the target discharging duration range is from a few seconds to a few minutes. The life cycle is around 10-200 times, and the lower boundary is suitable for residential areas.

3.5 ESS for Power Loss Reduction

ESS is widely used in DN to reduce the power loss. In reference [72][73][74] the authors considered the optimal size and placement of ESS in DN to reduce the power loss. Reference [75] the authors concentrated on the locations of DG and ESS and their cooperation for power loss reduction in DN. Reference [76] considered the size of wind generation units and ESSs as well as ESS operation strategy by considering the ESS's reactive power contribution for power loss minimisation in DN. Researchers considered shift load from on-peak to off-peak time period in DN by using ESS to reduce the power loss [77]. Researchers considered optimal operation of ESS to reducing power loss by reducing energy cost while satisfying battery physical constraints [78]. Reference [79] considered the key parameters identification of ESS for TN and DN line power loss. In [80] the authors developed an advanced ESS management model to accommodate the penetration of DG and Photovoltaic panels by

considering power loss reduction in DN. Reference [81] considered the cooperation's between two ESSs for power loss reduction caused by large penetration of EV in DN by minimising the operation costs of the ESS.

All these researchers have used ESS to reduce to power loss indicated ESS has a great advantages for TN and DN power loss reduction.

3.6 Chapter Summary

In this chapter the ESS was introduced. It consists of three main components; storage, which can be of different types: PCS, which is designed to supply active and reactive power to the system and SMS, which controls the different control variables in ESS for various operation purposes; it is the brain of the ESS. Moreover, other research example of how to use ESS to reduce power loss in both TN and DN were discussed. Finally, the physical characteristics of ESS were also discussed to reveal its technical benefits.

Chapter 4 The Optimization for Power Loss Reduction

Chapter four presents Mathematical Optimization Techniques (MOTs) such as Linear Programming (LP), Nonlinear Programming (NP) and Quadratic Programming (QP); as well as Artificial Intelligence (AI) optimisation technique and its applications in the power system.

4.1 Overview

The power system is suffering increased pressures from government, large industries, and investors in favour of privatization. Facing such a complicated existence, power utilities need efficient tools and aims to ensure the system can be operated in a safe and stable way: meanwhile, providing the lowest cost. This makes the overall objective, no matter whether for long term operating or for short term operating, to find a balance between security and stability and economic requirements.

Optimization and evolution techniques are the most common techniques used in power system operation, planning and control. Due to the nature of problems inherent in the system, some of them being very complex and nonlinear, not all of them can be formulated mathematically. In order to find solutions to these problems, it is vital to choose the proper problem-solving techniques for power systems.

MOTs and AI are widely used in power systems. MOTs are all based on mathematical models; suitable mathematical models are needed to solve problems. AI does not have the strict requirements of MOTs and is based on evolution theory: it can be used in much wider areas in power systems and is more robust than conventional MOTs [82].

4.2 Mathematical Optimization Techniques

MOT is highly reliant on mathematical formulations. A one-dimensional problem can be solved simply. However, to solve problems which have more than one dimension, specific software and coding skills may be needed. Some power system problems are optimization problems, and MOT is a suitable tool to solve these [83]. MOT can be classified into [84]:

LP: The objective function and constraints are given in linear forms with continuous control variables.

NP: Either objective function or constraints, or both, are in nonlinear forms with continuous control variables.

IP and MIP: The control variables are discrete. And for mixed-integer programming the control variables are both discrete and continuous.

4.2.1 Linear Programming

LP is a type of optimization technique which can be defined as the problem of maximizing or minimizing a linear objective function subject to linear constraints [85][86]. A standard mathematical model is given below:

The objective function:

$$C^T x = c_1 x_1 + c_2 x_2 + \cdots + c_n x_n \qquad (4-1)$$

Subject to the constraints

$$a_{11} x_1 + a_{12} x_2 + \cdots + a_{1n} x_n \leq b_1 \text{ or } \geq b_1 \qquad (4-2)$$

$$a_{21} x_1 + a_{22} x_2 + \cdots + a_{2n} x_n \leq b_2 \text{ or } \geq b_2 \qquad (4-3)$$

$$\vdots$$

$$a_{m1} x_1 + a_{m2} x_2 + \cdots + a_{mn} x_n \leq b_m \text{ or } \geq b_m \qquad (4-4)$$

$$aeq_{11} x_1 + aeq_{12} x_2 + \cdots + aeq_{1n} x_n = beq_1 \qquad (4-5)$$

$$\vdots$$

$$aeq_{q1} x_1 + aeq_{q2} x_2 + \cdots + aeq_{qn} x_n = beq_q \qquad (4-6)$$

and

$$x_1 \geq 0\,,\ x_2 \geq 0\,, \ldots, x_n \geq 0 \qquad (4-7)$$

where, x is the decision variable; c is the objective function linear coefficient; a is the inequality constraint function coefficient; and aeq is the inequality constraint coefficient function. Note that the main constraints are written as $\leqslant$ for the standard maximum problem, and $\geqslant$ for the standard minimum problem.

One of the general processes for solving this LP is to graph the inequalities and then to form a feasibility region. The coordinates of the corners of this feasibility region are then found and the points for which the highest and lowest values can be found are tested.

Compared with other optimization techniques, LP has several merits [86]. Firstly, it is very reliable, especially regarding convergence properties. Secondly, it can quickly identify infeasibility. Thirdly, it can accommodate a large variety of power system limits, including very important contingency constraints. On account of these features, LP is widely use in power system operation problems such as economic dispatch, optimal power flow, and steady-state security regions.

The drawbacks of LP based techniques are they can be inaccurate: for example, in terms of evaluation of the system losses, there are insufficient solutions to find an exact solution compared with an accurate nonlinear power system model.

4.2.2 Nonlinear Programming

Nonlinear Programming consists of the objective function, general constraints and variable bounds [87]. Compared with LP, the main difference is that NL consists of at least one nonlinear function, which can be the objective function or some of the constraints. A standard mathematic model is given below:

The objective function:

$$Max\ or\ Min\ f(x_1, x_2, \cdots x_n) \qquad (4-8)$$

Subject to:

$$a_1(x_1, x_2, \cdots x_n) \leq b_1 \qquad (4-9)$$

$$a_m(x_1, x_2, \cdots x_n) \leq b_m \qquad (4-10)$$

$$c_1(x_1, x_2, \cdots x_n) = beq_1 \qquad (4-11)$$

$$\vdots$$

$$c_q(x_1, x_2, \cdots x_n) = beq_q \qquad (4-12)$$

$$x_1 \geq 0\ ,\ x_2\ \geq 0\ , \ldots , x_n \geq 0 \qquad (4-13)$$

where x is the decision variable; a is the inequality constant function coefficient; and c is the equality constant function coefficient.

Compared with LP, NP is more accurate and it has wider applications; not only in the power system, but also in other areas. However, with some NPs. it is hard to distinguish a local optimum from a global optimal, and different starting points may lead to different final solutions. Moreover, it may be difficult to find a feasible starting point. NP is widely used in power system unit commitment, multi-area system economic dispatch, and active and reactive power optimizations.

4.2.3 Quadratic Programming

QP is a special form of NL. The objective function of the QP optimization model is quadratic, and the constraints can be in linear or nonlinear forms. QP has a higher accuracy than LP-based approaches. It is used in optimization problems, especially those for which the objective function is quadratic, such as generator cost minimization, or power loss reduction [87][88].

The standard objective function of QP is shown below:

$$f(x) = \left(\frac{1}{2}\right) x^T\ H\ x + \ C^T x\ +\ \alpha \qquad (4-14)$$

subject to

$$a_1(x_1, x_2, \cdots x_n)\ \leq\ b_1 \qquad (4-15)$$

$$\vdots$$

$$a_m(x_1, x_2, \cdots x_n)\ \leq\ b_m \qquad (4-16)$$

which is usually further defined by a number of constraints. ($\frac{1}{2}$ factor is included in the quadratic term to avoid the appearance of the factor of 2 in derivatives) $f(x)$ is the objective

function, H is the Hessian symmetric matrix, c is the constant vector, and α is the scalar constant.

The value of the objective function can be deduced from the equations below

$$H = \begin{bmatrix} H_{x11} & H_{x12} & H_{x13} \\ H_{x21} & H_{x22} & H_{x23} \\ H_{x31} & H_{x32} & H_{x33} \end{bmatrix} \qquad (4-17)$$

$$H_1^i = \frac{\partial f(x)}{\partial x_{1i}} \geq 0, \quad i = 1, \cdots\cdots\cdots n, H\,x + \ C^T \geq 0 \qquad (4-18)$$

$$H_2^i = \frac{\partial f(x)}{\partial x_{2i}} \geq 0, \quad i = 1, \cdots\cdots\cdots n\,, H\,x + \ C^T \geq 0 \qquad (4-19)$$

$$\mathrm{H}_3^i = \frac{\partial \mathrm{f(x)}}{\partial \mathrm{x_{3i}}} \geq 0, \mathrm{i} = 1, \cdots\cdots\cdots \mathrm{n}, H\,x + \ C^T \geq 0 \qquad (4-20)$$

$$C_i^T = \frac{\partial\ C^T x}{\partial\ x_i} \geq 0, i = 1, \cdots\cdots\cdots n, x_i \geq 0 \qquad (4-21)$$

$$\alpha = c, \qquad c \in R \qquad (4-22)$$

The above example assumes no constraints, and is the easiest QP problem to solve. The problem reduces the setting of the gradient of the objective function equation to zero and solves the problem.

For QP the gradient G is

$$G = Hx + c \qquad (4-23)$$

Setting the gradient equation

$Hx + c = 0$ to zero, then is become $Hx = -c$

where A is H, and b is – c

For the system to be solved, which becomes $[A]\ [x] = \ [b]$ $(4-24)$

Then the problem comes down to solving the N equations in N unknowns. A simple example of this method is given below:

The objective function is

$$f(x) = \left(\frac{5}{2}\right)x_1^2 - 2x_1x_2 - x_1x_3 + 2x_2^2 + 3x_2x_3 + \left(\frac{5}{2}\right)x_3^2 + 2x_1 - 35x_2 - 47x_3 + 5 \qquad (4-25)$$

in this case

$$H = \begin{bmatrix} 5 & -2 & -1 \\ -2 & 4 & 3 \\ -1 & 3 & 5 \end{bmatrix} \qquad (4-26)$$

All of the eigenvalues of the H matrix must be great than 0. Therefore, the H matrix is positive definite

$$C^T = [2 \quad -35 \quad -47],\ \alpha = 5 \qquad (4-27)$$

$$A = \begin{bmatrix} 5 & -2 & -1 \\ -2 & 4 & 3 \\ -1 & 3 & 5 \end{bmatrix},\quad b = \begin{bmatrix} 2 \\ -35 \\ -47 \end{bmatrix},\quad x = \begin{bmatrix} x_1 \\ x_2 \\ x_3 \end{bmatrix} \qquad (4-28)$$

Then it becomes $$\begin{bmatrix} 5 & -2 & -1 \\ -2 & 4 & 3 \\ -1 & 3 & 5 \end{bmatrix}\begin{bmatrix} 2 \\ -35 \\ -47 \end{bmatrix} = \begin{bmatrix} x_1 \\ x_2 \\ x_3 \end{bmatrix} \qquad (4-29)$$

$$\begin{bmatrix} x_1 \\ x_2 \\ x_3 \end{bmatrix} = \begin{bmatrix} 3 \\ 5 \\ 7 \end{bmatrix} \qquad (4-30)$$

Compared with LP, the QP approach allows modelling and investigation between variables: for example, a power demand change may result from electricity price change and both will affect total profits. QP also has higher accuracy than LP, especially when the problem's properties match the QP, such as optimization based on power loss reduction.

4.3 The Artificial Intelligence

AI is the branch of computer science which creates intelligent machines that work and react like humans. AI was invented and designed for problem-solving, planning, and learning. It has been useful for solving power system problems, especially when the problems' characteristics match the features of AI tools. AI is also widely used in power systems in system operations, planning, and control: for example, it can be used for system energy management, relay settings determination, automatic generation control and fault detection. As one of optimisation methods, GA is very robust optimisation and suitable for large scale problems.

4.3.1 Genetic Algorithm

GA is a probabilistic search approach which is founded and based on the principle of genetics and evolution. The GA uses genetics as its model for problem solving. It is a search technique to find approximated solutions to optimization and search problems. The GA was created based on natural biological evolution: it is a stochastic algorithm so randomness is one of its features since both selection and reproduction need random procedures.

Robustness is also a very significant feature of GA, because it always considers a population of solutions rather than searching for a single solution. Therefore, the chance of reaching the global optimum is greatly increased. Moreover, there is no particular requirement in terms of the problem itself before GA is used: for example, GA can be used for continuous/discrete, constrained/unconstrained and sequential/parallel optimization problems. All these features have enabled GA to become very powerful optimization tool.

Genes are the basic instructions for building a GA. Thus the required design variables are encoded into binary string as a set of genes corresponding to chromosomes in biological systems. It is a bit string of arbitrary length, and can be represented as a binary number. *Gene* may also describe a possible solution to a problem. In figure 4.3, several genes are shown. The *Chromosome* consists of a set of genes and is the raw genetic information that the GA deals with: it contains the solutions' information. Figure 4.3 also illustrates the basic structure of the chromosome. The general principle of GA is survival of the fitness. The concepts of

natural selection and survival of the fittest are applied to searching space to determine the optimal string by exchanging randomized input information [89]. As a result, the fittest individuals are selected for reproduction. *Selection* compares each individual in the population, and is done by using the fitness function. Each chromosome has its associated value corresponding to its fitness. *Fitness* is the value of the objective function for its phenotype. It indicates how close the chromosome is to the optimum answer.

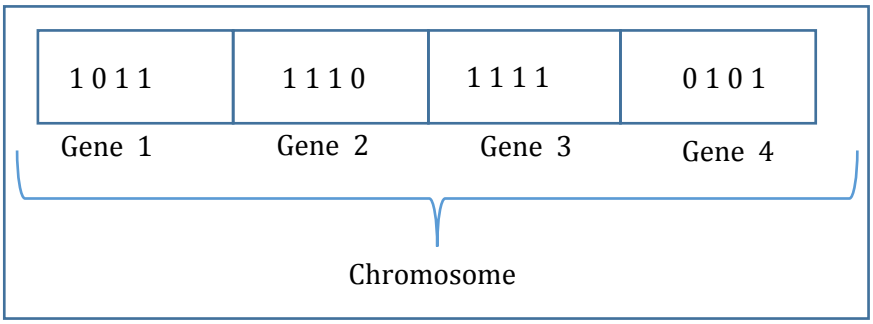

Figure 4.1 Genes and Chromosome Structure

The GA starts by creating an initial population of chromosomes randomly. The population size depends on the complexity of the problem, since it must show the diversity of genetic materials.

Then GA loops through an iteration process in order to make the population evolve. Each iteration consists of four steps:

- Selection: This is done randomly and through this process, the relative fitness individuals are chosen for reproduction.
- Reproduction: The offspring are fed: meanwhile new chromosomes are generated by recombination and mutation.
- Evaluation: The fitness of the new chromosomes is evaluated.
- Replacement: The new generated individuals from the population are used instead of the old ones.

The GA is stopped when the end conditions are satisfied. If there is no change to the population's best fitness for a specified number of generations, GA will stop when the maximum generation number has been reached. It will also stop when the required time has passed.

The GA can be divided into several steps as follows shown in figure 4.2:

Step 1. A set of potential random solutions is generated. Every potential solution can be defined as a string or chromosome of discrete symbols. Normally, a binary coding system is used to encode these symbols. The format of the encode is very important, if every string is encoded in a suitable bits number, then the calculation speed will improve dramatically.

Step 2. After creating the potential random solutions, all the solutions need to be scored by fitness function. In some environments, the fitness function is also called the objective function: for instance, in the optimization tool box of MATLAB. Fitness function is used to assess the fitness values of each string. It is a slightly similar to the objective function. According to B.A.Nicholson's thesis, the fitness function is the modification of the objective function, and it can formulated using principles such as explicit or implicit inclusion of constraint function."

Step 3. If all the acceptable solutions are found, and they all converge into one optimal solution, then the optimization process finishes.

Step 4. If the above is not achieved, the genetic operator needs to create a new population; usually this process is called reproduction. The purpose of reproduction is to increase parents' number of next generation. The reproduction process is based on a stochastic process: the higher fitness values potential solutions have, the more frequently they can be selected as the parents.

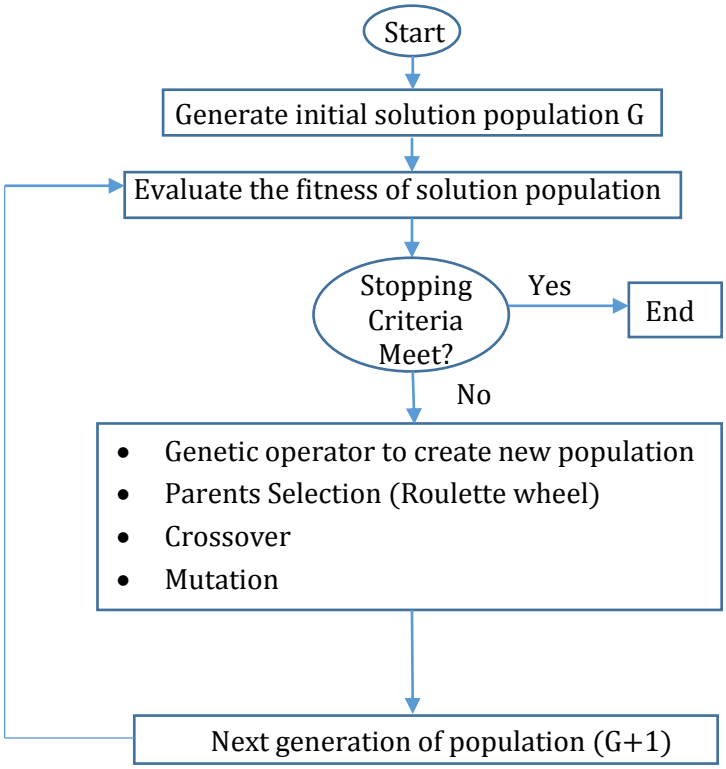

Figure 4.2 Flowchart of Genetic Algorithm

In terms of selection, a probabilistic technique, such as Roulette Wheel selection, is used. After selection, the most suitable and fit parents are selected. Once parents are selected, in order to create offspring, a crossover occurs by exchanging genetic information between selected chromosomes.

The final operation is mutation. The purpose of this operator is to maintain genetic diversity by narrowing down the possibility of potential loss of notions in a limited size population, which means this operator helps GA to search the different zones of searching space.

Step 5. The steps above are repeated until all the solutions converge and satisfy the stopping criteria.

Compared with other conventional optimal methods, GA is more suitable for solving any optimization problems because the fitness function of GA can be in any form, there is no

restriction on its properties, and it can be discrete, nonlinear, or linear. The other main advantages of GA are listed below [90][91]:

- GA uses evolution theory for optimization: as a result GA, can be applied to any kind of optimization problem, and it can also be used for problems which have a multi-objective function.

- GA uses a population of solutions rather than a single point to search for the optimum one. This makes GA more robust compared with conventional methods, and it also increases opportunities for reaching the global optimum.

- GA copes with the coding of the solution set rather than the solution itself. It may reduce the complexity of the problem and performs well for large-scale optimization problems.

- GA requires no knowledge in terms of further mathematical calculations, such as gradient or derivation calculations.

The GA also has several limitations such as [92]:

- The data process speed is very much depends on the computer processor, data process can be slow especially when the problems are very complex and have large number of input parameters.

- There is no stander rules to decide the size of population, mutation rate, cross over rate and the size of each gene.

- To a non-professional, the return encoded results may not be able to understand.

Considering both the advantages and disadvantages of GA, it is most suitable for use GA in power system optimal power flow, economic load dispatch, power station location choice, power loss reduction and load forecasting.

4.4 Power Loss Minimization Methods

There are many optimization methods for power loss Minimization. These methods include the mathematical optimization methods as well as other optimization methods.

Researchers used the MATLAB quadratic programming by considering the different levels of EV penetrations and different loads types for power loss reduction in DN [93]. Reference [94] concentrated on using Newton Raphson method for TN power loss reduction by the setting of flexible AC transmission system (FACTS) devices. Reference [94] considered using the penalty function combined with MTALAB optimization programming to optimise the power flow problem so as to reduce the power loss in DN. Reference [95][96] proposed the particle swarm optimization method for DG placement and sizing as well as considering the reactive power optimisation problem for power loss reduction in DN. In [97][98] the researchers developed GA for network reconfiguration and capacitor control for power loss reduction in the DN. Reference [99] developed A fuzzy adaptive particle swarm optimisation method for power loss minimization in DN.

In order to choose the suitable optimisation methods we have to fully understand the problem itself. The detailed analysis of the methods used in this thesis can be found in chapter 5.32 and 8.1.

4.5 Chapter Summary

In this chapter the different mathematical optimization and one of the artificial intelligence techniques have been introduced: LP, QP, and GA. The advantages and disadvantages of these techniques have been presented, and it has been shown that all of them are used in power system operation, control and planning. As the power system is moving towards a smart system, they strongly influence its operation’s decision making and are extremely necessary. With the penetration of renewable energy and uncontrollable new types of loads such as EV, security and economic issues of power system are being coordinated more tightly than before [90]. Therefore, such much faster and more robust optimization tools are needed to support power system control and operation.

Chapter 5 Active and Reactive Power Dispatch (ARPD) for Power Loss Reduction with Electric Vehicle Penetration

Chapter five presents two optimisation methods based on active and reactive power dispatch for power loss reduction. They are the uncoordinated optimal active-reactive power flow (UA-RPF) of the ESS and the coordinated optimal active-reactive power flow (CA-RPF) of the ESS. Results for the IEEE 33-bus distribution system are presented.

5.1 Overview

With modern technological development, and raising awareness of environmental protection, EVs will become alternatives, cheaper and less environmentally damaging, to traditional vehicles. Customers can charge their EVs either using electric outlets in their homes, or public stations with charging plugs. These EVs can only be driven over a limit range, some of the EVs may have larger batteries and better drive systems, but their range is still limited [100][25].

The charging process can affect the DN significantly, especially when large amounts of the EVs are connected to the DN at the same time. Because these vehicles use considerable amounts of energy, if this scenario happens at peak time, it worsens the insecurity level of the DN, and causes a great deal of active power loss. Meanwhile, this put huge pressures on the system operators in terms of keeping the system secure. It has been shown that, if EV penetration increases by 10% between 18:00-21:00 hours, energy losses raise by almost 3.7% [29].

From the system operator's view point the power losses are an economic concern and need to be reduced. One of the reduction methods is to add ESS into the DN. Usually ESSs in the DN are combined with any available renewable energy sources to accommodate variations in these sources, making the system more stable. Some areas do not have sufficient sources of renewable energy generation, for this situation, how to use ESS to improve the system performance such as reducing power loss is a concern of this chapter. Also from the EV owner's view point, they want to use cheaper electricity when they charge their EVs, this also has been considered.

Previously, active and reactive power dispatches were considered separately for loss reduction. Some researchers concentrate on intalling capacitors for reactive power optimisation [101]. Some researchers use an algorithm for optimal location selection to reduce active power losses [102], others to remove load imbalances in the radial network for loss reduction [103]. Alternatively, the methods proposed in this chapter consider the reduction of both active and reactive power losses. Also, two optimisation methods, both based on the ESSs were used and compared for losses reduction caused by the different levels of EV penetration. Renewable energy sources can be also implemented in the model for this research, including wind power generation and PV generation. In this optimisation problem, only active, and reactive power losses and the power imported from the TN are considered.

The proposed method emphasizes the improvements and the differences in terms of power loss reduction when using the two charging methods, which are UA-RPF of the ESS and the CA-RPF of the ESS. It also indicates how much active power can be reduced from the TN.

5.2 System Modelling

This section covers the EV modelling (the specification of EV, the charging place and period of EV), loads modelling, and ESS modelling.

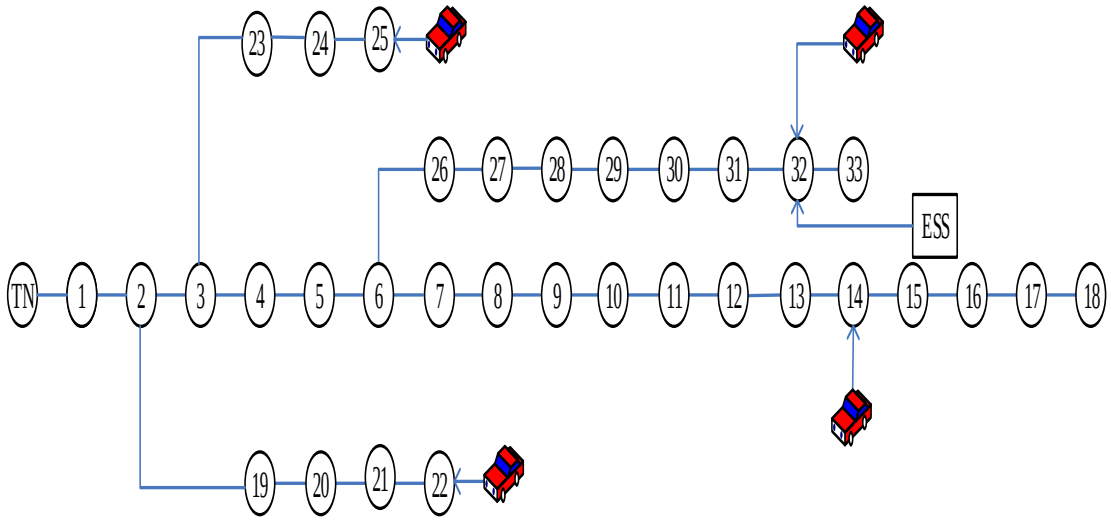

Figure 5.1 Tested IEEE 33-bus DN

5.2.1 EV Modelling

The EVs are added in to the IEEE 33-bus DN randomly, in this chapter they are added in bus 25, 32, 22, and bus 14. The topology of the tested IEEE 33-bus DN with EV penetration can be seen from figure 5.1.

A. Specifications of EV

Recent market data shows that, EV sales are led by the Chevrolet Volt plug-in hybrid with 48,218 units, followed by Nissan Leaf all electric cars with 35,588 units. The Toyota Prius Plug-in Hybrid occupies the third largest market with 20,724 units, with the fourth being the Tesla Model S with over 15,000 units [104][105][106]. Accordingly, it can be seen that the Chevrolet Volt plug-in hybrid occupies the 41% of the whole EV market, the Nissan Leaf all-electric car account for 30%, the Toyota Prius Plug-in Hybrid takes up 17%, while the Tesla Model S shares the rest of the market which is 12%. Therefore, an assumption is made, each load feeder, 41 people use Chevrolet Volt Plug-in Hybrid cars, 30 people use Nissan Leaf all-electric cars, 17 people buy Toyota Prius Plug-in Hybrid cars, and 12 people use the Tesla Model S. The characteristics of the different EVs are shown in table 5.1 [107].

Each EV has a battery and, the charging characteristic can be seen in table 5.1. For the Tesla Roadster 0.0168 MW power are needed to be fully charged, for the Nissan Leaf it is 0.06MW, for the Chevrolet Volt is 0.003MW, and for the Toyota Prius it is 0.003MW. The battery can only be charged during the charging time, which means energy flow is unidirectional, so the concept of EVs to grid is not considered here. Fast charging is taken into consideration, but requires a higher short-circuit power. Customers can purchase an electrical outlet to fit the high short-circuit power from the auto-supply shop. Extra costs are needed to install the high voltage connection equipment, but it can charge the EV faster than others. The scenario studied up to 40% EVs penetration in 10% increments, based on the 20% penetration. For example at 20% EVs penetration, it is assume that there are 20 EVs, Chevrolet Volt occupies the 41% which is 8 Chevrolet Volts, 6 Nissan Leafs, 3 Toyota Prius, and 2 Teslas.

Table 5.1 The characteristics of the EV

Load Type	Type	Power Demand (MW)	Battery Size
Tesla Roadster	Battery	0.0168MW	53 kWh
Nissan leaf	Battery	0.06MW	24 kWh
Chevrolet Volt	Plug-in	0.003MW	16 kWh
Toyota Prius	Plug-in	0.003MW	4.0 kWh

The maximum power demand (PD) for all 41 Tesla Roadsters is 0.688MW, for all 30 Nissan Leafs is 1.8MW, for all 17 Chevrolet Volts is 0.051MW, and for all 12 Toyota Prius is 0.036MW. The total power demand (TPD) is 2.575MW, and it is added into the node 22, node 25, node 32, and node 14 respectively which is chosen randomly. The load feeder data is shown in table 5.2.

Table 5.2 Load feeder data

Load feeder	PD(MW)	TPD(MW)	PD'(MW)
22	0.09	2.575	2.675
25	0.21	2.575	2.785
32	0.42	2.575	2.995
14	0.12	2.575	2.695

B. Charging Period and Place

Although the EV is becoming more popular, charging stations are not as common as petrol stations, therefore, EVs are assumed to be charged at home or at the work place. Figure 5.2 shows the percentage of vehicles arriving at home [108]. From that figure three periods are proposed. The first one is from the 8:30 t to 14:30 people arrive home and plug their EVs in to the charging station nearby or their garage. The second charging period takes place between 14:30 and to 19:30 and, this period coincides with the peak load during the day and also more EVs arriving home. These penetrations can lead to more power losses in the DN. The last charging period is from 19:30 to 23:30, with less people arriving home and charging their EVs during night. This assumes that, there is only one EV per house and that the charging places are usually either at home, at the office or in the centre of town.

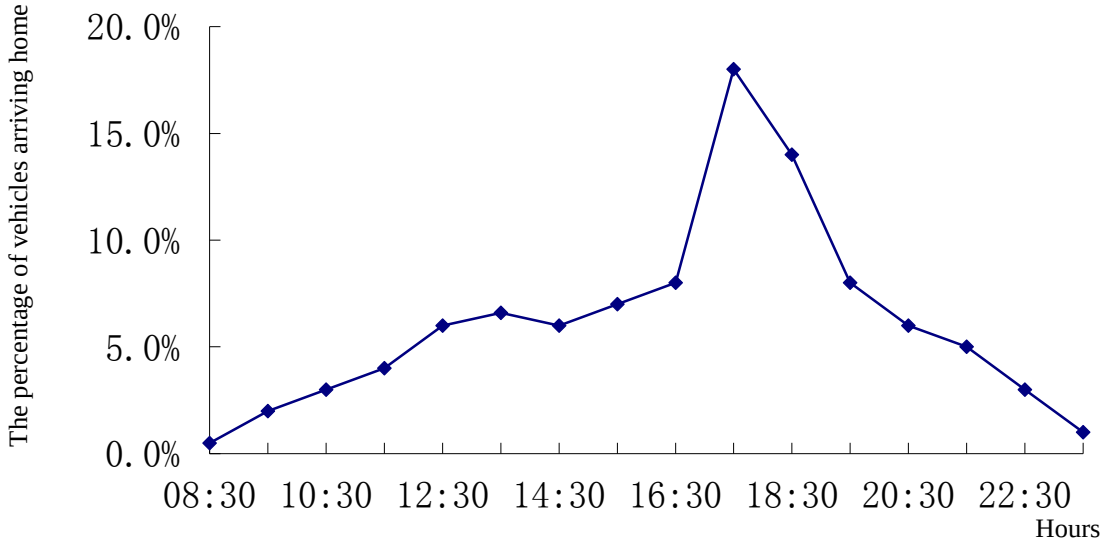

Figure 5.2 Percentage of vehicles arriving home

5.2.2 Loads Modelling

From the available household load measurements data [42], a daily electricity demand (excluding heating) in the UK residence has been drawn below.

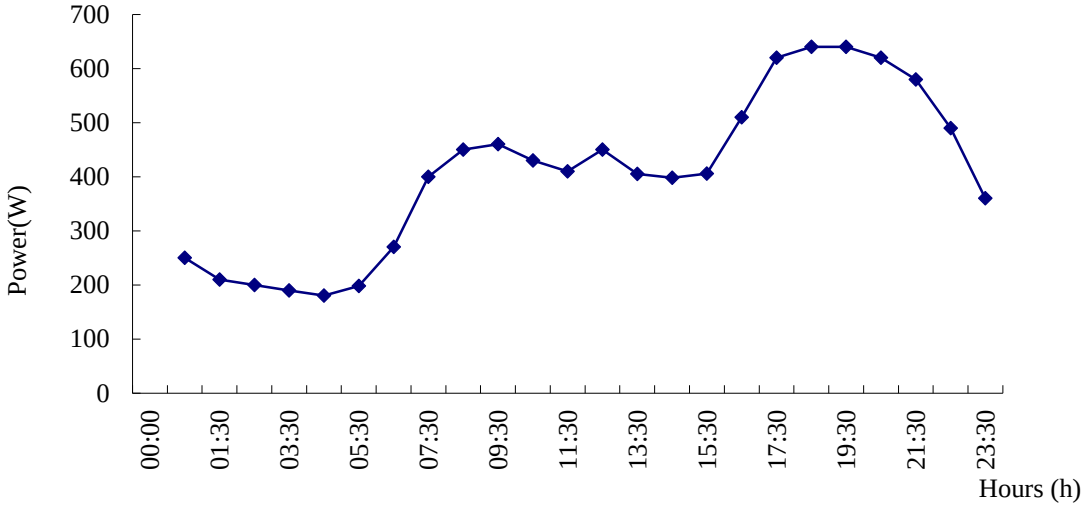

Figure 5.3 Daily electricity demand in a typical UK resident

The hourly household load was scaled to a suitable range for the IEEE 33-bus test DN by using MATPOWER, which can be used for power flow analysis. The detailed steps can be found in 5.3.2 Methodology part in the first step.

In order to test the smart charging and discharging method in next section, IEEE test distribution systems were compared and one of them was chosen as the test system for new method in this project for power loss reduction.

Generally speaking, IEEE power energy society collected several distribution test networks, such as 13-bus network, 33-bus network, 34- bus network, 37- bus network, and 123-bus network. These test networks are all used by others researchers. In this current project, 33-bus test network was chosen, the main reasons for that are shown below.

Firstly, compare with other feeders, 33-bus DN is very suitable for a middle size community. The topology can be seen from figure 5.1. Currently, not many customers want to purchase EVs, not only from battery technology aspect, also form the price-quality ratio. Therefore a middle size community can represent that number of EVs holders.

Secondly, the rated voltage is 12.66KV of selected network. That voltage level is close to the UK's 11KV distribution level, which makes simulation results more close to practical in this country.

Thirdly, 33-bus test DN's reactive load and reactive power supply are relative low compare with other feeders. It is convenient for comparison in terms of impacts of adding EVs into DN because the EV does not need reactive power to support driving. Therefore, IEEE 33-bus DN was chosen as the test system.

The 33-bus DN structure is shown below. The rated voltage is 12.66kV. Real power and reactive power of the load are 3.7MW and 2.3 Mvar respectively. Node 1 is regarded as the voltage source in the system, the total on-line capacity for the active and reactive is 100MW and 300-300MVar respectively, and other nodes can be seen as load feeders. The System total losses are 0.2MW.

5.2.3 ESS Modelling

The EES can provide the energy to the customers in a given time periods. It consists several Battery Storage Systems (BSS). These BSS consist PCSs, which can provide both active and reactive power to the DN [61]. When the PCS discharges to the network it can be seen as an inverter, whereas when it charges from the system can be regarded as the rectifier. A simple PCS consists of capacitors, diodes as well as transformers. The detailed model can be seen from section 3.2 in chapter three.

The active and reactive power discharge of the ESS should not exceed the maximum apparent power S_{PSCmax} of ESS [62] in equation 5-1. The active power in terms of charging and discharging must be positive values, in equation 5-2. Moreover the upper and lower bound of the storage units should be satisfied in equation 5-3.

$$P_{disc}^2 + Q_{disc}^2 \leq S_{PSCmax}^2 \quad (5\text{-}1)$$

$$P_{char} \geq 0,\ P_{disc} \geq 0 \quad (5\text{-}2)$$

$$E_{min} \leq E \leq E_{max} \quad (5\text{-}3)$$

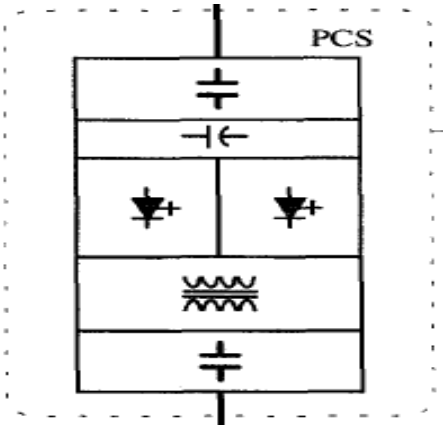

Figure 5.4 Power condition system

The apparent power of the ESS should be larger than the maximum power demand which is 2.995MW as can be seen in table 5.1. The installed capacity of the ESS also needs to exceeded the total install battery capacity of the total EVs which is calculate by $(41 \times 53\text{kWh}) + (30 \times 24\text{ kWh}) + (17 \times 16\text{ kWh}) + (12 \times 4.4\text{ kWh}) = 3217.8$ kWh. Therefore, the whole capacity is chosen to be 3.3MWh.

5.3 The method of reducing power losses in the tested DN

This section consists objective function and constraints of power loss reduction, optimisation method, methodologies, and results of these methodologies.

5.3.1 Objective Function and Constraints

The previous section illustrates power losses in the IEEE 33-bus DN. For reducing these losses, the ESS was embedded into the DN as shown in the figure 5.1 meanwhile, the objective function, which is Min $P_L = \sum_{\forall k,m}^{k,m \in S_B} I_i^2 R_i$ was built.

In order to analyse the power losses in the DN, a π model combined with ESS and DN of a particular distribution line between nodes k and m was modelled, with real and the reactive power flow through node k (the sending point) and m (the receiving end) as given bellows.

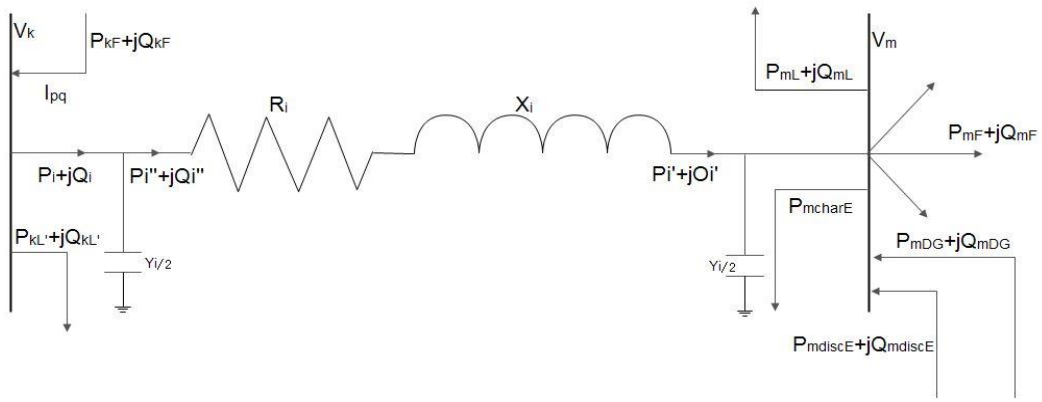

Figure 5.5 A simple model of a distribution line

From figure 5.5 it can be seen that

$$P_i' = P_{mL} + P_{mcharE} + P_{mF} - P_{mDG} - P_{mdiscE} \quad (5\text{-}4)$$

$$P_i = P_i'' = P_i' + R_i \frac{P_i'^2 + Q_i'^2}{V_m^2} \quad (5\text{-}5)$$

$$Q_i' = Q_{mL} + Q_{mF} - Q_{mDG} - Q_{mdiscE} - V_m^2 \frac{Yi}{2} \quad (5\text{-}6)$$

$$Q_i = Q_i'' - V_k^2 \frac{Yi}{2} = Q_i' + X_i \frac{P_i'^2 + Q_i'^2}{V_m^2} - V_k^2 \frac{Yi}{2} \quad (5\text{-}7)$$

Where P_i and Q_i are the sending active and reactive power through the branch i between node k and m, the series impedance and shunt admittance between nodes k and m are $(R_i + j\,X_i)$ and $\frac{Yi}{2}$ respectively, P_{mDG} and the Q_{mDG} are the active and reactive power injected by the distribution generation, P_{mL} and the Q_{mL} are the total active and reactive power load at bus m. P_{mF} and Q_{mF} are the sum of active (reactive) power flows through all the downstream branches connected to bus m. P_{mcharE}, P_{mdisE}, Q_{mdisE}, are the active and reactive power charging and discharging of the ESS respectively.

$$V_m = V_k - I_i Z_i = V_k - \frac{S_i''^*}{V_k^*}(R_i + j\,X_i) \tag{5-8}$$

$$V_m = V_k - \frac{P_i'' - jQ_i''}{V_k}(R_i + j\,X_i) = \left(V_k - \frac{P_i''R_i + Q_i''X_i}{V_k}\right) - j\left(\frac{P_i''X_i - Q_i''R_i}{V_k}\right) \tag{5-9}$$

$$V_m = \sqrt{V_k^2 - 2(P_i''R_i + Q_i''X_i) + (P_i''^2 + Q_i''^2)(R_i^2 + X_i^2)/V_k} \tag{5-10}$$

V_k and V_m are the voltage at bus k and m, I_i is the current through the branch, where S_i'' $=P_i''+Q_i''$, $P_i''=P_i$, $Q_i''= Q_i+V_k^2\frac{Yi}{2}$, so the value of the current flow through the branch connected between nodes k and m can be calculated by [109]. Mathematically, objective function of the power losses is given as:

$$I_i = \sqrt{\frac{P_i^2+Q_i^2}{V_k{}^2}} \tag{5-11}$$

$$Min\ P_L = \sum_{\forall k,m}^{k,m\in S_B} I_i^2\,R_i = \sum_{\forall k,m}^{k,m\in S_B}\left(\frac{P_i^2+Q_i^2}{V_k{}^2}\right)R_i \tag{5-12}$$

$$P_i = P_{mL} + P_{mcharE} + P_{mF} - P_{mDG} - P_{mdiscE} + R_i\frac{P_i'^2+Q_i'^2}{V_m^2} \tag{5-13}$$

$$P_i'^2 = \left(P_{mL} + P_{mcharE} + P_{mF} - P_{mDG} - P_{mdiscE}\right)^2 \tag{5-14}$$

$$Q_i'^2 = \left(Q_{mL} + Q_{mF} - Q_{mDG} - Q_{mdiscE} - V_m^2 \frac{Yi}{2}\right)^2 \quad (5\text{-}15)$$

$$P_i = P_{mL} + P_{mcharE} + P_{mF} - P_{mDG} - P_{mdiscE} + R_i \frac{\left(P_{mL}+P_{mcharE}+P_{mF}-P_{mDG}-P_{mdiscE}\right)^2+\left(Q_{mL}+Q_{mF}-Q_{mDG}-Q_{mdiscE}-V_m^2\frac{Yi}{2}\right)^2}{V_m^2} \quad (5\text{-}16)$$

$$Q_i = Q_{mL} + Q_{mF} - Q_{mDG} - Q_{mdiscE} - V_m^2 \frac{Yi}{2} + X_i \frac{P_i'^2+Q_i'^2}{V_m^2} - V_k^2 \frac{Yi}{2} \quad (5\text{-}17)$$

$$Q_i = Q_{mL} + Q_{mF} - Q_{mDG} - Q_{mdiscE} - V_m^2 \frac{Yi}{2} + X_i \frac{(P_{mL}+P_{mcharE}+P_{mF}-P_{mDG}-P_{mdiscE})^2+\left(Q_{mL}+Q_{mF}-Q_{mDG}-Q_{mdiscE}-V_m^2\frac{Yi}{2}\right)^2}{V_m^2} - V_k^2 \frac{Yi}{2} \quad (5\text{-}18)$$

It can be seen from the equation above, the object function is very complex, in order to simplify the objective function P_L in terms of analysing the relationship between the control variables which are the active power of DG (P_{mDG}), the active power of the ESS discharge (P_{mdiscE}). A method is used, by setting the rest values of the equation P_i and Q_i to be the constant value c, except the P_{mDG} and P_{mdiscE}.So the equation P_i and Q_i become

$$P_i = \{(c - P_{mDG} - P_{mdiscE}) + c\,[(c - P_{mDG} - P_{mdiscE})^2 + c]\} \quad (5\text{-}19)$$

$$Q_i = \{c + c\,[(c - P_{mDG} - P_{mdiscE})^2 + c]\} \quad (5\text{-}20)$$

$$P_i^2 = \{(c - P_{mDG} - P_{mdiscE}) + c\,[(c - P_{mDG} - P_{mdiscE})^2 + c]\}^2 \quad (5\text{-}21)$$

$$Q_i^2 = \{c + c\,[(c - P_{mDG} - P_{mdiscE})^2 + c\}^2 \quad (5\text{-}22)$$

then the objective function becomes $P_L = \sum_{\forall k,m}^{k,m\in S_B} I_i^2 \, R_i \; = \frac{P_i^2+Q_i^2}{V_k^2} R_i$ (5-23)

$$P_L = \frac{\{(c-P_{mDG} - P_{mdiscE})+c\,[(c-P_{mDG} - P_{mdiscE})^2+c]\}^2+\{c+c\,[(c-P_{mDG} - P_{mdiscE})^2+c]\}^2}{V_k^2} R_i \quad (5\text{-}24)$$

P_L is subject to the equality and inequality constraints as bellows:

The active and reactive power flow in branch must satisfy the equations below:

$$\mathrm{P_i} - \mathrm{P_i'} - \mathrm{R_i}\frac{\mathrm{P_i'^2+Q_i'^2}}{\mathrm{V_m^2}} = 0 \quad (5\text{-}25)$$

$$\mathrm{Q_i} - \mathrm{Q_i'} - \mathrm{X_i}\frac{\mathrm{P_i'^2+Q_i'^2}}{\mathrm{V_m^2}} + \mathrm{V_k^2}\frac{\mathrm{Yi}}{2} = 0 \quad (5\text{-}26)$$

The voltage magnitudes at the sending point and receiving point must be satisfy the equation below for all branches in the DNs

$$V_m^2 - \left\{V_k^2 - 2(P_i'' R_i + Q_i'' X_i) + \frac{(P_i''^2+Q_i''^2)(R_i^2+X_i^2)}{V_k}\right\} = 0 \quad (5\text{-}27)$$

The power factor of the DG connected to the bus m must be satisfy the following equations

$$\frac{P_m^{DG}}{\sqrt{(P_m^{DG})^2+(Q_m^{DG})^2}} = \cos\alpha_m \quad (5\text{-}28)$$

The hourly energy balance in each ESS can be written as

$$E_{h+1} - E_h - \eta_{char} P_{mcharE} + \frac{P_{mdiscE}}{\eta_{disc}} = 0 \quad (5\text{-}29)$$

Where $\mathrm{E_h}$ is the energy level in ESS during the hour h, efficiency η_{char} and η_{disc} are the charge and discharge efficiency [64].The active power charging should be zero during the on-peak time, the discharging should also be zero during the off-peak time.

$$P_{mcharE\,(h1)} = 0,\ h_1 \in \text{on} - \text{peak time} \quad (5\text{-}30)$$

$$P_{mdiscE\,(h2)} = 0,\qquad h_2 \in \text{off} - \text{peak time} \quad (5\text{-}31)$$

The line current flow for each branch should be within the thermal limit. The bus voltage at each bus should not exceed maximum and minimum voltage

$$I_i \leq I_i^{rated},\ \ \forall m \in S_B \quad (5\text{-}32)$$

$$V_m^{min} \leq V_m \leq V_m^{max}, \quad (5\text{-}33)$$

$$V_k^{min} \leq V_k \leq V_k^{max} \quad (5\text{-}34)$$

The distribution generation's capacity must not exceed the total load of the network

$$\sum_m^{S_B} \sqrt{(P_m^{DG})^2 + (Q_m^{DG})^2} \leq \sum_m^{S_B} \sqrt{(P_m^L)^2 + (Q_m^L)^2} \quad (5\text{-}35)$$

The active and reactive power discharge of the ESS should not exceed the maximum apparent power $S_{BESSMAX}$ of ESS

$$P_{mdiscE}^2 + Q_{mdiscE}^2 \leq S_{BESSMAX}^2 \quad (5\text{-}36)$$

The active power in terms of charging and discharging must be the positive values. Moreover the upper and the lower bound of the storage units should be satisfied

$$P_{mcharE} \geq 0,\ P_{mdiscE} \geq 0 \quad (5\text{-}37)$$

$$E_{min} \leq E \leq E_{max} \quad (5\text{-}38)$$

5.3.2 Methodology

The minimization of power losses, which is treated as nonlinear minimization problem, can be tackled as a time series sequential optimisation. This has been achieved in the research

here using the MATLAB optimisation programming. This optimisation was carried out using three periods for a typical day, two off-peak periods (8:30-14:30 hours and 19:30-23:30 hours), and one peak period (14:30-19:30 hours) this can be seen from figure 5.6 below. The overnight part of the day was not considered, because few EVs arrive homes or arrive at working places, and there is little load demand during this period. Two different control methods were proposed, optimised and compared. These were Uncoordinated Active-Reactive Power Flow of ESS (UA-RPF ESS) and Coordinated Active-Reactive Power Flow of ESS (CA-RPF ESS) for power loss reduction. For the UA-RPF the active, reactive power discharge and active power charge of the ESS are optimised in order to reduce overall demand from the TN and reduce power losses ignoring the peak and off-peak costs. For the CA-RPF, the minimization not only relates to optimisation of the above three variables, but also considers different costs for peak and off-peak energy. So CA-RPF ESS can charge during the two off-peak periods and discharge during the peak period, whereas the UA-RPF ESS does not distinguish between these periods.

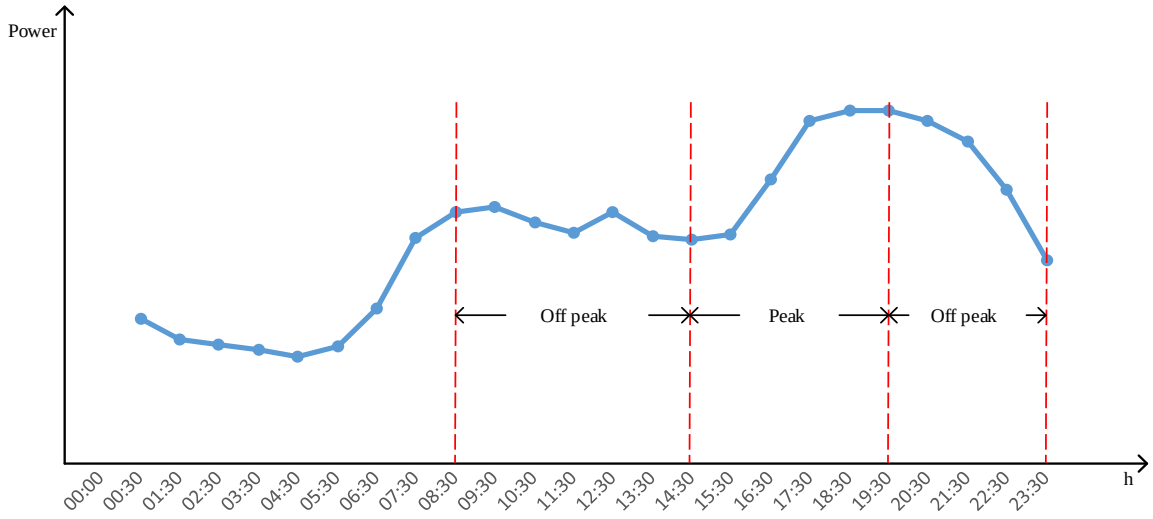

Figure 5.6 Three chosen periods of the typical daily load

The implementation of the methodology was divided into six steps.

Step 1: Scale the typical daily load of the 33-bus test DN.

Step 2: Place EVs into the 33-bus test DN.

Step 3: Add ESS near to the largest power loss feeder.

Step 4: Build an objective function based on the distribution line model in terms of power flow analysis for power loss reduction and active power demand reduction.

Step 5: Use the optimisation programming available from the MATLAB optimisation function to optimise P_{mcharE} (h), P_{mdiscE} (h), as well as Q_{mdiscE} (h).

Step 6: Present and analyse the results obtained from the optimisation process.

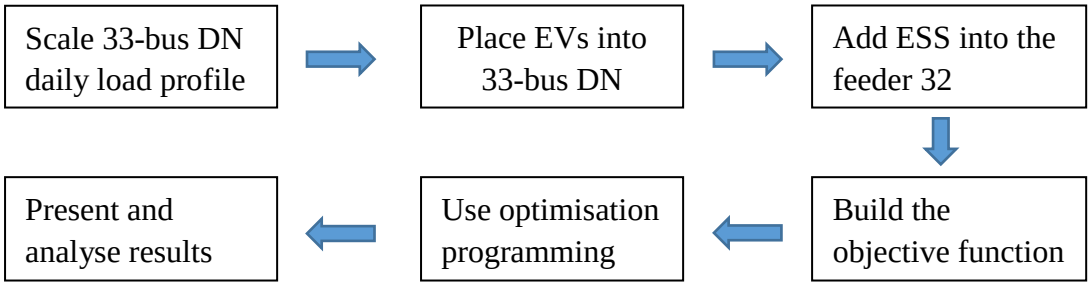

Figure 5.7 Procedure of methodology

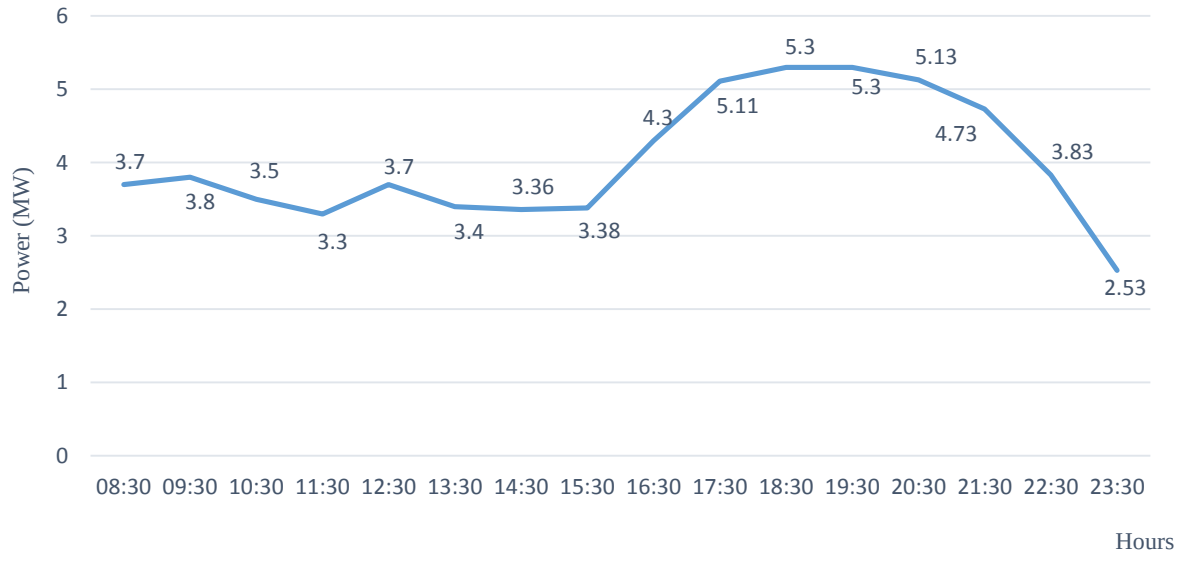

Figure 5.8 Typical daily 33-bus test DN'load

These six steps are shown in figure 5.7. Each step will now be explained in more detailed. For the first step, the typical daily load was scaled to a suitable range for the 33-bus test DN. For example, given that for the IEEE 33-bus DN 3.7 MW is the total base load at time point 8:30 hours, each hourly load between 8:30-14:30 hours was scaled according to the ratio of the load at 8:30 hours and this 3.7 MW base load. The same method was used to build the whole daily load profile. The process can be seen from the figure 5.8 below.

For the second step, EVs were added at feeders 25, 22, 32 and 14 respectively. As shown in the original 33-bus test DN load data sheet, in Appendix A, these four feeders have relative high power demands, so it is assumed there are high populations and higher EVs penetrations.

For the third step, with ESS and using the MATPOWER power flow analysis, the feeder that had the largest power loss was found (by comparing the different time points' load loss of the different feeders during each of the three chosen periods). For this system this was feeder 33. So the ESS was added at feeder 32 next to that feeder.

For the fourth step, the objective function was built, as previously described in equation 5-12. The control variables, (P_{mcharE} (h), and P_{mdiscE}(h) ,which are the active power charge and discharge, and Q_{mdiscE}(h) the reactive power discharge of the ESS were optimised to achieve an optimal operation for total power loss and power demand reduction (i.e. the active power provided from the TN).

For the fifth step, power loss was calculated. Figure 5.9 shows the iterative loop that allows the optimiser to find a solution.

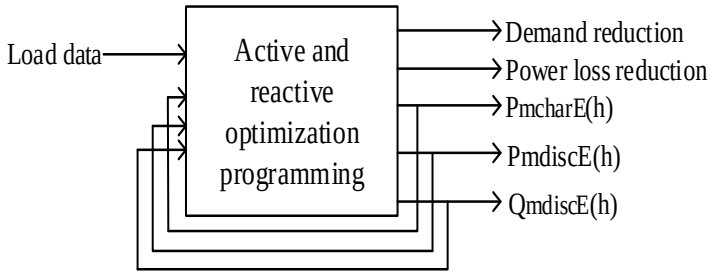

Figure 5.9 Input and output chart

First of all, power loss was calculated as the instant value at each time slot. For example, by adding the EVs into the DN during period 14:30-19:30 hours, at 14:30 hour the power loss was 0.23MW, expressed as $P_L(14:30) = 0.23$ MW. The method used in this research was to use the average power loss value instead of every individual power loss for each of the three different periods. For example, the average power loss over the period 14:30-19:30, can be

seen from figure 5.10 below. Whereas, the energy loss for the period 14:30 -19:30 hours can be measured by using that average value multiplied by 5 hours.

The instantaneous power loss for each time slot was optimised using the optimisation program. Using the variables at the end of optimisation, in equation 5-12, gives the power loss for node 32 only at that stage. Finally, the MATPOWER power flow for the whole system to determine the total system power loss was carried out by adding the optimal variables for node 32.

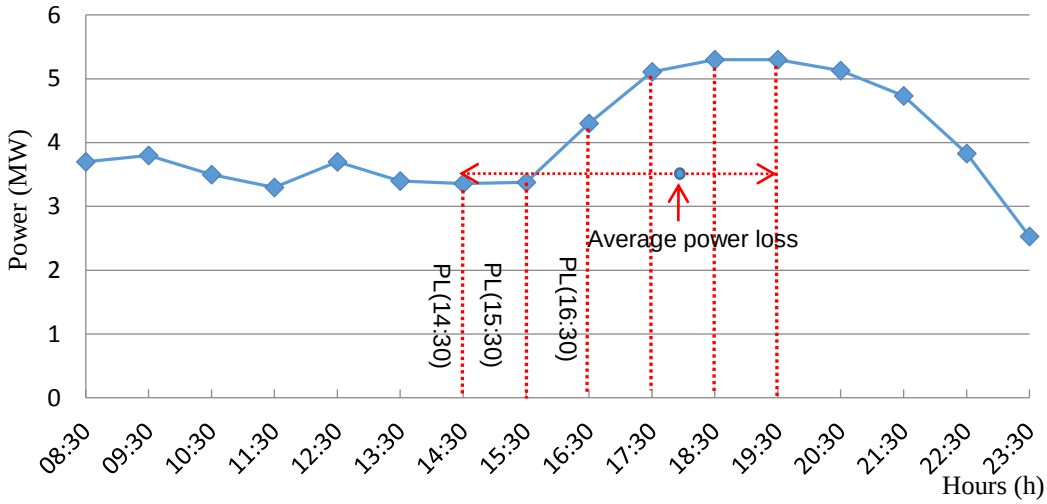

Figure 5.10 The average power loss

5.3.3 The Optimiser

The problem in this chapter is to minimise the system power loss, it is the optimization problem. Meanwhile, the mathematic model of the problem itself is highly non-liner. In order to solve this problem the proper optimiser needs to be chosen.

The non-liner optimisation problems can be solved by many solvers, such as R Languages non-linear solver, or AMPL Nonlinear solvers. In this chapter the mathematical model of problem

is presented in equation 5-12 in Section 5.3.1. It is solved by an open source MATLAB solver called Quadratic Function with Quadratic Constraints (QFQC). Because the nature of the problem is to minimise the $P_L = \sum_{\forall s_1,s_2}^{s_1,s_2 \in S_B} I_i^2 R_i = \sum_{\forall s_1,s_2}^{s_1,s_2 \in S_B} \left(\frac{P_i^2+Q_i^2}{{V_{s_1}}^2}\right) R_i$, the optimized variables are quadratic, which are $P_{mcharE}(h)$, $P_{mdiscE}(h)$, $Q_{mdiscE}(h)$. Therefore, the quadratic function is a good choice as the optimiser. A generic quadratic problem as follows:

$$min\ \frac{1}{2}x^T Hx + c^T x \tag{5-39}$$

Subject to

$$\frac{1}{2}x^T H_i x + K_i^T x + d_i \leq 0 \tag{5-40}$$

The Function below is used to call the quadratic solver in MATLAB, and it is defined as:

[x,fval] = quadprog (H , f, A, b, ub, lb, x0, nonlconstr, opts)

Input Parameters

H:Symmetric matrix of doubles. Represents the quadratic in the expression $\frac{1}{2}x^T Hx + c^T x$

f: Vector of doubles. Represents the linear term in the expression $\frac{1}{2}x^T Hx + c^T x$

A: Matrix in linear inequality constraints $Aeq * x \leq bineq$

b: Vector in linear equality constraints $Aeq * x \leq beq$

ub:Vector of upper bounds

lb: Vector of lower bounds

x0: Initail point for x

nonlconstr: Matrix in non-linear constraints

Output values:

x: Optimal values of the decision variables

fval: Value of $\frac{1}{2}x^T Hx + c^T x$ at the solution x

Once the input parameters are fed into the QFQC, the optimisation results of the objective function can be obtained.

5.3.4 The Method of the Load Flow Analysis

A load flow analysis in terms of total power losses(TPLs), total generation, and PD was performed by the MATPOWER using the IEEE 33-bus tested DN, combined with different EVs penetration levels, different load profiles, and different charging periods. Two scenarios are chosen to be analysed, depending on the different penetration levels.

Table 5.3 Percent between total power losses and total power generated in terms of uncoordinated charging

Penetration / Charging period	0%	20%	30%	40%
8:30-14:30	3.16%	4.39%	5.07%	5.92%
14:30-19:30	3.25%	4.41%	5.23%	6.03%
19:30-23:30	3.24%	4.15%	4.92%	5.69%

The first case for each scenario is taken as the base value, which is without adding any EVs into the distribution grid, but with different load profiles in three different charging periods. The next cases are with the EVs penetration 20%, 30%, 40%, respectively in three charging period. The percent between total power losses and total power generated in terms of uncoordinated charging can be seen from table 5.3.

5.3.5 Results

The numbers of EVs used were 100, as this is a reasonable number of EVs for a medium size community. The results show the percentage of TPLs to the total power received from TN.

In all cases with the EV penetrations increase, the percentage of the TPL increases. The highest power losses take place between 14:30 and 19:30. Two reasons for it, one is the load during that period is higher than the other periods, the other is more EVs arrive at home during that period. Knowledge of these power losses are vital to the system operators, in order to them to compensate for the system losses and choosing the appropriate methods to do this.

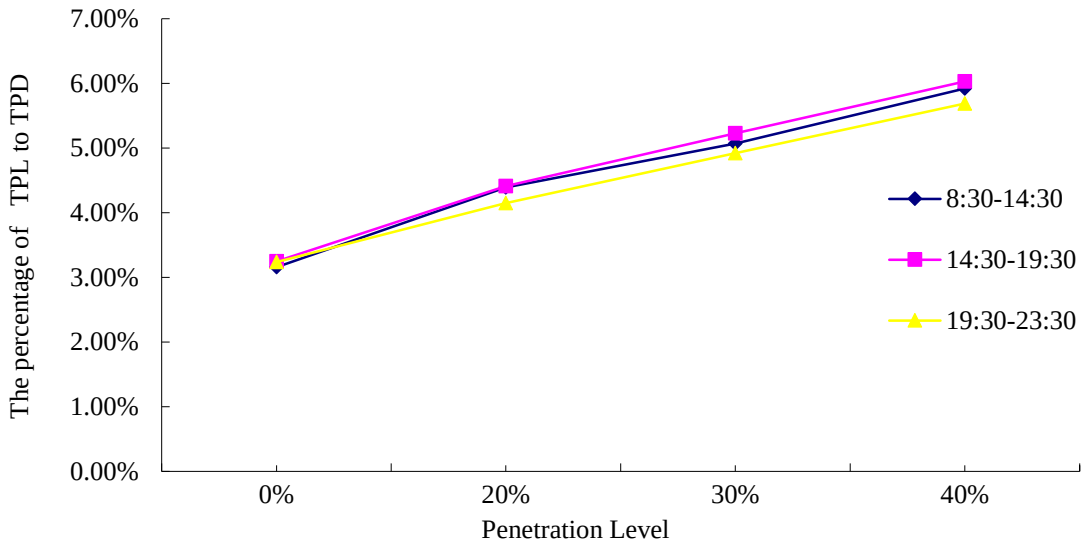

Figure 5.11 Total power loss against EV penetration level for different time of day

5.4 Results and analysis

From the above sections, power losses in terms of two different optimisation methods were obtained by using the MATLAB optimisation programming. In general, the losses are reduced when the ESS adds into the IEEE 33-bus tested DN.

The table of load demands was built and can be seen from table 5.4, based on the daily household load and the demand of the EV at different penetration levels. From the table 5.4, 3.7MW is the load of the IEEE 33-bus tested DN. This load is regarded as the base load for the period 8:30 – 14:30. Then according to the ratio between 8:30 – 14:30 and 14:30 19:30 in terms of daily household load which is 1.053, the load for 14:30-19:30 is calculated 3.7 × 1.05 = 3.9MW. The Same method is used to calculate the load between 19:30 and -23:30.

4.13 MW is calculated by 3.7 + 0.43MW＝4.13MW where 0.43MW is the total power demand of 20% EVs penetration for 4 different types of EV.

Table 5.4 Load demand for the IEEE 33-bus tested DN

Charging Period	EVs Penetration	0%	20%	30%	40%
8:30-14:30	LD (MW)	3.7	4.13	4.33	4.57
14:30-19:30	LD (MW)	3.9	4.33	4.56	4.77
19:30-23:30	LD (MW)	3.3	3.73	3.96	4.17

Table 5.5 The average active power losses with ESS and without ESS

Charging period	Penetration level	0%	20%	30%	40%
8:30-14:30	Without ESS(MW) With ESS	0.12 0.53	0.25 0.09	0.34 0.13	0.45 0.18
14:30-19:30	Without ESS(MW) With ESS	0.05 0.13	0.26 0.10	0.36 0.25	0.47 0.32
19:30-23:30	Without ESS(MW) With ESS	0.11 0.50	0.22 0.08	0.31 0.22	0.41 0.27

The table 5.5 shows the differences of total active power losses (APL) in the tested DN with and without A-RPF ESS for UA-RPF case, during the different periods with different EV penetrations. From that table, the APL reduced dramatically when adding ESS to the DN.

The total active power (TAP) reductions are 0.64MW, which is calculated by the sum of the difference of APL between the pattern with ESS and without ESS in terms of three different EVs penetration levels, for the period between 8:30-14:30. During the period 14:30-19:30 it is 0.42MW, whereas, for the period 19:30-23:30 it is 0.37MW. Therefore, the TAP can be reduced 1.43MW between 8:30 and 23:30.

The charging period between 14:30and -19:30 is chosen to see the differences between the two methods which are UA-RPF and CA-RPF. For the CA-RPF ESS, during the off peak periods of 8:30-14:30 and 19:30-23:30, the ESS has to be charged, but for the peak period

between 14:30and-19:30, the ESS has to discharge to the DN, without charging. However, for the UA-RPF these factors are not taken into account.

Table 5.6 The APL, RPL, TAP without ESS between 14:30-19:30

Power / Penetration	APL	RPL	TAP
0%	0.05	0.09	4.03
20%	0.26	0.19	5.88
30%	0.36	0.27	6.89
40%	0.47	0.35	7.84

Table 5.7 below indicates these two different methods in terms of APL, reactive power losses (RPL), and the TAP from the TN during the period between 14:30 and 19:30. The gaps can be seen by comparing the UA-RPF ESS and CA-RPF ESS. As shown in table 5.7, the active and reactive power losses are decreased by using the UA-RPF and CA-RPF compare with the results from table 5.6 (without using any active and reactive methods). Meanwhile, under the different EVs penetrations, large amount of active power from the TN can also be reduced by using the proposed method.

Table 5.7 APL, RPL, TAP between 14:30-19:30

Pattern / EVs penetration	With ESS UA-PRF(MW)			With ESS CA-PRF(MW)		
	APL	RPL	TAP	APL	RPL	TAP
0%	0.05	0.04	2.42	0.11	0.11	1.01
20%	0.10	0.08	3.85	0.10	0.08	3.84
30%	0.25	0.19	5.91	0.25	0.19	5.90
40%	0.32	0.24	6.64	0.32	0.24	6.61

Figure 5.12 is drawn, in order to make the APL clearer as to the three different charging patterns, it is noticed the APL is much lower by using the proposed methods than not using it.

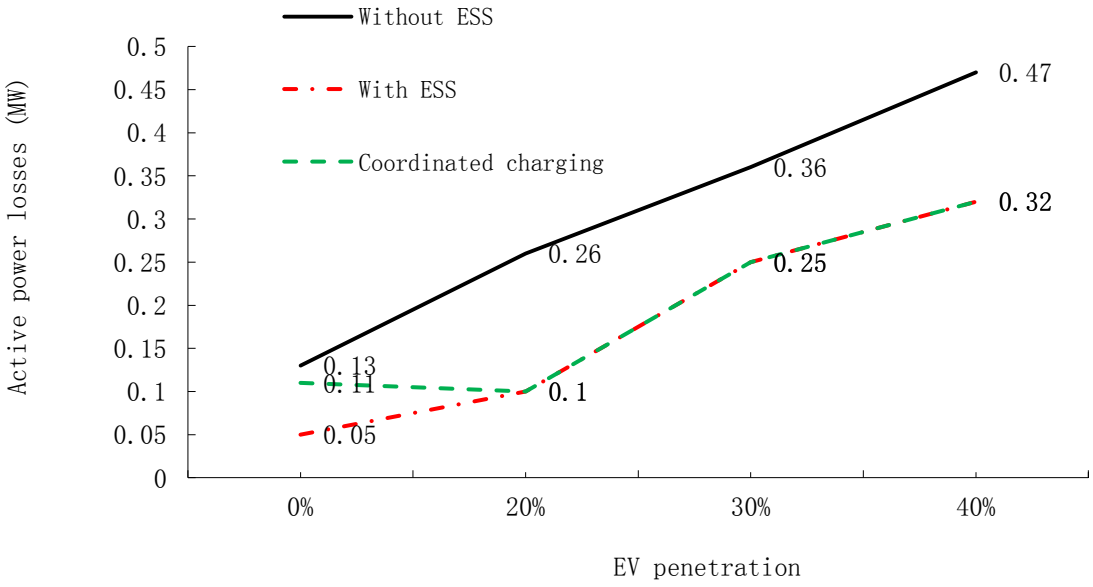

Figure 5.12 The comparison between the 3 different charging methods

It is very interesting to see that, the APL is a little bigger at the beginning of the coordinated charging compare with the uncoordinated one, the reason for this is in this scenario the loads of the DN are not increase, ESS has to use active and reactive power which are already stored in the ESS during the off peak time, so it generates more active and reactive power than the situation in terms of UA-RPF ESS. However, with the loads raise, the active power losses are almost the same as the UA-RPF ESS.

Although, by using the CA-RPS ESS charging method power losses are slightly higher than the UA-RPF ESS charging method, the charging price of ESS is much lower than the UA-RPF ESS, in terms of using the peak and off peak electricity price. During the same period, the active power can be decreased from the TN by installing the ESS in the DN. In the UA-RPF ESS pattern, 1.61MW power can be reduced which is calculated by 4.03-2.42=1.61MW. In the CA-RPF ESS pattern, 3.0 MW power calculated by 4.03-1.01 can be reduced for 0% EV penetration. For the 20% EV, the power reductions are 2.03MW and 2.04MW respectively. For the 30% they are 0.98Mw, 0.99MW, for 40% the power from TN that can be reduced are 1.2MW, 1.23MW.

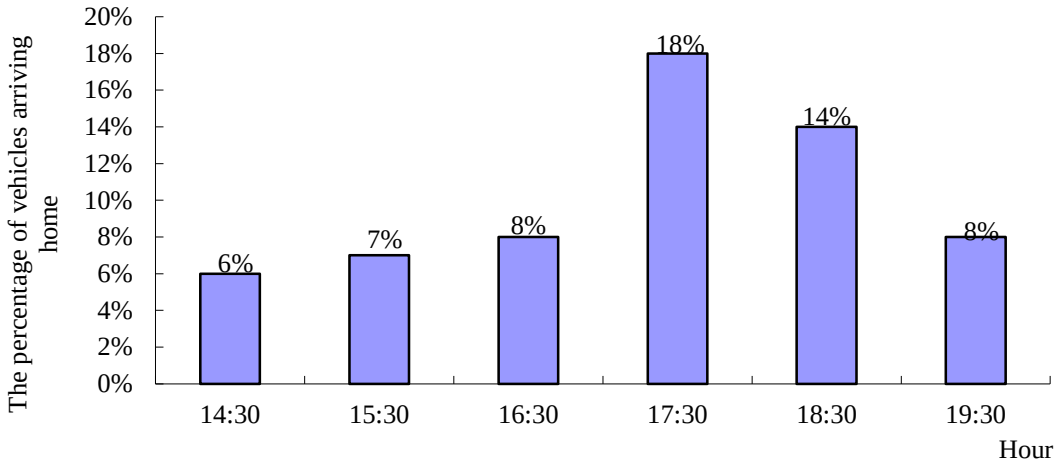

Figure 5.13 Percentage of vehicles arriving home

Figure 5.14 is made for comparing the TPL of the CA-RPF ESS and the TPL without ESS during the period between 14:30 and 19:30 at the 30% EV penetration. According to the figure 5.13 at 14:30, 6% EVs are not under way, the total power demand for the EVs at this time is 6% ×0.66=0.0039 MW, and 0.66 MW is the TPD for 30% EV of the 100 EVs. At 15:30 the TPD is 7% ×0.66=0.00462 MW, 16:30 is 8% ×0.66=0.0039 MW, 17:30 is 18% ×0.66=0.1188 MW, 18:30 is 14% ×0.66=0.0924 ,19:30 is 8% ×0.66=0.0528 MW. These loads are connected to the feeder 14, 22, 25, and 32 respectively, for each time.

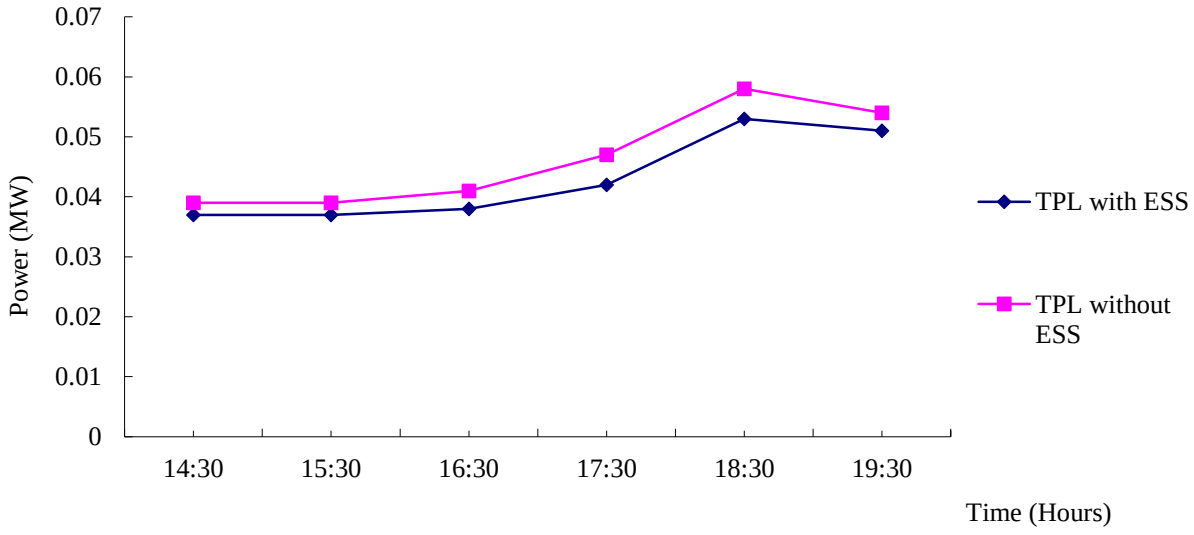

Figure 5.14 The total power losses of the tested network in terms of different charging patterns

Adding these demands into the tested DN is shown in the table 5.8. At 14:30 for the feeder 14 the power demand including EVs and daily loads is 0.016 + 0.0039 = 0.0556MW, 0.016 MW is the house hold loads at feeder 14.

Table 5.8 Total power demand of each feeder

Feeder / Time	14 (MW)	22 (MW)	25(MW)	32(MM)
14:30	0.0556	0.0516	0.0946	0.066
15:30	0.0622	0.0582	0.1062	0.0762
16:30	0.0701	0.0702	0.123	0.095
17:30	0.1428	0.1370	0.2042	0.1615
18:30	0.1174	0.1114	0.1814	0.1364
19:30	0.0778	0.0713	0.1418	0.0968

From figure 5.14 the TPL increases from 14:30 to 18:30 and then decreases from 18:30 to 19:30. One of the main reasons of this is that demands for the electricity rises and then declines. It is worth noticing that the maximum TPL which is 0.058 MW with the ESS is much less than the TPL 0.053MW without the ESS.

Table 5.9 Total power losses of different charging pattern

Time / Pattern	14:30	15:30	16:30	17:30	18:30	19:30
TPL with ESS	0.037	0.037	0.038	0.042	0.053	0.051
TPL no ESS	0.039	0.039	0.041	0.047	0.058	0.054

The active power and reactive power discharge of the ESS is shown in figure 5.15 below. During the period between 14:30- 17:30 the active and reactive power increases all the time, at 17:30 it reaches the highest point and then decreases for the rest of the time. The gap between the active and reactive power discharge is very high, because the EV doesn't need the reactive power and, the householders do not need lots of reactive power, moreover it also does not change a great deal during time as it goes by.

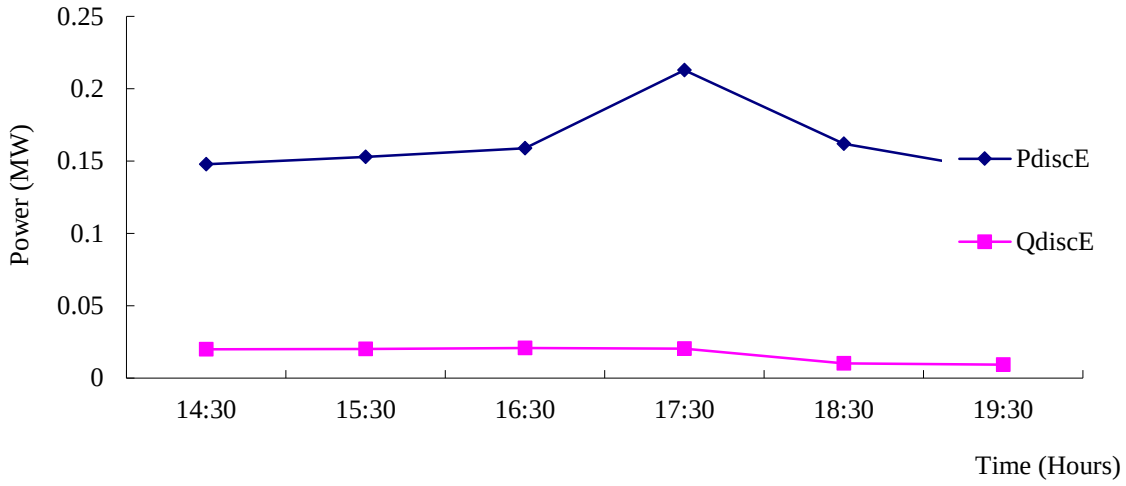

Figure 5.15 PdiscE and QdiscE during the time between 14:30-19:30

Table 5.10 PdiscE and QdiscE during the time between 14:30 -19:30

Time / Pattern	14:30	15:30	16:30	17:30	18:30	19:30
P discE (MW)	0.0147	0.1529	0.1599	0.2130	0.1629	0.1431
Q discE (MVAr)	0.0198	0.0201	0.0202	0.0204	0.1020	0.093

Figure 5.16 shows that the TAP receives from the TN with the ESS without ESS, and the TAP provides the DN with ESS. It can be seen that from the period 14:30 to 18:30 (for the DN with ESS) with power demand increases the TAP from the TN rises from 0.59MW at 14:30 to 1.75MW, then declined to a low of 1.63MW at 19:30. It is noticeable that the ESS reduces a great deal of active power from the network compared to the one without ESS, at 18:30, 0.13MW active power reduced, at 17:30 0.19MW active power does not need to import from the TN, moreover the total 0.75MW active power can be reduced by using the ESS.

Table 5.11 TAP from the TN with and without ESS

Time / Pattern	14:30	15:30	16:30	17:30	18:30	19:30
TAP from TN with ESS (MW)	0.59	0.62	0.74	1.08	1.75	1.63
TAP from TN No ESS(MW)	0.69	0.73	0.87	1.27	1.88	1.72

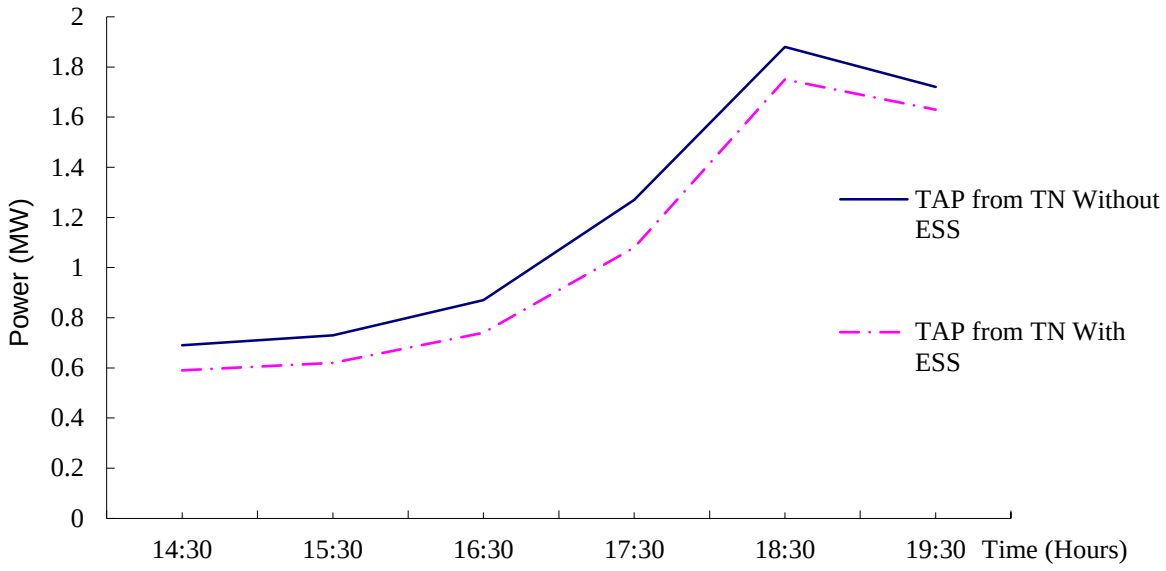

Figure 5.16 TAP from the TN with and without ESS

5.5 Chapter Summary

Previously, many studies used optimisation methods based on either active or reactive power dispatch in terms of capacitor placement, network reconfiguration, as well as charger design for power loses reduction caused by EVs within in the DN. The power losses were compared with, and without, optimisation methods. But unlike these methods, in this chapter we proposed, and compare, two different methods both based on the active, and reactive power optimisation dispatch of the ESS for power loss reduction. In addition, the power imported from the TN has also been reduced.

In the section 5.2 of this chapter, by using historical data for daily load, charging demand for EVs was analysed and modelled. Meanwhile, EVs were added into the IEEE 33-bus test DN, the percent between total power losses and total power generated raises from 3.16% at 0% EV penetration to 5.69% at 40% penetration between 8:30-23:30 hours. Therefore, when EV penetration levels increase, the power losses increase dramatically, the trend of losses is almost linear from figure 5.11 so with the more EVs penetration, and losses will rise predictably.

In the section 5.3 of this chapter, using the combined problem formulation for the active and reactive power dispatch of the ESS lowers the active power losses. 1.43MW of total active power losses can be reduced. Moreover two novel charging and discharging methods, which are coordinated active-reactive power flow of the ESS and uncoordinated active-reactive power flow of the ESS, were used in the IEEE 33-bus test DN during the peak time between 14:30-19:30 hours. Although for the former method the active power losses are a little higher, compare with the latter method, 1.64MW does not need to be imported from the TN, making the charging price of the ESS lower for the first method. Overall, adding ESS is an efficient method for the DN to achieve power loss reduction.

The results were obtained by using the optimisation algorithms described in this section, the applied methodologies and techniques can also be used to other objective functions, for instance to reduce the voltage drop, reactive power balancing or coordination of the wind power and ESS operation .

Chapter 6 Active and Reactive Power Dispatch (ARPD) for Optimal Placement of Charging Stations in Power System

In the last chapter, we proposed active and reactive power dispatch of ESS for power loss minimisation with EV penetration. However, with the increasing number of EVs, more customers are paying attention to relevant charging facilities, such as charging stations. As a consequence, several problems are occurring concerning EVs for DN planners or relevant stake holders; one of them is where to install the charging stations in the DN to facilitate EV charging.

In this chapter, a concept of a charging station combined with BESS is given. Based on this concept, a new analytical method is proposed using the stations' cooperation, in terms of optimal active and reactive power dispatch and power flow analysis, for locating the optimal placement of charging stations so as to reduce power losses. This method is compared with the previously developed current density method for a single charge station using system simulation results. It is demonstrated that the methods proposed in this chapter are more accurate than the current density method, and 17% of average active power loss can be saved for three different types of load profile. In addition, 27% of the average active power loss was saved by installing two charging stations, rather than having no charging stations in the test-line. It is shown that this could represent a 2.6% annual yield above inflation for investing in installing and running such charging stations. The proposed method is tested in an IEEE 33-bus DN and 36-bus DN.

6.1 Overview

In order to reduce CO_2 emissions, much attention is being paid to EVs. However, driving range limitation is still a big concern for all EV drivers. This problem can be solved either by improving the state-of-the-art EV batteries or by building charging stations into DN and TN [110][111] .

Developments in state-of-the-art batteries are restricted by materials science and physics, but the charging station is a relatively mature technology and, with an increasing number of EVs, will become an essential part of the commercial chain. In reference [112], the researchers

concentrated on designing multi-charging stations for vehicles, together with their utilisation in the grid, by considering battery replacement, charging and vehicle to grid. In references [113][114] , the authors considered EV arrival time, departure time, energy demands, and real world parking statistics. Based on these data, the papers provided charging station scheduling strategies. References [115][116][117]concentrated more on optimal planning and the economic aspects of a charging station for EVs by considering various costs to achieve comprehensive cost and energy loss minimisation. As an alternative, references [118][119], focused on optimisation of EV charging station location by using the conservation theory of regional traffic flows, taking EVs as fixed load points for the charging station. Maintenance and capital cost minimisation for a charging station was also considered in this work.

Research focusing on BESS has investigated various options. In [120], BESS was considered as a design criterion for charging stations. By using this criterion, EV charge efficiency and time was improved. In [121], the concept of combined photovoltaic systems and battery unit multi-supply systems was mentioned. In [122], the BESS was installed in fast charging stations as an energy supplier. The daily operating cost was minimised by optimising the active power of the BESS, allowing charging loads to be smoothed and high-price electricity absorption from the grid avoided.

The common drawback of these papers is that no matter what type of method was used to optimise size and location and to minimise the various costs of those stations, the energy transfer between charging stations was not considered: for example, combined BESSs' in charging stations can store off-peak energy and use it to provide energy to EVs during peak-time. However, these charging stations do not provide energy to each other. In this chapter, cooperation between two charging stations, in order to transfer energy to each other, is specified and tested for four different operation scenarios. This cooperation makes charging stations able to support each other, reduces losses further and provides energy to customers.

Installing combined BESS charging stations brings some additional problems; one of which is where to install these charging stations in the power system. In the existing literature, the optimal location problem has been treated in the following ways. In [123], the author proposed a maximisation of the wind energy method based on Ontario's standard offer program for locating a BESS in a DN with high penetration of wind energy. In [124], the author used a hybrid GA combined with quadratic programming to size and site the BESS to

reduce network losses and costs. In [125], a hybrid method relying on dynamic programming with a GA was described. Through this method, the location, rating and control strategy of the BESS were found, and overall investments and network costs were minimized. The methodology proposed in [126] was to optimise the location of the BESS in DNs and also to mitigate problems created by high penetration of renewable DG. A two segment current density integration method was used in [127] to choose the optimal location of DG in a single-DG system. The method was tested and proved using an 11-bus distribution line network.

However, these methods did not consider the active and reactive power transference between two BESSs when choosing the location. The research described by the author of this chapter expands on the current density integration method for a two-charge station system. The new method identifies the optimal location for the second charging station given the optimal location of the first charging station. The developed method is tested in the same system as [127] using four different operational scenarios. It is found that the current density method is accurate for a system with one charging station, but it could not be applied to a system that has two charging stations, under several different operational scenarios, because it only considers one current component from the BESSs. Therefore, an analytical cooperation approach, combining active and reactive power optimisation methods, is proposed to address this. This method is more accurate than the current density method. The results are compared with the current density method, not only as a mathematic model, but also considering the cost of power loss.

After finding the optimal locations of charging stations, the costs and profits of the charging stations is analysed. From the results, the owners of the charging stations can earn 0.84 million dollars over 15 years'. More benefits: for example, by providing voltage support and load peak shaving services to the DN, could be obtained from operation.

The rest of the chapter is structured as follows: In section 6.2 system modelling is introduced. Section 6.3 provides a theoretical analysis of the optimal placement of a charging station for power loss reduction and a costs and profits analysis. In this section, the current density integration method and the analytical method, combined with a π line model, are presented. In section 6.3, the old [127] and new methods' results are compared and analysed. Both methods are used with the 11-bus test-line used in [127]. Based on that test-line, four

different operation scenarios were used. These cover normal working conditions (scenario one and four) and energy cooperation conditions (scenario two and three) for two charging stations, identifying the optimal location for them. Section 6.4 and 6.5 give the outcomes and discussions. Moreover the IEEE 33-bus DN and 36-bus DN are also test in this chapter.

6.2 System Modelling

This section covers the EV modelling (the specification of EV, the charging place and period of EV), loads modelling, and BESS modelling.

A. System load modelling

The 11-bus distribution test-line with three different types of load profile, which can illustrate the majority of load patterns in such power systems, was used in this chapter for identifying the optimal location of the charging stations [127].

It can be seen from figure 5.6 that during the first and second off-peak periods the BESS can store energy from the TN, This energy can be purchased at a low price, whereas during the on-peak period the BESS can dispatch the stored energy to customers. This will not only save money on their electricity bill, but also enhance system stability [61].

B. Specifications and modelling of EVs

According to recent EV market surveys [128][129]][130][131], the Chevrolet Volt plug-in hybrid occupied 41% of the whole EV market, the Nissan Leaf all-electric car accounted for 30%, the Toyota Prius Plug-in Hybrid took up 17%, while the Tesla Model S had the remaining 12% of the market. Therefore, an assumption was made that, for 100 EV owners, 41 used Chevrolet Volt Plug-in Hybrid cars, 30 used Nissan Leaf all-electric cars, 17 used Toyota Prius Plug-in Hybrid cars, and 12 used the Tesla Model S. The characteristics of the different EVs are shown in table 6.1 [39].

Level 1 Charging is the slowest level. It provides a single phase 120V/15A AC plug. This type of charge is suitable for the home charge during the night, no additional infrastructure is necessary [39].

Level 2 Charging is the primary option for a public or commercial charging station. This charge option can operate at up to 80A and 19.2 kW. This charging is not suitable for home and private use, but is suitable for public charging [132].

DC Fast Charging is much faster than other methods. It can be installed in charging stations, but usually requires a 480V AC input [132] and power electronics to convert AC to DC.

Table 6.1 Characteristic of the EV

EV Types	Level 1 Charge		Level 2 Charge		DC Fast	
	Power Demand	Time	PD	Time	PD	Time
Chevrolet Volt	0.96-1.4 kW	5-8 hours	3.8kW	2 hours	n/a	n/a
Nissan Leaf	1.8 kW	12-16 hours	3.3kW	7 hours	50kW+	15-30 m
Prius	1.4kW (120v)	3 hours	3.8kW (240v)	2.5 hours	n/a	n/a
Tesla Model S	1.8kW	30+ hours	16.8 kW	4 hours	n/a	n/a

In this research Level 2 Charging was chosen. The charge time was chosen as the average charge time of the four types of EV, which was four hours.

The power demand of each type of EV in one timeslot can be calculated by using equation 6-1 [131].

$$P_i(t) = \frac{[b_i - x_i(t)] \times C_i}{E_i H_{aver}}, \forall i, t \qquad (6-1)$$

where $P_i(t)$ is the power demand of the EV at any timeslot t. b_i is the SOC of EV's battery. $x_i(t)$ is the SOC at the beginning of t. C_i is the capacity of the EV. E_i is the battery charging efficiency of the EV, $H_{aver}$is the EV's average charge time.The total power demand of all EVs can be express as shown in equation 6-2.

$$P_T(t) = \sum_{i=1}^{41} P_{i(t)c} + \sum_{i=1}^{30} P_{i(t)n} + \sum_{i=1}^{17} P_{i(t)p} + \sum_{i=1}^{12} P_{i(t)t} \qquad (6-2)$$

where $P_T(t)$ are the total power demands of all types of EVs. $P_{i(t)c}$, $P_{i(t)n}$, $P_{i(t)p}$, and P_{itt} are the power demand for each type, i.e. Chevrolet, Nissan Leaf, Prius, and Tesla.
These EVs were added into the test-line at the locations seen in figure 6.1.

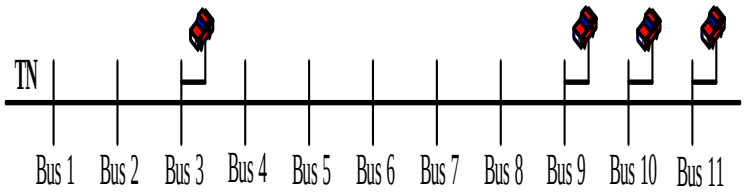

Figure 6.1 A test-line with EVs

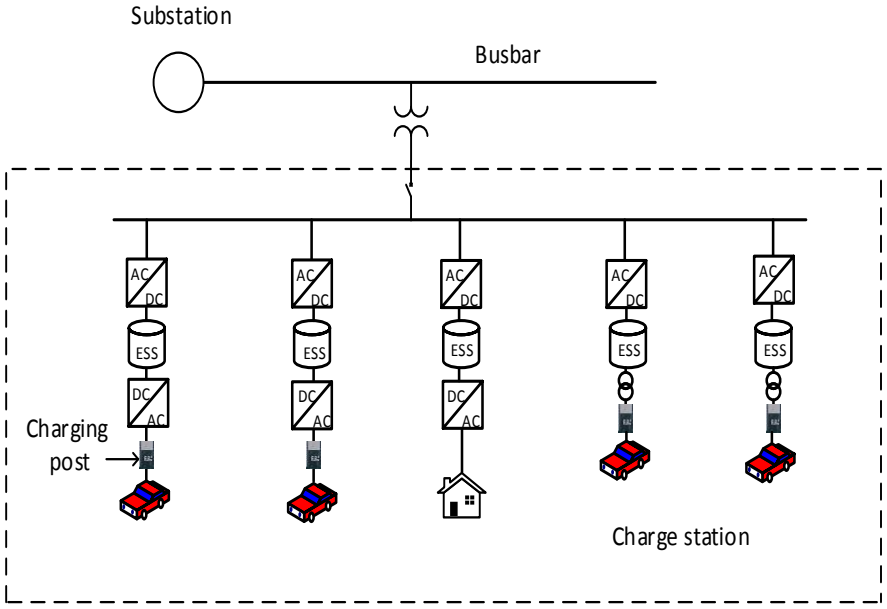

Figure 6.2 Charge station's configuration

C. The modelling of combined BESS charging station

The combined BESS charging station is different compare with the traditional charging station. Traditional stations are not able to store off-peak energy and sell it to EVs and local residents at any time. Whereas, BESS can make the profits by utilising electricity price differences between peak and off-peak times. The configuration of the stations can be seen in figure 6.2.

The charging station consists of BESSs, normal charging points and relevant charging facilities such as transformers, active and reactive compensators, inverters and converters, charging spaces, working staff. The BESS consists of batteries and PCSs [61][62]. A simple PCS consists of electronic devices such as capacitors, diodes and transformers, the structure

can be seen in figure 5.4 and the PCS capability is show in figure 3.2 in chapter five and chapter three. At operation point 1 active and reactive power is being discharged to the system. At operation point 2 the system is being charged, absorbing both active and reactive power from the TN [63]. Based on the independent and rapid control capability of the PCS, active discharge and reactive power dispatch were set as controlled variables when identifying charging station two's optimal location. It is noted that active power can be either charging or discharging at any given time.

D. The EV's impact modelling and four operation scenarios

For the sake of modelling the EV's impact in terms of active and reactive power losses, and observing the power losses for the test-line without a charging station, with one charging station and with two charging stations, power flow analysis was used.

Four different operation scenarios, in terms of the cooperation between two charging stations, are listed below. The first scenario is for normal EV charge requirements, where a regular amount of drivers charge their EVs at the charging station. The second and the third scenario are designed for some exceptional events, where one charging station runs out of energy and needs to borrow it from other sources. The last scenario is where the EV's energy requirements exceed both charging stations' designed capacity; this time both stations need external energy from the TN.

(1) The first scenario is the most common one, both charging stations used their full charged capacity to charge EVs without any optimised power charge and discharge.

(2) The second scenario considers both charge and discharge processes as charging station two runs out of rated energy. Charging station one needs to transfer energy to charging station two. The active and reactive discharge power from station one will be optimised.

(3) The third scenario also considers both charge and discharge processes, but here charging station one runs out of rated energy. Charging station two needs to transfer energy to charging station one. The active discharge and reactive dispatch power from station two will be optimised.

(4) The fourth scenario is where both charging stations one and two cannot supply the EVs and loads. External energy from the TN is used to charging stations one and two. The active and reactive power from the TN will be optimised to charge both stations. Tables 6.2-6.4 show comparisons of active and reactive power losses without charging stations, with one charging station and with two charging stations in 11-bus distribution test-line.

Table 6.2 First scenario comparison of power loss

First scenario	Without stations		Charging station one		Both charge stations	
	Ploss	Qloss	Ploss	Qloss	Ploss	Qloss
Uniform	0.682	0.59	0.616	0.53	0.190	0.25
Central	0.251	0.22	0.215	0.18	0.058	0.06
Increasing	0.565	0.49	0.532	0.46	0.171	0.21

Table 6.3 Second scenario comparison of power loss

Second scenario	Without stations		Charging station one		Both charge stations	
	Ploss	Qloss	Ploss	Qloss	Ploss	Qloss
Uniform	0.682	0.59	0.801	0.69	0.596	0.51
Central	0.251	0.22	0.319	0.27	0.215	0.18
Increasing	0.565	0.49	0.655	0.56	0.387	0.33

Table 6.4 Third scenario comparison of power loss

Third scenario	Without stations		Charging station one		Both charge stations	
	Ploss	Qloss	Ploss	Qloss	Ploss	Qloss
Uniform	0.682	0.59	0.741	0.64	0.136	0.14
Central	0.251	0.22	0.284	0.24	0.093	0.08
Increasing	0.565	0.49	0.609	0.52	0.094	0.08

6.3 Theoretical Analysis

The main focus of this chapter is to identify charging station two's optimal location. In practice, there are many additional constrains for the optimisation of charging station's location, such as different countries' energy policies and geographic factors. This chapter does not consider these factors.

6.3.1 Analytical Approach for Optimal Location

In order to reduce the power loss caused by EV penetration, a DN with charging stations one and two, which are S_1 and S_2 are shown in figure 6.3, and the π line model [109]was created and developed for analysing the location of station two for loss reduction. The active, reactive power flow, bus voltage and current of π line model are given by equations 6-3 to 6-9.

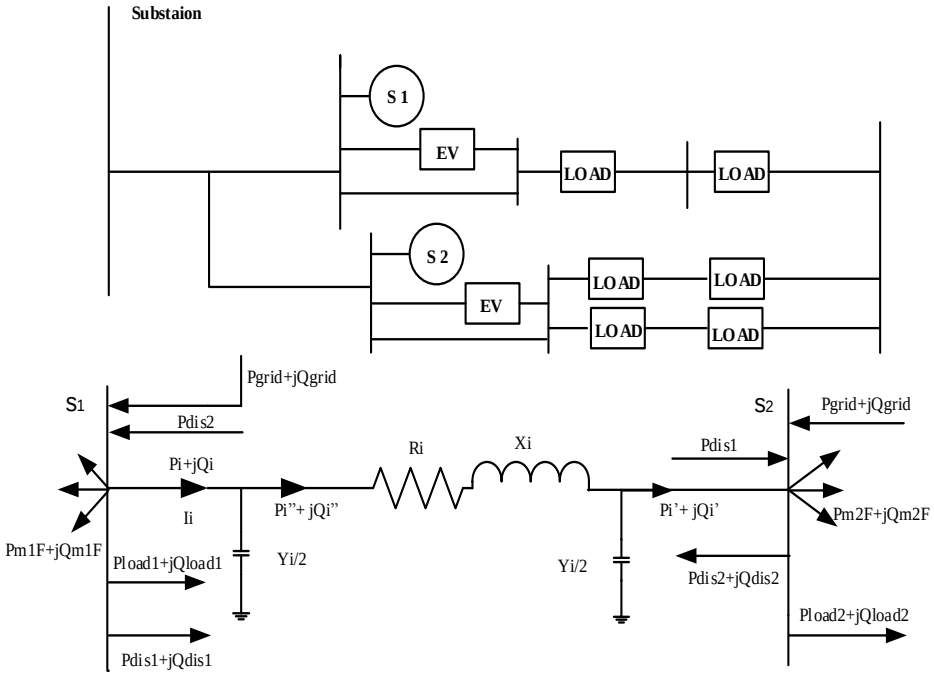

Figure 6.3 Power flow analysis

P_i and Q_i are the sending-end active and reactive power through bus S_1 and S_2.

$$P_i = P_i' + R_i \frac{P_i'^2 + Q_i'^2}{V_{s2}^2} \qquad (6-3)$$

$$Q_i = Q_i'' - V_{s1}^2 \frac{Yi}{2} = Q_i' + X_i \frac{P_i'^2 + Q_i'^2}{V_{s2}^2} - V_{s1}^2 \frac{Yi}{2} \qquad (6-4)$$

P_i' and Q_i' are the injection active power and reactive power to bus S_2 respectively

$$P_i' = P_{dis2} + P_{load2} + P_{m2F} - P_{grid} - P_{dis1} \qquad (6-5)$$

$$Q_i' = Q_{dis2} + Q_{load2} + Q_{m2F} - Q_{grid} - Q_{dis1} - V_{s2}^2 \frac{Yi}{2} \qquad (6-6)$$

The voltage at bus S_2 is

$$V_{s2} = V_{s1} - I_i Z_i = V_{s1} - \frac{S_i''^*}{V_{s1}^*}(R_i + \mathrm{j}\, X_i) \qquad (6-7)$$

$$V_{s2} = V_{s1} - \frac{P_i'' - jQ_i''}{V_{s1}}(R_i + \mathrm{j}\, X_i)$$

$$= \left(V_{s1} - \frac{P_i'' R_i + Q_i'' X_i}{V_{s1}}\right) - \mathrm{j}\left(\frac{P_i'' X_i - Q_i'' R_i}{V_{s1}}\right) \qquad (6-8)$$

The current through the π line model is

$$I_i = \sqrt{\frac{P_i^2 + Q_i^2}{V_{s1}^2}} \qquad (6-9)$$

The series impedance and shunt admittance between bus S_1 and S_2, are $(R_i + \mathrm{j}\, X_i)$ and $\frac{Y_i}{2}$ respectively. P_i' and Q_i' are the injection active power and reactive power to bus S_2 respectively. P_{dis} and Q_{dis} are the active and reactive discharge power of station.

Where $S_i'' = P_i'' + Q_i''$, $P_i'' = P_i$, $Q_i'' = Q_i + V_{s1}^2 \frac{Y_i}{2}$. P_{grid} and the Q_{grid} are the active and reactive power injected by the TN. P_{load1}, P_{load2}, Q_{load1}, and Q_{load2} are the total active and reactive power load at bus S_1 and S_2. P_{m1F}, P_{m2F}, Q_{m1F} and Q_{m2F}, are the sum of active and reactive power flows through all downstream branches connected to buses S_1 and S_2.

To find the optimal location of charging station two, an objective function was built and can be seen from equation 6-10.

$$f_j = \sum_{i=1}^{j} R_{1i(j)} |P_i' + jQ_i'|^2 \qquad j = 3,4,5 \cdots \cdots N \qquad (6-10)$$

The goal is to find the optimal location for charging station two, where equation 6-10 reaches the minimum value.

$$F_m = Min f_j \qquad (6-11)$$

The $R_{1i(j)}$ is the resistance between two charging stations. N is the test system's total bus number. P_{load2} is the load at bus S_2. P_{m2F} is active power injection from bus S_2. P_{dis1} and P_{dis2} can be obtained from equation 6-12 by using the MATLAB optimisation programming.

$$Min\ P_L = \sum_{\forall s_1,s_2}^{s_1,s_2 \in S_B} I_i^2\, R_i = \sum_{\forall s_1,s_2}^{s_1,s_2 \in S_B} \left(\frac{P_i^2 + Q_i^2}{V_{s_1}^{\ 2}}\right) R_i \qquad (6-12)$$

Both equation 6-11 and 6-12 must satisfy the constraints, based on equations from 6-13 to 6-18. The active and reactive power flow in π line model must satisfy the equations 3-2 to 3-6.

$$P_i - P_i' - R_i \frac{P_i'^2 + Q_i'^2}{V_{s2}^2} = 0 \qquad (6-13)$$

$$Q_i - Q_i' - X_i \frac{P_i'^2 + Q_i'^2}{V_{s2}^2} + V_{s1}^2 \frac{Yi}{2} = 0 \qquad (6-14)$$

The voltage magnitudes at the sending bus and receiving bus must satisfy the equation 6-15.

$$V_{s2}^2 - \left\{V_{s1}^2 - 2(P_i'' R_i + Q_i'' X_i) + \frac{(P_i''^2 + Q_i''^2)(R_i^2 + X_i^2)}{V_{s1}}\right\} = 0 \qquad (6-15)$$

The line current of the π line model should be within the thermal limit. The bus voltages should not exceed the maximum and below the minimum voltage.

$$I_i \le I_i^{rated} \qquad (6-16)$$

$$V_{s1}^{min} \le V_{s1} \le V_{s1}^{max} \qquad (6-17)$$

$$V_{s2}^{min} \le V_{s2} \le V_{s2}^{max} \qquad (6-18)$$

The theoretical procedures to find the optimal bus to locate station two are summarized below:

(1) Add EVs randomly into the test network.

(2) Run simulations and use power flow analysis to find the largest power loss bus and install charging station one there for 11-bus test line and 36-bus test network are both bus 2.

(3) Use the π line model in figure 6.3 to analyse the power loss between S_1 and S_2, which can be seen from equation 6-3 to 6-12.

(4) Set P_{dis1}, P_{dis2}, Q_{dis1}, Q_{dis2}, as the variables for power losses minimisation.

(5) Use MATLAB optimisation programming to obtain these variables' values from equation 6-12.

(6) Use these values as the input values for objective function 16 and get values of each bus.

(7) Compare the objective function's values with the simulation results.

6.3.2 Current Density Method for Optimal Location

In previous research, the current density method was used for analysis of power losses and identifying a DG's optimal location in a one DG system [127]. In this chapter, phase current I_i density was used for the same purpose, but different power cooperation strategies between charging stations one and two were considered.

Using the current density method, the phasor feeder current at point x is

$$I(x,T_i) = \int_0^x I_d\,(x,T_i)dx \qquad (6-19)$$

The incremental power loss at point x is

$$dP(x,T_i) = \left(\left|\int_0^x I_d\,(x,T_i)dx\right|\right)^2 \cdot Rdx \qquad (6-20)$$

The total power loss along the feeder within the time duration T_i is

$$P_{loss}(T_i) = \int_0^l dP(x,T_i) = \int_0^l \left(\int_0^x I_i(x,T_i)\,dx\right)^2 \cdot Rdx \qquad (6-21)$$

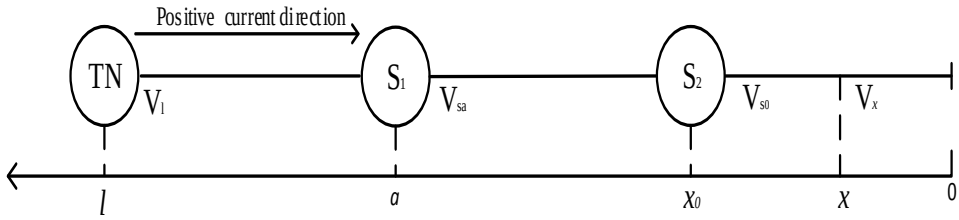

Figure 6.4 A test-line with distributed load

Firstly, it is considered that there is only one charging station in the test distribution line at location x_0, shown in figure 6.4. As a result of charging station two being added into the distribution line, two parameters (load current density $I_d(x, T_i)$ and load current) are changed in terms of current. The load current density will decrease, caused by voltage improvements due to adding station two, this decrease causes the feeder current to decrease. Meanwhile, with station two's current injection, the feeder current between the TN at l and the location of station two at x_0 will also change. But, compared with the change of load current density, the change of injected current from station two is influenced more by the change in feeder current. Hence, the change of load current density, caused by adding charging station two is neglected in this chapter [127]. Therefore, the feeder current after adding station two can be obtained by using the load current density $I_d(x, T_i)$.

Secondly, consider the second charging station which is station one adds in to test-line similarly. The change in the feeder current caused by injected current from station one is much higher than the change in the load current density. Therefore, the feeder current $I(x, T_i)$can be expressed by using the $I_d(x, T_i)$ after adding the charging station one and two. It can be seen from equation 6-22.The feeder current $I(x, T_i)$ through that test line can be expressed as:

$$I(x,T_i) = \begin{cases} \int_0^x I_d(x,T_i)dx & 0 \le x \le x_0 \\ \int_0^x I_d(x,T_i)dx - I_{disc2} & x_0 \le x \le a \\ \int_0^x I_d(x,T_i)dx - I_{disc1} & a \le x \le l \end{cases} \qquad (6-22)$$

The corresponding power loss in the feeder is

$$P_{loss}(x_0, T_i) = \int_0^{x_0} \left(\left| \int_0^x I_d(x, T_i) dx \right| \right)^2 R d_x + \int_{x_0}^a \left(\left| \int_0^x I_d(x, T_i) dx - I_{disc2} \right| \right)^2 R d_x + \int_a^l \left(\left| \int_0^x I_d(x, T_i) dx - I_{disc1} \right| \right)^2 R d_x \quad (6-23)$$

The average power loss in a given time period T is

$$\overline{P_{loss}}(x_0) = \frac{1}{T} \sum_{i=1}^{N_t} P_{loss}(x_0, T_i)\, T_i \quad (6-24)$$

Where N_t is the number of time durations in the time period T. The target to minimise total average power loss

$$Target = Min\, P_{loss}(T) \quad (6-25)$$

The solution x_0 of the equation 6-26 will give equation 6-25 the optimal site for power loss minimising.

$$\frac{\overline{P_{loss}}(x_0)}{d_{x_0}} = 0 \quad (6-26)$$

Assuming that charging station two is located at point x_0 according to equation 6-23 the effective power loss of the test feeder is

$$P_{loss}(x_0, T_i) = A + B + C \quad (6-27)$$

$$A = [I_d^2(T_i) \cdot R\, \frac{x_0^3}{3})] \quad (6-28)$$

$$B = \left[I_d^2(T_i) \cdot R\, \frac{a^3 - x_0^3}{3} + I_{disc2}^2(T_i) \cdot R(a - x_0) + I_d\,(T_i) I_{disc2}(T_i) R(a^2 - x_0^2) \right] \quad (6-29)$$

$$C = \left[I_d^2(T_i) \cdot R \ \frac{l^3 - a^3}{3} + I_{disc1}^2(T_i) \cdot R(l-a) + I_d\ (T_i) I_{disc1}(T_i) R(l^2 - a^2) \right] \quad (6-30)$$

where $\mathrm{I_d(x, T_i)} = \frac{\mathrm{I_{load}(x,T_i)}}{\mathrm{l}}$, $\mathrm{I_{load}}$ is the load current at the sending-end of the feeder.

From the equation 6-28 to 6-30, equation 6-26 can be deduced as below

$$I_d^2(T_i)\ R x_0 - I_{dis2}^2(T_i) \cdot R - 2 I_d\ (T_i) I_{dis2}(T_i) R x_0 = 0 \quad (6-31)$$

x_0 is obtained as below:

$$x_0 = \frac{l \cdot \sum_{i=1}^{N_t}\ I_{dis2}^2(T_i) T_i}{2 \sum_{i=1}^{N_t}\ I_{load}\ (T_i) I_{dis2}(T_i) T_i} \quad (6-32)$$

Assuming the bus voltage along the feeders are in acceptable range, x_0 can be approximated as below:

$$x_0 = \frac{l \cdot \sum_{i=1}^{N_t}\ P_{dis2}^2(T_i) T_i}{2 \sum_{i=1}^{N_t}\ P_{load}\ (T_i) P_{dis2}(T_i) T_i} \quad (6-33)$$

The goal is achieved by considering the power cooperation between both charging stations and using the equation 6-26 to identify the optimal location for station two. It is assumed that the voltage along the feeder is within the acceptable range 1 ± 0.05 p.u., and the transferred power is under the line thermal limit.

The solution of $x_0$of gives the optimal location of station two for the minimising of power loss for the test-line. It is assured that the voltage and transferred power are within system limitations. The theoretical procedures to find the optimal location of charging station two are summarised as follows:

(1) Add EVs randomly into 11-bus test-line.

(2) Run power flow analysis, and find the largest power loss bus and install charging station one there for four different operation scenarios.

(3) Find the distributed load $I_d(x, T_i)$ along the feeder l.

(4) Express the feeder current by using three segment current density integration methods.

(5) Use equation 6-22 and 6-26 to calculate the average power loss and identify the optimal location x_0 for charging station two.

(6) Compare the optimal location x_0 with the system simulation's location.

6.3.3 The Annual Profit of the Charging Station

In order to calculate the profit of charging station, the revenues and costs of the station are obtained.

The profit of the charging station is in equation 6-34.

$$P_{EVCSi}(t) = \sum_{t=1}^{T} R_{EVCSi}^{T}(t) - \sum_{t=1}^{T} C_{EVCSi}^{T}(t) \qquad (6-34)$$

where $P_{EVCSi}(t)$ is the annual profit of charging station, $R_{EVCSi}^{T}(t)$ is revenue of charging station and $C_{EVCSi}^{T}(t)$ is total cost of station, T is the life time of station.
$R_{EVCSi}^{T}(t)$ can be expressed in equation 6-35.

$$R_{EVCSi}^{T}(t) = \sum_{t=1}^{T} [C_{pi}^{on}(t) E_{EV} T_{CHi} + C_{pi}^{off}(t) E_{Re} T_{CHi}] \qquad (6-35)$$

where $C_{pi}^{on}(t)$ is the on-peak electricity price, C_{pi}^{off} is the off-peak price. E_{EV} and E_{Re} are the energy demand of EVs and local residents. T_{CHi} is the annual utilization hours of charging devices.

The cost of the charging station includes investment cost$C^{I}_{EVCSi}(t)$, operation cost $C^{O}_{EVCSi}(t)$, maintenance cost $C^{M}_{Evcsi}(t)$ the network loss cost [118]can be shown in equation 6-36.

$$C^{T}_{EVCSi}(t) = \sum_{t=1}^{T}[C^{I}_{EVCSi}(t) + C^{O}_{EVCSi}(t) + C^{M}_{Evcsi}(t)] \quad (6-36)$$

The investment cost of charging station can be expressed in equation 6-37.

$$C^{I}_{EVCSi}(t) = C^{I}_{ETi}(t)S_{ETi} + C^{I}_{CHi}(t)S_{CHi} + C^{I}_{DEi}(t)S_{DEi} + C^{I}_{EAi}(t)F_{EAi} + C^{I}_{Bsi}(t)\frac{E_B}{\eta CHij} \quad (6-37)$$

where C^{I}_{ETi}, C^{I}_{CHi} , C^{I}_{DEi} and C^{I}_{Bsi} are the capacity per-unit investment cost of transformers, charging devices, other devices and batteries. C^{I}_{EAi} is the land utilization cost. S_{ETi} are the transformers' capacities. S_{CHi} is the total capacity of the charging devices (including chargers, charging points). S_{DEi} is the total capacity of other devices except transformers and charging devices (for example loads and lighting). F_{EAi} is the area of ith charging station. E_B is the capacity of battery. ηCHij is the charging efficiency.

$$S_{ETi} = \frac{(S_{CHi} + S_{DEi})}{L^{max}_{EVCSi}} \quad (6-38)$$

where L^{max}_{EVCSi} is the daily maximal load rate of the ith EV charging station. S_{CHi} is the rated power.

$$S_{CHi} = K_i \sum_{j=1}^{n_i} S_{CHi} \quad = K_i \sum_{j=1}^{n_i} (P_{CHij/\eta CHij \cos \emptyset CHij}) \quad (6-39)$$

where n_i and K_i are the number and simultaneity coefficient of the charging devices in ith charging station. P_{CHij} is the output active power. cos ∅ CHij is the power factor and ηCHij is the charging efficiency in charging station.

The operation cost of ith charging station can be expressed in equation 6-40, which include charging cost $C^{O}_{CHi}(t)$, power consumption cost $C^{O}_{EEi}(t)$, active power filtering and reactive power compensation cost $C^{O}_{VCi}(t)$, battery operation cost $C^{O}_{CBi}(t)$, and human resources cost $C_{HRi}(t)$.

$$C^{O}_{EVCSi}(t) = C^{O}_{CHi}(t) + C^{O}_{EEi}(t) + C^{O}_{VCi}(t) + C^{O}_{CBi}(t) + C_{HRi}(t)$$
$$= C^{off}_{pi}(t)P^{N}_{chi}T_{CHi} + C^{off}_{pi}(t)P^{max}_{EEi}T_{EEi} + C^{O}_{VCi}(t) + C^{O}_{Bsi}(t)P_{ES} + C_{HRi}(t) \quad (6-40)$$

where P^{N}_{chi} is the rated power of charging devices. T_{CHi} is the annual utilization hours of charging devices. P^{max}_{EEi} and T_{EEi} are the maximal power consumed and annual utilization hours of the electric devices respectively. $C^{O}_{Bsi}(t)$ is the operation cost of battery per unit and P_{ES} is capacity of battery.

The maintenance cost of charging station in the planning period can be express in equation 6-41.

$$C^{M}_{Evcsi}(t) = C^{M}_{ETi}(t)S_{ETi} + C^{M}_{CHi}(t)S_{CHi} + C^{M}_{DEi}(t)S_{DEi} + C^{M}_{BSi}(t)P_{ES} \quad (6-41)$$

where $C^{M}_{ETi}(t)$, $C^{M}_{CHi}(t)$, $C^{M}_{DEi}(t)$ and $C^{M}_{BSi}(t)$ are the transformers, charging devices, other devices and batteries' battery per-unit capacity maintenance cost in ith charging station.

Network loss cost can be expressed in equation 6-42.

$$C^{L}_{PS}(t) = C^{on}_{Pi}(t)T_{h}P_{Loss} \quad (6-42)$$

where $C^{on}_{Pi}(t)$ is the on-grid price of electricity. T_h is the annual utilization hour, and P_{Loss} is the entire network loss.

The yield per year for charging station can be express in equation 6-43.

$$Y_{EVCSi}(t) = \frac{\sum_{t=1}^{T} P_{EVCSi}(t)}{[\sum_{t=1}^{T} C^{T}_{EVCSi}(t)]T} \times 100\% \quad (6-43)$$

where $Y_{EVCSi}(t)$ is the annual yield of charging station. T is the life time of charging station. In order to mitigate the price inflation in 15 years the Net Present Value (NPV) is used, where P_{Rt} is the net cash flow, P_{NPV} is the NPV, i is the discount rate, t is the time of cash flow.

$$P_{Rt}(t) = P_{NPV} \times (1+i)^t \qquad (6-44)$$

6.4 Results

The proposed method is applied to four different types of load profile in a test-line. The main aim is to demonstrate that the analytical method is suitable for identifying station two's locations under four different operational scenarios for power loss reduction. The comparison between two different methods is illustrated in Table 6.5.

Table 6.5 The Comparisons between two methods for the first scenario centrally load

Method	Power Loss expressions	Location expression	Bus	Simulation results	Power loss($)
Current density	$P_{loss}(T_i) = \int_0^l dP(x,T_i)$	$\frac{\overline{P_{loss}}(x_0)}{d_{x_0}} = 0$	$0.22l$ Bus9	Bus 8	$12,90
P,Q dispatch	$P_{loss}(T_i) = \sum_{\forall s_1,s_2}^{s_1,s_2 \in S_B} \left(\frac{P_i^2+Q_i^2}{V_{s_1}{}^2}\right) R_i$	$Min\ f_j = \sum_{i=1}^{j} R_{1i(j)} \lvert P_i' + jQ_i' \rvert^2, j = 3,4,5 \cdots\cdots N$	Bus 8	Bus 8	$11,69

6.4.1 First Scenario Three Different Load Profiles

For a uniformly distributed load, by comparing the objective function's values from equation 6-10 at each bus, bus 10 was obtained as the optimal location, as the result of adding charging station two. By using the current density method the optimal location is $0.09l$, which is near bus 10. In this case both methods have the same result.

For the centrally distributed load, by using the analytical method, the optimal location x_0 is bus 8, whereas by using the current density method, the optimal location x_0 is $0.22l$, which is near bus 9: not very accurate when compared with the simulation results. It is important to

remember that a non-optimal location can lead to $ 1,210 of power loss more than the optimal one.

To the increase the distributed load, optimal location x_0 is bus 10: bus 11 does not meet the design requirement as it can only provide energy to the load at bus 10. With the current density method, the optimal location is $0.21l$, near bus 9. Compared with the simulation results, this is not accurate.

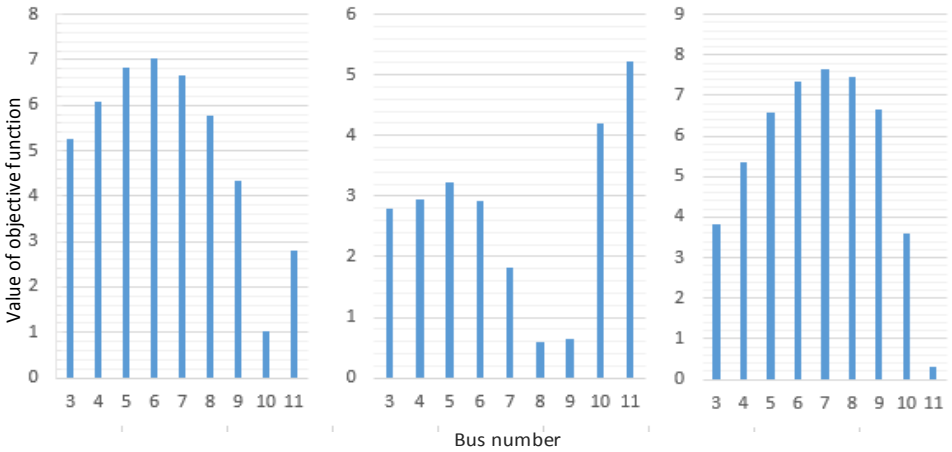

Figure 6.5 Objective function's values of the first scenario of three load profiles

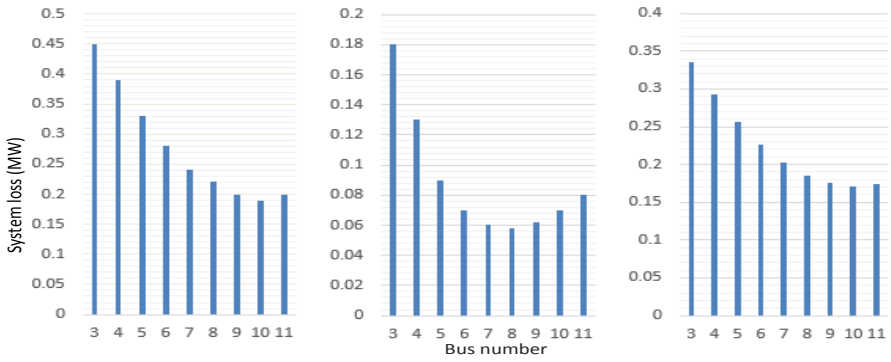

Figure 6.6 Simulation results of the first scenario of three load

The Objective function's values and simulation results are shown in figure 6.5 and figure 6.6. By using the analytical method, the optimal location for charging station two for both uniformly load and increasingly load type profiles are bus 10. For centrally load is bus 8. Simulation results prove the analytical approach.

6.4.2 Second Scenario Three Different Load Profiles

For the second scenario P_{dis1} and Q_{dis1} is optimised. $P_{dis2} = 0$, $Q_{dis2} = 0$, $P_{char2} = P_{dis1}$,$P_{optimal} = P_{dis1}$. Different optimised active and reactive power of charging station one are shown in table 6.6. They are used as input data of equation 6-10.

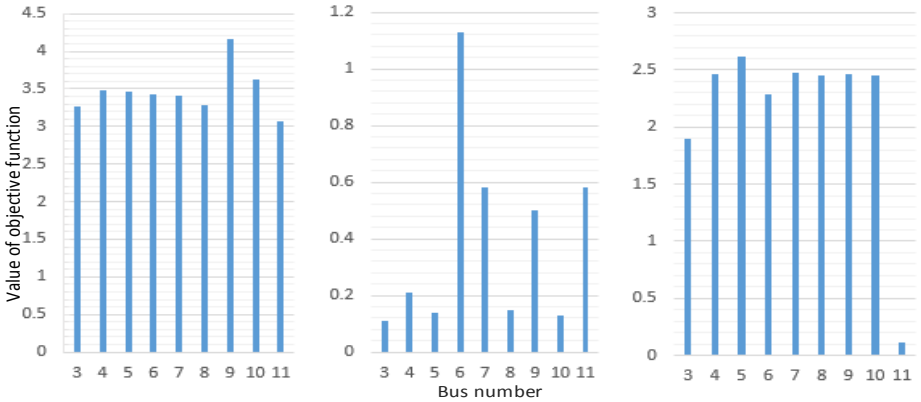

Figure 6.7 Objective function's values for the second scenario of three load profiles

The objective function's values for three types of load profile are shown in Figure 6.7. The simulation results demonstrate the validity of the analytical approach: bus 11 in this scenario does not meet the design requirements as it cannot provide energy to the load nearby. Therefore, bus 3 is chosen for three types of load.

Table 6.6 P, Q station one at different locations for uniformly load

No. / P,Q	3	4	5	6	7	8	9	10	11
Pdis	3.88	3.84	3.80	3.58	3.25	2.69	2.08	1.47	1.15
Qdis	1.25	1.37	1.61	1.21	1.05	0.93	0.62	0.48	0.27

6.4.3 Third Scenario Three Different Load Type

For the third scenario, P_{dis2} and Q_{dis2} is optimised. $P_{dis1} = 0$, $Q_{dis1} = 0$, $P_{char1} = P_{dis2}$, $P_{optimal} = P_{dis2}$. Differently optimised active and reactive power of charging station two shows in table 6.7.

Table 6.7 P,Q station two at different locations for uniformly load

No. / P,Q	3	4	5	6	7	8	9	10	11
Pdis	3.81	3.79	3.77	3.63	3.20	2.68	2.03	1.09	0.58
Qdis	1.47	1.50	1.56	1.29	1.19	0.93	0.61	0.48	0.27

The objective function's values meet the simulation results in this scenario for three different types of load profile. The optimal location for uniformly load type is bus7, for centrally load type is bus 5, for increasingly load type is bus 8. The simulation results prove the analytical method.

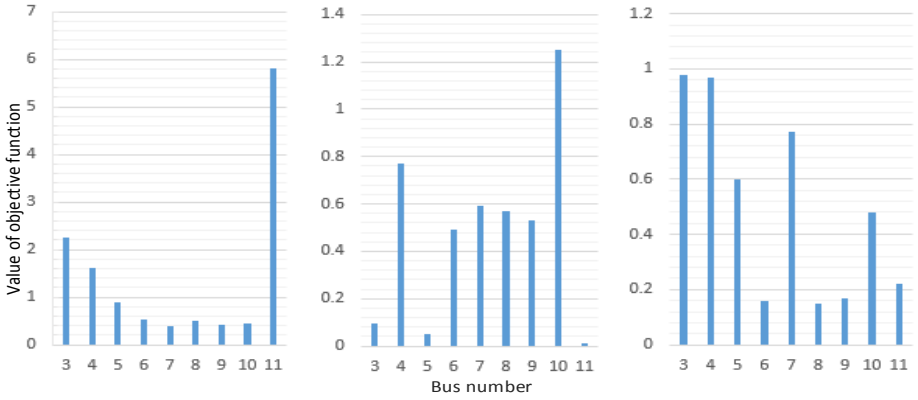

Figure 6.8 Objective function's values for the third scenario of three load profiles

6.4.5 Fourth Scenario Three Different Load Profiles

For the fourth scenario,$P_{dis1} = 0$,$Q_{dis1} = 0$,$P_{dis2} = 0$, $Q_{dis2} = 0$. Active and reactive power from grid are optimised and obtained by using the MATLAB optimisation programming. The table 6.8 shows the different active and reactive power from the TN for uniformly load.

For this scenario, both charging stations are regarded as the loads. The charging station one is added into bus 2, charging station two is added to the flowing bus except bus 2. The differently optimised active and reactive power from TN are set as the input data of equation 6-10.

Table 6.8 Pgrid ,Qgrid from TN at different locations for uniformly load

No. / P,Q	3	4	5	6	7	8	9	10	11
Pdis	9.45	9.51	9.56	9.62	9.67	9.72	9.77	9.83	9.85
Qdis	2.95	3.00	3.04	3.09	3.14	3.18	3.22	3.25	3.27

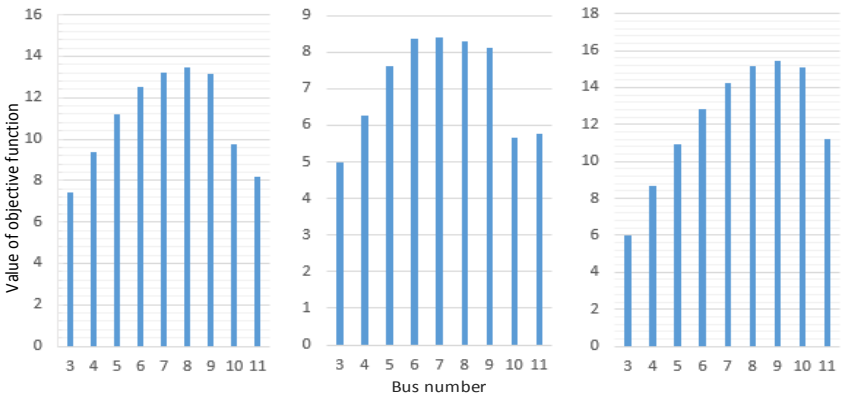

Figure 6.9 Objective function's values for the fourth scenario of three load types

Regarding the first scenario, for the uniform load and increasing load, station two's location is bus 10, which is relatively far from bus one's location. Therefore, the power loss caused by the edge of the test line is much smaller than that caused by the one installed in the middle. For the central load, station two's location moves a little closer to the centre because of the load type.

For the second scenario, station one needs to transfer energy to station two. For all three types of load, the location of station two is bus 3 because in this situation, station two is regarded as the largest load and cannot provide any energy to the loads. Therefore, the optimal locations for all three types of load are bus 3.

For the third scenario, charging station two needs to deliver energy to station one. For the uniform load type, station two's location is bus 7. Since bus 7 is in the middle area of test line, it is not far from station one and the load at the edge. For the central load type, the location is bus 5, which is in the centre of the test line, near to the largest load bus 6 and the second largest load bus 2. For the increasing load type, the location is bus 8. For this load type, if station two is installed at the end of the test line, the power loss will increase during the energy transmission to station one. Hence, bus 8 is the ideal location.

With regard to the fourth scenario, when both charging stations run out of rated energy, charging station two's location is bus 3 for the three different loads because for the uniform load and the central load, buses 2 and 3 are the largest load buses. Bus 3 is the nearest bus to the transmission network, so that the network does not need to deliver as much power to bus 3 as to others. For the increasing load, the largest load is bus 10 when the station is seen as load and added to that bus. Bus 3 is the second largest load of the system, and only less than the largest load bus 10, 0.87MW. Bus 10 is at nearly the end of this test line so that much more energy needs to be transferred to that bus. Therefore, for this scenario the location for station two is bus 3.

6.5 Discussion

The table 6.9 shows the optimal locations for charging station two in the test-line for power loss reduction. From the system operating view point, four different operation scenarios have different station two's locations. They give system operators suggestions for power loss reduction operations. However in reality, there is low possibility for moving station two's locations along the test-line according to different operation scenarios, unless every bus has charging stations. Yet it is expensive to install them in every bus. Therefore, from system planning view point, for each load type of four operation scenarios, charging station two's locations should be fixed.

Table 6.9 Optimal location of charging station two

Different scenarios	Uniformly load	Centrally load	Increasingly load
First scenario	Bus NO.10	Bus NO.8	Bus NO.10
Second scenario	Bus NO.3	Bus NO.3	Bus NO.3
Third scenario	Bus NO.7	Bus NO.5	Bus NO.8
Fourth scenario	Bus NO.3	Bus NO.3	Bus NO.3

As mentioned above, the method to identify fixed charging station two's locations show below.

In most operation states, charging stations work under the first scenario. Therefore, a compromise is made, if the station two's locations in the second scenario and the third scenario can be changed to the first scenario's locations, the fixed station two's locations can be obtained. In order to observe the differences in terms of active -reactive power loss. When

changing the third and second to the first scenario, and to analyse the possibilities of swapping station two's locations. The increasingly load type for the second and the third scenario is chosen as a case study.

When station two moves from bus 3 to bus 10 for the second scenario, and moves from bus 8 to bus 10 for the third scenario. As can be seen from table 6.10, station two moves from bus 3 to bus 10 the test-line's power loss increases greatly for the second scenario. However, for the third scenario, active and reactive power loss do not increase dramatically when changing charging station two's location from bus 8 to bus 10. Therefore, if charging station two can move from bus 8 to 10 rather than from bus 3 to 10, 0.319Mw power loss can be saved.

Table 6.10 Power loss difference for increasingly load type

For the second scenario				For the third scenario		
Bus NO.	3	10	Difference	8	10	Difference
Ploss	0.387	0.741	0.354	0.094	0.129	0.035
Qloss	0.33	0.64	0.31	0.08	0.11	0.03

Based on above analysis, an assumption is made that charging station one should always run out of energy before station two. Meaning that the third scenario always occurs before the second scenario For the sake of implementing it, charging station two's capacity has to be increased, whereas station one's capacity needs to be decreased.

Table 6.11 BESS related parameters

	Original		Current	
Stations	Power	Capacity	Power	Capacity
Station one	1.02MW	4.08MWh	0.68MW	2.72MWh
Station two	1.02MW	4.08MWh	1.36MW	5.44MWh

The capacity of station two rises a little by $\frac{4}{3}$ of original capacity and station one's capacity declines by $\frac{2}{3}$ of original capacity. From table 6.11 the current parameters of both stations are used for an increasingly load type for the first, and the third scenario.

Table 6.12 Charging station two's locations for increasingly load of first scenario of new capacity

No. / P,Q	3	4	5	6	7	8	9	10	11
Ploss	0.48	0.42	0.34	0.32	0.29	0.26	0.24	0.23	0.24
Qloss	0.42	0.36	0.32	0.28	0.25	0.25	0.21	0.21	0.21

Table 6.13 P,Q and power loss for the third scenario of increasingly load

No. / P,Q	3	4	5	6	7	8	9	10	11
Pdisc	4.58	4.80	4.37	3.75	3.55	2.99	2.57	2.20	1.15
Qdis	2.13	2.26	1.85	1.34	1.23	0.85	0.62	0.48	0.27
Ploss	0.35	0.26	0.19	0.14	0.10	0.095	0.10	0.12	0.28
Qloss	0.30	0.22	0.16	0.12	0.09	0.08	0.09	0.10	0.24

Table 6.12 shows the active and reactive power loss of charging station, in terms of different locations. Although, the rated power of station two increased to 1.36MW, and station one decreased to 0.68MW, the optimal location for station two is still bus 10. Table 6.12 indicates charging station two's active and reactive power of new capacity. Using the changed capacity of both stations in the third scenario of increasingly load type, the optimal location for station two is still bus 8. Also from table 6.13, if station two's locations change to bus 10, the active and reactive power loss will not change significantly compared with other changes. Therefore, replacing station two's location from bus 8 to bus 10 can be applied in the test-line from a system planning point view.

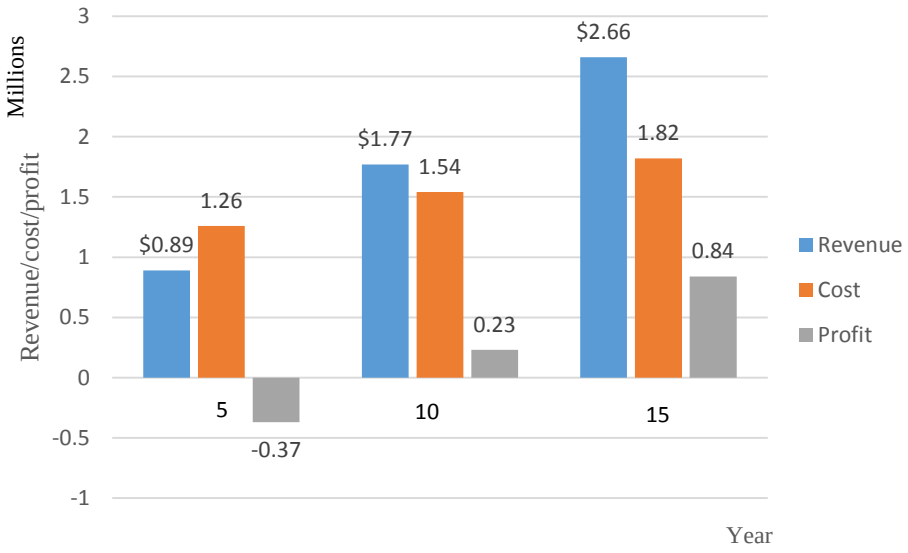

Figure 6.10 Revenue, cost, profit of charging station in every 5 year

Figure 6.10 shows commercial aspects of charging stations. The blue one is 5 years revenue, the red one is cost and the grey one is profit. As we can see from figure 6.10 in the first 5 years, station owners need to invest charging facilities that makes negative profits. However, in the after 5 years state owners can not only repay the investment cost, but 0.23 million profit can be taken by selling the cheaper electricity to local residents and EVs. In the 15 years the station owners can obtain 0.84 million profits. These profits can be obtained from equation 6-34 and 6-44.

Overall, from above analysis due to choosing the fixed locations of station two. Comparisons are made for replacing station two' locations from bus 3 and 8 in two different scenarios to bus 10 and, the result of moving station two from bus 8 to bus 10 is more suitable than 3 to 10. In order to apply this, the capacities of station one changed to 2.72MWh, and station two's capacity changed to 5.44MWh making scenario three always occurs before scenario two.

As a result of swapping station two's location from bus 8 to bus 10, the difference of active and reactive power loss only changes 0.025MW and 0.02Mvar. Therefore, bus 10 can be used instead of other buses for installing station two for power loss reduction both from system operation and planning points of view. All the results are obtained from MATPOWER and MATLAB optimisation programming.

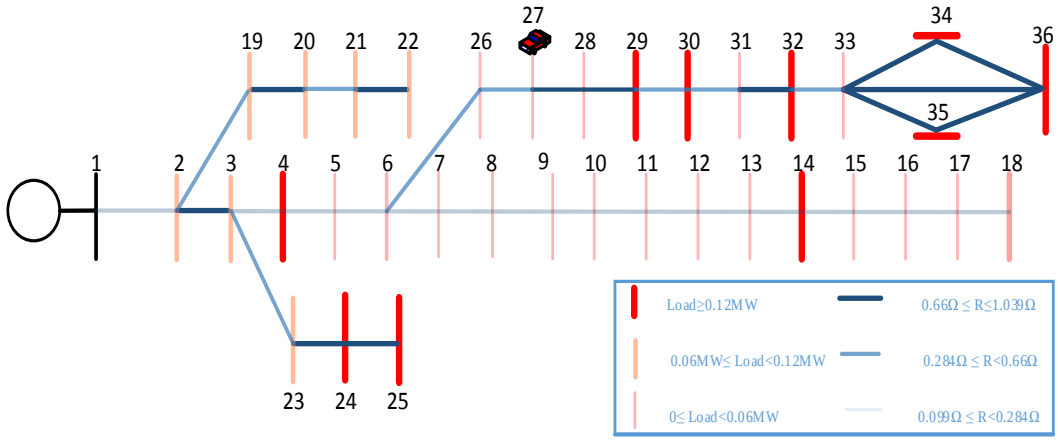

Figure 6.11 Topology of 36-bus distribution network

The proposed method is tested in a 36-bus DN [133]. The EV is connected into bus 27 by random choosing, which shows in figure 6.11. The EVs' demands are calculated by using

equation 6-2. The simulation results prove the accuracy of the proposed method. The objective function values and the simulation results can be seen in figure 6.12 and figure 6.13.

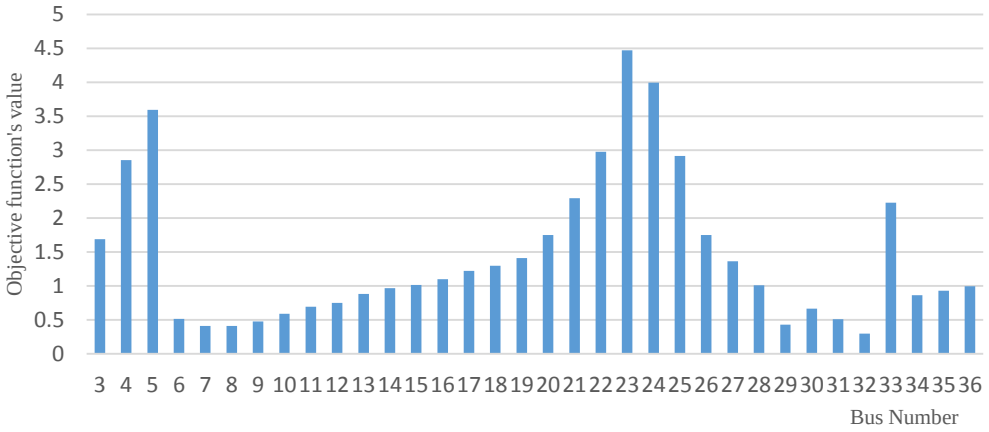

Figure 6.12 Objective function's values of 36-bus test distribution network

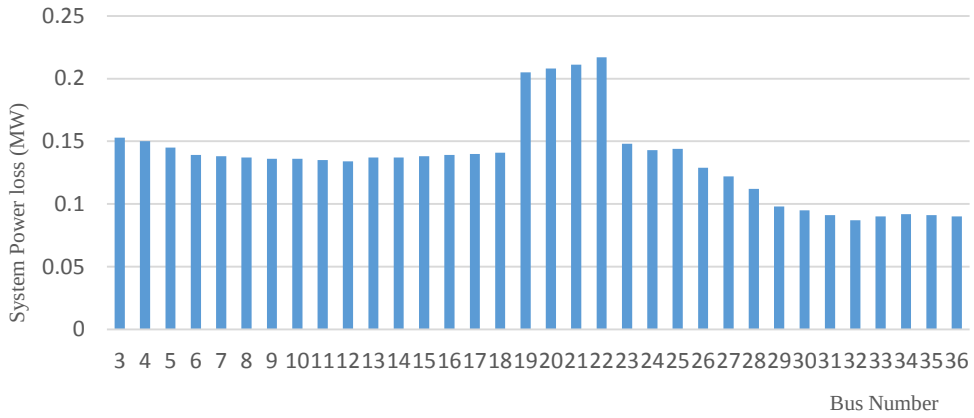

Figure 6.13 Power loss of the 36-bus test distribution network

The objective function values were obtained by using the already proposed method and are shown in figure 6.12. It can be seen that the optimal location for charging station two in terms of power loss reduction is bus 32. From the simulation results in figure 6.13, it can be seen that the proposed method is accurate, installing charging station two at bus 32 leads the system to have the lowest power loss.

The proposed method active and reactive power dispatch location choosing method is also tested in an IEEE 33-bus test DN, which is used in chapter five the topology can be seen from figure 6.14. The EVs are added into bus 10 by random. The EV load is calculated by using the equation 6-2.

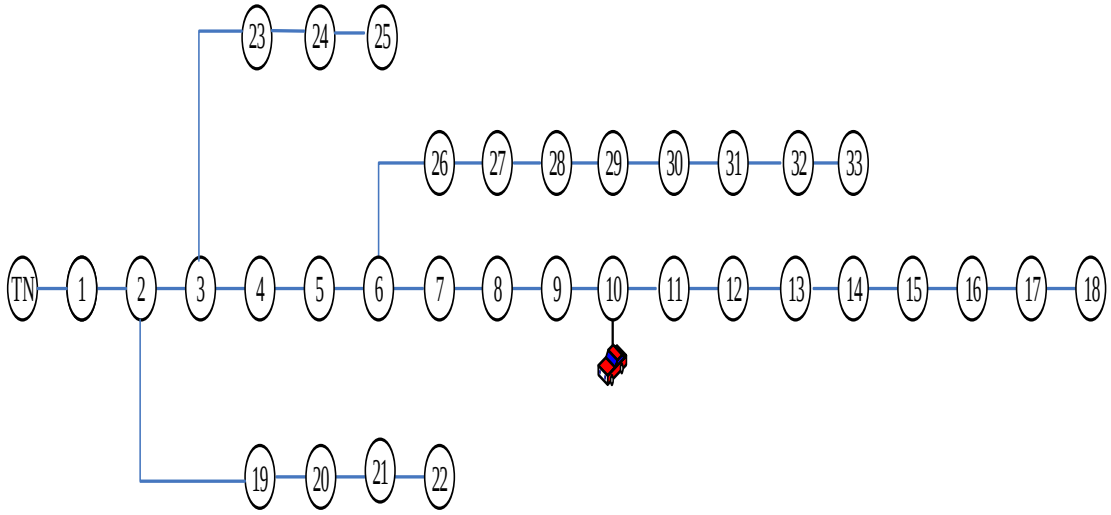

Figure 6.14 Topology of IEEE 33-bus distribution network

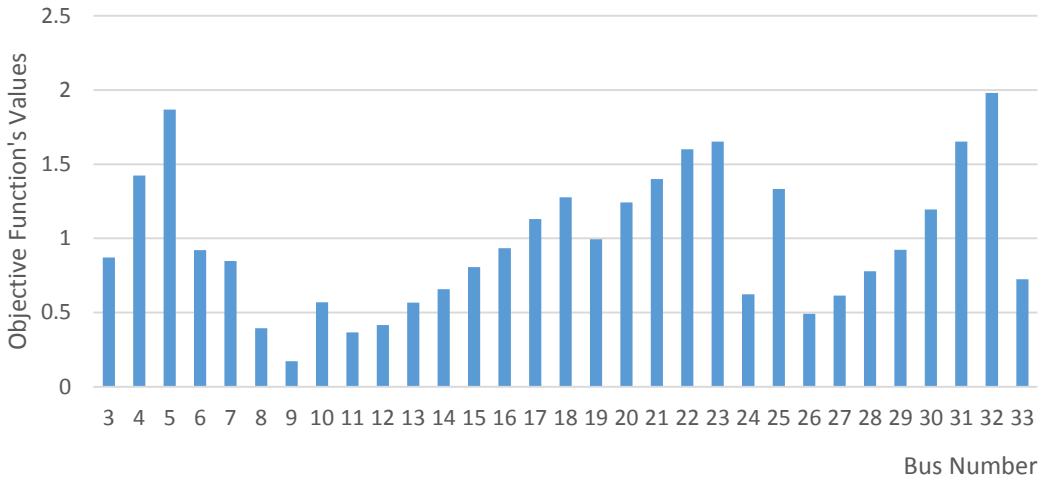

Figure 6.15 Objective function's values of IEEE 33-bus test distribution network

From figure 6.15, it can be seen that when the charging station installed in bus 9, the system power loss reach the minimum. The simulation results prove it, which can be seen from figure 6.16.

The proposed active and reactive power dispatch location choosing method was tested in 11-bus distribution line with three different loads patterns, which are uniform, central, and increasing, as well as the IEEE 33-bus test DN, and 36-bus test DN. It can be seen that the optimal location of charging station are influenced by network topology, different load patterns, and line parameters such as resistance and reactance, it is difficult to say how single

factor affect the optimum location of charging station. The more detailed analysis of how these factors affect the optimal location of charging station is shown in the next chapter.

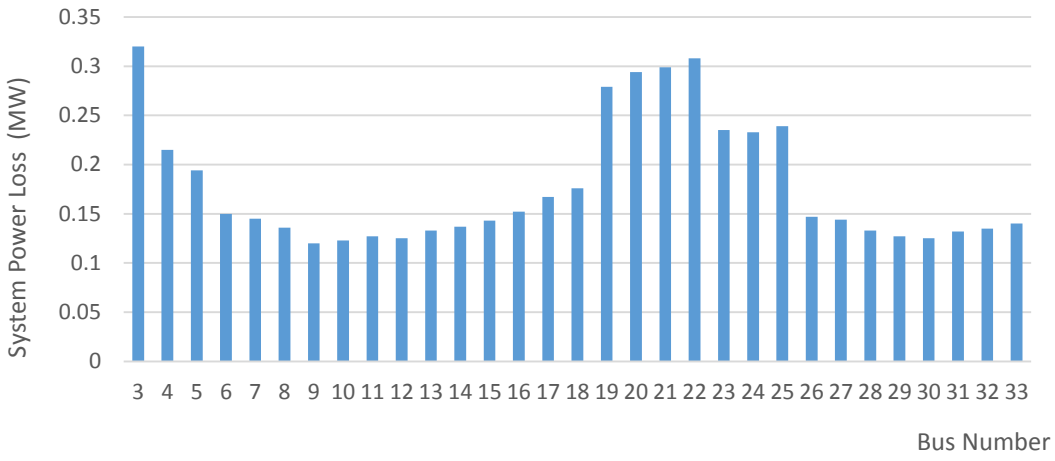

Figure 6.16 Power loss of the IEEE 33-bus test distribution network

6.6 Chapter Summary

Charging stations have been considered in many previous studies in order to mitigate the driving range limitations of EVs. Some researchers consider battery replacements, or using smart charge schedules based on various EV data. Others concentrate on optimisation methods to minimise the capital and operational costs of those charge stations. Unlike these methods, BESS is considered in this chapter not only for compensating for driving limitations, but also for reducing power loss. However, where to install such combined BESS charging stations in networks then becomes an essential issue.

In this chapter, we used a new analytical analysis combined with active and reactive power optimisation methods to identify charging station two's best location for power loss reduction. The method was tested in an 11-bus distribution line, IEEE 33-bus DN and 36-bus DN. A previously developed current density method [127] was also tested and the results compared for the same test-line with four different operational scenarios for power loss reduction.

A daily load curve was used to illustrate how BESS can shift energy between different operating periods. Next, EVs were added to the 11-bus test-line and a BESS model was built and also added to the test-line. As a result, it was shown that 27% of average active power

loss can be saved by installing two charging stations rather than no charging stations. A Comparison between one charging station and two charging stations, in terms of power loss, is depicted in tables 6.2 to 6.4.

The previously developed current density method was compared to the proposed method using a new analytical analysis combined with active and reactive power optimisation. From the power flow analysis, it was proved that the current density method is not accurate for choosing charging stations two's location. Based on four different operation scenarios, 17% of average active power loss can be saved for three different types of load using the new method described in this chapter, compared with the current density method. In particular, a case study showed that for both system operation and planning viewpoints, the optimum location of charging station two is identified at bus 10.

From the results and discussion part of this chapter, it can be seen that the optimal location of charging station two is influenced by network topology, load patterns and distribution line parameters. How these factors affect the optimum location is shown in chapter 7.

Chapter 7 The Impact Factors of Optimum Charging Station Location Analysis

In chapter six we proposed active and reactive power dispatch for charging station location choice. By using the proposed method, the optimal location for charging station two was found in terms of power loss minimisation.

Additionally, in chapter six, it was found that the optimal charging station location was influenced by factors such as network topology, load patterns and distribution line parameters. This chapter gives a detailed analysis, based on three case studies and five scenarios, of how these factors affect the optimal location of a charging station.

7.1 Overview

With the increasing number of EVs in modern society, a number of challenges and opportunities are presenting themselves: for example, how to choose charging station locations to minimize DN power loss when a large number of EVs are connected to it. How impact factors, such as different load patterns, EV charging locations and network topology, affect charging station location is becoming vital.

By using a new charging station location methodology, which was proposed in chapter six, a detailed analysis of how these impact factors affect the optimal location of a charging station is given in this chapter. Results for the 36-bus test DN with three different scenarios are presented. In addition, a more realistic model, based on EV daily travel patterns, is built to illustrate how these impact factors affect charging station location. It is demonstrated that the optimal charging station location, in terms of power loss minimization, is not affected by the EVs' charging location and load patterns; it is affected by the simultaneously change of these factors.

In [134] the authors developed a mixed-integer programming model to determine the optimal location of a charging station by considering EV parking demands, local job recruitment and a community's population density. In [135] the authors considered the impacts of limiting an EV's full state of charge on the total charge energy for charging station planning. Reference [136] considered the environmental factors and service radius for charging station location choice by using a two-step screening method. In reference [137] a new charging station

model, which is influenced by electricity consumption along the roads in cities, and oil sales, was proposed. Reference [138] considered how traffic flow and EV battery capacity affect a charging station's location choice and size.

Unlike these papers, the proposed method in this chapter uses the new charging station location choosing method proposed in chapter six to analyse how the charging station locations change as a consequence of changing the network's resistance, reactance and EV charging locations, which can be chosen at any bus in the test 36-bus DN. The structure of this chapter is as follows: In section 7.2, a theoretical analysis of this method is given. In section 7.3, three cases based on five scenarios are given and the simulation results are discussed. In section 7.4, the conclusion and summary of this chapter are presented.

7.2 Theoretical Analysis

The main focus of this chapter is to analyse how impact factors, such as loads and network resistance and reactance, affect optimal charging station location choices in terms of power loss minimization. In order to quantify the impacts on the DN, charging station two's location needs to be obtained. The same test 36-bus DN, which was used in chapter six, is used again. The EV to grid concept is not considered in this chapter.

7.2.1 Base Case and Model Explanation

The base case is used for power loss comparison with case 1 and case 2. The test network is the 36-bus DN [133], and there are two charging stations in the DN: charging station one has already been installed at bus two because the system's largest loss occurs in the line between bus one and two. The 36-bus DN voltage is 11KV and the total active reactive loads are 3.97MW and 2.08Mvar. The system's topology and the specifications are shown in figure 7.1 and reference [133]. Also, in order to analyse the power flow between each busbar, a simple test-line with distribution load model is built and shown in figure 6.4. The objection function was built to find charging station two's location.

$$f_j = \sum_{i=1}^{j} R_{1i(j)} |P_i' + jQ_i'|^2 \qquad j = 3,4,5 \cdots \cdots N \qquad (7-1)$$

where $P_i' = P_{dis2} + P_{load2} + P_{m2F} - P_{grid} - P_{dis1}$ (7 − 2)

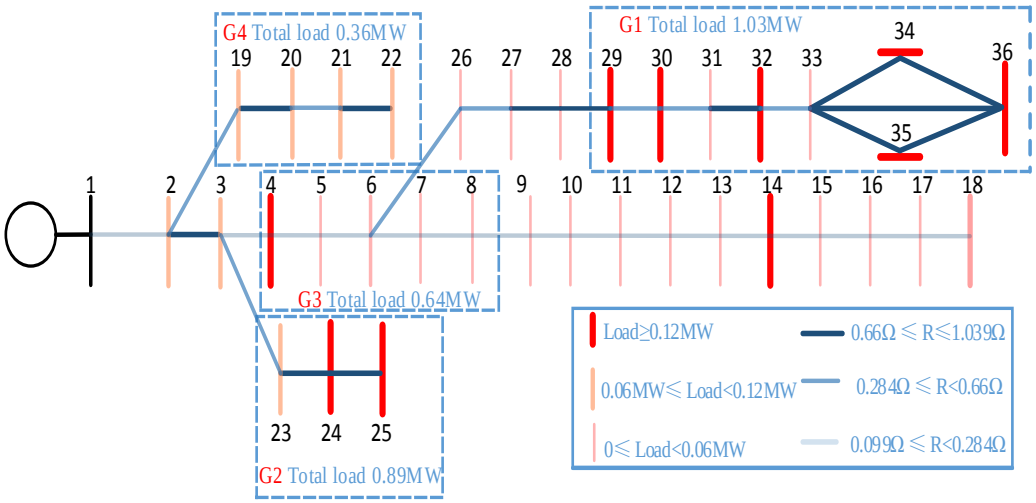

Figure 7.1 The topology of 36-bus distribution network

$$Q_i' = Q_{dis2} + Q_{load2} + Q_{m2F} - Q_{grid} - Q_{dis1} - V_{s2}^2 \frac{Yi}{2} \qquad (7-3)$$

The goal is to find the optimal location for charging station two, where equation 7-4 reaches the minimum value.

$$F_m = Min f_j \qquad (7-4)$$

The $R_{1i(j)}$ is the resistance between two charge stations. N is the test system's total bus number. P_{load2} is the load at bus S_2. P_{m2F} is active power injection from bus S_2.

$$Min\ P_L = \sum_{\forall s_1, s_2}^{s_1, s_2 \in S_B} I_i^2 R_i = \sum_{\forall s_1, s_2}^{s_1, s_2 \in S_B} \left(\frac{P_i^2 + Q_i^2}{V_{s_1}^{\ 2}} \right) R_i \qquad (7-5)$$

P_i and Q_i can be seen in chapter six in equations 6-3 to 6-4. The active and reactive power flow in the π line model must satisfy the equations 6-13 to 6-14. The voltage magnitudes at the sending bus and receiving bus must satisfy the equation 6-15.The line current of the π line

model should be within the thermal limit. The bus voltages should not exceed the maximum or be below the minimum voltage. They can be seen from equations 6-16 to 6-18.

7.3 Case Study and Result Discussion

In this section, three cases based on a 36-bus DN are analysed. The base case is used for power loss comparison. The first case, without any EV charging, shows how network loads, resistance and reactance affect charging station two's locations. The second case is with EV charging, and shows how EV charging location change affects charging station two's locations.

7.3.1 The Base Case

Before analysing the first and second case, the optimal charging station location for station two needs to be found by using the proposed method in chapter six: because if we know the optimal charging station location, then we can analyse how the impact factors affect the optimal location. Therefore, the optimal location result for charging station two obtained in chapter six is used as the base case. The objective function's values and real system power loss are shown in figure 7.2 and figure 7.3.

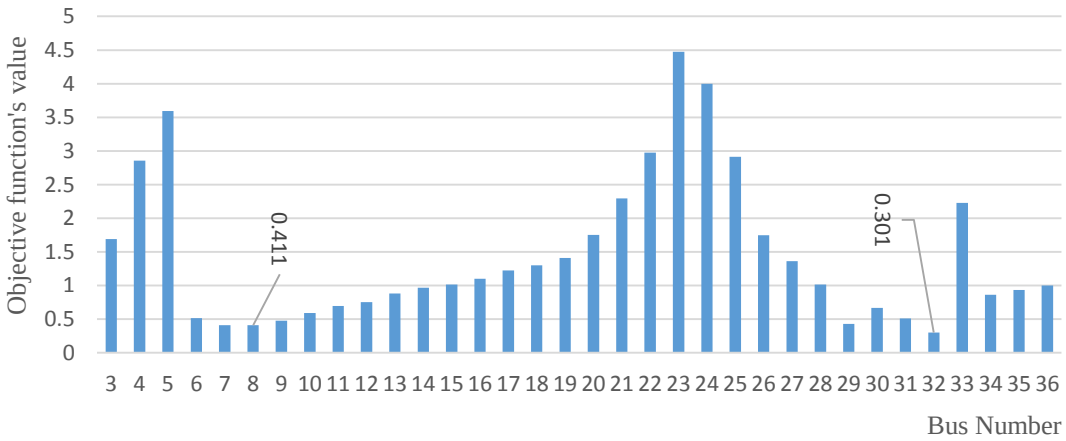

Figure 7.2 Objective function's values of 36-bus test distribution network

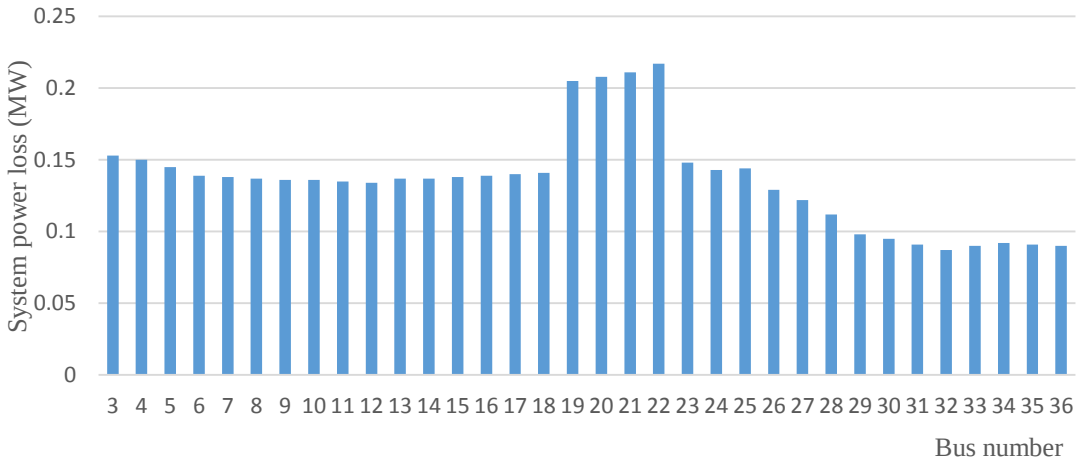

Figure 7.3 Power loss of the 36-bus test distribution network

The simulation results are shown in figure 7.3. It is proved that the optimal location for charging station two is bus 32. Regarding the objective function's values and simulation results, in general, the heavier load demands of the test system and the relatively further the distance from station one, the lower the power loss and objective functions we have: for example, bus 32 is in the system heaviest loads area G_1, which can be seen from figure 7.1. Installing station two in the heavier loads area can cause lower power loss than in the lighter loads area.

7.3.2 The First Case

The first case without any EV penetrations shows how loads, resistance, and reactance changes influence the optimal location of charging station two.

This has three scenarios. The first scenario is to change the test system's resistance, reactance and keep the load the same as the original system's loads. The second scenario is to change the test system's loads, but keep resistance and reactance the same as the original system's ones. The third scenario is to change the test system's resistance: meanwhile changing the system's loads.

In the first scenario, the resistances and reactance between bus 9 to bus 18 and bus 29 to bus 36 are changed to the new resistances and reactance as shown in table 7.1 in the appendix.

The system's loads are kept the same as the original. The 36-bus test DN with the changed R and X parameters is shown in figure 7.4.

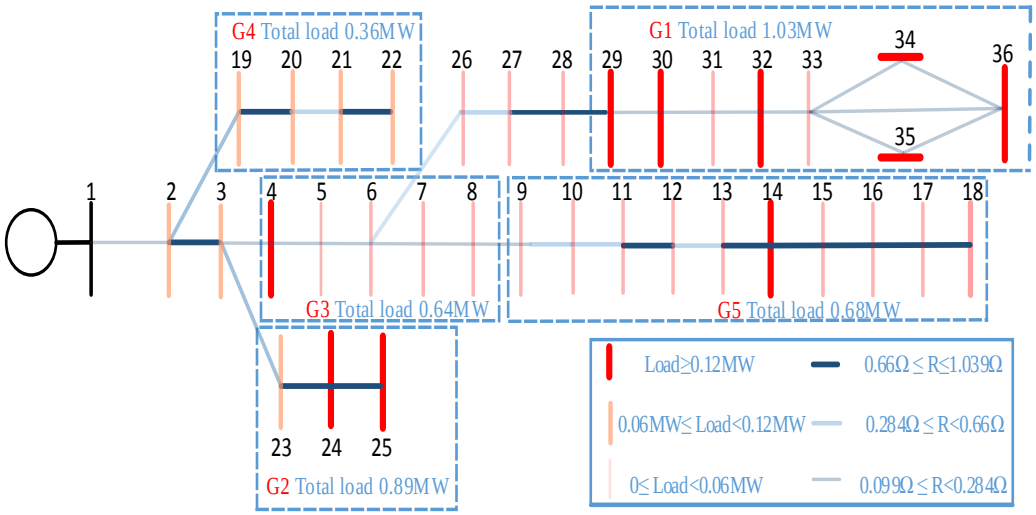

Figure 7.4 36-bus test distribution network with changed R and X

Simulation results shown in figure 7.5 illustrate the following: blue is the system's original power loss at each bus. Yellow is the changed system's power loss at each bus. Although R and X have changed, the optimal location for charging station two is still the same.

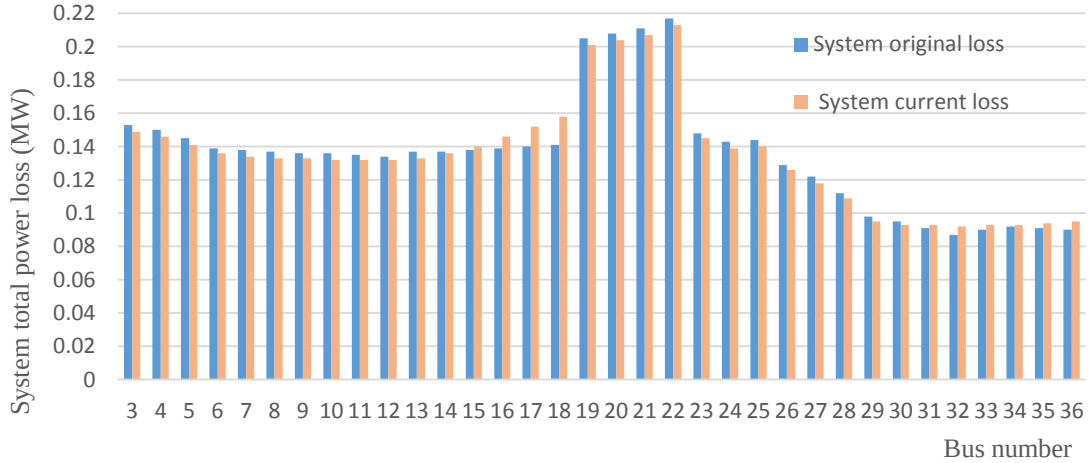

Figure 7.5 Total power loss comparison for the first scenario

Regarding this scenario, increasing system's R and X from bus 9 to bus 18, and decreasing it from bus 29 to bus 30, raises the total power loss at each bus from bus 15 to bus 18 and bus 31 to bus 36: but charging station two's location is not changed. Therefore, by only changing

the system's R and X in area G_1 and G_5, the optimal location of charging station two is not influenced.

In the second scenario, the system's loads from bus 11 to bus 18 and from bus 29 to bus 36 are changed to new loads, as shown in table 7.2 in the appendix. The system's R and X remain the same as the original.

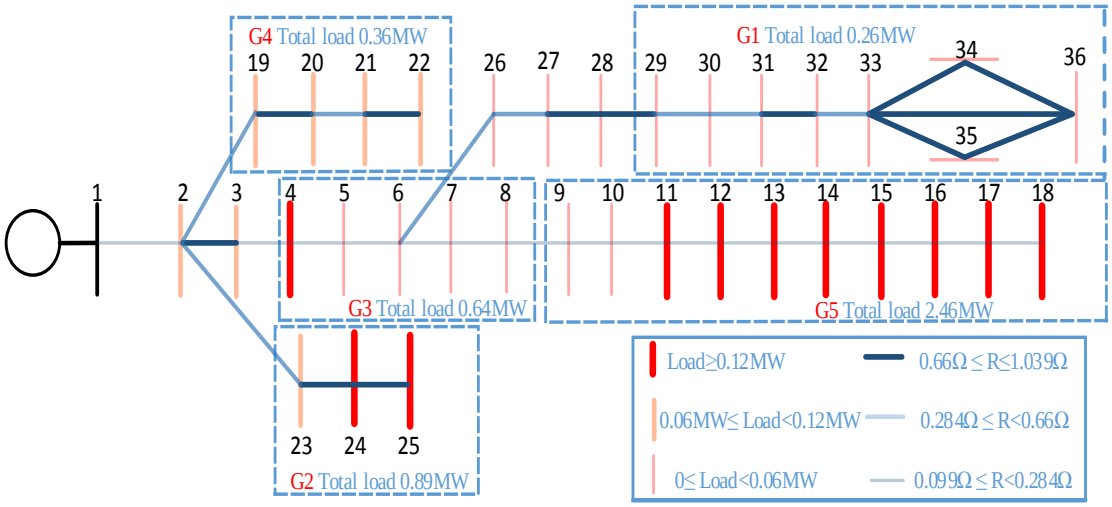

Figure 7.6 36-bus test distribution network with changed loads

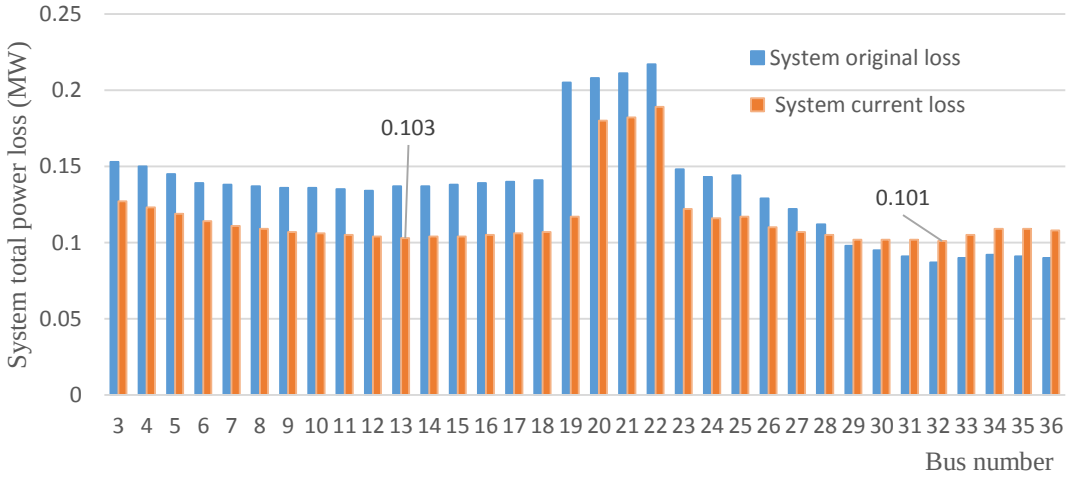

Figure 7.7 Total power loss comparison for the second scenario

From simulation results shown in figure 7.9, the blue column shows the system's original power loss at each bus. The yellow shows the new system's power loss at each bus. Increasing the load at each bus between bus 11 to 18 to the original's four times and decreasing the load at each bus between bus 29 to 36 to original one's four times raises the

total power loss, but the optimal location for charging station two is still the same: bus 32. Therefore, by only changing the system loads in area G_1 and G_5, the optimal location for charging station two does not change.

In the third scenario, the system's loads from bus 11 to bus 18 are changed to new loads, as shown in figure 7.6. Meanwhile, the system's R and X from bus 9 to bus 18 and between bus 29 and bus 30 are changed to the new values. The new loads, R and X, are shown in table 7.3 and table 7.4 in the appendix.

From the simulation results shown in figure 7.9, we can see the blue shows system original power loss at each bus and the yellow shows the new test-system's power loss with changed loads, R and X. For the new test system, the optimal location of station two has changed to bus 16.

The previous secured charging station two's location, which was bus 32, has moved to bus 16 in the third scenario. This illustrates that station two's optimal location is influenced by changing both system loads, R and X simultaneously. If only one is changed, the location will not change. Also, in this third scenario, the optimal location tends to near heavy loads and big resistance, which means by installing charging station two in a bus between bus 11 to 18, the power loss will be smaller than installing it in the other buses.

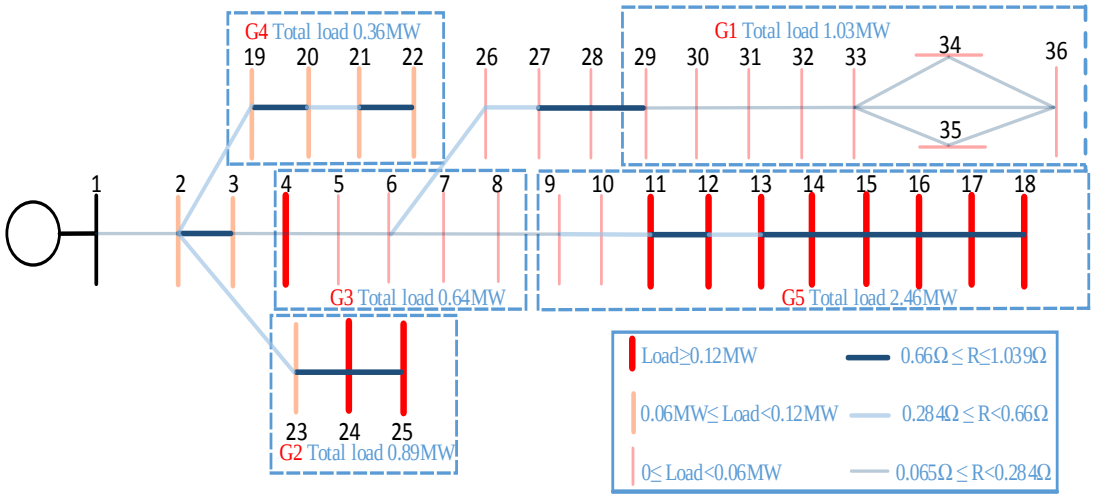

Figure 7.8 36-bus test distribution network with changed loads

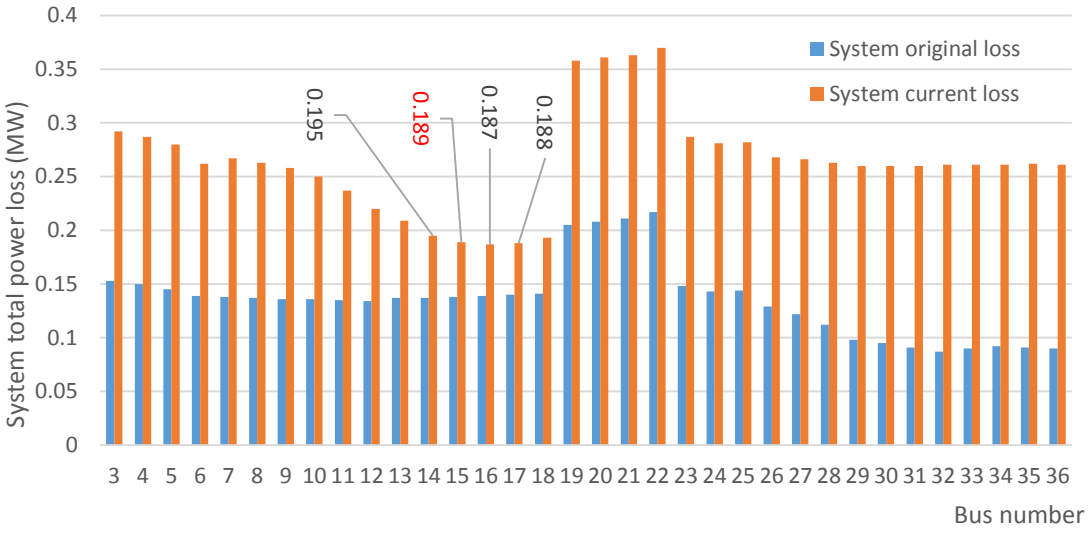

Figure 7.9 Total power loss comparison for the third scenario

Overall, the much heavier loads and the higher system R and X the bus has, the higher possibilities it can be chosen to be the optimal location for charging station two. However, in a real DN, the line parameters, such as R and X, are hardly changed. Therefore, more realistic scenarios are given in the second case.

7.3.3 The Second Case

The main aim for the second case is to test whether by changing the system loads and EV charging locations, the optimal charging station's locations can be affected or not. Two scenarios are developed for this case.

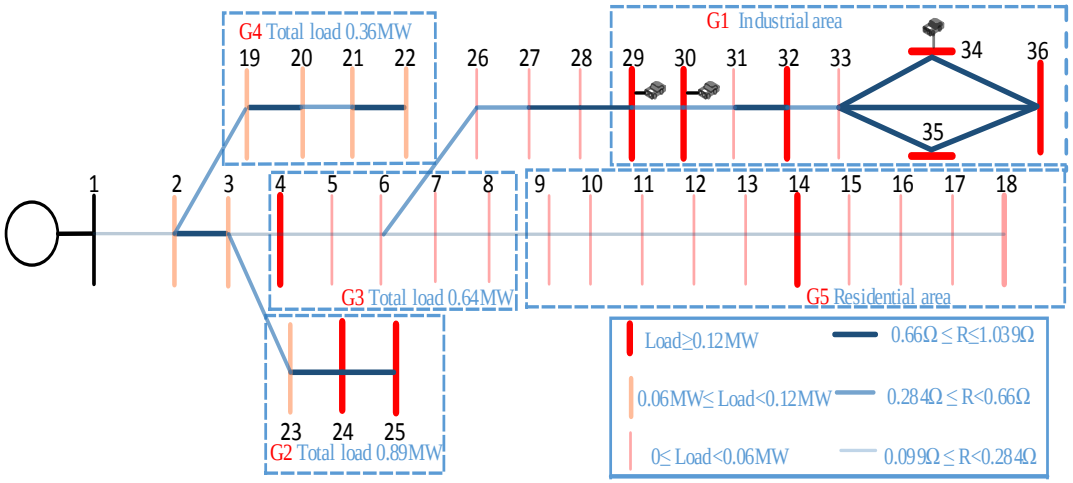

Figure 7.10 The first scenario Charing pattern

In the first scenario, EVs can charge at any time between 9:00 to 17:00. According to national travel survey statistics and the daily load profile [139][42], between 7:00 to 9:00 people leave their homes from G_5 area to go to working places G_1 area and start working. In figure 7.10, it is assumed that G_5 is the residential area because the loads are much lighter than in G_1, which is the industrial area, during the period between 9:00 to 13:00: as can be seen from figure 7.11. In this case, it is also assumed that the EV charging place is randomly chosen in the G_1 area.

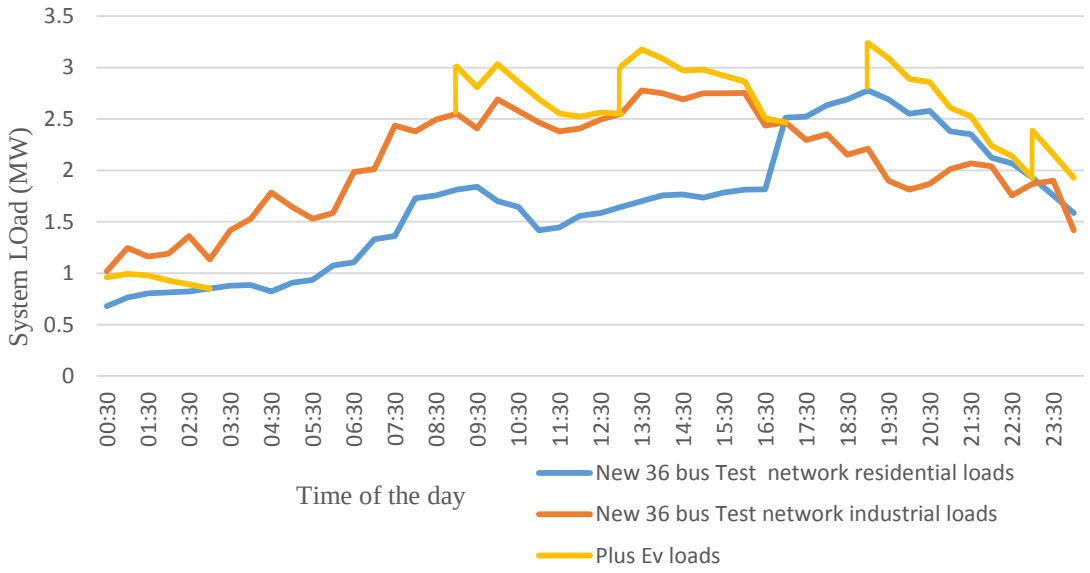

Figure 7.11 Network's load profiles after adding EVs' load between 9:00 to 17:00

In order to prove the optimal location for charging station two in bus 32, in terms of power loss minimization. The EVs are charged in the G_1 area randomly during the daytime. Two cases for daytime charging are listed below:

Case 1. The EVs' charging starts at 9:00 and finishes at 13:00. In order to simulate the hourly power loss of the whole test network, three different load patterns: the industrial load pattern, residential load pattern and EVs loads, are scaled in figure 7.11[140].

All 100 EVs, which were used in chapter six, are charged in the G_1 area during the period between 9:00 to 13:00. In this case, these EVs start charging at 9:00 in the morning and finish at 13:00 in the afternoon. These EVs' power demands increase the industrial loads profiles, which can be seen from figure 7.11. After 13:00, these EVs are fully charged, and a new

charging recycle starts from 13:00 to 17:00. Meanwhile, the residential load profiles do not change.

Case 2. The EVs start charging at 13:00 and finish at 17:00. Figure 7.12 shows the average power loss for the 36-bus test DN in the period between 9:00 and 17:00. From the simulation results, we can see the optimal location of charging station two is bus 32. Although the EVs are charged randomly in the industrial area, bus 32 is still the optimal location for charging station two.

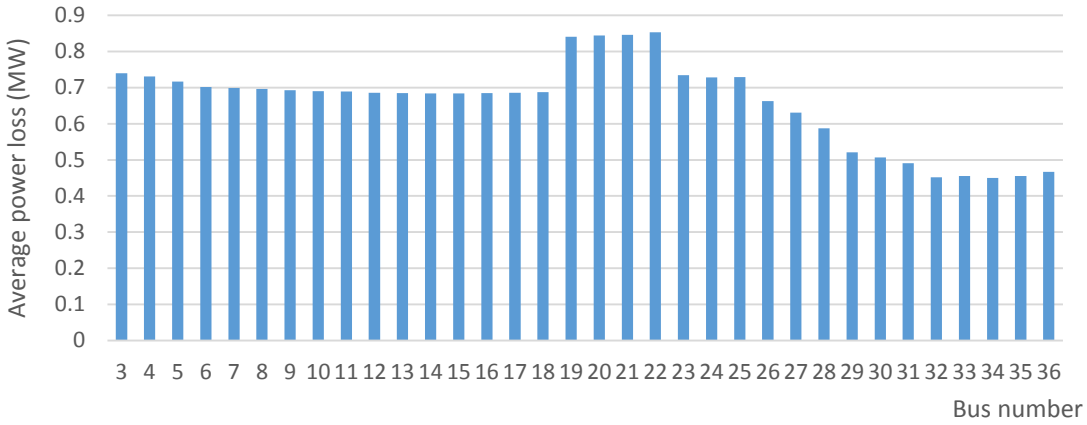

Figure 7.12 Average power loss for 36-bus test DN in the period 9:00 to 17:00

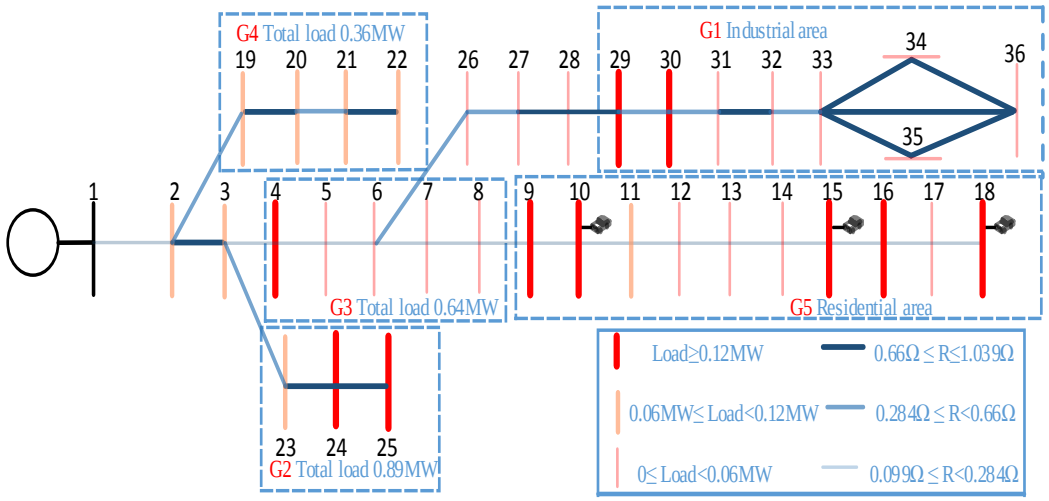

Figure 7.13 The second scenario charging pattern

In the second scenario, EVs can charge at any time between 19:00 and 24:00 because according to the national travel survey [42], most people do not use their vehicles during this period. In this scenario, people go home from their working places, from the G_1 area to the G_5 area, as shown in figure 7.13. These EVs are charged randomly in the G_5 area.

The simulation results for average power loss of the 36-bus test DN can be seen in figure 7.14. In the first charging pattern (the day time charging pattern), the average power loss is higher than in the second charging pattern (the night time charging pattern).

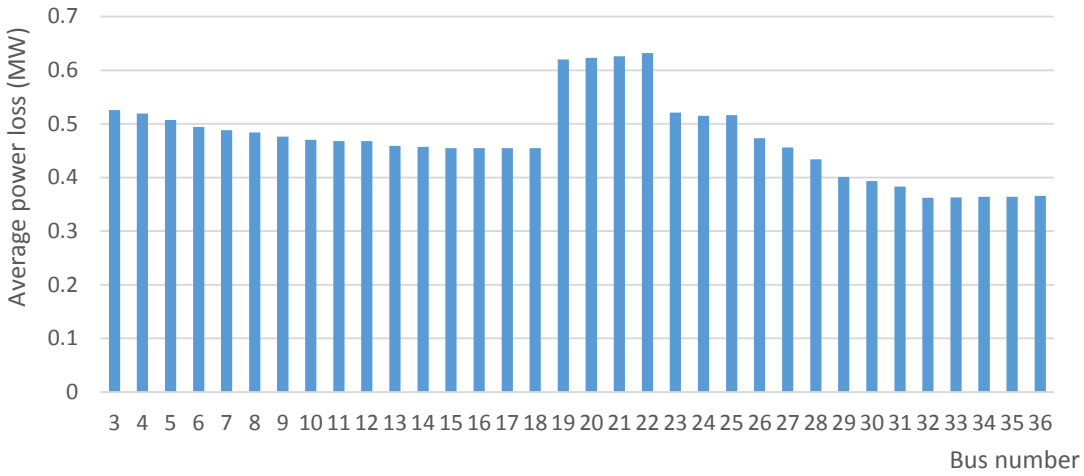

Figure 7.14 Average power loss for 36-bus test DN in the period 19:00 to 3:00

The reason for this is that in the day time charging pattern, EVs are connected to the industrial area, and in the night time charging pattern, the EVs are connected to the residential area. Comparing the two patterns' total base loads (industrial's loads plus the residential loads), the day time charging pattern's base loads are much higher than the night time's. This makes the average power loss of the first charging pattern higher than the second pattern. However, irrespective of the charging pattern, bus 32 is always the optimal location for charging station two.

From the above two different charging patterns' simulation results, we can see the optimal location for charging station two is bus 32. This proves that whether EVs are charged in the industrial area or in the residential area, by installing charging station two at bus 32, the total system's power loss is at the lowest point. In other words, the EVs' changing the charging location and load patterns will not influence charging station two's location.

7.4 Chapter Summary

In this chapter, we used active and reactive power dispatch to analyse how impact factors, such as different loads patterns, EV charging locations and network parameters, affect charging station location choice for power loss reduction. It has been shown that the charging

station’s location is not affected by the individual changes of these impact factors. It was affected by changing the network’s resistance, reactance and load patterns simultaneously. This is also proved by testing the 36-bus DN with EV penetrations.

Chapter 8 Genetic Algorithm for Charging Station Location Choosing

In chapters six and seven, the optimal locations for charging stations were found and the impact factors analysed by using the active and reactive power dispatch method. The complex calculation process for location choosing has been noted and only two charging stations' locations in the test systems were considered in chapter six for power loss minimisation. However, in reality, the situation can be more complicated: for example, it may be necessary to install more than two charging stations to provide energy to customers. Consequently, the need for a more robust and quick optimisation method is required to find multiple charging station locations to achieve power loss reduction. In order to deal with this problem, in this chapter, GA has been chosen to optimise the charging stations' locations and numbers. The GA is tested in the 36-bus DN.

8.1 Overview

GA is the most widely used artificial intelligence for optimisation. It has been used in power systems to solve power flow calculations, economic dispatch, and unit commitment. GA is used in this chapter to find the optimal locations for charging stations because it is designed for solving large-scale optimisation problems and can be much quicker than the conventional mathematical optimisation methods.

The locations problem can be very complicated: for example, to find charging station two's location in a 36-bus test DN when station one's location is fixed, there are $C_{35}^{1} = 35$ potential locations; to find the third charging station's location, there are $C_{35}^{2} = 595$ locations; to find the fourth charging station's location, there are $C_{35}^{3} = 6545$; and for the seventh charging station, there are $C_{35}^{6} = 1{,}623{,}160$ locations. If optimisation is used through a conventional mathematical optimisation method, such as the quadratic method, the objective value has to be calculated $C_{35}^{1} + C_{35}^{2} + C_{35}^{3} \cdots\cdots + C_{35}^{6} > 2{,}000{,}000$ times: thus one calculation using a traditional method takes one second, and it will take 555.56 hours to finish all the calculations. However, a GA with a 300 population size and requiring 300 generations, only requires 90,000 calculations, which is 22 times as fast as the traditional method. Hence, it is very suitable for finding the optimal locations of the charging stations.

The fitness function based on power flow analysis is built and results from GA prove the accuracy of the quadratic method, as used in chapter six. In addition the maximum number of charging stations is found by analysing how different numbers of charging stations affect the network power loss. Moreover, the calculation time of GA and the quadratic method is compared; the analysis in the summary shows GA is much quicker than the quadratic method.

8.2 Genetic Algorithm Implementation

The goal for GA is to find the best charging stations' locations to minimise network power loss. The fitness function is the same as the objective function in equation 7-1.

$$f_j = R_{1i(j)}|P_i' + jQ_i'|^2 \quad j = 3,4,5\cdots\cdots N \;\; i = 3,4,5\cdots\cdots N \qquad (8-1)$$

where

$$P_i' = P_{dis2} + P_{load2} + P_{m2F} - P_{grid} - P_{dis1} \qquad (8-2)$$

$$Q_i' = Q_{dis2} + Q_{load2} + Q_{m2F} - Q_{grid} - Q_{dis1} - V_{s2}^2 \frac{Yi}{2} \qquad (8-3)$$

The variables are $P_{dis2} = x_1$, $Q_{dis2} = x_2$, $P_{m2F} = x_3$, and $Q_{m2F} = x_4$. GA is used to decide charging station two's optimal location for power loss minimisation. It is tested in the 36-bus DN which was used in chapters six and seven. In this scenario, there are only two charging stations in the test 36-bus DN. The first charging station has already been installed in bus two because the largest power loss occurs between bus one and bus two. The same 36-bus test DN, used in chapters six and seven, is chosen and shown in figure 8.1.

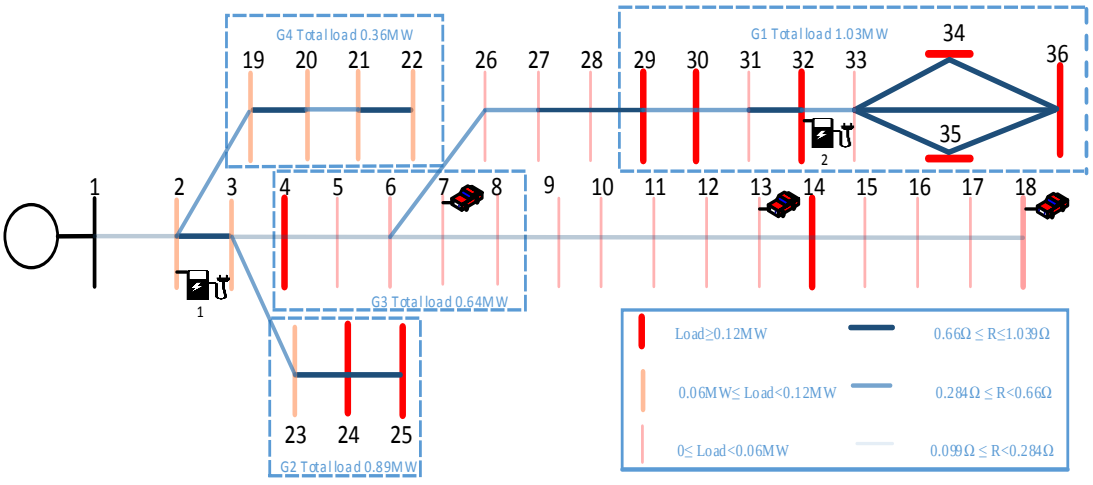

Figure 8.1 The topology of 36-bus distribution network

The GA results can be seen from figure 8.2 and figure 8.3. The EVs are connected to bus 7, 14 and 17 randomly; as can be seen from figure 8.1. From figure 8.2 it can be seen that the optimal location for charging station two is still bus 32, which proves the active-reactive location method used in chapter six.

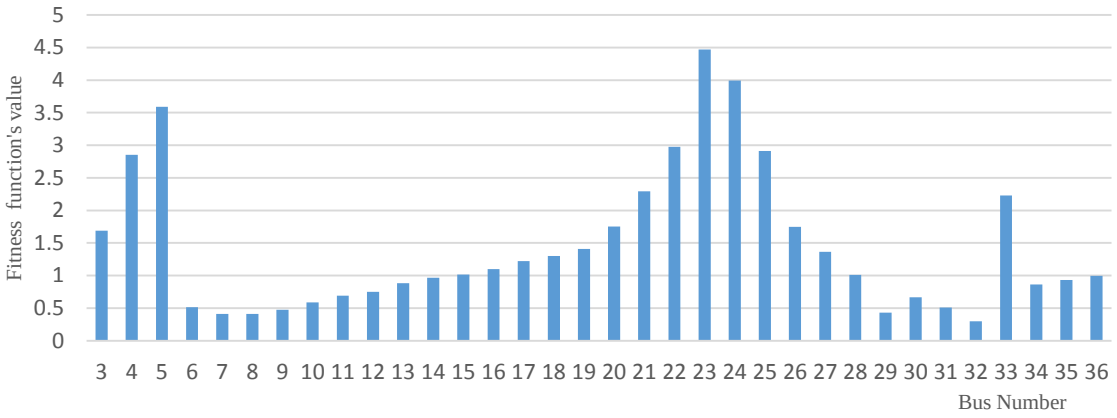

Figure 8.2 The fitness function's values of 36-bus DN

In order to test how different settings affect the GA performance, the following results are given. The default settings of the GA are shown in table 8.1.

Table 8.1 GA's setting

Population size	300
Crossover Probability	0.8
Mutation Probability	0.2
Stall Generations	300
Current iterations	100

Figure 8.3 shows the best and mean fitness values and average distance between each individual in the GA. They were obtained by using the default GA settings in table 8.1. Figure 8.4 upper plot shows the best and mean fitness values coincide at the same point at generation number 55: after this number, the best fitness and mean fitness values are the same. The GA has found the best solution to the problem.

From the lower plot in figure 8.4, we can see that around generation 230, the average distance between individuals becomes zero, which means all the individuals are the same. The best solution has been found. The average distance between each individual also shows the diversity of the population. If the average distance between individuals is large, then the diversity is high:

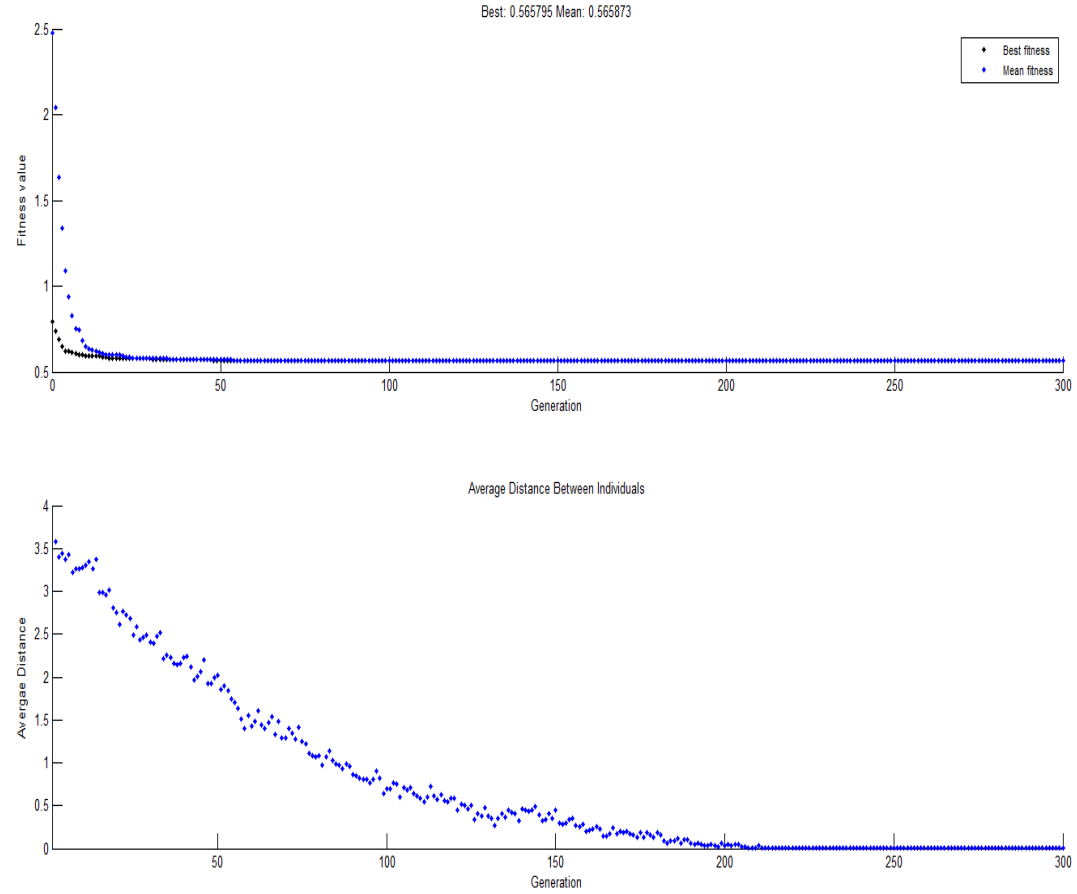

Figure 8.3 Fitness value of default settings

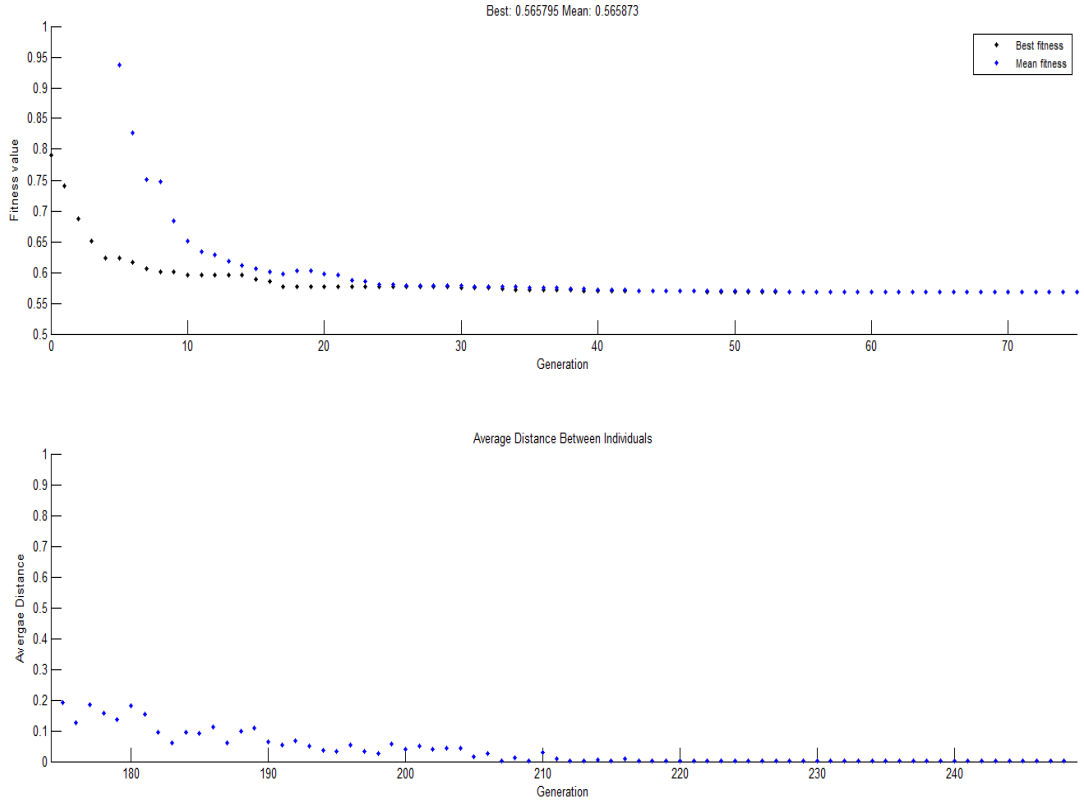

Figure 8.4 The enlarged version of figure 8.3

if the distance is small, the diversity is low. Getting the right amount of diversity is very important for using GA. If diversity is too high or too low, the GA might not perform well. Figure 8.4 shows the best and mean fitness values, and average distance between each individual in the GA.

8.2.1 Different GA Settings

In order to analyse how different settings affect the GA's performance, the GA's population size, crossover possibility, mutation possibility and elite count are changed individually. Based on these changes, two scenarios with three cases are given, which can be seen in table 8.2.

Table 8.2 Four different GA's settings

Scenario		Population Size	Crossover Probability	Mutation Probability	Stall Generation
One		400	0.8	0.2	300
Two	One	300	1.0	0	300
	Two	300	0.0	1.0	300
	Three	200	0.8	0.2	300

The first scenario's results can be seen from figure 8.5: compared with the default setting, the population size increases from 300 to 400. The rest settings remain the same.

One of the most important factors that determine GA performance is the diversity of the population. The diversity of the GA is greatly dependent on population size. In principle, increasing the population size enables GA to search for more potential solutions in the searching areas; and thereby a better result can be obtained. However, the larger the population size the GA has, the longer time it takes to compute each generation. By increasing the population size from 300 to 400, as can be seen from figure 8.4, the best and mean fitness values decrease to 0.0010 and 0.0015 respectively.

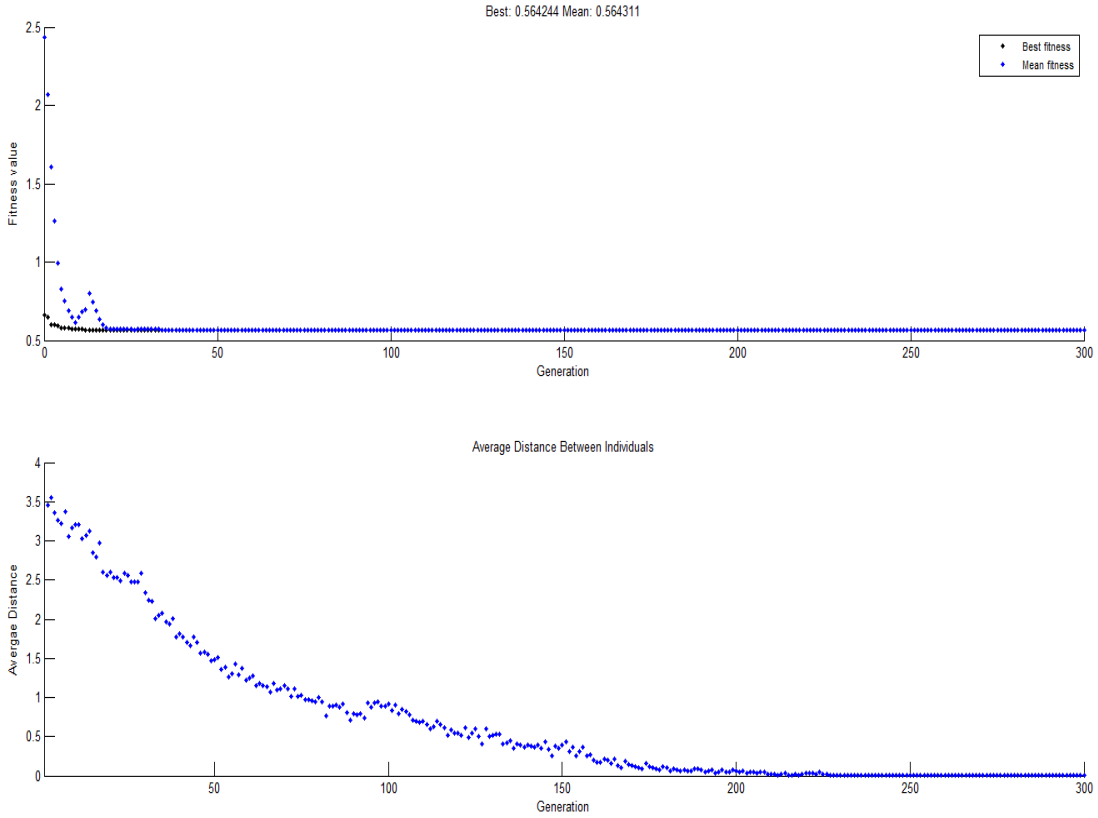

Figure 8.5 Fitness values, average distance between individuals with 400 generations

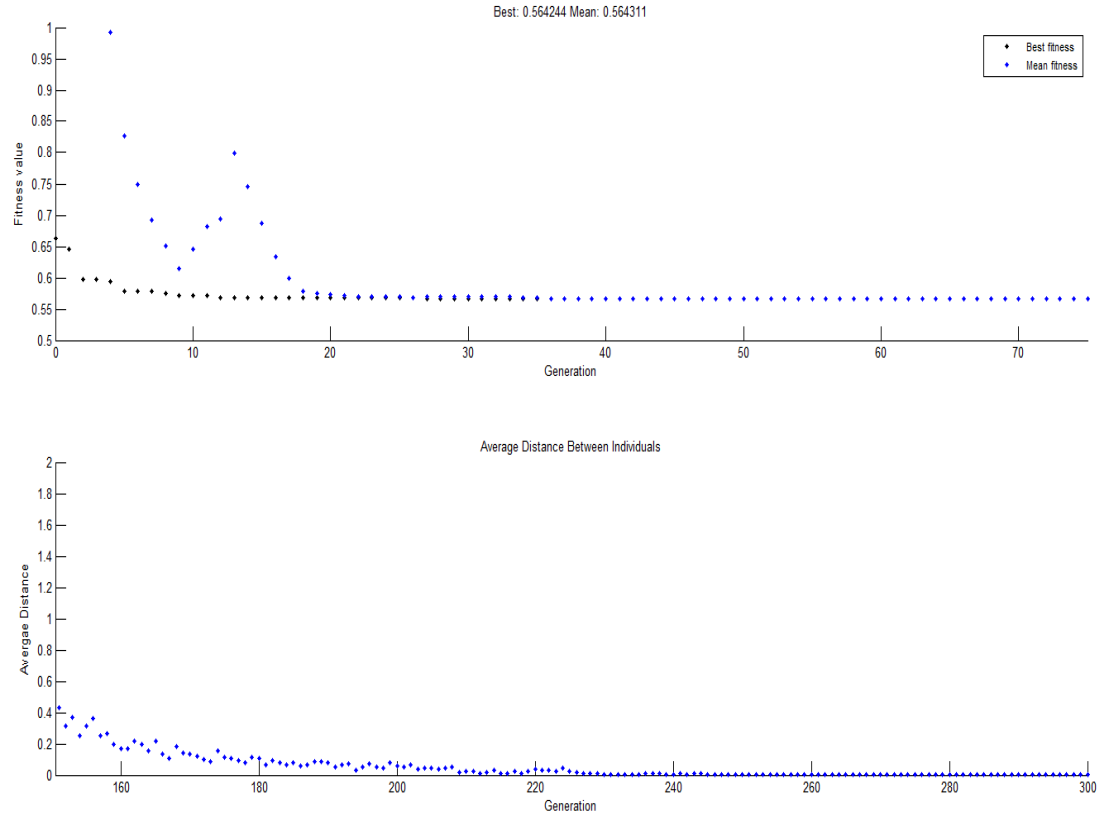

Figure 8.6 The enlarged version of figure 8.5

From figure 8.6, we can see that the GA generates the best individual, which has the best fitness values, at generation number 35, which is quicker when compared with the one in figure 8.4. This is because increasing the population size causes the population diversity to increase. Therefore, the GA can find the best solution more quickly. The average distance between each individual in the lower plot in figure 8.6 is higher than the average distance in figure 8.4, which proves increasing the population size increases the diversity of a population.

GA uses the individuals of the current generation to create the next generation. Except for elite children, which correspond to the individuals with the best fitness values in the current generation, the GA produces the following:

Crossover children: selecting genes to form a pair of individuals in the current gene pool and combine them to create a child.

Mutation children: applying random changes to a single individual in the current gene pool and forming a child.

The second scenario is to test how crossover and mutation affect GA performance. It has three cases. In the first case, the crossover possibility is changed and the mutation possibility is set to zero. In the second case, the mutation possibility is changed and the crossover possibility is set to zero. In the third case, the system default crossover and mutation possibility remain the same as the default setting, but the population size decreases from 300 to 200.

Case 1. Crossover without Mutation

Figures 8.7 shows the first case's fitness and mean values. In this case the crossover possibility is 1: which means there is no mutation. In this case, the genes are selected and recombined by the GA from the individuals in the initial population. There are no new genes because there is no mutation. Figure 8.8 shows the GA generates the best parents at generation number 9, where the best fitness plot becomes level. After this, they create the individual with the best fitness values, which are selected from the next generation. As there is no mutation, the average distance between individuals does not converge, which means the GA does not find the best solution to the question.

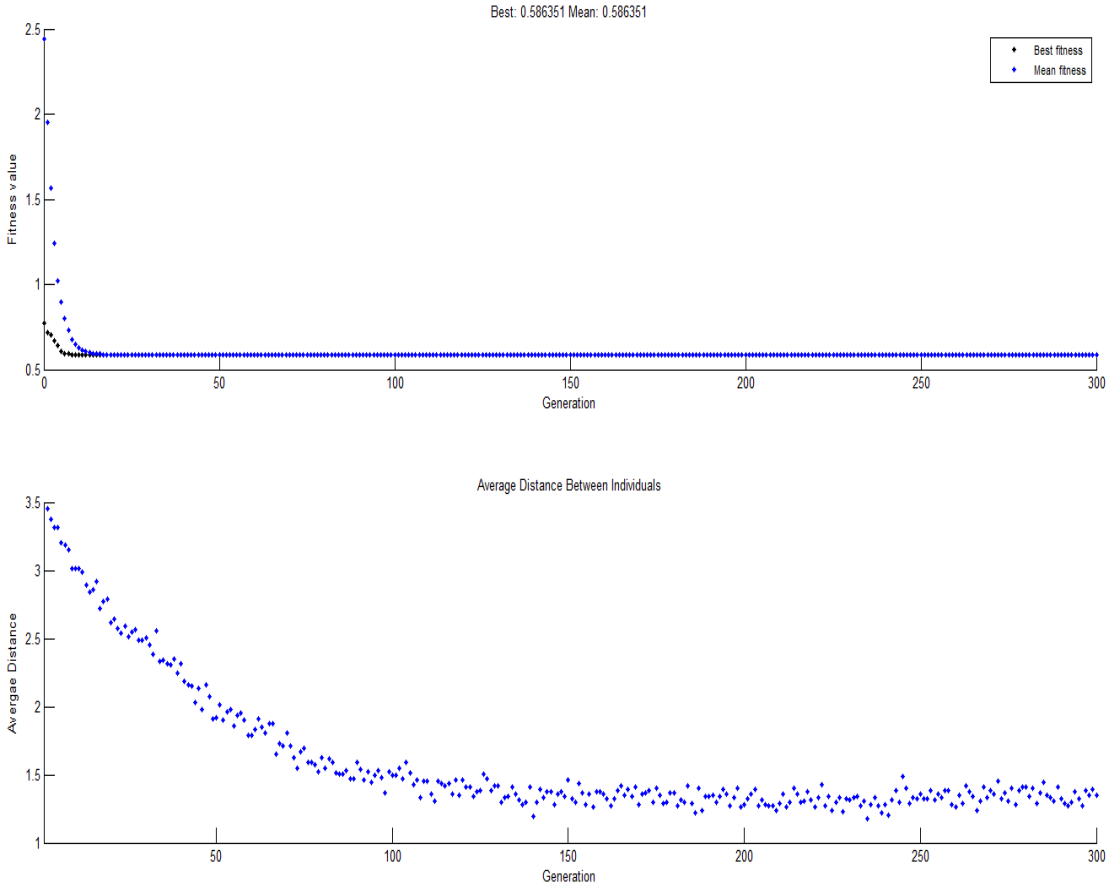

Figure 8.7 Fitness values: Crossover without Mutation

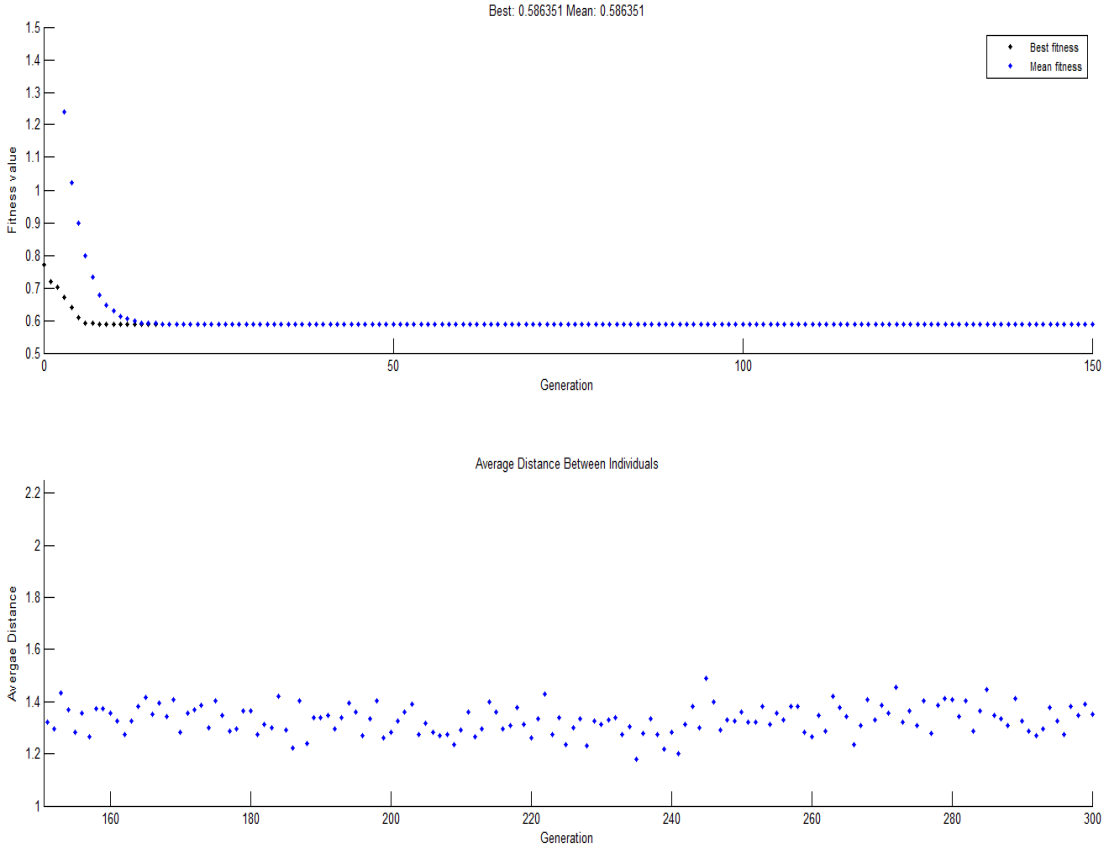

Figure 8.8 The enlarged version of figure 8.7

Case 2. Mutation without Crossover

Figure 8.9 shows the second case's fitness and mean values. In this case, the crossover possibility is set to zero, which means there is no crossover possibility. The best fitness value is approximately 0.572.

The fitness value of the best individual at the first generation will never improve through the random changes that the GA applies. Since there is no crossover possibility, it can be seen from the upper plot in figure 8.10 that the best fitness values remain the same from the first generation to the last generation. The offspring are made from exact copies of their parents. As there is no crossover, all the individuals in each generation are the same after generation 31, which means the GA finds a solution, but not the best one, much more quickly than in the other cases.

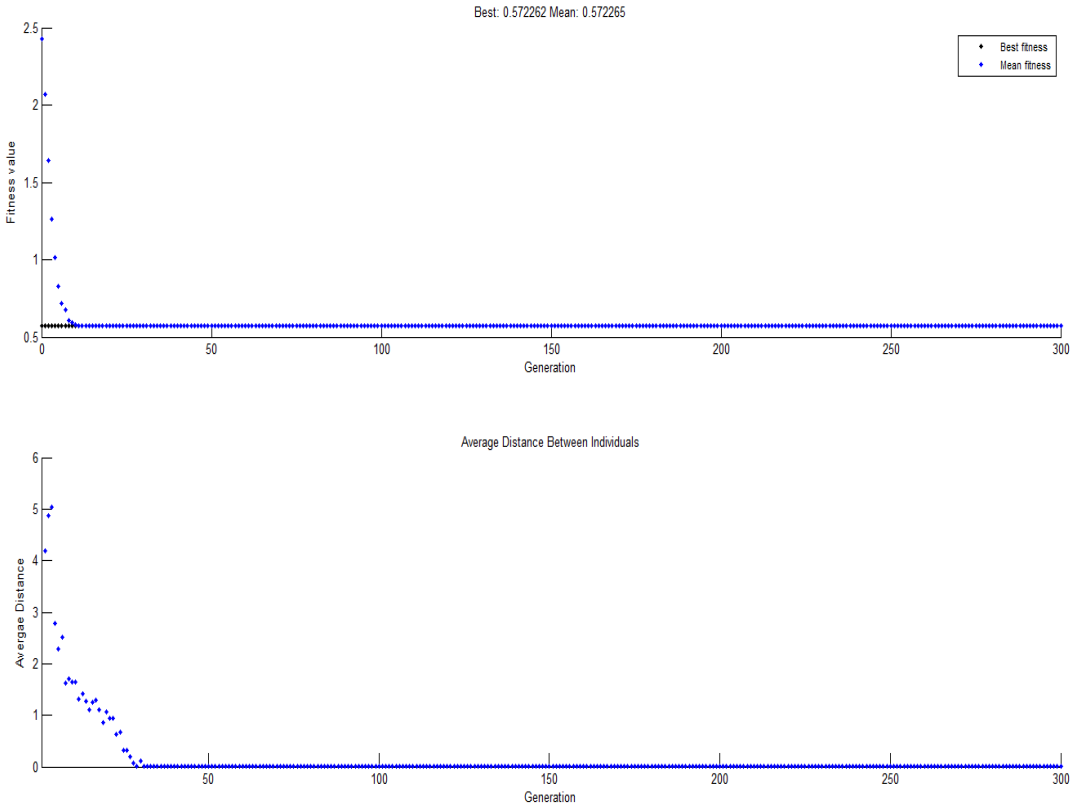

Figure 8.9 Fitness values: Mutation without Crossover

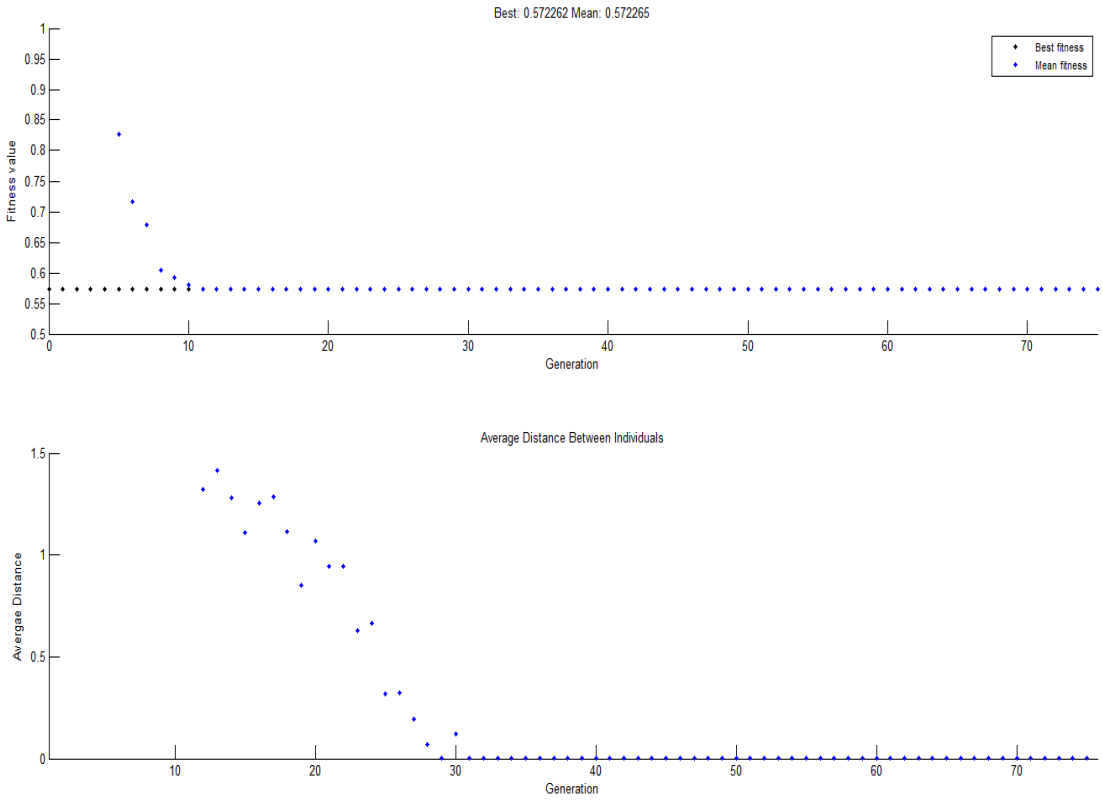

Figure 8.10 The enlarged version of figure 8.9

Case 3. The system default crossover and mutation possibility.

Figure 8.11 shows the third case's fitness and mean values. In this case, the GA can not only select genes and recombine them from individuals by crossover, but can also create some new genes through mutations: for example, when the population size is 10, the elite count is 2, and the crossover possibility is 0.8, the number of each type of children in the next generation is as follows:

There are 2 elite children. There are 8 normal individuals, including crossover mutation children. Apply the crossover possibly to these normal individuals to calculate the number of crossover children: $0.8 \times 8 = 6.4$, which means there are 6 crossover children. The remaining two individuals are the mutation children.

From upper plot in figure 8.12, we can see that the GA generates the best individuals that can use both mutation and crossover genes at generation 11, where the best fitness plot becomes level. After this generation, all the best fitness values are the same, but not until generation 21 do the mean and best fitness values coincide. That is because although mutation and

crossover occurs, there are still some individuals, who do not have the best fitness value: the fitness values of these individuals are still not close enough to the mean fitness value.

By generation 214, all individuals in the population are the same, and the best solution to the problem is found. It can be seen from the lower plot in figure 8.12 that the average distance between individuals is 0. This means there are no differences between each individual in the population: the GA cannot change any individuals in the population.

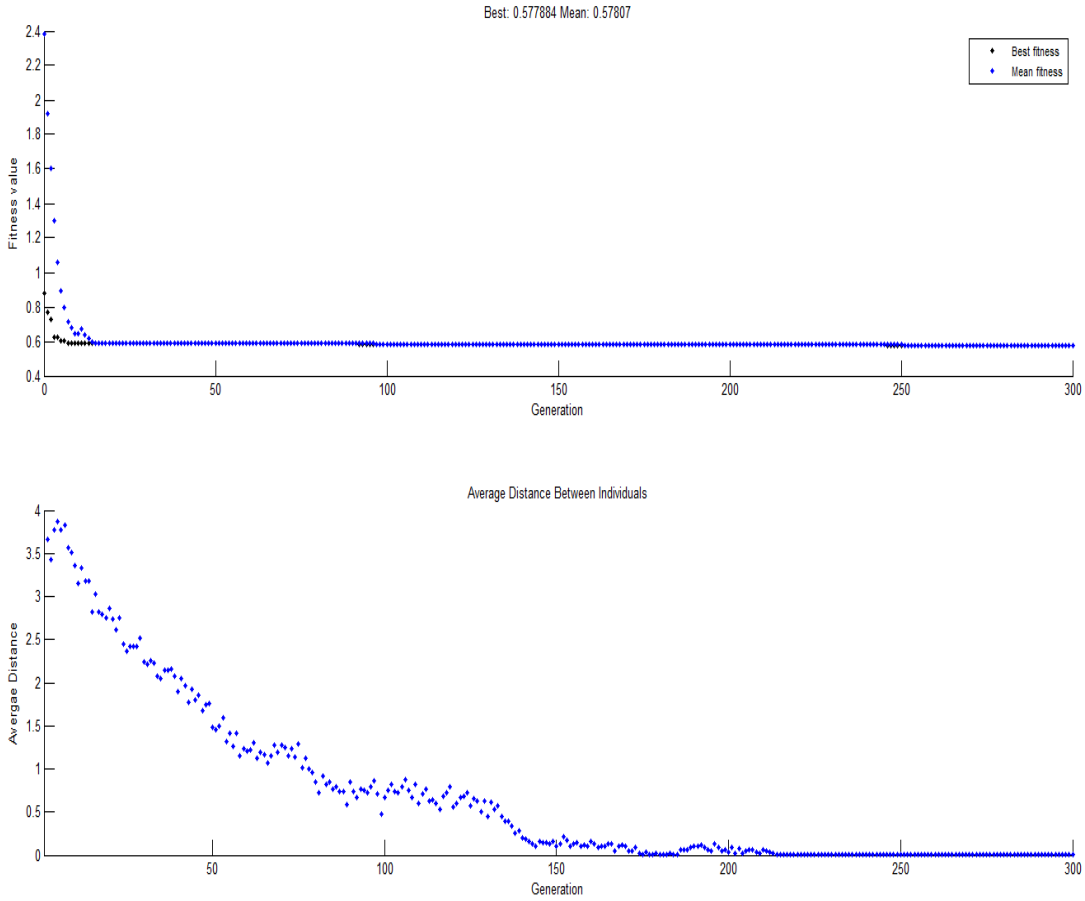

Figure 8.11 Fitness values: Mutation with Crossover

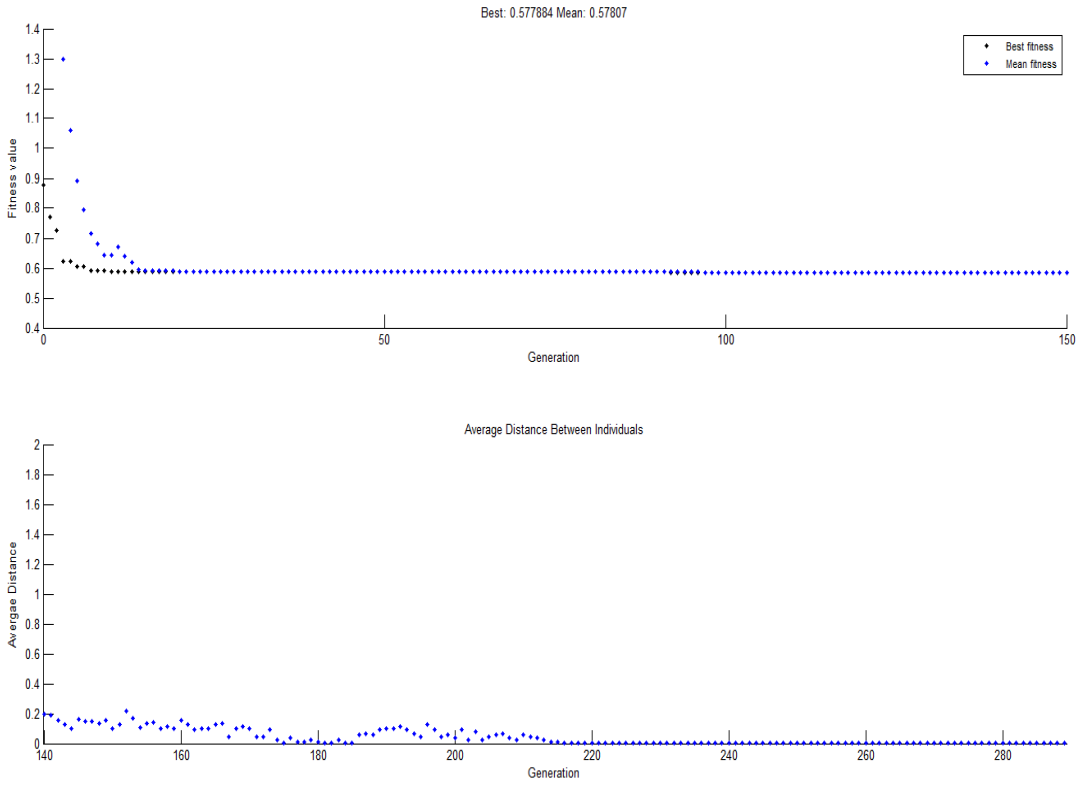

Figure 8.12 The enlarged version of figure 8.11

From the above analysis, it is evident that by using the GA with default settings, the GA can find the best solution quickly and accurately. The results from the GA show the optimal location for charging station two is still bus 32, which proves the active and reactive location method used in chapter six and chapter seven. However, in practice, there may be more than two charging stations needed to be installed in test DN. With the loads and EV numbers increase, multiple charging stations may be needed to supply the increased loads.

In order to analyse how the increased number of charging stations affect power loss reduction, a third and a fourth charging stations are installed in 36-bus DN. The GA is still used to decide their optimal location. With more charging stations installed in the DN, the model for analysing the power flow between two charging stations, which was built in figure 6.3, needs to be modified.

8.2.2 GA for n Charging Stations

Figure 8.13 shows the modified model for analysing power flow between charging stations. The fitness function remains the same as that which is shown in equation 8-1.

The new injected real and reactive power to bus S_n shows below, n is the number of charging station:

$$P_i' = P_{disn} + P_{loadn} + P_{mnF} - P_{grid} - P_{dis(n-1)} \quad (8-4)$$

$$Q_i' = Q_{disn} + Q_{loadn} + Q_{mnF} - Q_{grid} - Q_{dis(n-1)} - V_{s2}^2 \frac{Yi}{2} \quad (8-5)$$

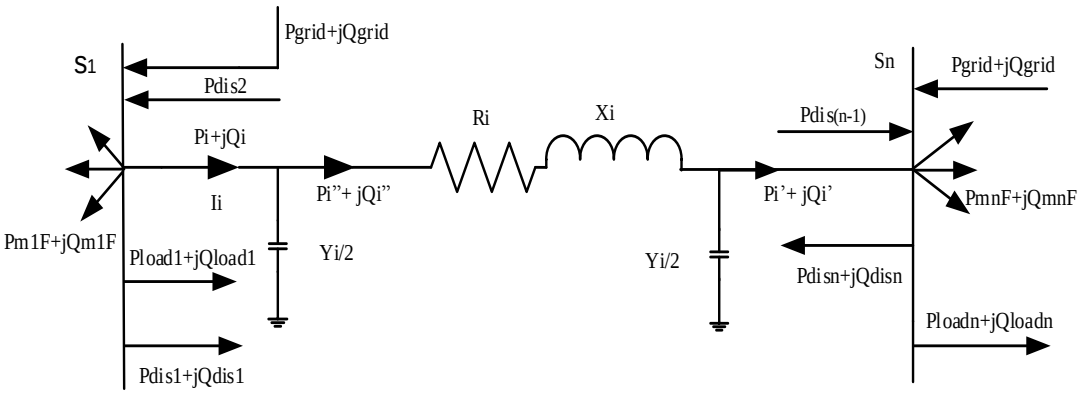

Figure 8.13 The multiple charging stations model

In the third charging station case, charging station one has already been installed in bus two, and station two installed in bus 32. The third charging station's optimal location in terms of power loss minimization is found by the GA: the fitness values of the 36-bus test DN are shown in figure 8.14.

The simulation results of the third charging station case are shown in figure 8.15. The fitness function values match the simulation results. The third charging station's location can be seen from figure 8.16, which shows that bus 14 is the optimal location for charging station three.

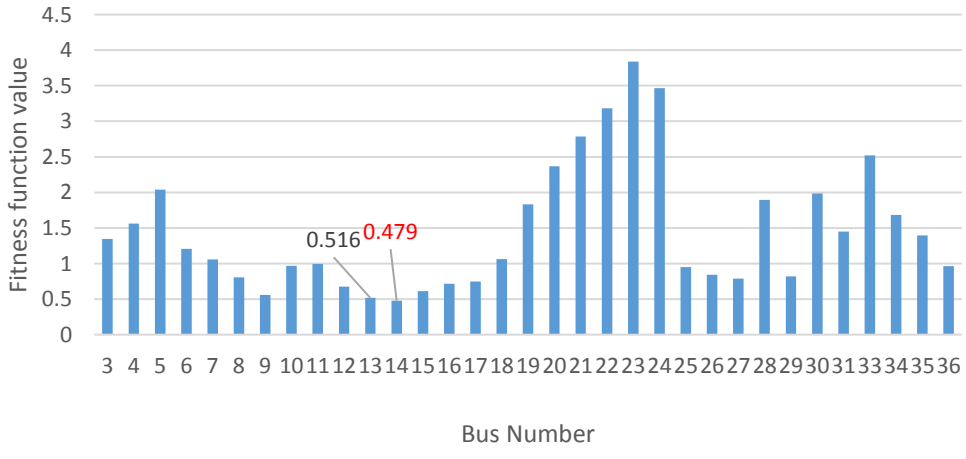

Figure 8.14 Fitness function values for the third charging stations

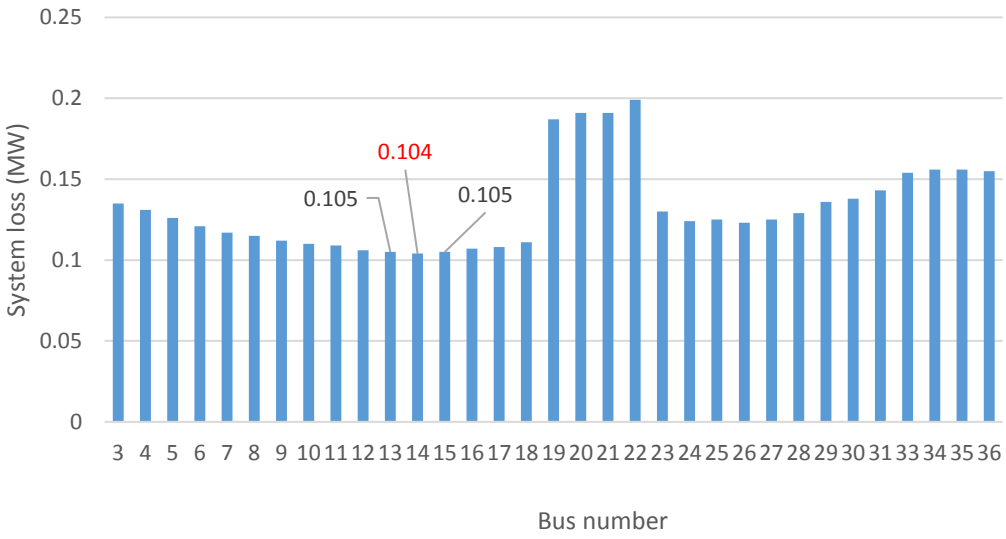

Figure 8.15 The simulation results for the third charging stations

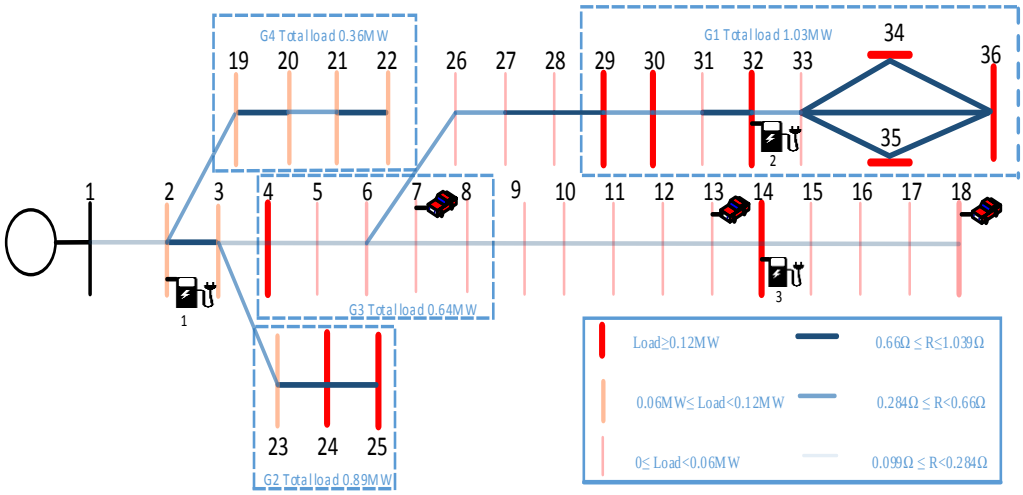

Figure 8.16 The optimal locations for the third charging station

Form figure 8.16 we can see that the optimal location for the third charging station is located relative far from station one. This is a reasonable location for charging station Form figure 8.16, we can see that the optimal location for the third charging station is located relatively far from station one. This is a reasonable location for charging station two in terms of power loss minimisation because if charging station three is installed near charging station one or two, such as in area G_3 or G_1, the energy provided by stations one and two needs to be transferred a long distance to load buses from eight to 18. If the test network voltage remains the same, more energy is needed to increase the current through the distribution line; therefore, power loss will increase. If charging station three is installed in area G_4, the power loss will also increase because station one can provide energy to the G_4 area, but in reality,

compared with the G_2 area, the line resistance between bus two to three is higher than bus two to bus 19, and that means the energy is relatively easier to transfer from charging station one to the G_4 area then to the G_3 and G_2 areas.

Therefore, there is low possibility to install charging station two in the G_4 area. However, the G_2 area has a high power demand, which means more energy needs to be transferred from charging station one. Therefore, due to the high demand in the G_2 area, there is high possibility for the fourth charging station to be installed in this area.

In the fourth charging station case, the station needs to be installed in the test DN for power loss minimisation. Before choosing the optimal location for charging station four, the test DN already installed three charging stations, which are charging station one, two and three. The GA is also used to find the optimal location for the fourth station.

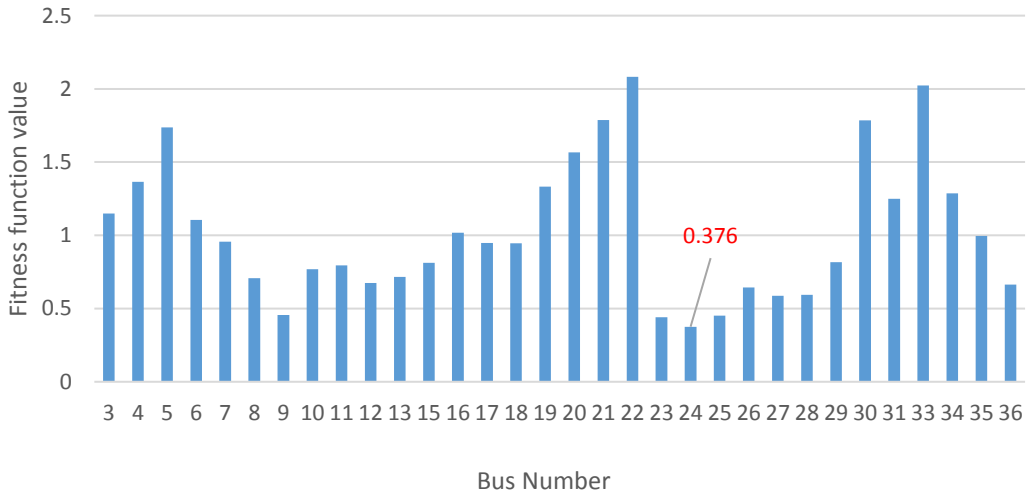

Figure 8.17 Fitness function values for the fourth charging stations

The results from figure 8.17 show that bus 24 has the lowest fitness values. The simulation results in figure 8.18 prove that when the fourth charging station is installed in the test DN, the system power loss reduces significantly compare with three charging station case.

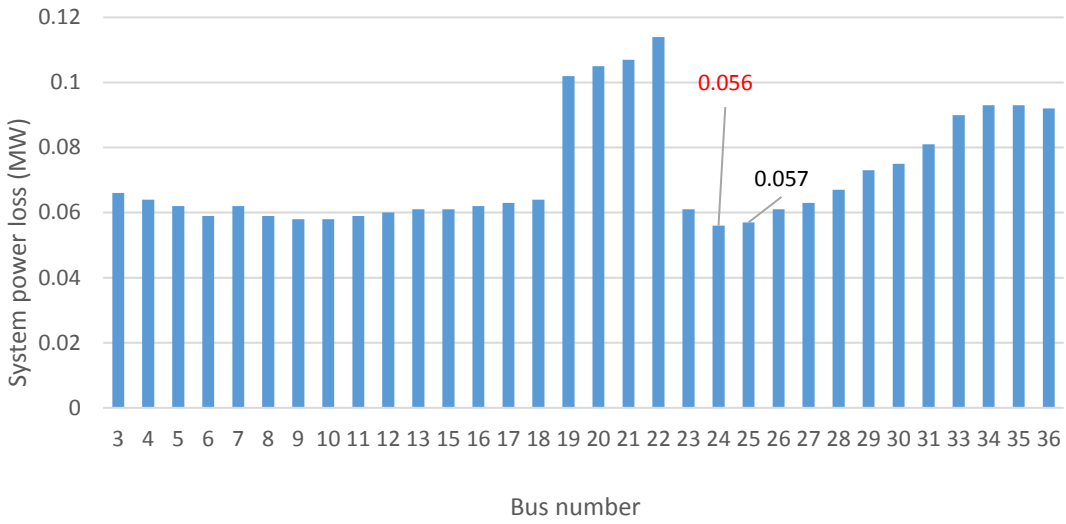

Figure 8.18 The simulation results for the fourth charging stations

Figure 8.19 shows the optimal charging station location of the fourth charging station. It is located in bus 24, which proves the deduction in the third charging station's analysis.

By installing charging station four in bus 24, this can not only provide energy to the heavy loads in bus 23, 24 and 25, but also reduce charging station one's energy supply burden. If charging station four were to be installed too near to station one, charging station one could not be fully utilised for providing energy to loads.

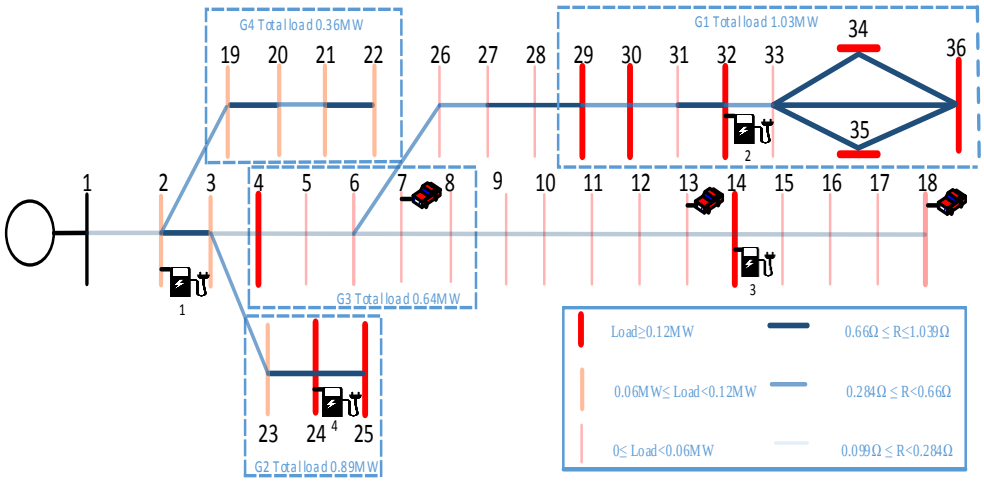

Figure 8.19 The optimal locations for the fourth charging stations

Similarly, if the fourth charging station were installed too near to station two or three, the system power loss will increase. If there is a possibility for a fifth charging station to be

installed in the test 36-bus DN, the highly possible locations are from bus seven to bus nine, or bus 26 to 28. The locations from bus seven to bus nine are near the EV charging bus, which is bus seven. That means heavy loads are there. The energy transfer distance can be reduced. The resistance between bus six and bus 26 is high, which means the energy from charging station one or other stations is hard to transfer to the loads at bus 29 and 30. Therefore, station five is also more likely to be installed between buses 26 to 28.

From figure 8.19 and the above analysis, charging station one is mainly responsible for providing energy to part of the G_3 area and the whole G_4 area. Since the distribution line's resistance from bus three to bus eight is low, this means that the energy provided by station one can be easily transferred. Although the line resistance between buses two to 19 is relativity high, compared with the resistance between bus two and bus three, it is lower, and this causes station one to be able to provide energy to the G_4 area more easily than to the G_3 area.

Charging station two is installed in the G_1 area. Not only does G_1 have high loads, but also, if there is not a charging station in this area, the energy from station one needs to be transferred a long distance and there is high resistance to the G_1 area. Therefore, the G_1 area does need a charging station to minimise power loss. If charging station two is installed towards the edge of the G1 area, the heavy loads' demands in buses 34, 35 and 36 can be satisfied, but the power loss will increase compared with installing it in the middle this area, because of high line resistance from that area.

Charging station three is installed in bus 14, which is in the middle, between buses nine and 18. Meanwhile, bus 14 also has a large power demand: the energy can be dispatched directly from station three to the loads with less power loss.

Charging station four is installed in bus 24. This is because the high resistance between buses three and 23 results in the energy from station one being difficult to transfer to the G_2 area. Although the loads in buses 23, 24 and bus 25 are near station one, high power loss will occur if there is not a charging station in the G_2 area due to high resistance. Similarly, station four may hardly provide energy to the loads in the G_3 and G_4 areas from the perspective of power loss minimisation.

8.3 Results and Analysis

Overall, from the above analysis, the choosing charging stations' location for power loss minimisation much depends on the test network's topology, line parameters and loads. By installing the charging stations in the proper locations, the power loss can be reduced.

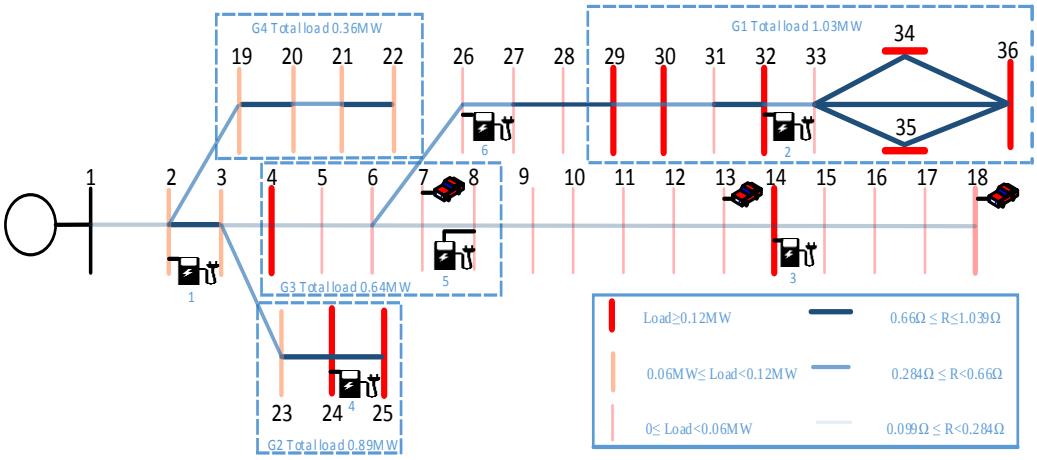

Figure 8.20 The optimal locations for the fifth and sixth charging stations

By using the same method, the fifth and sixth charging station's optimum locations are found. The optimum locations for the six charging stations can be seen from figure 8.20. Charging station five is installed in bus eight and station six is installed in bus 26, which prove the deduction in the above analysis. Installing station five in bus eight can not only provide the energy to the nearest EV charging bus, which is bus seven, but also to the loads between buses nine to 12. Charging station six, installed in bus 26, can reduce the pressure on station two in terms of transferring energy to loads between buses 26 to 30.

The sixth charging station's fitness value is also plotted, and can be seen from figure 8.21, which shows the best fitness value is 0.144. From the lower plot in figure 8.22, the GA finds the best fitness value at generation 54.

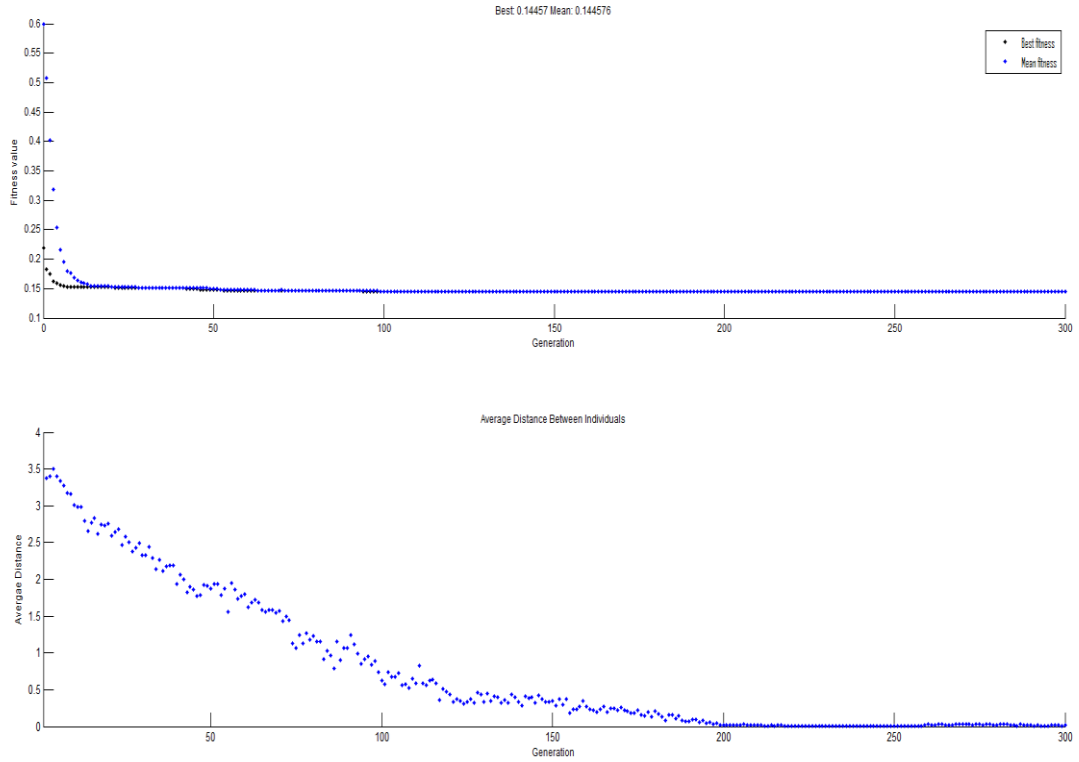

Figure 8.21 Fitness value of sixth charging station

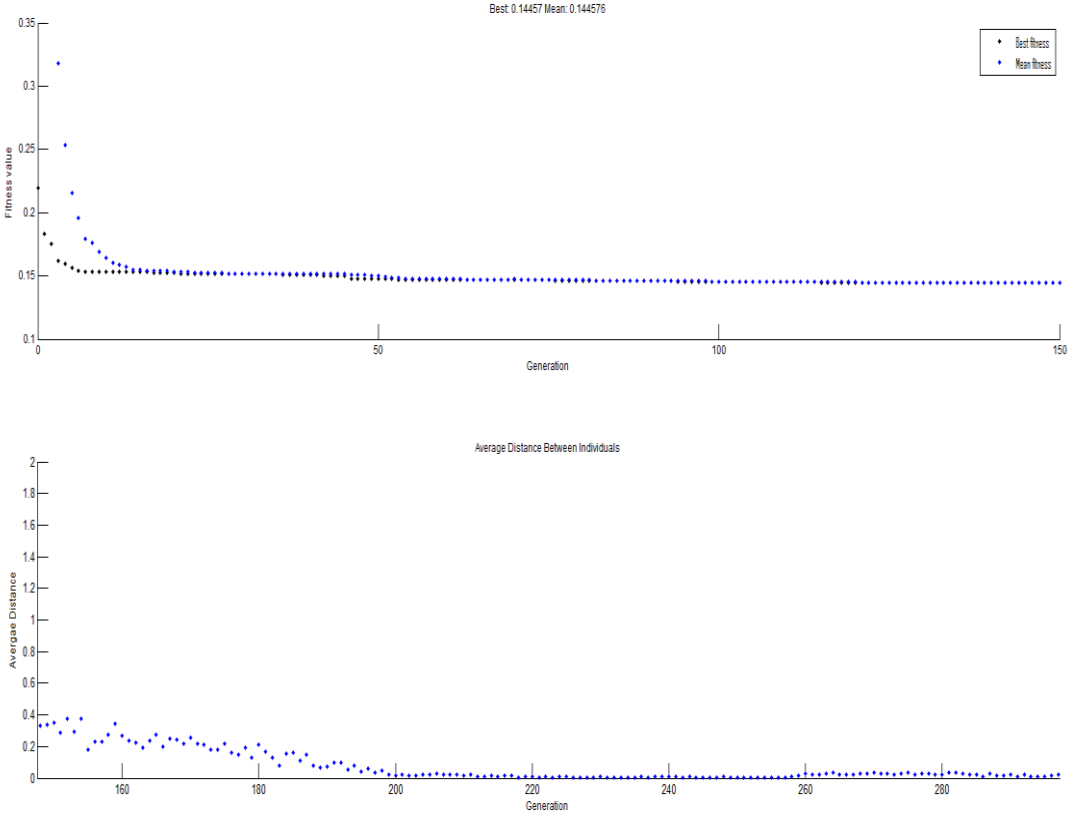

Figure 8.22 The enlarged version of figure 8.21

In order to analyse how the best fitness function values change with the increased number of stations, figure 8.23 is plotted. It can be seen that installing charging stations in the test DN results in the best fitness function's value decreasing. This is because adding charging stations to the test DN reduces the injected power to each charging station and that reduces the best fitness function's values.

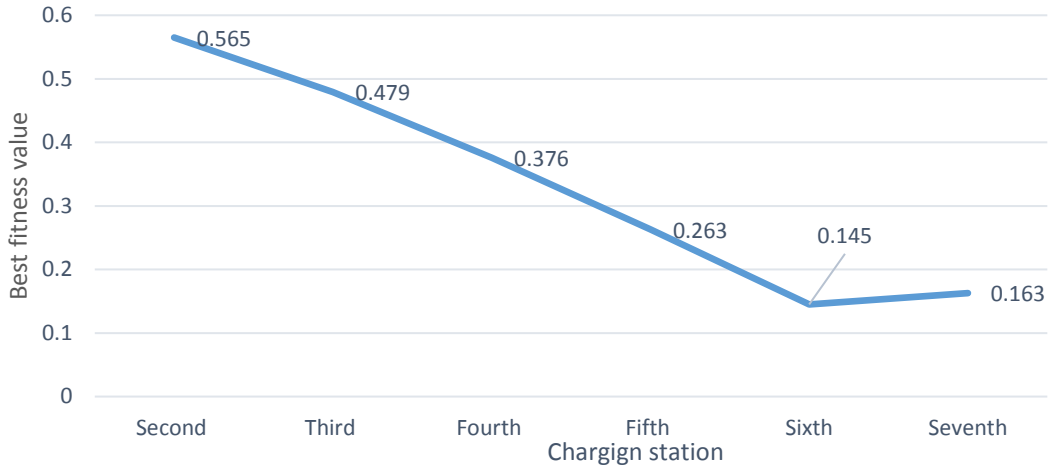

Figure 8.23 The best fitness function values and charging station

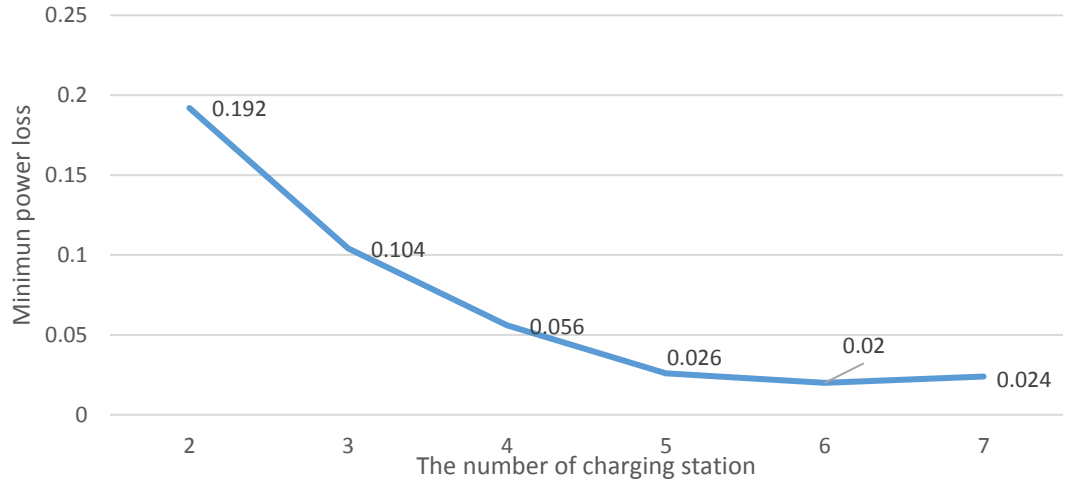

Figure 8.24 The minimum power loss of different number of stations

Installing reasonable numbers of charging stations can significantly decrease the test DN's power loss, as can be seen from figure 8.24. By installing three stations in the network, power loss reduces by 0.088 MW, compared with the situation with two stations. Compared with installing three charging stations, with six charging station, power loss is much lower. The network power loss reduces by 0.84MW when three more stations are installed in the network. Moreover, from figure 8.24, the knee point is found, we can see that by installing

charging station seven in the test DN, power loss does not decrease, but increases from 0.02 to 0.024, which means the maximum charging station number for the test DN is six, in terms of network power loss minimisation. This is because adding more than six charging stations to the DN results in the power loss increasing, so the extra power generation is wasted.

8.4 Chapter Summary

The GA is used in this chapter to find the optimal locations for charging stations for power loss reduction. The same 36-bus test DN, which is used in chapter six and seven with different loads is tested in this chapter. The results match the results in chapter six in the case of two charging stations. Compared with the quadratic optimisation method, which is used in chapter six for charging station location optimisation, the GA is much quicker to find the optimal location and is more suitable for the larger and more complex test network.

The problem of charging station location can be very complicated: for example, by using the conventional quadratic method to find six charging stations' optimal locations in a 36-bus test DN, will take more than 2,000,000 minutes, whereas by running the GA once, the objective function value of each bus can be obtained. From figure 8.21, it can be seen that the GA stalls at the 300th generation. In the GA, one generation has 300 populations: the GA needs to calculate $6 \times 300 \times 300 = 420{,}000$ times, where six means using the GA six times. If the time of one calculation is the same as with the quadratic method, then the GA can be five times quicker than this method. In reality, as shown in figure 8.22, the GA converges much more quickly (around 54 generations) than the 300 generations, so it outperforms the traditional method 22 times in terms of calculation time. This is only for the 36-bus test DN: if the DN is larger than this the GA can be much quicker than the conventional method. Therefore, the GA is a more suitable optimisation method for a larger system and for the problem of choosing more charging station locations.

Chapter 9 Conclusions and Future Work

The main target of this thesis was to minimise the power loss caused by EV penetration. In order to achieve this target, four stages were developed. The main conclusions of each of these four stages are shown below:

In the first stage, the optimised active and reactive power dispatched from the ESS was optimised to reduce the power loss. The objective function was built based on the power flow between two ESSs. Quadratic programming was chosen to be the optimiser for the optimisation. That is because of the nature of problem, the power loss of the DN is highly quadratic. The results show that by using the proposed method with 40% EV penetration, the average power loss can be reduced by 0.57MW during the time periods between 8:30 and 23:30. Moreover, 1.64MW average power can also be reduced from TN.

In the second stage, charging stations were introduced into this study for power loss minimisation. The locations of the charging stations were optimised. A comparison between the current density method used in other authors' papers and the active and reactive power dispatch method proposed in this study was made. The results showed that the current density method is not accurate for optimising the problem of two charging stations' locations, but the active and reactive power dispatch method is accurate for optimising this problem. Based on the proposed method in this study, 17% of average active power loss can be saved from three different types of loads profile. 27% of average active power loss is saved by installing two charging stations rather than no charging stations in the test-line. Finally, 2.6% of annual yield above inflation was obtained from an economic analysis of the charging stations.

In the third stage, the charging station impact factors were listed and how these impact factors affect the optimal locations was analysed. The EV charging location, line resistance, reactance, and different loads patterns were chosen as the impact factors. The active and reactive power dispatch was also used for analysing how these impact factors affect the optimal locations. The results showed that the optimal location changes simultaneously to these impact factors.

In the last stage, GA was chosen for reducing the calculation times of multiple charging stations' location choice for power loss minimisation. GA was chosen because using

traditional quadratic optimisation, the calculations take a huge amount of time: for example, to find the optimal locations for six charging stations, the traditional quadratic optimisation method takes nearly 555.56 hours, whereas by using GA, the calculations can be completed 22 times faster. The GA was tested in a 36-bus DN, and optimal locations for two charging stations proved the accuracy of the quadratic method, which was used in chapter seven and six. In addition, the optimal number of charging stations was found by analysing the results from fitness values and power loss of the test 36-bus DN.

9.1 Thesis Summary

The first chapter gives this research's motivations and challenges. With the world population increasing, so does the demand for more power. Figure 1.1 shows that in the year 2030, world electricity demand will reach 28.9 TWh. The related CO_2 emissions will reach 40.2 GT. Compared with emissions in 2015, this is an increase of nearly 5GT. CO_2 emissions are rapidly rising and this directly affects our living environment. Currently, many people are suffering from various negative impacts, such as bad air quality and global warming. In order to reduce CO_2 emissions, the majority of countries have set emission reduction targets.

In order to meet such targets, the power system has to become more environmentally friendly. However, the traditional power system cannot meet these targets. Therefore, a more advanced system is needed. By applying information and communication techniques, the system can become smarter. However, the smart power system is facing several challenges with the emergence of the large penetration of renewable energy and new types of loads, such as EV. Consequently, the system's stability and security are under pressure. In order to relieve this pressure, demand side response can be applied to the system.

As a part of an energy management system, demand side response is designed to reduce average generation costs, avoiding or delaying additional investment in TN and DN, as well as balancing loads and generation. When a large number of EVs connect to the DN, the loads increase dramatically, and this massively increased load can result in a significant amount of power loss. For the sake of decreasing power loss caused by EVs, the ESS is introduced into the grid. It has several merits, such as voltage support and power loss reduction, especially

for the power loss caused by EVs and power quality improvement. Therefore, ESS is chosen to reduce the power loss caused by EV penetration.

The second chapter illustrates the impacts of EVs on the DN. With the petrol price growing and rising awareness of the need for environmental protection, the EV will become the alternative to traditional vehicles. If EVs occupy 50% of the total vehicle market, then electricity has to increase by 8% per year.

As a new type of load (this study only considers grid to EV, EV to grid is not considered), the EV is a future alternative to traditional vehicles not only because it is less polluting to the environment because it does not produce CO_2, but also because it does not rely on petrol. These merits give the EV many advantages as a replacement for traditional vehicles, and a number of countries have encouraged people to buy EVs: the data from recent market analysis shows Norway and Netherlands have the most EV users. The next highest market shares are those of Sweden, Iceland and France.

However, an issue arises when these EVs are connected to the grid since power loss can increase dramatically. Connecting a large number of EVs to the DN can result in significant load unbalancing. Especially when these EVs connect to the DN simultaneously during on-peak time, the power loss increases dramatically, and, at the same time, it increases the insecurity levels of the DN. The energy loss rises by almost 3.7% if EV penetration increases by 10% between 18:00 and 21:00. In order to reduce the power loss caused by EVs, the ESS is introduced.

The third chapter shows why the ESS is chosen to reduce power loss in the DN, and summarises its history, specifications and benefits. As part of DSR, ESS is used for various purposes, such as voltage support, transmission and DN congestion relief, power quality improvement, and electric energy time shifting.

As shown in the second chapter, large penetration of EVs can cause a huge amount of power loss in the DN. The ESS is designed to provide energy to customers when they need it. It has the ability to store off-peak energy and dispatch it during peak times: this greatly reduces the power loss of the DN, especially during EV on-peak connection time. By installing the ESS in the DN and optimising the active and reactive power dispatches from the ESS, power loss

can be greatly reduced. A final element of this chapter is that different storage options and the ESS model are shown and built.

The fourth chapter includes mathematical optimisation and artificial intelligence techniques. These mathematical optimisations are those most commonly used in different aspects of the power system. LP is widely used in economic dispatch, optimal power flow and steady-state security region analysis. NP is used for system unit commitment, multi-area system economic dispatch, and active, reactive power optimisation. A special form of NP, QP, is especially suitable for quadratic optimisation problems, such as power loss minimisation.

AI has been used in power systems for various purposes for many years. One of them is GA. Power system operators use it to estimate generator parameters, locate TN and DN fault locations and to assess system security levels.

GA is a probabilistic search approach which is founded and based on the principle of genetics and evolution theory. It has also been used in power systems to cover power flow optimisation, economic load dispatch, power station location choice, power loss reduction. Compared with other optimisation methods, it is very suitable to solve large scale optimisation problems because it is created based on natural biological evolution.

These problem-solution tools are used in power systems for different purposes, how to choose and use the proper solution tools for minimising power loss caused by large penetration of EVs is given in chapter five.

The fifth chapter creates a new active and reactive power optimisation dispatching method based on analysing the power flow between two ESSs for power loss minimisation. QP is chosen to be the optimiser because the nature of the problem is to reduce power loss, and the power loss is highly quadratic.

Also in this chapter, the power loss caused by EV penetration is quantified. When the EVs are added to an IEEE 33-bus test DN, the percentage between total power loss and total power generation raises from 3.16% at 0% EV penetration to 5.69% at 40% penetration between 8:30 to 23:30 hours. As the EV penetration numbers increase, the power loss can increase dramatically.

In order to reduce this amount of power loss, two novel charging and discharging methods have been developed based on active and reactive power dispatching. These are coordinated active-reactive power flow of ESS and uncoordinated active-reactive power flow. These two methods are tested in the IEEE 33-bus test DN. A comparison between these two methods, in terms of power loss, is made. The coordinated charging pattern can reduce power loss by 0.03MW more than the uncoordinated one. Both coordinate and uncoordinated methods can save more power loss than the random charging method.

Installing ESS in the DN is an efficient method to achieve power loss reduction targets. With more EVs in use, the relevant charging facilities are paid more attention to than before. Chapter six discusses how to find the optimal charging station locations for power loss minimisation.

The sixth chapter develops a new active and reactive power dispatch analytical method for charging station optimisation. The proposed new method was not only tested in 11-busdistribution line, and IEEE 33-bus test DN, but also in a 36-bus test DN.

The charging station plays a key role in the EV charging process. The BESS is considered as the main part of charging station. The new analytical analysis, combined with the active and reactive power optimisation method, is developed to find the optimal locations for charging stations to minimise power loss. As the results show, 27% of average active power loss can be saved by installing two charging stations rather than no charging station.

In addition, the previously developed current density method proposed in other papers is compared with the new analytical method developed in this chapter, and the results show the current density method is not accurate for finding the optimal locations in the two stations case.

To further investigate power loss minimisation, four different operation scenarios are made. Based on these scenarios, 17% average power loss is saved by using the new method described in this chapter. In addition, an economic model for a charging station is built, the revenue, cost and profit of charging station is plotted by using that economic model, and the results show 2.6% annual yield above inflation for investing in installing and running such charge stations can be obtained.

The seventh chapter uses the active-reactive power dispatch method to analyse how impact factors, such as network loads, resistances, reactance and different EV charging locations, affect the optimal charging station's location.

Two cases are designed to test how these impact factors affect optimal charging station two's location. The first one, without any EV charging, tests how the network's loads, resistance and reactance affect optimal location. The second one tests how EV charging location changes affect the optimal charging station's location. Both these cases are tested in the 36-bus DN. Moreover, in order to illustrate how these factors affect the charging station's location, a more realistic model based on EV daily travel patterns is built and used for analysis.

The results of the analysis show that the optimal charging station location is not influenced by any single change of load pattern, line resistance, reactance or different EV charging locations. The optimal location is affected by the network topology and simultaneous changes of these impact factors.

The eighth chapter develops a GA to find the multiple charging stations' optimal locations for power loss minimisation. The purpose of using the GA is stated. The comparisons of calculation time between the quadratic optimisation method, which is used in chapter six, and GA is made. The results show the GA is more suitable for finding optimal locations with the multiple charging stations in a complex network. Moreover, the results show the GA is 22 times faster than the quadratic optimisation method.

In chapters six and seven, only two charging stations' optimal locations are found by using the quadratic optimisation method. With more EVs connected to the DN, more charging stations are needed. Installing these stations brings several problems, one of which is the optimal locations for these charging stations.

The location problem can be very complicated: if the traditional quadratic optimisation method is used to find the six charging station's optimal locations in the 36-bus test DN, it will take more than 2,000,000 times of calculations. One calculation takes one second, so the whole calculation will take nearly 555.56 hours. This is a huge amount of time, and needs high performance computers to achieve.

Overall, GA is very suitable for solving this large scale calculation problem so it is used to find six charging stations optimal locations in this chapter. A 36-bus DN is used to test the calculations. After analysis, the maximum charging station numbers for this test DN are also found. By installing these six charging stations in the DN, the whole test DN power loss reaches the minimum.

9.2 The key Conclusion and Contribution

This section contains the key conclusions and contributions of this study.

9.2.1 The Key Conclusions

This study really focuses on how to use ESS to reduce power loss caused by EV penetrations.

The mathematical model of power loss minimisation is built based on the power flow between two ESSs. Due the problem itself, it is highly quadratic and nonlinear; quadratic optimisation is chosen to be the optimiser in chapters five, six and seven.

The active-reactive power dispatch method is proposed to reduce the power loss in this study. This method is tested in an IEEE 33-bus DN. The results show how power loss changes with ESS and without ESS in different cases. The power loss difference between using the coordinated optimal active-reactive power flow method and the uncoordinated optimal active-reactive power flow method in the IEEE 33-bus test DN is also compared. By using the coordinated optimal active-reactive power flow method, the power loss is significantly reduced, and the active power from the upper substation can be reduced.

With more EVs connecting to the DN, relevant charging facilities, such as charging stations, need building more than in the past. However, installing charging stations into the DN results in several problems. One of them is how to find the optimal locations of these charging stations. This study uses a new analytical analysis combined with the active and reactive power optimisation method to identify charging station two's location. This method is tested in an 11-bus distribution line, IEEE 33-bus and 36-bus DN. The simulation results prove the accuracy of this method. Moreover, the current density method, which is proposed by other authors, is compared with the new analytical method. The results show that the analytical

method is more accurate than the current density method for finding charging station two's optimal location.

After finding the optimal location of charging station two, the same method is used to analyse how impact factors, such as different EV charging locations, line resistance, reactance and different loads, influence the optimal location of charging stations. The results show the optimal location is highly influenced by the simultaneous changes of these impact factors.

In order to optimise more charging stations in the test DN, GA based on power flow analysis is used to find the multiple charging stations' optimal locations. As shown in chapter eight, by using the traditional quadratic method, the whole calculation takes nearly 555.56 hours. That is only for six charging stations in a 36-bus test DN. When the size of the test network and the number of charging stations increase, the calculation times increase dramatically. In that situation, GA is chosen to be the optimiser. By using the GA, the optimal locations of six charging stations in the 36-bus test DN are found. The results from the GA prove the accuracy of the active and reactive optimisation method developed in chapter six. Also, by analysing the power loss of the test DN, the maximum number of charging stations are found.

9.2.1 The key Contributions

The key contributions in this thesis involves:

- Building a mathematical model based on power flow analysis between two ESS for power loss minimisation and developing the active and reactive power dispatch method to reduce the power loss caused by EV penetration.

- Developing a new analytical location choosing method to find the optimal location of charging station two in an11-bus distribution line, and a 33-bus and 36-bus test DN and comparing this with the current density method which is used in other papers.

- Developing an annual profits model for a charging station. The annual yield above inflation is calculated. The annual profit, revenue and the total cost of the charting station are also obtained.

- Using the new analytical location choosing method to analyse how different impact

factors, such as different EV charging locations, line resistance, reactance and different loads, influence optimal station location.

- Developing a GA for choosing charging station location for power loss minimisation. The GA is tested in the same 36-bus DN, and the maximum number of charging stations and their locations are optimised by the GA. The GA's result for charging station two's optimal location is compared with the traditional quadratic optimisation method's result. GA proves the accuracy of the quadratic method. Moreover, the calculation time of these two different optimisation methods is compared.

9.3 Future Work

This chapter provides several future recommendations in the area of this research. These cover voltage magnitude deviation, voltage phase imbalance and distribution transformer overload problems. In addition, since the EV to grid is not considered in this study, more research can be done in terms of using the EVs to balance loads, as well as to mitigate the shortages of renewable energy. Moreover, the research based on the optimal settings of GA can be done by other researchers.

9.3.1 The Voltage and Transformer of DN

It has been demonstrated in the thesis that connecting a large number of EVs to the DN can cause a significant increase in power losses. However, such large numbers of EVs charging may also affect DNs significantly in other aspects. These aspects include:

- Voltage drop: Voltage drop in DN can occur during the EV charging process. With more power transferred from the TN or other charging stations to satisfy EV demand, the DN line voltage drop may occur with large penetration of EV.

- Voltage phase imbalance: When DNs connect with large number of EVs the voltage at certain buses may experience imbalance because of connecting these single-phase loads. This voltage imbalance may also decrease power system security and stability level.

- Distribution transformer Overloads. The large power demands may also cause local residential transformers to overload when the apparent power loadings on the transformers exceed their rated values.

The above impacts need to be quantified with different EV penetration levels. In addition, since this thesis only considers the grid to EVs, the EV discharging process (EVs to grid) is not considered. An EV also can be regarded as a signal storage system which can provide power to the DN when fully or partly charged. This alternative energy source has two main benefits:

- Balancing Loads: It helps balance loads by peak shaving (sending the power to grid when the demands are high).

- Combining with Renewable Energy: It can store the excess energy generated by wind turbines or solar panels through the grid. When the energy is needed, it can send this energy to loads. The ESS purchasing and installing fee can be saved by using EVs as alternatives.

9.3.2 The GA Settings

In chapter eight, GA is used for choosing multiple charging station locations. The system default setting of the GA is used. Chapter eight analyses how changes in the GA default settings (such as the population size, crossover probability, mutation probability and the stall generation) influence GA performance. However, the optimised GA settings are not obtained. The GA optimal settings directly influence its performance. Therefore, finding the optimal GA settings is an avenue for future research. There is one possible solution to find the optimal setting for GA.

- Using the tradition mathematical optimisations to obtain the optimal GA settings. If the relationships between each setting and the input variables are known, the mathematical model can be built: for example, to optimise the population size of the GA, if we know the number of binary bits in each gene or the average number of bits in each chromosome, the population size can be maximised.

9.3.3 The Different GA for Location Choosing

In chapter eight, the GA is used seven times to analyse the maximum number of charging stations and the locations of each charging station. The maximum number of charging stations is obtained through analysing the sixth and seventh station's fitness function values.

However, in this case GA is only used once, and then the optimal location and number of the station can be obtained. The fitness function of this GA is built and can be seen from equation 8-1.

In order to obtain the optima number of charging station. The new variable α is embedded in the fitness function, and this variable can be optimised. When α equals one it means there is a charging station in the test DN, when α equals zero it means there is not a charging station in the test DN. The number of charging stations can also be limited by the ratio of the facility cost and service benefit, so future research needs to be completely addressing this.

The Publications

Journal Paper

C. Wang, R. Dunn, F. Robinson, B. Lian, W. Yuan, and M. Redfern, “Active-reactive power approaches for optimal placement of charge stations in power systems,” *Int. J. Electr. Power Energy Syst.*, vol. 84, pp. 87–98, 2017.

Conference papers

C.Wang,R.Dunn,Q.Yang,B.Lian,W.Yuan,J.Li, “The Active and Reactive Power Dispatch for Charging Station Location Impact Factors Analysis,” *Symp. Appl. Energy*, vol. 103, no. April, pp. 237–243, 2016.

C.Wang,R.Dunn,B.Lian,“Power loss reduction for electric vehicle penetration with embedded energy storage in distribution networks,” *2014 IEEE Int. Energy Conf.*, pp. 1417–1424, 2014.

Active-Reactive Power Approaches for Optimal Placement of Charge Stations in Power Systems

Cheng Wang, Roderick Dunn, Bo Lian, Weijia Yuan, and Miles Redfern

***Abstract*—Electric vehicles (EVs) have been suggested as alternatives to conventional vehicles for reducing petrol consumption and carbon dioxide (CO_2) emissions. When a large number of EVs connect to the grid, they can cause a large amount of power loss. Where to install multiple charge stations in the grid, so as to mitigate losses caused by EVs when providing energy to those EVs, is becoming vitally important. In this paper, a distribution test-line model is described. A new analytical method is proposed, using the stations' cooperation in terms of optimal active and reactive power dispatch as well as power flow analysis for locating the optimal placement of charge stations, so as to reduce power losses. This method is compared with the previously developed current density method [18] for single charge stations using system simulation results. It was demonstrated that the methods proposed in this paper are more accurate than the current density method, and that 17% of the average active power loss can be saved for three different types of load profile. In addition, 27% of the average active power loss was saved by installing two charge stations rather than no charge stations in the test-line. It is shown that this could represent a 2.6% annual yield above inflation for investing in installing and running such charge stations.**

***Index Terms*—Charge stations' location, EVs, active and reactive power optimisation, power loss reduction.**

Introduction

IN order to reduce CO_2 emissions, more attention is being paid to Electric Vehicles (EV) than before. However, the driving range limitation is still a big concern for all EV drivers. This problem can be solved either by improving the state-of-the-art of EV batteries or by building charge stations into Distribution Networks (DN) and Transmission Networks (TN)[1][2].

The state-of-the-art of batteries is restricted by material science and physics. The charge station is a relatively mature technology and with an increasing number of EVs will become an essential part of the commercial chain. In reference [3] the researchers concentrated on designing multi-charge stations for vehicles together with their utilisation in the grid by considering battery replacement, charging and vehicle to grid. In references [4][5] the authors considered both EV arrival time, departure time, energy demands, and real world parking statistics. Based on these data the papers provided charge station scheduling strategies. References [6][7][8] concentrated more on the optimal planning and economic aspects of a charge station for EV; by considering various costs, to achieve comprehensive cost and energy loss minimisation . As an alternative, references [9][10] focused on optimisation of EV charge station location; by using the conservation theory of regional traffic flows, taking EVs as fixed load points for the charge station. The maintenance and capital cost minimisation for a charge station was considered in this work.

In [11] the Battery Energy Storage System (BESS) was considered as a design criteria in charge stations. By using this criteria the EV charge efficiency and time was improved. In [12] the concept of combined photovoltaic systems and battery unit multi-supply systems was mentioned. In [13] the BESS was installed in fast charge stations as an energy supplier. The daily operating cost was minimised by optimising the active power of the BESS. Meanwhile, charging loads were smoothed and high-price electricity absorption from the grid was avoided.

The common drawback of these papers is that no matter what type of method were used to optimise the size and location, and to minimise the various costs of those stations, the energy transfer between charge stations was not considered. For example, combined BESSs' in charge stations can store off-peak energy and use it to provide energy to EVs during peak-time. But these charge stations do not provide energy to each other. In this paper cooperation between two charge stations, in terms of transferring energy to each other, is specified and tested for four different operation scenarios. This cooperation makes charge stations able to support each other, reduce losses further and provide energy to customers.

Installing combined BESS charge stations brings some additional problems, one of which is where to install these charge stations in the power system. In existing literature the optimal location problem has treated in the following ways. In [14] the author proposed a maximisation of the wind energy method based on Ontario's standard offer program for locating a BESS in a DN with high penetration of wind energy. In [15] the author used a hybrid Genetic Algorithm (GA) combined with quadratic programming to size and site the |BESS, so as to

reduce network losses and cost. In [16] a hybrid method relying on dynamic programming with a GA was described. Through this method the location, rating and control strategy of the BESS were found, and overall investments and network costs were minimized. A methodology proposed in [17] was to optimise the location of the BESS in DNs and also to mitigate problems created by high penetration of renewable Distribution Generation (DG). A two segment current density integration method was used in [18] for choosing the optimal location of DG in a single-DG system. The method was tested and proved using an 11-bus distribution line network.

However, these methods did not consider the active and reactive power transferring between two BESSs when choosing the location. The research described by the authors of this paper expands on the current density integration method for a two charge station system. The new method identifies the optimal location for the second charge station given the optimal location of the first charge station. The developed method was tested in the same system as [18] using four different operational scenarios. It was found that the current density method was accurate for the system with one charge station, but it could not be applied to a system that had two charge stations, under several different operational scenarios, because it only considered one current component from the BESSs. Therefore, an analytical cooperation approach, combining active and reactive power optimisation methods, was proposed to address this. This method was more accurate than the current density method. The results were compared with the current density method not only as a mathematic model, but also the cost of power loss.

After finding the locations of charge stations, the costs and profits of the charge stations were analyzed. From the results, the owners of the charge stations can earn 0.84 million dollars over 15 years'. More benefits, for example by providing voltage support and load peak shaving services to the DN could be obtained from operation.

The rest of this paper is structured as follows. In section II system modelling is introduced and an BESS model is built. Section III provides a theoretical analysis of the optimal placement of a charge station for power loss reduction and a costs and profits analysis. In this section a current density integration method and the analytical method, combined with a π line model, are presented. In section IV the old [18] and new methods' results are compared and analysed. Both methods are used with the 11-bus test-line used in [18]. Based on that test-line, four different operation scenarios were used. These cover normal working conditions (scenario one and four) and energy cooperation conditions (scenario two and three) for two charge stations, identifying the optimal location for the charge stations. Section V gives the outcomes and conclusions of the research.

System modelling

A. System load modelling

In order to test the proposed method three load periods, two off-peak (00:30-05:30 hours and 05:30-20:30 hours) and one peak (20:30- 23:30 hours), for a typical day [19] were chosen to separate each 24 hours into three power demand periods. These can be seen in Fig.1. The 11-bus distribution test-line with three different types of load profile, which can illustrate the majority of load patterns in such power systems, was used in this paper for identifying the optimal location of the charge stations [18].

It can be seen from Fig.1 that during the first and second off-peak periods the BESS can store energy from the TN, This energy can be purchased at a low price, whereas during the on-peak period the BESS can dispatch the stored energy to customers. This will not only save money on their electricity bill, but also enhance system stability [20].

B. Specifications and modelling of EVs

According to recent EV market surveys [21]-[24], the Chevrolet Volt plug-in hybrid occupied 41% of the whole electric vehicle market, the Nissan Leaf all-electric car accounted for 30%, the Toyota Prius Plug-in Hybrid took up 17%, while the Tesla Model S had the remaining 12% of the market. Therefore, an assumption was made that, for 100 EV owners, 41 used Chevrolet Volt Plug-in Hybrid cars, 30 used Nissan Leaf all-electric cars, 17 used Toyota Prius Plug-in Hybrid cars, and 12 used the Tesla Model S. The characteristics of the different electric vehicles are shown in Table I [25].

Level 1 Charging is the slowest level. It provides a single phase 120V/15A AC plug. This type of charge is suitable for the home charge during the night, no additional infrastructure is necessary [25].

Level 2 Charging is the primary option for a public or commercial charge station. This charge option can operate at up to 80A and 19.2 kW. This charging is not suitable for home and private use, but is suitable for public charging [26].

DC Fast Charging is much faster than other methods. It can be installed in charge stations, but usually requires a 480V AC input [26] and power electronics to convert AC to DC.

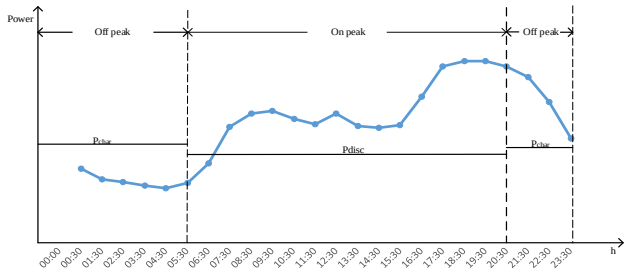

Fig.1. Three periods of daily electricity demand [15]

TABLE I
CHARACTERISTIC OF THE EV

EV Types	Level 1 Charge		Level 2 Charge		DC Fast	
	Power Demand	Time	PD	Time	PD	Time
Chevrolet Volt	0.96-1.4 kw	5-8 hours	3.8kw	2 hours	n/a	n/a
Nissan Leaf	1.8 kw	12-16 hours	3.3kw	7 hours	50k w+	15-30 m
Prius	1.4kw (120v)	3 hours	3.8kw (240v)	2.5hours	n/a	n/a
Tesla Model S	1.8kw	30+ hours	16.8 kw	4 hours	n/a	n/a

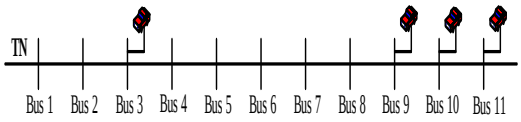

Fig.2.A test-line with EVs

In this research Level 2 Charging was chosen. The charge time was chosen as the average charge time of the four types of EV, which was four hours.

The power demand of each type of EV in one timeslot can be calculated by using equation 1 [27].

$$P_i(t) = \frac{[b_i - x_i(t)] \times C_i}{E_i H_{aver}}, \forall i, t \qquad (1)$$

where $P_i(t)$ is the power demand of the EV at any timeslot t. b_i is the desired State of Charge (SOC). $x_i(t)$ is the SOC at the beginning of t. C_i is the capacity of the EV. E_i is the battery charging efficiency of the EV., H_{aver} is the EV's average charge time.

The total power demand of all EVs can be express as shown in equation 2.

$$P_T(t) = \sum_{i=1}^{41} P_{i(t)c} + \sum_{i=1}^{30} P_{i(t)n} + \sum_{i=1}^{17} P_{i(t)p} + \sum_{i=1}^{12} P_{i(t)t} \qquad (2)$$

where $P_T(t)$ is the total power demand of all types of EVs. $P_{i(t)c}$, $P_{i(t)n}$, $P_{i(t)p}$, and P_{itt} are the power demand for each type, i.e. Chevrolet, Nissan Leaf, Prius, and Tesla.

These EVs were added into the test-line at the locations seen in Fig.2.

C. *The modelling of combined BESS charge station*

The combined BESS charge station is different compare with the traditional charge station. Traditional stations are not able to store off-peak energy and sell it to EVs and local residents at any time. Whereas, BESS can make the profits by utilising electricity price differences between peak and off-peak times. The configuration of the stations can be seen in Fig.3.

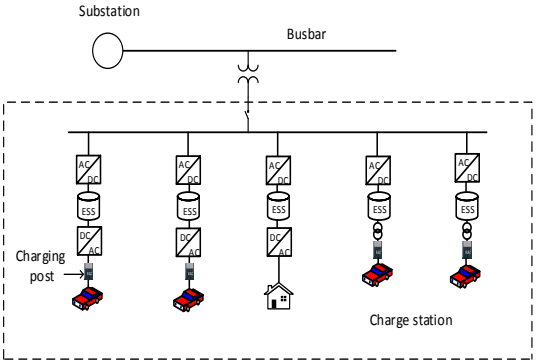

Fig.3. Charge station's configuration

The charge station consists of BESSs, normal charging points and relevant charging facilities such as transformers, active and reactive compensators, inverters and converters, and charging spaces.

The BESS consists of batteries and Power Conditioning Systems (PCS) [20][28].

A simple PCS consists of electronic devices such as capacitors, diodes and transformers, the structure can be seen in Fig.4. The PCS capability is show in Fig.5. At operation point 1 active and reactive power is being discharged to the system. At operation point 2 the system is being charged, absorbing both active and reactive power from the TN [29]. Based on the independent and rapid control capability of the PCS, active discharge and reactive power dispatch were set as controlled variables when identifying charge station two's optimal location. It is noted that active power can be either charging or discharging at any given time.

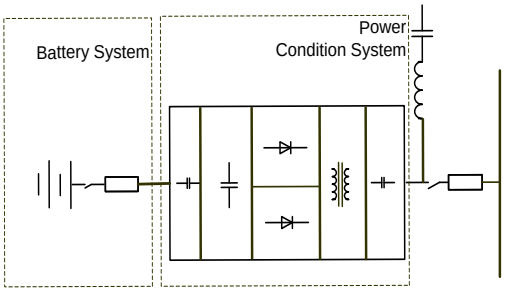

Fig.4.The structure of BESS

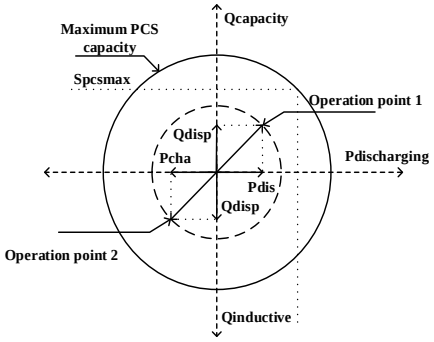

Fig.5. Active and reactive power capability [29].

The active and reactive power discharge of the BESS should not exceed the maximum apparent power S_{max} of the BESS [30].

$$P_{dis}^2 + Q_{dis}^2 \leq S_{ESSmax}^2 \quad (3)$$

$$P_{char}^2 + Q_{disc}^2 \leq S_{ESSmax}^2 \quad (4)$$

The active power for charging and discharging must be positive values

$$P_{char(k,h)} \geq 0, \qquad P_{dis(k,h)} \geq 0 \quad (5)$$

$$-S_{ESSmax(k,h)}^2 \leq Q_{dis\,(k,h)} \quad (6)$$

Moreover the upper and lower bound of the storage capacity should satisfy.

$$E_{min} \leq E_{Low}, \qquad E_{Up} \leq E_{max} \quad (7)$$

D. The EV's impact modelling and four operation scenarios

For the sake of modelling the EV's impact in terms of active and reactive power losses, and observing the power losses for the test-line without a charge station, with one charge station and with two charge stations, power flow analysis was used.

Four different operation scenarios, in terms of the cooperation between two charge stations, are listed below. The first scenario is for normal EV charge requirements, where a regular amount of drivers charge their EVs at the charge station. The second and the third scenario are designed for some exceptional events, where one charge station runs out of energy and needs to borrow it from other sources. The last scenario is where the EV's energy requirements exceed both charge stations' designed capacity; this time both stations need external energy from the TN.

(1)The first scenario is the most common one, both charge stations used their full charged capacity to charge EVs without any optimised power charge and discharge.

(2)The second scenario considers both charge and discharge processes as charge station two runs out of rated energy. Charge station one needs to transfer energy to charge station two. The active and reactive discharge power from station one will be optimised.

(3)The third scenario also considers both charge, discharge processes, but here charge station one runs out of rated energy. Charge station two needs to transfer energy to charge station one. The active discharge and reactive dispatch power from station two will be optimised.

(4)The fourth scenario is where both charge stations one and two cannot supply the EVs and loads. External energy from the TN is used to charge stations one and two. The active and reactive power from the TN will be optimised to charge both stations. Tables II-IV show comparisons of active and reactive power losses without charge stations, with one charge station and with two charge stations in 11-bus distribution test-line.

TABLE II
FIRST SCENARIO COMPARISON OF POWER LOSS

First scenario	Without stations		Charge station one		Both charge stations	
	P_{loss}	Q_{loss}	P_{loss}	Q_{loss}	P_{loss}	Q_{loss}
Uniform	0.682	0.59	0.616	0.53	0.190	0.25
Central	0.251	0.22	0.215	0.18	0.058	0.06
Increasing	0.565	0.49	0.532	0.46	0.171	0.21

TABLE III
SECOND SCENARIO COMPARISON OF POWER LOSS

Second scenario	Without stations		Charge station one		Both charge stations	
	P_{loss}	Q_{loss}	P_{loss}	Q_{loss}	P_{loss}	Q_{loss}
Uniform	0.682	0.59	0.801	0.69	0.596	0.51
Central	0.251	0.22	0.319	0.27	0.215	0.18
Increasing	0.565	0.49	0.655	0.56	0.387	0.33

TABLE IV
THIRD SCENARIO COMPARISON OF POWER LOSS

Third scenario	Without stations		Charge station one		Both charge stations	
	P_{loss}	Q_{loss}	P_{loss}	Q_{loss}	P_{loss}	Q_{loss}
Uniform	0.682	0.59	0.741	0.64	0.136	0.14
Central	0.251	0.22	0.284	0.24	0.093	0.08
Increasing	0.56	0.49	0.609	0.52	0.094	0.08

Theoretical analysis

The main focus of this paper is to identify charge station two's optimal location. In practice, there are many additional constrains for the optimisation of charge station's location, such as different countries' energy policies and geographic factors. This paper does not consider these factors.

Analytical approach for optimal location

In order to reduce the power loss caused by EV penetration, a distribution network with charge stations one and two, which are S_1 and S_2 are shown in Fig.6, and the π line model [31] was created and developed for analysing the location of station two for loss reduction. The active, reactive power flow, bus voltage and current of π line model are given by equations 8-14.

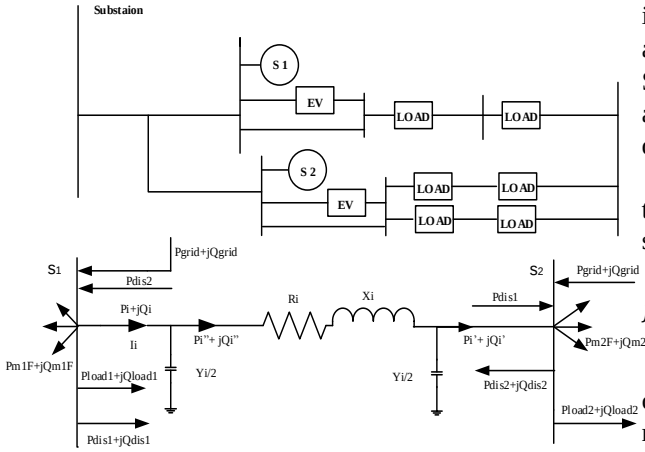

Fig.6. Power flow analysis

P_i and Q_i are the sending-end active and reactive power through bus S_1 and S_2

$$P_i = P_i' + R_i \frac{P_i'^2 + Q_i'^2}{V_{s2}^2} \quad (8)$$

$$Q_i = Q_i'' - V_{s1}^2 \frac{Yi}{2} = Q_i' + X_i \frac{P_i'^2 + Q_i'^2}{V_{s2}^2} - V_{s1}^2 \frac{Yi}{2} \quad (9)$$

P_i' and Q_i' are the injection active power and reactive power to bus S_2 respectively

$$P_i' = P_{dis2} + P_{load2} + P_{m2F} - P_{grid} - P_{dis1} \quad (10)$$

$$Q_i' = Q_{dis2} + Q_{load2} + Q_{m2F} - Q_{grid} - Q_{dis1} - V_{s2}^2 \frac{Yi}{2} \quad (11)$$

The voltage at bus S_2 is

$$V_{s2} = V_{s1} - I_i Z_i = V_{s1} - \frac{S_i''^*}{V_{s1}^*}(R_i + \mathrm{j}\, X_i) \quad (12)$$

$$V_{s2} = V_{s1} - \frac{P_i'' - jQ_i''}{V_{s1}}(R_i + \mathrm{j}\, X_i) = \left(V_{s1} - \frac{P_i'' R_i + Q_i'' X_i}{V_{s1}}\right) - \mathrm{j}\left(\frac{P_i'' X_i - Q_i'' R_i}{V_{s1}}\right) \quad (13)$$

The current through the π line model is

$$I_i = \sqrt{\frac{P_i^2 + Q_i^2}{V_{s1}^2}} \quad (14)$$

The series impedance and shunt admittance between bus S_1 and S_2, are $(\mathrm{R_i} + \mathrm{j\, X_i})$ and Yi/2 respectively. P_i' and Q_i' are the injection active power and reactive power to bus S_2 respectively. P_{dis} and Q_{dis} are the active and reactive discharge power of station.

Where $S_i'' = P_i'' + Q_i''$, $P_i'' = P_i$, $Q_i'' = Q_i + V_{s1}^2 \frac{Yi}{2}$. P_{grid} and the Q_{grid} are the active and reactive power injected by the TN. P_{load1}, P_{load2}, Q_{load1}, and Q_{load2} are the total active and reactive power load at bus S_1 and S_2. P_{m1F}, P_{m2F}, Q_{m1F} and Q_{m2F}, are the sum of active and reactive power flows through all downstream branches connected to buses S_1 and S_2.

To find the optimal location of charge station two, an objective function was built and can be seen from equation 16.

$$f_j = \sum_{i=1}^{j} R_{1i(j)} |P_i' + jQ_i'|^2 \quad j = 3,4,5 \cdots\cdots N \quad (15)$$

The goal is to find the optimal location for charge station two, where equation 16 reaches the minimum value.

$$F_m = Min f_j \quad (16)$$

The $R_{1i(j)}$ is the resistance between two charge stations. N is the test system's total bus number. P_{load2} is the load at bus S_2. P_{m2F} is active power injection from bus S_2. P_{dis1} and P_{dis2} can be obtained from equation 17 by using the MATLAB optimisation programming.

$$Min\ P_L = \sum_{\forall s_1, s_2}^{s_1, s_2 \in S_B} I_i^2 R_i = \sum_{\forall s_1, s_2}^{s_1, s_2 \in S_B} \left(\frac{P_i^2 + Q_i^2}{\mathrm{V_{s_1}}^2}\right) R_i \quad (17)$$

Both equation 16 and 17 must satisfy the constraints, based on equations in 3-7 and 18-23.

The active and reactive power flow in π line model must satisfy the equations 18-19.

$$P_i - P_i' - R_i \frac{P_i'^2 + Q_i'^2}{V_{s2}^2} = 0 \quad (18)$$

$$Q_i - Q_i' - X_i \frac{P_i'^2 + Q_i'^2}{V_{s2}^2} + V_{s1}^2 \frac{Yi}{2} = 0 \quad (19)$$

The voltage magnitudes at the sending bus and receiving bus must satisfy the equation 20.

$$V_{s2}^2 - \left\{V_{s1}^2 - 2(P_i'' R_i + Q_i'' X_i) + \frac{(P_i''^2 + Q_i''^2)(R_i^2 + X_i^2)}{V_{s1}}\right\} = 0 \quad (20)$$

The line current of the π line model should be within the thermal limit

$$I_i \le I_i^{rated} \quad (21)$$

The bus voltages should not exceed the maximum and below the minimum voltage

$$V_{s1}^{min} \le V_{s1} \le V_{s1}^{max} \quad (22)$$

$$V_{s2}^{min} \le V_{s2} \le V_{s2}^{max} \quad (23)$$

The theoretical procedures to find the optimal bus to locate station two are summarized below:

(1)Add EVs randomly into the 11-bus test-line.

(2)Run simulations and use power flow analysis to find the largest power loss bus and install charge station one there.

(3)Use the π line model in Fig.6 to analyse the power loss between S_1 and S_2, which can be seen from equation 8 to 17.

(4)Set P_{dis1}, P_{dis2}, Q_{dis1}, Q_{dis2}, as the variables for power losses minimisation.

(5)Use MATLAB optimisation programming to obtain these variables' values from equation 17.

(6)Use these values as the input values for objective function 16 and get values of each bus.

(7)Compare the objective function's values with the simulation results.

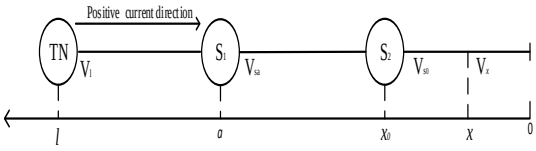

Fig.7.A test-line with distributed load

The current density method for optimal location

In previous research the phase current density method was used for analysis of power losses and identifying a DG's optimal location in a one DG system [18]. In this paper phase current I_i density was used for the same purpose, but different power cooperation strategies, between charge station one and two, were considered.

Using the current density method, the phasor feeder current at point x is

$$I(x,T_i) = \int_0^x I_d\,(x,T_i)dx \tag{24}$$

The incremental power loss at point x is

$$dP(x,T_i) = \left(\left|\int_0^x I_d\,(x,T_i)dx\right|\right)^2 \cdot Rdx \tag{25}$$

The total power loss along the feeder within the time duration T_i is

$$P_{loss}(T_i) = \int_0^l dP(x,T_i) = \int_0^l \left(\int_0^x I_i(x,T_i)\,dx\right)^2 \cdot Rdx \tag{26}$$

Firstly, it is considered that there is only one charge station in the test distribution line at location x_0 shown in Fig.7. As a result of charge station two being added into the distribution line, two parameters (load current density $I_d(x,T_i)$ and load current) are changed in terms of current. The load current density will decrease, caused by voltage improvements due to adding station two, this decrease causes the feeder current to decrease.

Meanwhile, with station two's current injection, the feeder current between the TN at l and the location of station two at x_0 will also change. But, compared with the change of load current density, the change of injected current from station two is influenced more by the change in feeder current. Hence, the change of load current density, caused by adding charge station two is neglected in this paper [18]. Therefore, the feeder current after adding station two can be obtained by using the load current density$I_d(x,T_i)$.

Secondly, consider the second charge station which is station one adds in to test-line similarly. The change in the feeder current caused by injected current from station one is much higher than the change in the load current density. Therefore, the feeder current $I(x,T_i)$can be expressed by using the $I_d(x,T_i)$ after two adding the charge station one and two. It can be seen from equation 27.

The feeder current $I(x,T_i)$ through that test line can be expressed as:

$$I(x,T_i) = \begin{cases} \int_0^x I_d(x,T_i)dx & 0 \le x \le x_0 \\ \int_0^x I_d(x,T_i)dx - I_{disc2} & x_0 \le x \le a \\ \int_0^x I_d(x,T_i)dx - I_{disc1} & a \le x \le l \end{cases} \tag{27}$$

The corresponding power loss in the feeder is

$$\begin{aligned} P_{loss}(x_0,T_i) &= \int_0^{x_0} \left(\left|\int_0^x I_d(x,T_i)dx\right|\right)^2 Rd_x \\ &+ \int_{x_0}^{a} \left(\left|\int_0^x I_d(x,T_i)dx - I_{disc2}\right|\right)^2 Rd_x \\ &+ \int_a^l \left(\left|\int_0^x I_d(x,T_i)dx - I_{disc1}\right|\right)^2 Rd_x \end{aligned} \tag{28}$$

The average power loss in a given time period T is

$$\overline{P_{loss}}(x_0) = \frac{1}{T}\sum_{i=1}^{N_t} P_{loss}(x_0,T_i)\,T_i \tag{29}$$

Where N_t is the number of time durations in the time period T.

The target to minimise total average power loss

$$Target = Min\,P_{loss}(T) \tag{30}$$

The solution x_0 of the equation 31 will give equation 30 the optimal site for power loss minimising.

$$\frac{\overline{P_{loss}}(x_0)}{d_{x_0}} = 0 \quad (31)$$

Assuming that charge station two is located at point x_0 according to equation 28, the effective power loss of the test feeder is

$$P_{loss}(x_0, T_i) = A + B + C \quad (32)$$

$$A = [I_d^2(T_i) \cdot R \frac{x_0^3}{3})] \quad (33)$$

$$B = \left[I_d^2(T_i) \cdot R \frac{a^3 - x_0^3}{3} + I_{disc2}^2(T_i) \cdot R(a - x_0) + I_d(T_i) I_{disc2}(T_i) R(a^2 - x_0^2) \right] \quad (34)$$

$$C = \left[I_d^2(T_i) \cdot R \frac{l^3 - a^3}{3} + I_{disc1}^2(T_i) \cdot R(l - a) + I_d(T_i) I_{disc1}(T_i) R(l^2 - a^2) \right] \quad (35)$$

where $I_d(x, T_i) = \frac{I_{load}(x, T_i)}{l}$, I_{load} is the load current at the sending-end of the feeder.

According to 31 and from the equation 33 to 35, equation 31 can be deduced as below

$$I_d^2(T_i)\, R x_0 - I_{dis2}^2(T_i) \cdot R - 2 I_d(T_i) I_{dis2}(T_i) R x_0 = 0 \quad (36)$$

x_0 is obtained as below:

$$x_0 = \frac{l \cdot \sum_{i=1}^{N_t} I_{dis2}^2(T_i) T_i}{2 \sum_{i=1}^{N_t} I_{load}(T_i) I_{dis2}(T_i) T_i} \quad (37)$$

Assuming the bus voltage along the feeders are in acceptable range, x_0 can be approximated as below:

$$x_0 = \frac{l \cdot \sum_{i=1}^{N_t} P_{dis2}^2(T_i) T_i}{2 \sum_{i=1}^{N_t} P_{load}(T_i) P_{dis2}(T_i) T_i} \quad (38)$$

The goal is achieved by considering the power cooperation between both charge stations and using the equation 31 to identify the optimal location for station two. It is assured that the voltage along feeder are in acceptable range 1 ± 0.05 p.u.and the transferred power is under line thermal limit.

The solution of $x_0$of gives the optimal location of station two for the minimising of power loss for the test-line. It is assured that the voltage and transferred power are within system limitations. The theoretical procedures to find the optimal location of charge station two are summarised as follows:

(1)Add EVs randomly into 11-bus test-line.

(2)Run power flow analysis, and find the largest power loss bus and install charge station one there for four different operation scenarios.

(3)Find the distributed load $I_d(x, T_i)$ along the feeder l.

(4)Express the feeder current by using three segment current density integration methods.

(5)Use equation 27 and 31 to calculate the average power loss and identify the optimal location x_0 for charge station two.

(6)Compare the optimal location x_0 with the system simulation's location.

The annual profit of the charge station

In order to calculate the profit of charge station, the revenues and costs of the station are obtained.

(1) The profit of the charge station is in equation 39.

$$P_{EVCSi}(t) = \sum_{t=1}^{T} R_{EVCSi}^T(t) - \sum_{t=1}^{T} C_{EVCSi}^T(\mathrm{t}) \quad (39)$$

where $P_{EVCSi}(t)$ is the annual profit of charge station, $R_{EVCSi}^T(t)$ is revenue of charge station and $C_{EVCSi}^T(\mathrm{t})$ is total cost of station, T is the life time of station.

$R_{EVCSi}^T(t)$ can be expressed in equation 40.

$$R_{EVCSi}^T(t) = \sum_{t=1}^{T} [C_{pi}^{on}(t) E_{EV} T_{CHi} + C_{pi}^{off}(t) E_{Re} T_{CHi}] \quad (40)$$

where $C_{pi}^{on}(t)$ is the peak electricity price, C_{pi}^{off} is the off-peak price. E_{EV} and E_{Re} are the energy demand of EVs and local residents. T_{CHi} is the annual utilization hours of charging devices.

(2) The cost of the charge station includes investment cost$C_{EVCSi}^I(\mathrm{t})$, operation cost$C_{EVCSi}^O(\mathrm{t})$, maintenance cost $C_{Evcsi}^M(t)$ the network loss cost [32] can be shown in equation 41.

$$C_{EVCSi}^T(\mathrm{t}) = \sum_{t=1}^{T} [C_{EVCSi}^I(\mathrm{t}) + C_{EVCSi}^O(\mathrm{t}) + C_{Evcsi}^M(t)] \quad (41)$$

The investment cost of charge station can be expressed in equation 42.

$$C_{EVCSi}^I(\mathrm{t}) = C_{ETi}^I(\mathrm{t}) S_{ETi} + C_{CHi}^I(\mathrm{t}) S_{CHi} + C_{DEi}^I(\mathrm{t}) S_{DEi} + C_{EAi}^I(\mathrm{t}) F_{EAi} + C_{Bsi}^I(t) \frac{E_B}{\eta CHij} \quad (42)$$

where C_{ETi}^I, C_{CHi}^I, C_{DEi}^I and C_{Bsi}^I are the capacity per-unit investment cost of transformers, charging devices, other devices and batteries. C_{EAi}^I is the land utilization cost. S_{ETi} are the transformers' capacities. S_{CHi} is the total capacity of the charging devices (including chargers, charging points). S_{DEi} is the total capacity of other devices except transformers and charging devices (for example loads and lighting). F_{EAi} is the area of *i*th charge station. E_B is the capacity of battery. ηCHij is the charging efficiency.

$$S_{ETi} = \frac{(S_{CHi} + S_{DEi})}{L_{EVCSi}^{max}} \quad (43)$$

where L_{EVCSi}^{max} is the daily maximal load rate of the *i*th EV charging station.

S_{CHi} is the rated power

TABLE V
THE COMPARISONS BETWEEN TWO METHODS FOR THE FIRST SCENARIO CENTRALLY LOAD

Method	Power Loss expressions	Location expression	Location	Simulation results	Power loss($)
Current density	$P_{loss}(T_i) = \int_0^l dP(x,T_i)$	$\frac{\overline{P_{loss}}(x_0)}{d_{x_0}} = 0$	$0.22l$ (BUS9)	BUS 8	$12,902
P,Q dispatch	$P_{loss}(T_i) = \sum_{\forall S_1,S_2}^{S_1,S_2 \in S_B} \left(\frac{P_i^2 + Q_i^2}{V_{s_1}^{\ 2}}\right) R_i$	$Min\, f_j = \sum_{i=1}^{j} R_{1i(j)} \lvert P_i' + jQ_i' \rvert^2, j = 3,4,5 \cdots\cdots N$	BUS 8	BUS 8	$11,692

$$S_{CHi} = K_i \sum_{j=1}^{n_i} S_{CHi}$$
$$= K_i \sum_{j=1}^{n_i} (P_{CHij/\eta CHij \cos \emptyset CHij}) \quad (44)$$

where n_i and K_i are the number and simultaneity coefficient of the charging devices in *i*th charge station. P_{CHij} is the output active power. $\cos \emptyset\, CHij$ is the power factor and ηCHij is the charging efficiency in charging station.

The operation cost of *i*th charge station can be expressed in equation 45, which include charging cost $C_{CHi}^O(t)$, power consumption cost $C_{EEi}^O(t)$, active power filtering and reactive power compensation cost $C_{VCi}^O(t)$, battery operation cost $C_{CBi}^O(t)$, and human resources cost $C_{HRi}(t)$.

$$C_{EVCSi}^O(\mathrm{t}) = C_{CHi}^O(t) + C_{EEi}^O(t) + C_{VCi}^O(t) + C_{CBi}^O(t) + C_{HRi}(t)$$
$$= C_{pi}^{off}(t) P_{chi}^N T_{CHi} + C_{pi}^{off}(t) P_{EEi}^{max} T_{EEi} + C_{VCi}^O(t) + C_{Bsi}^O(t) P_{ES} + C_{HRi}(t) \quad (45)$$

where P_{chi}^N is the rated power of charging devices. T_{CHi} is the annual utilization hours of charging devices. P_{EEi}^{max} and T_{EEi} are the maximal power consumed and annual utilization hours of the electric devices respectively. $C_{Bsi}^O(t)$ is the operation cost of battery per unit and P_{ES} is capacity of battery.

The maintenance cost of charge station in the planning period can be express in equation 46.

$$C_{Evcsi}^M(t) = C_{ETi}^M(t) S_{ETi} + C_{CHi}^M(t) S_{CHi} + C_{DEi}^M(t) S_{DEi} + C_{BSi}^M P_{ES} \quad (46)$$

where $C_{ETi}^M(t)$, $C_{CHi}^M(t)$, C_{DEi}^M and C_{BSi}^M are the transformers, charging devices, other devices and batteries' per-unit capacity maintenance cost in *i*th charging station.

Network loss cost can be expressed in equation 47.

$$C_{PS}^L(t) = C_{Pi}^{on}(t) T_h P_{Loss} \quad (47)$$

where $C_{Pi}^{on}(t)$ is the on-grid price of electricity. T_h is the annual utilization hour, and P_{Loss} is the entire network loss.

(3) The yield per year for charge station can be express in equation 48.

$$Y_{EVCSi}(t) = \frac{\sum_{t=1}^{T} P_{EVCSi}(t)}{[\sum_{t=1}^{T} C_{EVCSi}^T(\mathrm{t})\,]T} \times 100\% \quad (48)$$

where $Y_{EVCSi}(t)$ is the average annual yield of charge station. T is the life time of charge station.

In order to mitigate the price inflation in 15 years the Net Present Value (NPV) is used

$$P_{Rt}(t) = P_{NPV} \times (1+i)^t \quad (49)$$

where P_{Rt} is the net cash flow, P_{NPV} is the net present value, *i* is the discount rate, *t* is the time of cash flow.

Simulation results and discussions

The proposed method is applied to four different types of load profile in a test-line. The main aim is to demonstrate that the analytical method is suitable for identifying station two's locations under four different operation scenarios in terms of power loss reduction.

First scenario three different load profiles

For a uniformly distributed load, by comparing the objective function's values from equation 15 at each bus, bus 10 was obtained as the optimal location as the result of adding charge station two. By using the current density method the optimal location is $0.09l$ which is near bus 10. In this case both methods have the same result.

For the centrally distributed load, the optimal location x_0 is bus 8 using the analytical method. Whereas, by using current density method the optimal location x_0 is $0.22l$, which is near bus 9, not very accurate when compared with simulation results. Moreover, the non-optimal location can lead $ 1,210 of power loss than the optimal one.

For the increasing distributed load, the optimal location x_0 is bus 10, the bus 11 does not meet the design requirement as it can only provide energy to the load at bus 10. Whereas the current density method is $0.21l$, near bus 9. Compared with simulation results it is not accurate.

The Objective function's values and simulation results are shown in Fig.8, and Fig.9. By using the analytical method, the optimal location for charge station two for both uniformly load and increasingly

load type profiles are bus 10. For centrally load is bus 8. Simulation results prove analytical approach.

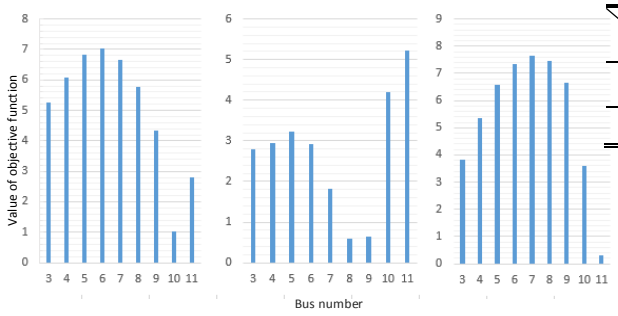

Fig.8. Objective function's values of the first scenario of three load profiles

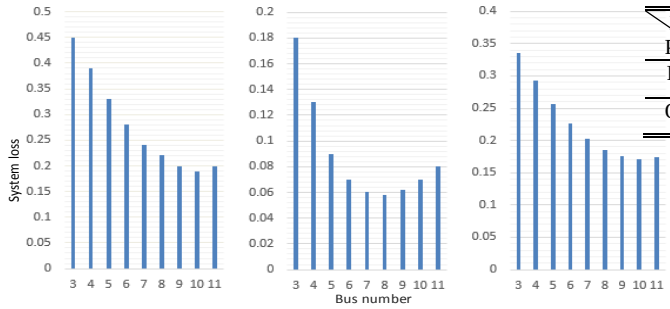

Fig.9. Simulation results of the first scenario of three load

Second scenario three different load profiles

For the second scenario P_{dis1} and Q_{dis1} is optimised. $P_{dis2} = 0$, $Q_{dis2} = 0$, $P_{char2} = P_{dis1}$, $P_{optimal} = P_{dis1}$. Different optimised active and reactive power of charge station one are shown in Table VI. They are used as input data of equation 15.

The objective function's values for three types of load profile show in Fig.10.

The simulation results demonstrate the analytical approach, bus 11 in this scenario does not meet the design requirements which cannot provide the energy to the load nearby. Therefore, bus 3 is chosen for three types of load.

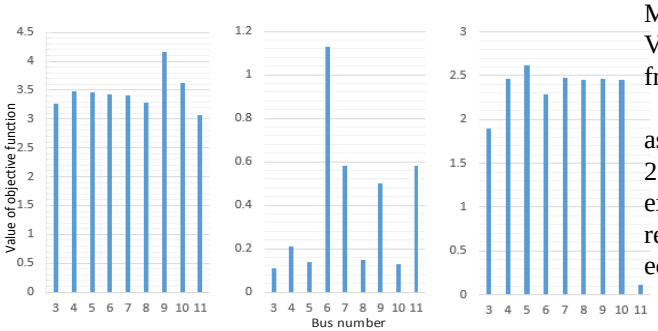

Fig.10. Objective function's values for the second scenario of three load profiles

TABLE VI
P , Q STATION ONE AT DIFFERENT LOCATIONS FOR UNIFORMLY LOAD

No. / P,Q	3	4	5	6	7	8	9	10	11
P_{dis}	3.88	3.84	3.80	3.58	3.25	2.69	2.08	1.47	1.15
Q_{dis}	1.25	1.37	1.61	1.21	1.05	0.93	0.62	0.48	0.27

Third scenario three different load type

For the third scenario, P_{dis2} and Q_{dis2} is optimised. $P_{dis1} = 0$, $Q_{dis1} = 0$, $P_{char1} = P_{dis2}$, $P_{optimal} = P_{dis2}$. Differently optimised active and reactive power of charge station two shows in Table VII.

TABLE VII
P,Q STATION TWO AT DIFFERENT LOCATIONS FOR UNIFORMLY LOAD

NO. / P,Q	3	4	5	6	7	8	9	10	11
P_{DIS}	3.81	3.79	3.77	3.63	3.20	2.68	2.03	1.09	0.58
Q_{DIS}	1.47	1.50	1.56	1.29	1.19	0.93	0.61	0.48	0.27

The objective function's values meet the simulation results in this scenario for three different types of load profile. The optimal location for uniformly load type is bus7, for centrally load type is bus 5, for increasingly load type is bus 8. The simulation results prove the analytical method.

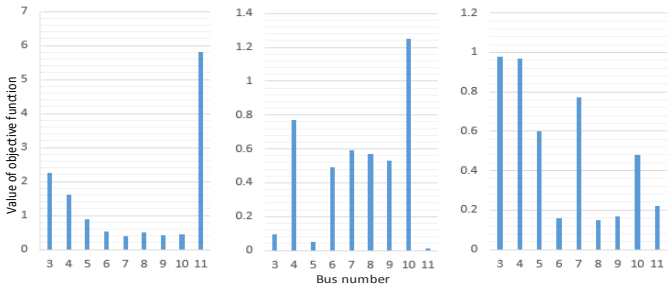

Fig.11. Objective function's values for the third scenario of three load profiles

Fourth scenario three different load profiles

For the fourth scenario, $P_{dis1} = 0$, $Q_{dis1} = 0, P_{dis2} = 0, Q_{dis2} = 0$. Active and reactive power from grid are optimised and obtained by using the MATLAB optimisation programming. The Table VIII shows the different active and reactive power from the TN for uniformly load.

For this scenario, both charge stations are regarded as the loads. The charge station one is added into bus 2, charge station two is added to the flowing bus except bus 2. The differently optimised active and reactive power from TN are set as the input data of equation 15.

TABLE VIII

P_{GRID} ,Q_{GRID} FROM TN AT DIFFERENT LOCATIONS FOR UNIFORMLY LOAD

No. / P,Q	3	4	5	6	7	8	9	10	11
P_{dis}	9.45	9.51	9.56	9.62	9.67	9.72	9.77	9.83	9.85
Q_{dis}	2.95	3.00	3.04	3.09	3.14	3.18	3.22	3.25	3.27

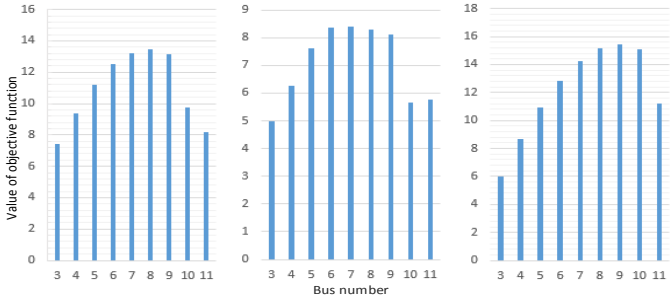

Fig.12. Objective function's values for the fourth scenario of three load types

Regarding the first scenario, for the uniformly load and increasingly load, the station two's location is bus 10 and it is relatively far from bus one's location. Therefore, the power loss caused by the edge of test line is much smaller than the one installed in the middle. For the centrally load the station two location moves a little closer to the centre because of the load type.

For the second scenario, station one needs to transfer energy to station two. For all three types of load the location of station two is bus 3, because in this situation station two was regarded as the largest load and cannot provide any energy to the loads. Therefore, the optimal locations for all three types of load is bus 3.

For the third scenario, charge station two needs to deliver energy to station one. For uniformly load type, station two location is bus 7. Because bus 7 is in the middle area of test line, it is not far from station one and the load at the edge. For the centrally load type the location is bus 5, which is in the centre of the test line, near to the largest load bus 6 and the second largest load bus 2. For increasingly load type the location is bus 8. For this load type, if station two is installed at the end of the test line the power loss will increase during the energy transmission to station one. Hence, bus 8 is the ideal location.

With regard to the fourth scenario. When both charge stations run out of rated energy, charge station two's location is bus 3 for three different loads. Because for uniformly load and centrally load, bus 2 and 3 are the largest load bus. Meanwhile, bus 3 is the nearest bus to the transmission network, so that the network does not need deliver as much power to bus 3 as to others. For increasingly load, although the largest load is bus 10 when the station is seen as load and added into that bus. Bus 3 is the second largest load of the system, and only less than the largest load bus 10, 0.87MW. Bus 10 is at nearly the end of this test line so that much more energy needs to be transferred to that bus. Therefore, for this scenario the location for station two is bus 3.

Discussion

The Table IX shows the optimal locations for charge station two in the test-line for power loss reduction. From the system operating view point, four different operation scenarios have different station two's locations. They give system operators suggestions for power loss reduction operations. However in reality, there is low possibility for moving station two's locations along the test-line according to different operation scenarios, unless every bus has charge stations. Yet it is expensive to install them in every bus. Therefore, from system planning view point, for each load type of four operation scenarios, charge station two's locations should be fixed.

As mentioned above, the method to identify fixed charge station two's locations show below.

In most operation states, charge stations work under the first scenario. Therefore, a compromise is made, if the station two's locations in the second scenario and the third scenario can be changed to the first scenario's locations, the fixed station two's locations can be obtained. In order to observe the differences in terms of active -reactive power loss. When changing the third and second to the first scenario, and to analyse the possibilities of swapping station two's locations. The increasingly load type for the second and the third scenario is chosen as a case study.

When station two moves from bus 3 to bus 10 for the second scenario, and moves from bus 8 to bus 10 for the third scenario. As can be seen from Table X, station two moves from bus 3 to bus 10 the test-line's power loss increases much for the second scenario. However, for the third scenario, active and reactive power loss do not increase dramatically when changing charge station two's location from bus 8 to bus 10. Therefore, if charge station two can move from bus 8 to 10 rather than from bus 3 to 10, 0.319Mw power loss can be saved.

TABLE IX
THE OPTIMAL LOCATION OF CHARGE STATION TWO

Different scenarios	Uniformly load	Centrally load	Increasingly load
First scenario	Bus NO. 10	Bus NO. 8	Bus NO.10
Second scenario	Bus NO. 3	Bus NO. 3	Bus NO. 3
Third scenario	Bus NO.7	Bus NO.5	Bus NO.8
Fourth scenario	Bus NO.3	Bus NO.3	Bus NO.3

TABLE X
POWER LOSS DIFFERENCE FOR INCREASINGLY LOAD TYPE

	For the second scenario			For the third scenario		
Bus NO.	3	10	Difference	8	10	Difference
P_{loss}	0.387	0.741	0.354	0.094	0.129	0.035
Q_{loss}	0.33	0.64	0.31	0.08	0.11	0.03

Based on above analysis, an assumption is made that charge station one should always run out of energy before station two. Meaning that the third scenario always occurs before the second scenario For the sake of implementing it, charge station two's capacity has to be increased, whereas station one's capacity needs to be decreased.

The capacity of station two rises a little by $\frac{4}{3}$ of original capacity and station one's capacity declines by $\frac{2}{3}$ of original capacity.

From Table XI the current parameters of both stations are used for an increasingly load type for the first, and the third scenario.

TABLE XI
BESS RELATED PARAMETERS

	Original		Current	
Stations	Power	Capacity	Power	Capacity
Station one	1.02MW	4.08MWh	0.68MW	2.72MWh
Station two	1.02MW	4.08MWh	1.36MW	5.44MWh

TABLE XII
CHARGE STATION TWO'S LOCATIONS FOR INCREASINGLY LOAD OF FIRST SCENARIO OF NEW CAPACITY

No. / P,Q	3	4	5	6	7	8	9	10	11
P_{loss}	0.48	0.42	0.34	0.32	0.29	0.26	0.24	0.23	0.24
Q_{loss}	0.42	0.36	0.32	0.28	0.25	0.25	0.21	0.21	0.21

TABLE XIII
P,Q AND POWER LOSS FOR THE THIRD SCENARIO OF INCREASINGLY LOAD

No. / P,Q	3	4	5	6	7	8	9	10	11
P_{disc}	4.58	4.80	4.37	3.75	3.55	2.99	2.57	2.20	1.15
Q_{dis}	2.13	2.26	1.85	1.34	1.23	0.85	0.62	0.48	0.27
P_{loss}	0.35	0.26	0.19	0.14	0.10	0.095	0.10	0.12	0.28
Q_{loss}	0.30	0.22	0.16	0.12	0.09	0.08	0.09	0.10	0.24

Table XII shows charge station two's locations of new capacity for both stations of the power loss. Although, the rated power of station two increased to 1.36MW, and station one decreased to 0.68MW, the optimal location for station two is still bus 10. Table XII indicates charge station two's active and reactive power of new capacity. Using the changed capacity of both stations in the third scenario of increasingly load type, the optimal location for station two is still bus 8. Also from Table XIII, if station two's locations change to bus 10, the active and reactive power loss will not change significantly compared with other changes. Therefore, replacing station two's location from bus 8 to bus 10 can be applied in the test-line from a system planning point view.

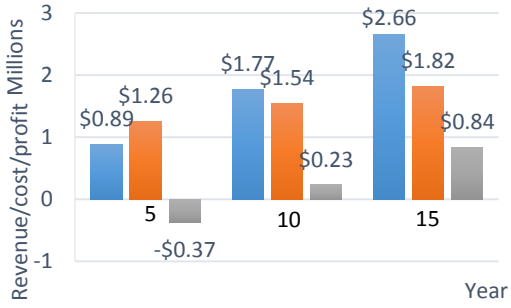

Fig.13. The revenue, cost, profit of charge station in every 5 year.

Fig.13 shows commercial aspects of charge stations. The blue one is 5 years revenue, the red one is cost and the grey one is profit. As we can see from fig.13 in the first 5 years, station owners need to invest charging facilities that makes negative profits. However, in the after 5 years state owners can not only repay the investment cost, but 0.23 million profit can be taken by selling the cheaper electricity to local residents and EVs. In the 15 years the station owners can obtain 0.84 million profits. These profits can be obtained from equation 39 and 49.

Overall, from above analysis due to choosing the fixed locations of station two. Comparisons are made for replacing station two' locations from bus 3 and 8 to bus 10 and, the result of moving station two from bus 8 to bus 10 is more suitable than 3 to 10. In order to apply this, the capacities of station one changed to 2.72MWh, and station two's capacity changed to

5.44MWh making scenario three always occurs before scenario two.

As a result of swapping station two's location from bus 8 to bus 10, the difference of active and reactive power loss only changes 0.025MW and 0.02Mvar. Therefore, bus 10 can be used instead of other buses for installing station two for power loss reduction both from system operation and planning points of view. All the results are obtained from MATPOWER and MATLAB optimisation programming.

Conclusion

In this paper, we used a new analytical analysis combined with active and reactive power optimisation methods for identifying charge station two's best location in terms of power loss reduction. The method was tested in an 11-bus distribution line. While, a previously developed current density method [14] is used and the results are compared for the same test-line with four different operational scenarios for power loss reduction.

As a results it was shown that 27% of average active power loss can be saved by installing two charge stations rather than no charge stations. From the power flow analysis, it was proved that the current density method is not accurate for choosing charge stations two's location. Based on four different operation scenarios, 17% of average active power loss can be saved for three different types of load, using the new method described in this paper compare with current density method, and the average annual yield above inflation is 2.6%, which can be refer to equation 48 for the station owners.

References

[1] A.Raskin, and S.Shah, "The Emergence of Hybrid Vehicles, "Researchon Strategic Change .Rep.3-41, 2006.

[2] M. A.bdelhamid, Singh, R. Singh, A. Qattawi, M. Omar, and I. Haque, "Evaluation of On-Board Photovoltaic Modules Options for Electric Vehicles," IEEE Journal of Photovoltaics, vol.4, no.6, pp.1576, 1584, Nov. 2014.

[3] M. Singh, P. Kumar, I. Kar, "Designing a multi charge station for Electric Vehicles and its utilization for the grid support," Power and Energy Society General Meeting, 2012 IEEE , vol., no., pp.1,8, 22-26 July 2012.

[4] Y. Ota, H. Taniguchi, T. Nakajima, K. M. Liyanage, J. Baba, and A. Yokoyama, "Autonomous distributed v2g (vehicle-to-grid) satisfying scheduled charge, " Smart Grid, IEEE Transactions on, vol. PP, no. 99,pp. 1 –6, 2011.

[5] J.Timpner, L.Wolf, "Design and Evaluation of Charge Station Scheduling Strategies for Electric Vehicles," Intelligent Transportation Systems, IEEE Transactions on, vol.15, no.2, pp.579, 588, April 2014.

[6] F.Xu, G.Q.Yu, L.F.Gu, H, Zhang, "Tentative analysis of layout of electrical vehicle charge stations," East China Electric Power, vol. 37, pp. 1678-1682, Oct. 2009.

[7] Z.F.Liu,W.Zhang, X.Ji, and k.li, "Optimal Planning of charge station for electric vehicle based on particle swarm optimization," Innovative Smart Grid Technologies - Asia (ISGT Asia), 2012 IEEE , vol., no., pp.1,5, 21-24 May 2012.

[8] Weifeng Yao; Junhua Zhao; Fushuan Wen; ZhaoYang Dong; Yusheng Xue; Yan Xu; Ke Meng, "A Multi-Objective Collaborative Planning Strategy for Integrated Power Distribution and Electric Vehicle Charging Systems," Power Systems, IEEE Transactions on , vol.29, no.4, pp.1811,1821, July 2014

[9] Y. Li, L. Li, J. Yong, Y. Yao, and Z. Li, " Layout Planning of Electrical Vehicle Charge Stations Based on Genetic Algorithm," Lecture Notes in Electrical Engineering, 1, Volume 99, Electrical Power Systems and Computers: 661-668,2011.

[10] Ge, S, Feng, L. and Liu. H,"The Planning of Electric Vehicle Charge Station Based on Grid Partition Method," IEEE Electrical and Control En gineering Conference, Yichang, China, 2011.

[11] Machiels, N.; Leemput, N.; Geth, F.; Van Roy, J.; Buscher, J.; Driesen, J., "Design Criteria for Electric Vehicle Fast Charge Infrastructure Based on Flemish Mobility Behavior," Smart Grid, IEEE Transactions on , vol.5, no.1, pp.320,327, Jan. 2014.

[12] Cairo, J.; Sumper, A., "Requirements for EV charge stations with photovoltaic generation and storage," Innovative Smart Grid Technologies (ISGT Europe), 2012 3rd IEEE PES International Conference and Exhibition on , vol., no., pp.1,6, 14-17 Oct. 2012

[13] Huajie Ding; Zechun Hu; Yonghua Song; Xiaorui Hu; Yongxiang Liu, "Coordinated control strategy of energy storage system with electric vehicle charging station," Transportation Electrification Asia-Pacific (ITEC Asia-Pacific), 2014 IEEE Conference and Expo , vol., no., pp.1,5, Aug. 31 2014-Sept. 3 2014

[14] Y.M. Atwa, E.F. El-Saadany, "Optimal Allocation of ESS in Distribution Systems with a High Penetration of Wind Energy," Power Systems, IEEE Transactions on, vol.25, no.4, pp.1815, 1822, Nov. 2010.

[15] G. Carpinelli, F. Mottola, D. Proto, and A. Russo, "Optimal allocation of dispersed generators, capacitors and distributed energy storage system sin distribution networks," Modern Electr. Power Syst., pp. 1–6, 2010.

[16] G. Celli, S. Mocci, F. Pilo, and M. Loddo, "Optimal integration of energy storage in distribution networks, "IEEE Power Tech, pp. 1–7, 2009.

[17] Y.Du, B.F.Yun,"Optimal allocation of energy storage system in distribution systems", Advanced in Control Engineering and Information Science, vol.15.2011.

[18] C.S. Wang, M.H. Nehrir, "Analytical approaches for optimal placement of distributed generation sources in power systems," *Power Engineering Society General Meeting, IEEE*, vol., no., pp.2393 Vol. 3, 12-16,2005.

[19] P.Owen, "Powering the Nation Household electricity-using habits revealed" Energy Saving trust," London.EST.Rep. 2011.

[20] N. W. Miller, R. S. Zrebiec, G. Hunt, and R. W. Deimerico, "Design and commissioning of a 5 MVA, 2.5MWh battery energy storage system," in Proc. IEEE Transaction. Distribution. Conf., Los Angeles, pp. 339–345, Aug.2007.

[21] J.Voeclcker.(2012).GreenCarreportWebpage.[Online].Available:http://www.greencarreporrts.com/news/1078116_july-plug-in-electric-car-sales-volt-steady-leaflethargic-again.

[22] J.Voelcker,(2012).GreenCarReportsWebpage.[Online].Available:http://www.greencarreports.com/news/1081419plug-in-electric-car-sales-triplei in2013-as-buyers-models-increase

[23] J.Cole,(2013).GreenCarReport.Webpage[Online].Available:http://insideevs.com/september-2013-plug-in-electric-vehicle-sales-report-card/

[24] J.Cole,(2013).GreenCarReport.Webpage[Online].Available:http://insideevs.com/june-2013-plug-in-electric-vehicle-sales-report-card/

[25] M. Yilmaz, P.T. Krein,"Review of charge power levels and infrastructure for plug-in electric and hybrid vehicles," Electric Vehicle Conference (IEVC), 2012 IEEE International , vol., no., pp.1,8, 4-8 March 2012.
[26] Alternative Fuels Data Center, Developing Infrastructure to Charge Plug-In Electric Vehicles.[online] http://www.afdc.energy.gov/fuels/electricity_infrastructure.html
[27] Chenrui Jin; Jian Tang; Ghosh, P., "Optimizing Electric Vehicle Charging With Energy Storage in the Electricity Market," Smart Grid, IEEE Transactions on , vol.4, no.1, pp.311,320, March 2013
[28] L. H. Walker, "10-MW GTO converter for battery peaking service," Industry Applications, IEEE Transactions on, vol.26, no.1, pp.63, 72, Jan/Feb 1990.
[29] A. Gabash, and P. Li, "Active-Reactive Optimal Power Flow in Distribution Networks With Embedded Generation and Battery Storage," Power Systems, IEEE Transactions on, vol.27, no.4, pp.2026, 2035, Nov. 2012.
[30] A. Gabash, and P. Li, "Evaluation of reactive power capability by optimal control of wind-vanadium redox battery stations in electricity market," Renewable Energy & Power Quality J., vol. 9, pp. 1–6, May2011.
[31] S.G.Nail, D.K.Khatod, and M.P.Sharma, "Optimal allocation of combined DG and capacitor for real power loss minimization in distribution networks," Electrical Power and Energy Systems, vol, 53, pp.967-973.2013.
[32] Zhipeng Liu; Fushuan Wen; Ledwich, G., "Optimal Planning of Electric-Vehicle Charging Stations in Distribution Systems," Power Delivery, IEEE Transactions on , vol.28, no.1, pp.102,110, Jan. 2013

APPENDIX:

TABLE XIV
THE PARAMETERS USED IN ECONOMIC ANALYSIS

T	Life time of charge station	15 years
$C_{pi}^{on}(t)$	Peak electricity price	\$0.068/kwh
C_{pi}^{off}	Off-peak electricity price	\$0.014/kwh
T_{CHi}	Annual utilization hours of charging devices	8h/ per-day
C_{ETi}^{I}(t)	Per-unit investment cost of transformers	\$40.84/KVA
C_{CHi}^{I}(t)	Per-unit investment cost of charging devices	\$34.71/KVA
C_{DEi}^{I}	Per-unit investment cost of other devices	\$30.94/KVA
C_{EAi}^{I}(t)	land utilization cost	\$95.63/m^2
C_{Bsi}^{I}	Per-unit investment cost of battery	\$5.21/KVA
$C_{VCi}^{O}(t)$	Active power filtering and reactive power compensation cost	\$10.16/KVA
$C_{HRi}(t)$	Human resources cost	\$16476.41
$C_{Bsi}^{OM}(t)$	Per-unit operation and maintain cost of battery	\$2500/MW
$C_{ETi}^{M}(t)$	Per-unit maintenance cost of transformers	\$11.92/KVA
$C_{CHi}^{M}(t)$	Per-unit maintenance cost of charging devices	\$8.92/KVA
C_{DEi}^{M}	Per-unit maintenance cost other devices	\$100/kwh
$\eta CHij$	Charging efficiency of charge devices	90%
$\cos\emptyset\, CHij$	Power factor of charge devices	0.95
K_i	Simultaneity coefficient	0.8
n_i	The number of charging devices	10
i	The discount rate	10%
E_i	Battery charging efficiency	90%
H_{aver}	The average EVs charging time	4h

Available online at www.sciencedirect.com

SciVerse ScienceDirect

Energy Procedia

www.elsevier.com/locate/procedia

Applied Energy Symposium and Forum, REM2016:
Renewable Energy Integration with Mini/Microgrid

The Active and Reactive Power Dispatch for Charging Station Location Impact Factors Analysis

ChengWang, RoderickDunn,QingqingYang, BoLian,WeijiaYuan,JianweiLi

Department of Electrical and Electronic Engineering, University of Bath
University of Bath, Bath, BA2 7AY, UK

c.wang@bath.ac.uk

Abstract

With the increasing number of Electric Vehicles (EVs) in modern society, a number of challenges and opportunities are presenting themselves. For example, how to choose charging station locations to minimize the Distribution Network's (DN) power loss when a large number of EVs are connected to the DN. How impact factors, such as different load patterns, EVs' charging locations and network topology, affect charging station location is becoming vital. In this paper a new charging station location methodology informed by impact factor analysis is proposed by using the Active and Reactive Power Dispatch of charging stations in terms of power loss minimization. Results for the 36 DN with three different scenarios are presented. In addition, a more realistic model based on EV's daily travel patterns is built to illustrate how these impact factors affect charging station location. It is demonstrated that the optimal charging station location in terms of power loss minimization can be found by using the new methodology, and it is not affected by the EVs' charging location and load patterns, it is affect by the network topology.

Introduction

Modern power systems are suffering pressures from government, large industries and investors. Especially when new type of loads are emerging, such as EVs. These new technologies make life easier and more comfortable. However, they also challenge the traditional power system. For example with a large level of EV penetration, are there enough charging stations to facilitate EVs' charging. How do we choose charging stations' locations, and how the impact factors such as different load patterns, EVs' charging locations and network topology affect this. This is becoming vital not only for power system operators, but also for EVs' users.

In [1] the authors developed a mixed-integer programming model to determine the optimal location of charging station by considering the EVs' parking demands, local jobs and a community's population density. In [2] the authors considered the impacts of limiting EV's full state of charge on the total charge energy for charging station planning. Reference [3] considered the environmental factors and service radius for charging station location choice by using a two-step screening method. Reference [4] proposed a new charging station model, which is influenced by the electricity consumption along the roads in cities and oil sales. Reference [5] considered how traffic flow and EVs' battery capacity affect a charging station's location choices and size.

Unlike these papers, the proposed method in this paper uses the active and reactive optimal power flow to analysis how the charging station locations change as a consequence of changing the network's resistance, reactance and EV's charging locations, which can be chosen at any bus in test 36 DN. The structure of this paper is as follows: In section two a theoretical analysis of this method is given, the charging station structure and the base case are also introduced for the cases studies and the results are discussed. In section three, two cases based on several scenarios are given and simulation results are discussed. In the final section, the conclusions of this paper are given.

Theoretical Analysis

The main focus of this paper is to analyse how the impact factors such as loads and network resistance and reactance affect optimal charging station location choice in terms of power loss minimization. In order to quantify the impacts on the DN, the optimal charging station location was obtained by using the active and reactive power approach. The EV to grid concept is not considered in this paper.

Charging Station Introductions

The charging station plays an essential role in EVs' power supply chain. It consists of a Battery Energy Storage System (BESS), which can not only provide the energy to EVs, but also can provide energy to local electricity customers. The BESS consists of batteries and Power Conditional Systems (PCS) [6][7].

A PCS has several electronic devices such as capacitors, diodes and transformers, the structure can be seen in [6].

It has two operation modes. The first operation is called discharging mode. In this operation mode BESS is being discharged to supply the active and reactive power to loads. The second operation mode is called charging mode. In this operation mode BESS is being charged, absorbing both active and reactive power from the DN. The active and reactive power discharge of the BESS should not exceed the maximum apparent power S_{ESSmax} of the BESS [8][9].

$$P_{dis}^2 + Q_{dis}^2 \leq S_{BESSmax}^2 \quad (1)$$

$$P_{char}^2 + Q_{disc}^2 \leq S_{BESSmax}^2 \quad (2)$$

The active power for charging and discharging must be positive values

$$P_{char(k,h)} \geq 0, \qquad P_{dis(k,h)} \geq 0 \quad (3)$$

$$S_{ESSmax(k,h)}^2 \geq Q_{dis\,(k,h)} \quad (4)$$

Moreover the upper and lower bound of the storage capacity should satisfy

$$E_{min} \leq E_{Low}, \qquad E_{Up} \leq E_{max} \quad (5)$$

The EVs power demand at each time slot can be calculated by using the equation

$$P_i(t) = \frac{[b_i - x_i(t)] \times C_i}{E_i \times H_{charging}}, \forall i, t \quad (6)$$

where $P_i(t)$ is the power demand of EVs at any time slot. b_i is the desired State of Charge (SOC) in this paper is 100%. $x_i(t)$ is the SOC at the beginning of t is 20%. C_i is the capacity of EV. E_i is the battery charging efficiency of EVs, $H_{charging}$ is the average charging period of all four types of EV. It is assume one charging station can charge 100 EVs simultaneously [10].

Base case and model explanation

The base case is the original network in this paper. It is the 36-bus DN [11] without any modifications, and it is assumed that there are two charging stations in the DN, charging station one's has already been installed in bus two because the system largest loss occurs there. The 36-bus DN voltage is 11KV and the total active reactive load are 3.97MW and 2.08Mvar. The system's topology is shown in Fig.1 and reference [11]. Also in order to analyse the power flow between each busbar, a simple π line model is built and shown in Fig.2.

The objection function is built to find the charging station two's station.

$$f_j = \sum_{i=1}^{j} R_{1i(j)} |P_i' + jQ_i'|^2 \qquad j = 3,4,5 \cdots \cdots N \quad (7)$$

where $P_i' = P_{dis2} + P_{load2} + P_{m2F} - P_{grid} - P_{dis1}$ (8)

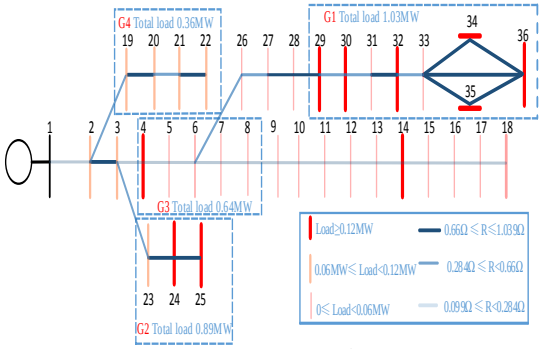

Fig.1. The topology of 36-bus distribution network

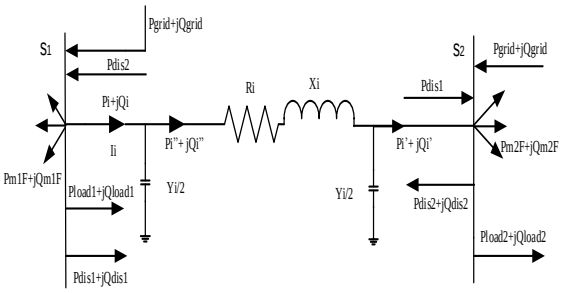

Fig.2. Power flow analysis

$$Q_i' = Q_{dis2} + Q_{load2} + Q_{m2F} - Q_{grid} - Q_{dis1} - V_{s2}^2 \frac{Yi}{2} \quad (9)$$

The goal is to find the optimal location for charge station two, where equation (10) reaches the minimum value.

$$F_m = Min f_j \quad (10)$$

The $R_{1i(j)}$ is the resistance between two charge stations. N is the test system's total bus number. P_{load2} is the load at bus S_2. P_{m2F} is active power injection from bus S_2.

$$Min\ P_L = \sum_{\forall s_1,s_2}^{s_1,s_2 \in S_B} I_i^2 R_i = \sum_{\forall s_1,s_2}^{s_1,s_2 \in S_B} \left(\frac{P_i^2 + Q_i^2}{V_{s_1}^{\ 2}} \right) R_i \quad (11)$$

$$P_i = P_i' + R_i \frac{P_i'^2 + Q_i'^2}{V_{s2}^2} \quad (12)$$

$$Q_i = Q_i'' - V_{s1}^2 \frac{Yi}{2} = Q_i' + X_i \frac{P_i'^2 + Q_i'^2}{V_{s2}^2} - V_{s1}^2 \frac{Yi}{2} \quad (13)$$

The active and reactive power flow in π line model must satisfy the Kirchhoff's current law.

Case Study and Result Discussion

In this section, two cases base on 36-bus DN are analysed. The first case is without any EVs charging, how the network's loads, resistances and reactance's changes affect charging station two's locations. The second one is with EVs charging, how EVs' charging locations change affect charging station two's location.

The Base Case

Before analysing the first and second case, the optimal charging station location for station two needs to be found by using the proposed method in chapter 6. Because if we know the optimal charging station location, then we can analysis how the impact factors affect the optimal location. It is installed in bus 32. The objective function's values and real system power loss are shown in Fig.3 and Fig.4.

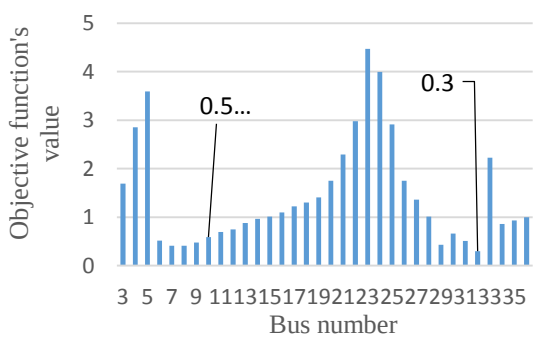

Fig.3. Objective function's values of 36-bus test DN

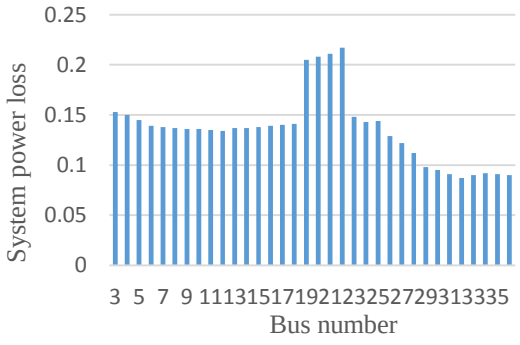

Fig.4. Power loss of the 36-bus test DN

The simulation results are shown in Fig.4. It is proved that the optimal location for charging station two is bus 32. Regarding to the objective function's values and simulation results. In general, the heavier load demands of test system, the relative further from station one, the lower power loss and objective functions we have. For

example bus 32 is in the system largest loads area G_1, installing station two in the larger loads area can cause lower power loss than small loads area.

The First Case

The first case is without any EV penetrations, how loads, resistance, and reactance change influence the optimal location of charging station two. It has three scenarios. The first scenario is to change the test system's resistance, keep load as the original system's loads. The second scenario is to change the test system's loads, keep resistance as the original system's resistance. The third scenario is to change the test system's resistance, meanwhile change system's loads.

In the first scenario the resistances and reactance between bus 9 to bus 18 and bus 29 to bus 36 are changed to the new resistance. The system's loads keep the same as original one. The 36 bus test-system with the changed *R* and *X* parameters shows in Fig.5.

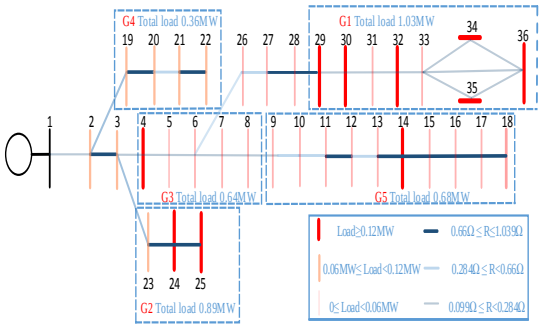

Fig.5. 36-bus test-system with changed R and X

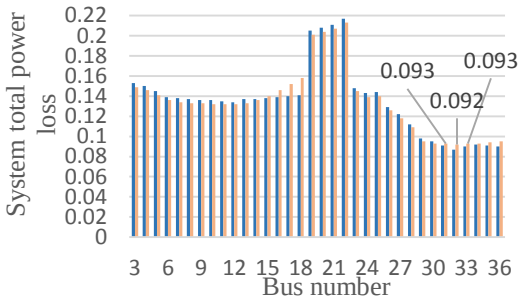

Fig.6. Total power loss comparison for the first scenario

From simulation results shown in Fig.6. The blue one is system original power loss at each bus. The yellow one is the changed system's power loss at each bus. Although the *R* and *X* have changed, the optimal location for charge station two is still the same. Regarding to this scenario, increase system's R and *X* between bus 9 to bus 18 and decrease bus 29 to bus 30, rise the total power loss at each bus between bus 15 to bus 18 and bus 31 to bus 36. But the charging station two's location is not changed. Therefore, only change system's *R* and *X* in area G_1 and G_5 , the optimal location of charging station two is not influenced. In the second scenario the system's loads from bus 11 to bus 18 and from bus 29 to bus 36 are changed to new loads. The system's *R* and *X* keep the same as original one.

From simulation results shown in Fig.7. The yellow one is the new system's power loss at each bus. Increase the load at each bus between bus 11 to 18 to original one's four times and decrease the load at each bus between bus 29 to 36 to original one's four times, rise the total power loss, but the optimal location for charge station two is still the same which is bus 32. Therefore, only change the system loads in area $G_1$and G_5, the optimal location for charge station two does not change.

In the third scenario the system's loads from bus 11 to bus 18 are changed to new loads. Meanwhile, the system's *R* and *X* between bus 9 to bus 18 and bus 29 to bus 30 are changed to the new values.

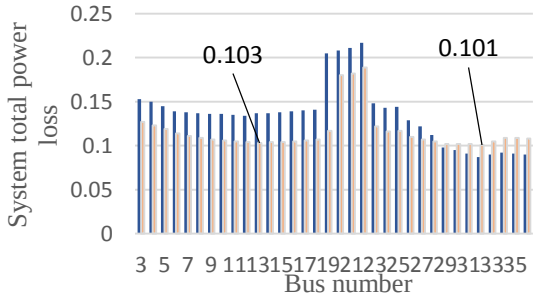

Fig.7. Total power loss comparison for the second scenario

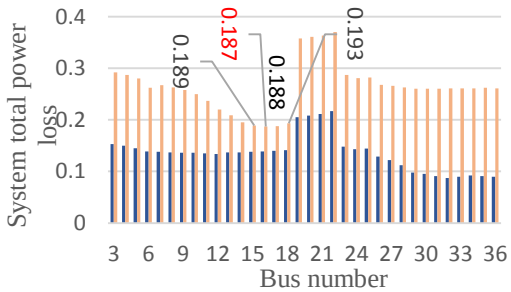

Fig.8. Total power loss comparison for the third scenario

From simulation results shown in Fig.8, we can see the blue one is system original power loss at each bus. The yellow one is new test-system's power loss with changed loads, *R* and *X*. For new test system the optimal location of station two has changed to bus 16.

The previous secured charge station two's location which is bus 32 has moved to bus 16 in the third scenario. This illustrates the station two's optimal location is influenced by changing both system loads, *R* and *X*

simultaneously. If only change one of them the location will not change. Also in this third scenario the optimal location tends to near heavy loads and big resistance. Which means install charge station two in the bus between bus 11 to 18, the power loss will be smaller than the other buses Overall, the much heavier loads and higher system R and X the bus has the higher possibilities it can be chosen to be the optimal location of charging station two. However, in the real DN the line parameters, such as R and X are hardly changed. Therefore more realistic scenarios are given in the second case.

The Second Case

The main aim for the second case is to test changing the system loads and EVs' charging locations the optimal charge station's locations can be affected or not. Two scenarios are developed for this case.

In the first scenario, EVs can charge at any time between 9:00 to 17:00. According the national travel survey statistics and daily load profile [12][13],between 7:00 to 9:00 people leave their homes from G_5 area to working places G_1 area and start working. In Fig.9 it assumes that G_5 is the residential area because the loads are much lighter than G_1, during the period between 9:00 to 13:00. In this case, it is also assumed that EV charging place is randomly chosen in G_1 area.

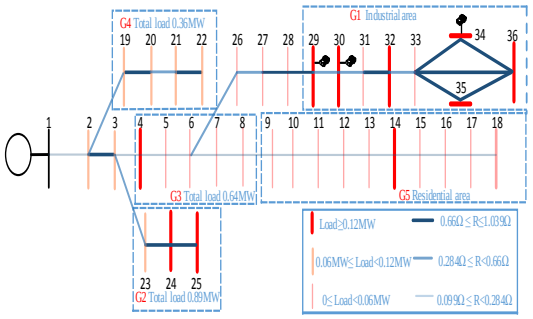

Fig.9. The first scenario Charing pattern

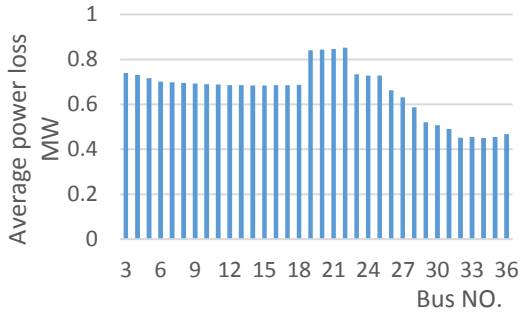

Fig.10. Average power loss for test DN during the period 9:00 to 17:00

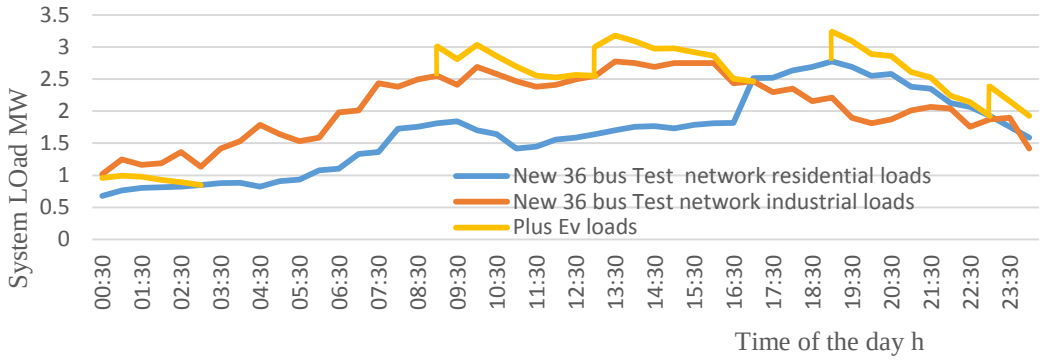

Fig.11. Network's load profiles after adding EVs' load between 9:00 to 17:00

In order to prove the best location for charge station two in terms of power loss minimization is bus 32. The EVs are charged in the G1 area randomly during the daytime. Two cases for the daytime charging are listed below:

Case 1. The EVs 'charging starts at 9:00 and finish at 13:00, In order to simulate hourly power loss of the whole test network, the two different load patterns, which are the industrial load pattern, residential load pattern and EVs loads are scaled in Fig.11 [14]. All 100 EVs are charged in the G1 area during the period between 9:00 to 13:00. In this case, these EVs start charging at 9:00 in the morning and finish at 13:00 in the afternoon. These EVs' power demands increase the industrial loads profiles, which can be seen from Fig.11. After 13:00 EVs are fully charged, and a new charging recycle starts from 13:00 to 17:00. Meanwhile, the residential load profiles do not change. Case 2. The EVs charging starts at 13:00 and finish at 17:00.

Fig.10 shows the average power loss for 36-bus test network in the period between 9:00 to 17:00. From the simulation results we can see the optimal location for charge station two is bus 32, which proves the method used in this paper. Although the EVs are charged randomly in the industrial area, the bus 32 is still the optimal location for charge station two in terms of power loss minimization. It is proved that the loads profile change, the optimal charge station two's location does not change.

In the second scenario, EVs can be charged at any time between 19:00 to 24:00 according to the national travel survey [12]. Because most of people do not use their vehicles during this period. In this scenario people go home from their working places, which is from G_1 area to G_5 area. These EVs are charged randomly in G_5 area.

The simulation results for average power loss of the 36-bus test network shows that, in the first charging pattern (the day time charging pattern) the average power loss is higher than the second charging pattern (the night time charging pattern). The reason for this is that in day time charging pattern, EVs are connected in industrial area, in night time charging pattern EVs are connected in residential area. Comparing the two patterns' total base loads (industrial's loads plus the residential loads) the day time charging pattern's base loads are much higher than the night time one. That makes average power loss of the first charging pattern higher than the second pattern. However, irrespective of the charging pattern bus 32 is always the optimal location for charge station two.

From above two different charging patterns' simulation results, we can see the optimal location for charge station two is bus 32. This proves whether EVs are charged in the industrial area or in the residential area, installing charge station two in bus 32, the total system's power loss can reach the lowest point. In other words, the EVs' location change and load patterns change will not influence charge station two's location.

Conclusions

In this paper, we used active and reactive power dispatch for analysing how impact factors such as different loads patterns, EVs' charging locations and network parameters affect charging station location choice for power loss reduction. It has been shown that the charging station's location is not affected by the individual changes of these impact factors. It was affected by changing the network's resistance, reactance and load patterns simultaneously. This was shown by testing the 36-bus distribution network with EVs' penetrations.

References

[1] Chen TD, Kockelman KM, Khan M. Locating electric vehicle charging stations parking-based assignment method for Seattle, Washington. Transp Res Rec 2013;2385:28–36.

[2] Fan PY, Sainbayar B, Ren SL. Operation analysis of fast charging stations with energy demand control of electric vehicles. IEEE Trans Smart Grid 2015;6:1819–26.

[3] Liu ZP, Wen FS, Ledwich G. Optimal planning of electric-vehicle charging stations in distribution systems. IEEE Trans Power Deliv 2013;28:102–10.

[4] Wang Z, Liu P, Cui J, Xi Y, Zhang L. Research on quantitative models of electric vehicle charging stations based on principle of energy equivalence. Math Probl Eng 2013;2013:1–10.

[5] Wang GB, Xu Z, Wen FS, Wong KP. Traffic-constrained multiobjective planning of electric-vehicle charging stations. IEEE Trans Power Deliv 2013;28: 2363–72.

[6] N. W. Miller, R. S. Zrebiec, G. Hunt, and R. W. Deimerico, "Design and commissioning of a 5 MVA, 2.5MWh battery energy storage system," in Proc. IEEE Transaction. Distribution. Conf., Los Angeles, pp. 339–345, Aug.2007.

[7] L. H. Walker, "10-MW GTO converter for battery peaking service," Industry Applications, IEEE Transactions on, vol.26, no.1, pp.63, 72, Jan/Feb 1990.

[8] A. Gabash, and P. Li, "Active-Reactive Optimal Power Flow in Distribution Networks With Embedded Generation and Battery Storage," Power Systems, IEEE Transactions on, vol.27, no.4, pp.2026, 2035, Nov. 2012.

[9] A. Gabash, and P. Li, "Evaluation of reactive power capability by optimal control of wind-vanadium redox battery stations in electricity market," Renewable Energy & Power Quality J., vol. 9, pp. 1–6, May2011

[10] Cheng Wang, R. Dunn and Bo Lian, "Power loss reduction for electric vehicle penetration with embedded energy storage in distribution networks," Energy Conference (ENERGYCON), 2014 IEEE International, Cavtat, 2014, pp. 1417-1424. doi: 10.1109/ENERGYCON.2014.6850608

[11] Ching-Tzong Su, Chen-Yi Lin, Ji-Jen Wong, Optimal Size and Location of Capacitors Placed on a Distribution System, WSEAS Transactions on Power Systems, Vol. 3, Issue 4, 2008, pp. 247-256.

[12] National Statistics, Department for Transport, Travel to Work-Personal Travel Factsheet, Jul. 2007

[13] O,Paula, F, Rosalyn. D,Penny. "Powering the Nation Household electricity-using habits revealed" Energy Saving trust, London. EST.Rep. 2011

[14] Kejun Qian; Chengke Zhou; Allan, M.; Yue Yuan, "Modeling of Load Demand Due to EV Battery Charging in Distribution Systems," in Power Systems, IEEE Transactions on , vol.26, no.2, pp.802-810, May 2011doi: 10.1109/TPWRS.2010.2057456

Power Loss Reduction for Electric Vehicle Penetration with Embedded Energy Storage in Distribution Networks

Cheng Wang , Rod Dunn, Bo Lian

Department of Electrical and Electronic Engineering, University of Bath
University of Bath, Bath, BA2 7AY, UK
c.wang@bath.ac.uk

Abstract—**Electric vehicles (EVs) are becoming more popular in modern society. These vehicles can be charged at home or in public areas with standard outlets. However, the extra power demand affects the distribution network (DN) in terms of power losses. If these vehicles are connected into the DN during peak times, it increases the power losses. One effective method to solve this issue would be the introduction of energy storage systems (ESSs). Therefore, both active and reactive power dispatch combined with different charging periods, off peak and peak, for the ESS is proposed in this paper. The research provides both uncoordinated optimal active-reactive power flow (UA-RPF) of the ESS and the coordinated optimal active-reactive power flow (CA-RPF) of the ESS, which improves the performance of the DN. Results for the IEEE-33 distribution system are presented. It is demonstrated that 1.43MW total power losses (TPL) and 1.64MW of imports from the transmission network (TN) can be reduced by using the proposed approach.**

Keywords: Power losses, optimization algorithm, ESS.

I. INTRODUCTION

With modern technological development, and raising awareness of environmental protection, EVs will become cheaper and less environmentally damaging alternatives, to traditional vehicles. Customers can charge their EVs either using electric outlets in their homes, working places or public stations with charging plugs. These EVs can only be driven over a limit range, some of the EVs may have larger batteries and better drive systems, but their range is still limited[1], [2].

The charging process can affect the DN a lot, especially when large amounts of the EVs are connected to the DN at the same time. Because these vehicles use considerable amounts of energy, if this scenario happens at peak time, it worsens the insecurity level of the DN, and causes a great deal of active power loss. Meanwhile, this put lots of pressures on the system operators in terms of keeping the system secure. It has been shown that, if EV penetration increases by 10% between 18:00-21:00 hours, energy losses raise by almost 3.7%.[3]

From the system operator's view point the power losses are an economic concern and need to be reduced. One of the reduction methods is to add ESS into the DN. Usually ESSs in the DN are combined with any available renewable energy sources to accommodate variations in these sources, making the system more stable. Some areas do not have sufficient sources of renewable energy generation, for this situation, how to use ESS to improve the system performance is a concern of this paper, for example to reduce the power losses. From the EV owner's point of view, they want to use cheaper electricity when they charge their EVs, this also has been considered.

Previously, active and reactive power dispatches were considered separately for loss reduction. Some researchers concentrate on installing capacitors for reactive power optimization [4]. Some researchers use an algorithm for optimal location selection to reduce active power losses [5], others to remove load imbalances in the radial network for loss reduction [6]. Alternatively, the methods proposed in this paper consider the reduction of both active and reactive power losses. Also, two optimization methods, both based on the ESSs were used and compared for losses reduction caused by the different levels of EV penetration.

Renewable energy sources were also implemented in the model for this research, including wind power generation and photovoltaic generation. In this optimization problem, only active and reactive power losses and the power imported from the TN are considered.

This article emphasizes the improvements and the differences when using the two charging methods, which are UA-RPF of the ESS and the CA-RPF of the ESS. It also indicates how much active power can be reduced from the TN.

II. ASSUMPTION AND MODLING

A. Load scenarios

From the available household load measurements data [7], a daily electricity demand (excluding heating) in the UK residence has been drawn above.

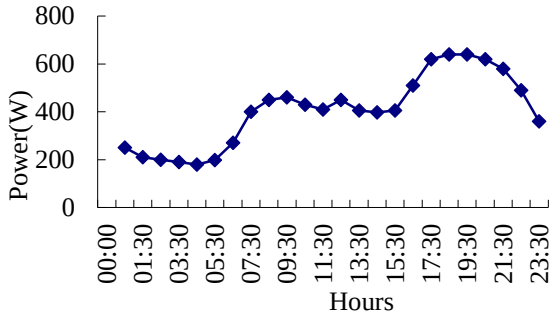

Fig.1. Daily electricity demand in a UK residence excluding heating

B. Specifications and modeling of EVs

Recent Recent market data shows that, EV sales are lead by the Chevrolet Volt plug-in hybrid with 48,218 units, followed by Nissan Leaf all electric cars with 35,588 units. The Toyota Prius Plug-in Hybrid occupies the third largest market with 20,724 units, with the fourth being the Tesla Model S with over 15,000 units [8][9][10][11]. Accordingly, it can be seen that the Chevrolet Volt plug-in hybrid occupies the 41% of the whole electric vehicle market, the Nissan Leaf all-electric car account for 30%, the Toyota Prius Plug-in Hybrid takes up 17%, while the Tesla Model S shares the rest of the market which is 12% . Therefore, an assumption is made, each load feeder, 41 people use Chevrolet Volt Plug-in Hybrid cars, 30 people use Nissan Leaf all-electric cars, 17 people buy Toyota Prius Plug-in Hybrid cars, and 12 people use the Tesla Model S. The characteristics of the different electric vehicles are shown below [12].

TABLE I. CHARACTERISTIC OF THE EV

Load Type	Type	Pd(MW)	BatterySize(kWh)
Tesla Roadster	**Battery**	0.0168	53
Nissan leaf	**Battery**	0.06	24
Chevrolet Volt	**Hybrid**	0.003	16
Toyata Prius	**Hybrid**	0.003	4.0

In In order to analyze the impacts of EVs on the distribution system, these vehicles are connected in the feeder 22, 25, 32, and 14 of the IEEE 33-bus distribution system [13]. Comparisons are made, to see the differences in terms of active power losses in some specific buses.

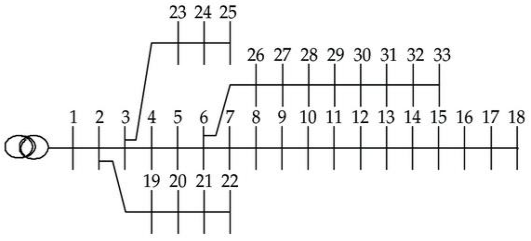

Fig.2.The tested DN

The maximum power demand (PD) for all 41 Tesla Roadsters is 0.688MW, for all 30 Nissian leafs is 1.8MW, for all 17 Chevrolet Volts is 0.051MW, and for all 12 Toyota Prius is 0.036MW. The total power demand (TPD) is 2.575MW, and it is added into the node 22, node 25, node 32, and node 14 respectively which is chosen randomly. The load feeder data is shown in the Table II.

Each Each EV has a battery and, the charging characteristic can be seen in Table.I. For the Tesla Roadster 0.0168 MW power are needed to be fully charged, for the Nissan Leaf it is 0.06 MW, for the Chevrolet Volt is 0.003MW, and for the Toyota Prius it is 0.003MW. The battery can only be charged during the charging time, which means energy flow is unidirectional, so the concept of EVs to grid is not considered here. Fast charging is taken into consideration, but requires a higher short-circuit power. Customers can purchase an electrical outlet to fit the high short-circuit power from the auto-supply shop. Extra costs are needed to install the high voltage connection equipment, but it can charge the EV faster than others. The scenario studied up to 40% EVs penetration in 10% increments, based on the 20% penetration. For example at 20% EVs penetration, it is assume that there are 20 EVs, Chevrolet Volt occupies the 41% which is 8 Chevrolet Volts, 6 Nissan Leafs, 3 Toyota Prius, and 2 Teslas.

TABLE II. LOAD FEEDER DATA

Load feeder	PD(MW)	TPD(MW)	PD'(MW)
22	0.09	2.575	2.675
25	0.21	2.575	2.785
32	0.42	2.575	2.995
14	0.12	2.575	2.695

C. Charging period and place

Although the EV is becoming more popular, charging stations are not as common as petrol stations, therefore, EVs are assumed to be charged at home or at the work place. Fig.3 shows the percentage of vehicles arriving at home [14]. From Fig. 3 periods are proposed. The first one is from the 8:30 t to 14:30 people arrive home and plug their EVs in to the charging station nearby or their garage. The second charging period takes place between 14:30 and to 19:30 and, this period coincides with the peak load during the day and also more EVs arriving home. These penetrations can lead to more power losses in the DN. The last charging period is from 19:30 to 23:30, with less people arriving home and charging their EVs during the night. This assumes that, there is only one EV per house and that the charging places are usually either at home, at the office or in the centre of town.

TABLE.III. PERCENT BETWEEN TOTAL POWER LOSSES AND TOTAL POWER

Penetration / Charging period	0%	20%	30%	40%
8:30-14:30	3.16%	4.39%	5.07%	5.92%
14:30-19:30	3.25%	4.41%	5.23%	6.03%
19:30-23:30	3.24%	4.15%	4.92%	5.69%

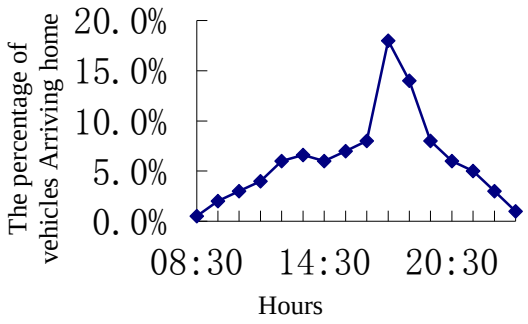

Fig.3. Percentage of vehicles not under way

D. *The method of load flow analysis*

A load flow analysis in terms of total power losses(TPLs), total generation, and PD was performed by the matpower using the IEEE 33-bus tested distribution system, combined with different EVs penetration levels, different load profiles, and different charging periods. Two scenarios are chosen to be analysed, depending on the different penetration levels. The first case for each scenario is taken as the base value, which is without adding any EVs into the distribution grid, but different load profiles in three different charging periods. The next cases are with the EVs penetration 20%, 30%, 40%, respectively in three charging periods. The charging feeders of the EVs are randomly chosen in the IEEE 33 node system.

E. *Result*

The results of the power losses in terms of the uncoordinated charging are shown in Table 3 below. The numbers of EVs used were 100, as this is a reasonable number of EVs for a medium size community. The results show the percentage of TPLs to the total power received from TN

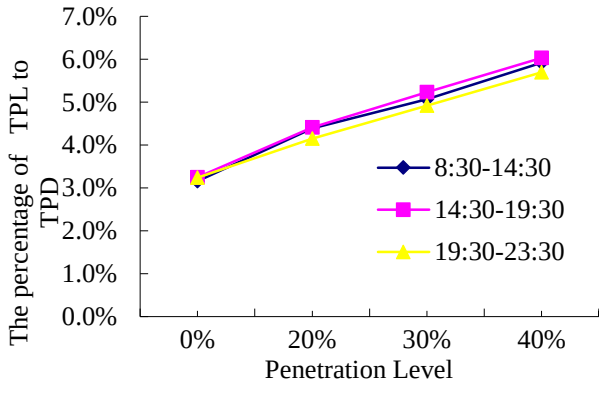

Fig.4.Different of the total power demand of three methods

In all cases with the EV penetrations increase, the percentage of the TPL increases. The highest power losses take place between 14:30 and 19:30. Two reasons for it, one is the load during that period is higher than the other periods, the other is more EVs arrive at home during that period. Knowledge of these power losses are vital to the system operators, in order to them to compensate for the system losses and choosing the appropriate methods to do this.

III. THE METHODS OF POWER LOSSES REDUCTION IN THE TEST NETWORK

A. *Objective function and constrains*

The previous section illustrates power losses in the IEEE 33 tested network. For reducing these losses, the ESS was embedded into the DN as shown in the Fig. 2, meanwhile, the objective function Min $P_L = \sum_{\forall k,m}^{k,m\in S_B} I_i^2 R_i$,based on the power flow analysis was built.

. In order to analyse the power losses in the DN, a π model combined with ESS and DN of a particular distribution line between nodes k and m was modelled, with real and the reactive power flow through node k (the sending point) and m (the receiving end) as given by bellows.

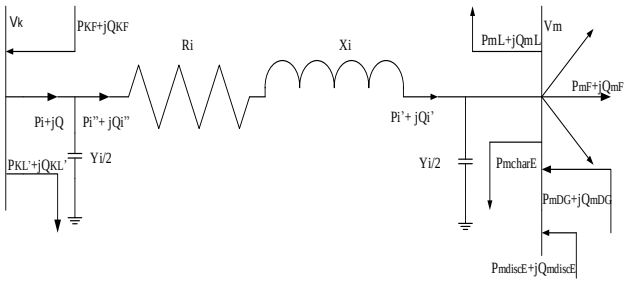

Fig.5.The model of a distribution network branch between node p and q

From the Fig .5, it can be seen that

$$P_i' = P_{mL} + P_{mcharE} + P_{mF} - P_{mDG} - P_{mdiscE}$$

$$P_i = P_i'' = P_i' + R_i$$

$$Q_i' = Q_{mL} + Q_{mF} - Q_{mDG} - Q_{mdiscE} - V_m^2 \frac{Yi}{2}$$

$$Q_i = Q_i'' - V_k^2 \frac{Yi}{2} = Q_i' + X_i \frac{P_i'^2 + Q_i'^2}{V_m^2} - V_k^2 \frac{Yi}{2}$$

Where P_i and Q_i are the sending active and reactive power through nodes k and m, the series impedance and shunt admittance between node k and m are $(R_i + j\,X_i)$ and $\frac{Yi}{2}$ respectively, P_{mDG} and the Q_{mDG} are the real and reactive power injected by the distribution generation, the P_{mDG} and the Q_{mDG} are not considered in the optimization. P_{mL} and the Q_{mL} are the total active and reactive power load at bus m.

P_{mF} and Q_{mF} are the sum of active (reactive) power flows through all the downstream branches connected to bus m . P_{mcharE} , P_{mdisE}, Q_{mdisE}, are the active and reactive power charging and discharging of the ESS respectively.

$$V_m = V_k - I_i Z_i = V_k - \frac{S_i''^*}{V_k^*}(R_i + j\,X_i)$$

$$V_m = V_k - \frac{P_i'' - jQ_i''}{V_k}(R_i + j\,X_i) = \left(V_k - \frac{P_i'' R_i + Q_i'' X_i}{V_k}\right) - j\left(\frac{P_i'' X_i - Q_i'' R_i}{V_k}\right)$$

$$V_m = \sqrt{V_k^2 - 2(P_i'' R_i + Q_i'' X_i) + \frac{(P_i''^2 + Q_i''^2)(R_i^2 + X_i^2)}{V_k}}$$

V_k V_k and V_m are the voltage at bus k and m, I_i is the current through the branch, where $S_i'' = P_i'' + Q_i''$, $P_i'' = P_i$, $Q_i'' = Q_i + V_k^2 \frac{Yi}{2}$, so the value of the current flow through the branch connected between nodes k and m can be calculated by[15].

$$I_i = \sqrt{\frac{P_i^2 + Q_i^2}{V_k{}^2}}$$

Mathematically, objective function of the power losses is given as

$$Min\ P_L = \sum_{\forall k,m}^{k,m \in S_B} I_i^2 R_i = \sum_{\forall k,m}^{k,m \in S_B} \left(\frac{P_i^2 + Q_i^2}{V_k{}^2}\right) R_i$$

P_L is subject to the equality and inequality constrains as bellows

The active and reactive power flow in branch must satisfy the equations below

$$P_i - P_i' - R_i \frac{P_i'^2 + Q_i'^2}{V_m^2} = 0$$

$$Q_i - Q_i' - X_i \frac{P_i'^2 + Q_i'^2}{V_m^2} + V_k^2 \frac{Yi}{2} = 0$$

The voltage magnitudes at the sending point and receiving point must be satisfy the equation below for all branches in the distribution networks

$$V_m^2 - \left\{V_k^2 - 2(P_i'' R_i + Q_i'' X_i) + \frac{(P_i''^2 + Q_i''^2)(R_i^2 + X_i^2)}{V_k}\right\} = 0$$

The power factor of the DG connected to the bus m must be satisfy the flowing equation

$$\frac{P_m^{DG}}{\sqrt{(P_m^{DG})^2 + (Q_m^{DG})^2}} = \cos\alpha_m$$

The hourly energy balance in each ESS can be written as $E_{(h+1)} - E_{(h)} - \eta_{char} P_{mcharE} + \frac{P_{mdiscE}}{\eta_{disc}} = 0$

Where the $E_{(h)}$ is the energy level in ESS during the hour, efficiency η_{char} and η_{disc} are the charge and discharge efficiency. [16].

The active power charging should be zero during the on- peak time, for the discharging should also be zero during the off-peak time.

$$P_{mcharE\,(h1)} = 0, \quad h_1 \in \text{on} - \text{peak time}$$

$$P_{mdiscE\,(h2)} = 0, \quad h_2 \in \text{off} - \text{peak time}$$

The inequality constrains the line current flow the each branch should be within the thermal limit

$$I_i \le I_i^{rated}, \quad \forall\, m \in S_B$$

The bus voltage at each bus should not exceed maximum and minimum voltage

$V_m^{min} \le V_m \le V_m^{max}$,

$V_k^{min} \le V_k \le V_k^{max}$

The distribution generation's capacity must not exceed the total load of the network

$$\sum_m^{S_B} \sqrt{(P_m^{DG})^2 + (Q_m^{DG})^2} \le \sum_m^{S_B} \sqrt{(P_m^L)^2 + (Q_m^L)^2}$$

B. *The model of the ESS*

The BSS is the most commonly used in the ESS. It consists of many power conditioning systems (PCS), which can provide both active and reactive power to the DN [17]. When the PCS discharges to the network it can be seen as an inverter, whereas when it charges from the system can be regarded as the rectifier. A simple PCS, consists of a capacitor, diode as well as transformer. The active and reactive power discharge of the ESS should not exceed the maximum apparent power S_{PSCmax} of ESS [18].

$$P_{mdiscE}^2 + Q_{mdiscE}^2 \le S_{PSCmax}^2$$

The active power in terms of charging and discharging must be the positive values

$$P_{mcharE} \ge 0, \qquad P_{mdiscE} \ge 0$$

Moreover the upper and the lower bound of the storage units should be satisfied

$$E_{min} \le E \le E_{max}$$

The apparent power of the ESS should be larger than the maximum power demand which is 2.995MW, as can be seen from the Table II, and the installed capacity of the ESS also needs to be exceeded than the total install battery capacity of the total EVs which is 3217.8 kWh, the configuration can be seen in Table I. Therefore, the whole capacity is chosen to be 3.3MWh.

C. Methodology

The minimizing of power losses which are treated as nonlinear minimization problem, can be tackled as a sequential optimization [19], and dealt with using matlab optimization programming. Two optimization methods, UA-RPF ESS and CA-RPF of the ESS are proposed for the power losses reduction based on that programming. For the UA-RPF the active, reactive power discharge and the active power charge of the ESS are optimized, by using the matlab nonlinear programming without considering the peak and off peak load periods. H, for the CA-RPF, the minimization not only relates to the optimization of active, reactive power discharge of the ESS, but also two charging time (off peak charging and peak charging) is taken into consideration.

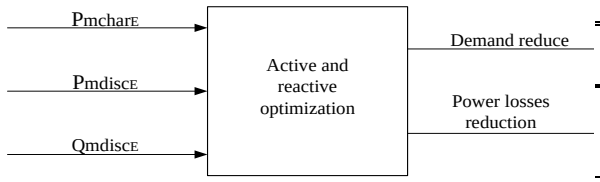

Fig.7.Input and output chart

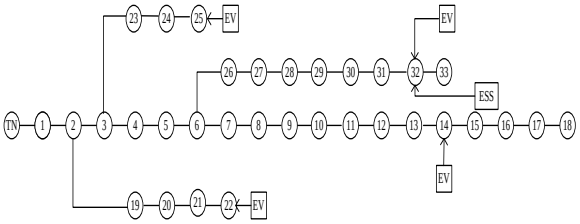

Fig.8.The tested DN

It is assumed that the ESS needs to be fully charged before it provides the active and reactive power to the DN, or before it is first installed into the networks active and reactive power to the DN, or before it is first installed in the networks. The figures for charging in terms of power losses are shown in the Table V, and these are 0.53MW and 0.50MW for the latter case.

IV. RESULTS AND ANALYSIS

From the above section, power losses in terms of two different optimization methods were obtained by using the matlab optimization programming. In general, the losses are reduced when the ESS adds into the IEEE 33 tested DN.

TABLE IV. LOAD DEMAND FOR THE IEEE 33 TESTED NETWORK

Charging Period	EVs Penetration	0%	20%	30%	40%
8:30-14:30	**LD (MW)**	3.7	4.13	4.33	4.57
14:30-19:30	**LD (MW)**	3.9	4.33	4.56	4.77
19:30-23:30	**LD (MW)**	3.3	3.73	3.96	4.17

The table of load demands (LD) was built and can be seen above, based on the daily household load and the demand of the EV at different penetration levels. From the table above, 3.7MW is the load of the IEEE 33 tested system. This load is regarded as the base load for the period 8:30 – 14:30. Then according to the ratio between 8:30 – 14:30 and 14:30 19:30 in terms of daily household load which is 1.053, the load for 14:30-19:30 is calculated $3.7 \times 1.05 = 3.9$MW. The Same method is used to calculate the load between 19:30 and -23:30. 4.13 MW is calculated by 3.7 + 0.43MW＝4.13MW where 0.43MW is the total power demand of 20% EVs penetration for 4 different types of EV.

TABLE V. THE ACTIVE POWER LOSSES WITH ESS AND WITHOUT ESS

Charging period	Penetration level	0%	20%	30%	40%
8:30-14:30	**Without ESS**	0.12	0.25	0.34	0.45
	With ESS(MW)	0.53	0.09	0.13	0.18
14:30-19:30	**Without ESS**	0.05	0.26	0.36	0.47
	With ESS(MW)	0.13	0.10	0.25	0.32
19:30-23:30	**Without ESS**	0.11	0.22	0.31	0.41
	With ESS(MW)	0.50	0.08	0.22	0.27

Table.V.shows the differences of total active power losses (APL) in the tested DN with and without A-RPF ESS for UA-RPF case, during the different periods with different EV penetrations. From that table, the APL reduced dramatically when adding ESS to the DN. The total active power (TAP) reductions are 0.64MW, which is calculated by the sum of the difference of APL between the pattern with ESS and without ESS in terms of three different EVs penetration levels, for the period between 8:30-14:30. During the period 14:30-19:30 it is 0.42MW, whereas, for the period 19:30-23:30 it is 0.37MW. Therefore, the TAP can be reduced 1.43MW between 8:30 and 23:30.

It also needs to be noticed that the APLs increase by installing the ESS during the charging period from 8:30-14:30 and 19:30-23:30 with 0% EV penetration. The reason for is that for these two periods the ESS needs to be fully charged. So it raises the loads when it charges from the DN. Whereas, when the EVs connect to the DN, the active power losses are significantly reduced by using the A-RPF ESS

The charging period between 14:30 and-19:30 is chosen to see the differences between the two methods which are UA-RPF and CA-RPF. For the CA-RPF ESS, during the off peak periods of 8:30-14:30 and 19:30-23:30, the ESS has to be charged, but for the peak period between 14:30 and-19:30, the ESS has to discharge to the DN, without charging. However for the UA-RPF these factors are not taken into account.

Table.VII. Table VI. below indicates these two different methods in terms of APL, reactive power losses (RPL), and the TAP from the TN during the period between 14:30 to 19:30. The gaps can be seen by comparing the UA-RPF ESS and CA-RPF ESS. As shown in that table, the active and reactive power losses are decreased by using the UA-RPF and CA-RPF. Meanwhile, under the different EVs penetrations, large amount of active power from the TN can also be reduced by using the proposed method.

TABLE VI. THE APL,RPL,TAP WITHOUT ESS BETWEEN 14:30-19:30

Power loss / Penetration	APL	RPL	TAP
0%	0.13	0.09	4.03
20%	0.26	0.19	5.88
30%	0.36	0.27	6.89
40%	0.47	0.35	7.84

TABLE.VII. THE APL,RPL,TAP BETWEEN 14:30-19:30

Feeder / Time	14 (MW)	22 (MW)	25(MW)	32(MM)
14:30	0.0556	0.0516	0.0946	0.066
15:30	0.0622	0.0582	0.1062	0.0762
16:30	0.0701	0.0702	0.123	0.095
17:30	0.1428	0.1370	0.2042	0.1615
18:30	0.1174	0.1114	0.1814	0.1364
19:30	0.0778	0.0713	0.1418	0.0968

Fig.8 Fig.8 is drawn, in order to make the APL clearer as to the three different charging patterns, the black one is without ESS, the green one is CA-RPF ESS, and the red one is UA-RPF ESS. It can be seen that APL is much lower by using the proposed methods than by not using it.

It is very interesting to notice that, the APL is a little bigger at the beginning of the coordinated charging compare with the uncoordinated one. The reason for this is in this scenario loads of the DN are not increased, ESS has to use active and reactive power which are already stored in the ESS during the off peak times. So it generates more active and reactive power than the situation in terms of UA-RPF ESS. However, with the loads raise, the active power losses are almost the same as for the UA-RPF ESS.

Although, by using the CA-RPS ESS charging method power losses are slightly higher than the UA-RPF ESS charging method, the charging price of ESS is much lower than the UA-RPF ESS, in terms of using the peak and off peak electricity price. During the same period, the active power can be decreased from the TN by installing the ESS in the DN. In the UA-RPF ESS pattern, 1.61MW power can be reduced which is calculated by 4.03-2.42=1.61MW. In the CA-RPF ESS pattern, 3.0 MW power calculated by 4.03-1.01 can be reduced for 0% EV penetration. For the 20% EV, the power reductions are 2.03MW and 2.04MW respectively. For the 30% they are 0.98Mw, 0.99MW, for 40% the power from TN that can be reduced are 1.2MW, 1.23MW.

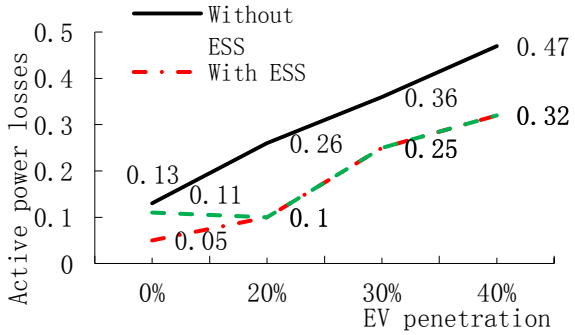

Fig.8. The comparison the between the 3 different charging method

Fig.10 is made for comparing the TPL of the CA-RPF ESS and the TPL without ESS during the period between 14:30 and 19:30 at the 30% EV penetration. According to the Fig. 9 at 14:30, 6% EVs are not under way, the total power demand for the EVs at this time is $6\% \times 0.66 = 0.0039$ MW , and 0.66 MW is the total power demand (TPD) of 30% EV for the 100 EVs. At 15:30 the TPD is $7\% \times 0.66 = 0.00462$ MW , 16:30 is $8\% \times 0.66 = 0.0039$ MW , 17:30 is $18\% \times 0.66 = 0.1188$ MW , 18:30 is $14\% \times 0.66 = 0.0924$,19:30 is $8\% \times 0.66 = 0.0528$ MW. These loads are connected to the feeder 14, 22, 25,and 32 respectively, for each time.

TABLE VIII. FEEDER'S LOAD

Pattern / EVs penetration	With ESS UA-PRF(MW)			With ESS CA-PRF(MW)		
	APL	RPL	TAP	APL	RPL	TAP
0%	0.05	0.04	2.42	0.11	0.11	1.01
20%	0.10	0.08	3.85	0.10	0.08	3.84
30%	0.25	0.19	5.91	0.25	0.19	5.90
40%	0.32	0.24	6.64	0.32	0.24	6.61

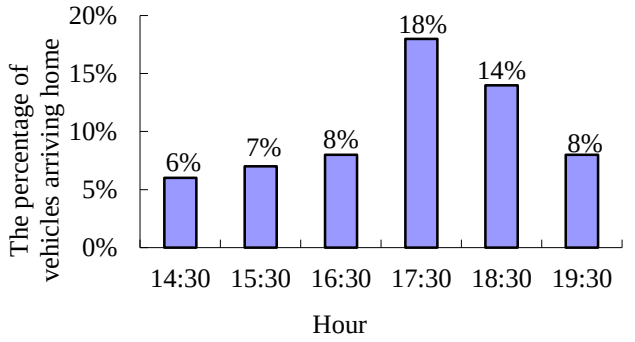

Fig.9. Percentage of vehicles arriving at home between 14:30 to 19:30

Adding these demands into the tested DN is shown in the table below. At 14:30 for the feeder 14 the power demand including EVs and daily loads is 0.016 + 0.0039 = 0.0556MW, 0.016 MW is the house hold loads at feeder 14.

From Fig .10 below the TPLs increases from 14:30 to 18:30 and then decreases from 18:30 to 19:30. One of the main reasons of this is that demands for the electricity raises and then declines. It is worth noticing that, the maximum TPL which is 0.058 MW with the ESS is much less than the TPL 0.053MW without the ESS.

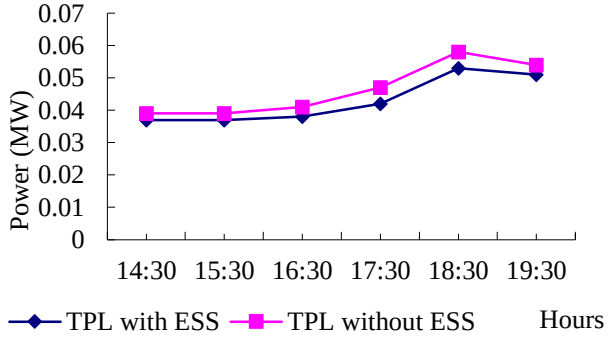

Fig.10.The total power losses of the tested network in terms of different charging pattern

TABLE IX.THE TOTAL POWER LOSSES OF THE TESTED NETWORK IN

Time / Pattern	14:30	15:30	16:30	17:30	18:30	19:30
TPL with ESS	0.037	0.037	0.038	0.042	0.053	0.051
TPLwithout ESS	0.039	0.039	0.041	0.047	0.058	0.054

TERMS OF DIFFERENT CHARGING PATTERN

The active power and reactive power discharge of the ESS is shown in Fig.11. Below. During the period between 14:30- 17:30 the active and reactive power increases all the time, at 17:30 it reaches the highest point and then decreases for the rest of the time. The gap between the active and reactive power discharge is very high, because the EV doesn't need the reactive power and, the householders do not need lots of reactive power, moreover it also does not change a great deal during time as it goes by.

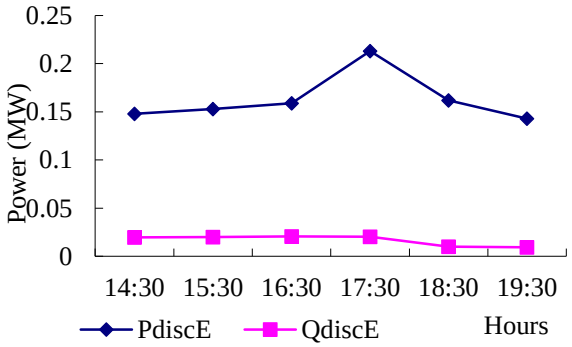

Fig.11. PDISCE AND QDISCE DURING THE TIME BETWEEN 14:30 - 19:30

TABLE X. PDISCE AND QDISCE DURING THE TIME BETWEEN 14:30 -

Time / Pattern	14:30	15:30	16:30	17:30	18:30	19:30
P discE (MW)	0.015	0.152	0.159	0.213	0.162	0.143
Q discE (Mvar)	0.019	0.020	0.020	0.020	0.102	0.090

19:30

Fig.12. shows that the TAP receives from the grid with the ESS without ESS, and the TAP provides by the DN with ESS. It can be seen that from the period 14:30 to 18:30 (for the DN with ESS) with power demand increases the TAP from the TN rise from 0.59MW at 14:30 to 1.75MW, then declined to a low of 1.63MW at 19:30. It is noticeable that the ESS reduces a great deal of active power from the network compare with the one without ESS, at 18:30, 0.13MW active power reduced, at 17:30 0.19MW active power does not need to import from the TN. Moreover the total 0.75MW active power can be reduced by using the ESS.

TABLE XI. THE TAP FROM THE TN

Time / Pattern	14:30	15:30	16:30	17:30	18:30	19:30
TAP from TN with ESS(MW)	0.59	0.62	0.74	1.08	1.75	1.63
TAP from TN without ESS(MW)	0.69	0.73	0.87	1.27	1.88	1.72
TAP provides by DN with ESS (MW)	0.74	0.77	0.90	1.29	1.92	1.77

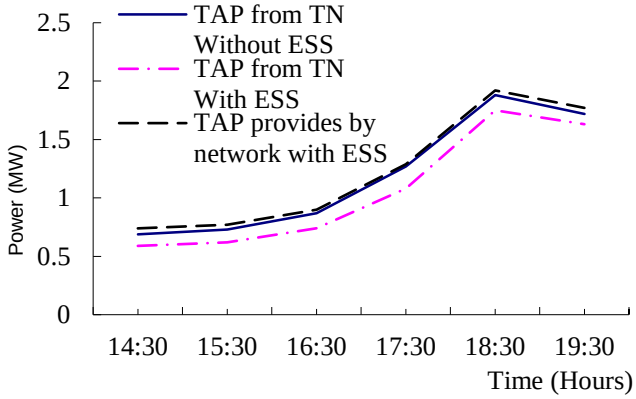

Fig.12.The TAP from the TN with and without ESS

III CONCLUSION:

Previously, many studies used optimization methods based on either active or reactive power dispatch in terms of capacitor placement, network reconfiguration, as well as charger design for power loses reduction caused by EVs within in the DN. The power losses were compared with, and without, optimization methods. But unlike these methods, in this paper we proposed, and compare, two different methods both based on the active, and reactive power optimization dispatch of the ESS for power loss reduction. In addition, the power imported from the TN has also been reduced..

In the first part of the paper, by using historical data for daily load, charging demand for EVs was analysed. Meanwhile, EVs were added into the IEEE 33 nodes test networks, the percent between total power losses and total power generated raises from 3.16% at 0% EV penetration to 5.69% at 40% penetration between 8:30-23:30 hours. Therefore, when EV penetration levels increase, the power losses increase dramatically, the trend of losses is almost linear from fig.4, so with the more EVs penetration, losses will rise predictably.

In the second part of the paper, using the combined problem formulation for the active and reactive power dispatch of the ESS lowers the active power losses. 1.43MW of total active power losses can be reduced. Moreover two novel charging and discharging methods, which are coordinated active-reactive power flow of the ESS and uncoordinated active-reactive power flow of the ESS, were used in the IEEE 33 node test network during the peak time between 14:30-19:30 hours. Although for the former method

the active power losses are a little higher, compare with the latter method, 1.64MW does not need to be imported from the TN, making the charging price of the ESS lower for the first method. Overall, adding ESS is an efficient method for the DN to achieve power loss reduction.

The results were obtained by using the optimization algorithms described in this paper, the applied methodologies and techniques can also be used to other objective functions, for instance to reduce the voltage drop, reactive power balancing or coordination of the wind power and the ESS operation

ACKNOWLEDGMENT

The author would like to thank the University of Bath for the opportunity to carry out the research described in this paper.

REFERENCES

[1]A.Raskin, and S.Shah, " The Emergence of Hybrid Vehicles," Research on Strategic Change .Rep.3-41, 2006.
[2]M.Anderman, "The challenge to fulfil electrical power requirements of advanced vehicles," *Journal. Power Sources*, vol.127, pp. 2–7, Mar.2004.
[3]J.Cole.(2013)InsideEVwebpage.[online].Available:http://insideevs.com/september-2013-plug-in-electric-vehicle-sales-report-card/
[4]J.Park, J.M.Sohn, and J.K.Park, "Optimal capacitor allocation in a distribution system considering operation costs," *IEEE Transactions Power System*, vol. 24, pp. 462–468, Feb. 2008.
[5]H.Falaghi, M.Ramezani, M.-R. Haghifam, and K. Milani. "Optimal conductor selection for radial distribution systems," *in Turin*,2005, paper. 63, pp. 95-103.
[6]D. K. Chembe, "Reduction of Power Losses Using Phase Load Balancing Method in Power Networks," *in San Francisco, USA*, pp. 492-497.
[7]P.Owen, "Powering the Nation Household electricity-using habits revealed" Energy Saving trust, London.EST.Rep. 2011.
[8]J.Voeclcker.(2012).GreenCarreportWebpage.[Online].Available: http://www.greencarreporrts.com/news/1078116_july-plug-in-electric-car-sales-volt-steady-leaflethargic-again.
[9]J.Voelcker,(2012).GreenCarReportsWebpage.[Online].Available: http://www.greencarreports.com/news/1081419plug-in-electric-car-sales-triplei in2013-as-buyers-models-increase
[10]J.Cole,(2013).GreenCarReport.Webpage[Online].Available:http://insideevs.com/september-2013-plug-in-electric-vehicle-sales-report-card/
[11]J.Cole,(2013)GreenCarReport.Webpage[Online].Available:http://insideevs.com/june-2013-plug-in-electric-vehicle-sales-report-card/
[12]J.Kassakian, R.Schmalensee, "The future of the electric grid", MIT STUDY ON THE FUTURE OF THE ELECTRIC GRID, MIT Press, 2001
[13]K.Schneider, G.Shirek, and S.K.Solanki, (2000) "IEEE Distribution SystemAnalysisSubcommittee"[online]Available:http://ewh.ieee.org/soc/pes/dsacom.
[14]G.Zeiss,(2011).ElectrifyingTransportation.Webside.[online].Available:http://geospatial.blogs.com/geospatial/2011/07/electrifying-transportation.htm
[15]S,G,Nail. D,K,Khatod. M,P,Sharma. "Optimal allocation of combined DG and capacitor for real power loss minimization in distribution networks," *Electrical Power and Energy Systems*,vol,53,pp.967-973.2013.
[16]A. Gabash, and P. Li, "Evaluation of reactive power capability by optimal control of wind-vanadium redox battery stations in electricity market," *Renewable Energy & Power Quality* J., vol. 9, pp. 1–6, May2011.
[17]N. W. Miller, R. S. Zrebiec, G. Hunt, and R. W. Deimerico, "Design and commissioning of a 5 MVA, 2.5MWh battery energy storagesystem," in Proc. IEEE Transm. Distrib. Conf., Los Angeles, pp. 339–345, Aug.2007
[18]L. H. Walker, "10-MW GTO converter for battery peaking service,"IEEE Transactions on industry application. vol. 26, no. 1, pp. 63–72, Jan./Feb. 1990.
[19]E.Haesen, J. Driesen, and R. Belmans, "Robust planning methodology for integration of stochastic generators in distribution grids," IET J.Renew. Power Gen, vol. 1, pp. 25–32, Mar. 2007.

Appendix A

The data for 11-bus distribution line uniformly load type

bus data

bus_i	type	Pd	Qd	Gs	Bs	area	Vm	Va	baseKV	zone	Vmax	Vmin
mpc.bus = [												
1	3	0.50	0.20	0	0	1	1	0	12.5	1	1.05	0.95
2	2	0.50	0.20	0	0	1	1	0	12.5	1	1.05	0.95
3	2	0.50	0.20	0	0	1	1	0	12.5	1	1.05	0.95
4	1	0.50	0.20	0	0	1	1	0	12.5	1	1.05	0.95
5	1	0.50	0.20	0	0	1	1	0	12.5	1	1.05	0.95
6	1	0.50	0.20	0	0	1	1	0	12.5	1	1.05	0.95
7	1	0.50	0.20	0	0	1	1	0	12.5	1	1.05	0.95
8	1	0.50	0.20	0	0	1	1	0	12.5	1	1.05	0.95
9	1	0.50	0.20	0	0	1	1	0	12.5	1	1.05	0.95
10	1	0.50	0.20	0	0	1	1	0	12.5	1	1.05	0.95
11	1	0.50	0.20	0	0	1	1	0	12.5	1	1.05	0.95
];												

branch data

f bus	t bus	r	x	b	rate A	rate B	rate C	ratio	angle	status	angmin	angmax
mpc.branch = [												
1	2	0.538	0.462	0	4.60	4.60	4.60	0	0	1	-360	360
2	3	0.538	0.462	0	4.10	4.10	4.10	0	0	1	-360	360
3	4	0.538	0.462	0	2.90	2.90	2.90	0	0	1	-360	360
4	5	0.538	0.462	0	2.90	2.90	2.90	0	0	1	-360	360
5	6	0.538	0.462	0	2.90	2.90	2.90	0	0	1	-360	360
6	7	0.538	0.462	0	1.50	1.50	1.50	0	0	1	-360	360
7	8	0.538	0.462	0	1.05	1.05	1.05	0	0	1	-360	360
8	9	0.538	0.462	0	1.05	1.05	1.05	0	0	1	-360	360
9	10	0.538	0.462	0	1.05	1.05	1.05	0	0	1	-360	360
10	11	0.538	0.462	0	1.05	1.05	1.05	0	0	1	-360	360
];												

The data for 11-bus distribution line centrally load type

bus data

bus_i	type	Pd	Qd	Gs	Bs	area	Vm	Va	baseKV	zone	Vmax	Vmin
mpc.bus = [												
1	3	0.05	0.20	0	0	1	1	0	12.5	1	1.05	0.95
2	2	0.10	0.20	0	0	1	1	0	12.5	1	1.05	0.95
3	2	0.20	0.20	0	0	1	1	0	12.5	1	1.05	0.95
4	1	0.30	0.20	0	0	1	1	0	12.5	1	1.05	0.95
5	1	0.40	0.20	0	0	1	1	0	12.5	1	1.05	0.95
6	1	0.50	0.20	0	0	1	1	0	12.5	1	1.05	0.95
7	1	0.40	0.20	0	0	1	1	0	12.5	1	1.05	0.95
8	1	0.30	0.20	0	0	1	1	0	12.5	1	1.05	0.95

```
9  1   0.20  0.20  0   0   1   1   0   12.5   1   1.05 0.95
10 1   0.10  0.20  0   0   1   1   0   12.5   1   1.05 0.95
11 1   0.05  0.20  0   0   1   1   0   12.5   1   1.05 0.95
];

branch data
f bus   t bus   r       x       b       rateA   rateB   rateC   ratio   angle   status angmin
angmax
mpc.branch = [
   1    2    0.538   0.462   0    4.60   4.60   4.60   0    0    1    -360   360
   2    3    0.538   0.462   0    4.10   4.10   4.10   0    0    1    -360   360
   3    4    0.538   0.462   0    2.90   2.90   2.90   0    0    1    -360   360
   4    5    0.538   0.462   0    2.90   2.90   2.90   0    0    1    -360   360
   5    6    0.538   0.462   0    2.90   2.90   2.90   0    0    1    -360   360
   6    7    0.538   0.462   0    1.50   1.50   1.50   0    0    1    -360   360
   7    8    0.538   0.462   0    1.05   1.05   1.05   0    0    1    -360   360
   8    9    0.538   0.462   0    1.05   1.05   1.05   0    0    1    -360   360
   9    10   0.538   0.462   0    1.05   1.05   1.05   0    0    1    -360   360
   10   11   0.538   0.462   0    1.05   1.05   1.05   0    0    1    -360   360
];
```

The data for 11-bus distribution line increasingly load type

```
bus data
bus_i   type   Pd  Qd  Gs  Bs  area   Vm  Va  baseKV  zone   Vmax   Vmin
mpc.bus = [
1  3   0.05  0.20  0   0   1   1   0   12.5   1   1.05 0.95
2  2   0.10  0.20  0   0   1   1   0   12.5   1   1.05 0.95
3  2   0.15  0.20  0   0   1   1   0   12.5   1   1.05 0.95
4  1   0.20  0.20  0   0   1   1   0   12.5   1   1.05 0.95
5  1   0.25  0.20  0   0   1   1   0   12.5   1   1.05 0.95
6  1   0.30  0.20  0   0   1   1   0   12.5   1   1.05 0.95
7  1   0.35  0.20  0   0   1   1   0   12.5   1   1.05 0.95
8  1   0.40  0.20  0   0   1   1   0   12.5   1   1.05 0.95
9  1   0.45  0.20  0   0   1   1   0   12.5   1   1.05 0.95
10 1   0.50  0.20  0   0   1   1   0   12.5   1   1.05 0.95
11 1   0.55  0.20  0   0   1   1   0   12.5   1   1.05 0.95
];


branch data
f bus   t bus   r       x       b       rateA   rateB   rateC   ratio   angle   status angmin
angmax
mpc.branch = [
1       2    0.538   0.462   0    4.60   4.60   4.60   0    0    1    -360   360
   2    3    0.538   0.462   0    4.10   4.10   4.10   0    0    1    -360   360
   3    4    0.538   0.462   0    2.90   2.90   2.90   0    0    1    -360   360
   4    5    0.538   0.462   0    2.90   2.90   2.90   0    0    1    -360   360
   5    6    0.538   0.462   0    2.90   2.90   2.90   0    0    1    -360   360
   6    7    0.538   0.462   0    1.50   1.50   1.50   0    0    1    -360   360
```

```
    7     8     0.538  0.462  0      1.05    1.05    1.05    0      0      1      -360    360
    8     9     0.538  0.462  0      1.05    1.05    1.05    0      0      1      -360    360
    9     10    0.538  0.462  0      1.05    1.05    1.05    0      0      1      -360    360
    10    11    0.538  0.462  0      1.05    1.05    1.05    0      0      1      -360    360
];
```

Appendix B

The data for IEEE 33-bus DN

bus data

bus_i	type	Pd	Qd	Gs	Bs	area	Vm	Va	baseKV	zone	Vmax	Vmin
mpc.bus = [												
1	3	0.00	0.00	0	0	1	1	0	12.66	1	1.05	0.95
2	1	0.021	0.06	0	0	1	1	0	12.66	1	1.05	0.95
3	1	0.002	0.04	0	0	1	1	0	12.66	1	1.05	0.95
4	1	0.253	0.08	0	0	1	1	0	12.66	1	1.05	0.95
5	1	0.013	0.03	0	0	1	1	0	12.66	1	1.05	0.95
6	1	0.013	0.02	0	0	1	1	0	12.66	1	1.05	0.95
7	1	0.042	0.10	0	0	1	1	0	12.66	1	1.05	0.95
8	1	0.042	0.10	0	0	1	1	0	12.66	1	1.05	0.95
9	1	0.013	0.02	0	0	1	1	0	12.66	1	1.05	0.95
10	1	0.013	0.02	0	0	1	1	0	12.66	1	1.05	0.95
11	1	0.010	0.03	0	0	1	1	0	12.66	1	1.05	0.95
12	1	0.013	0.035	0	0	1	1	0	12.66	1	1.05	0.95
13	1	0.013	0.035	0	0	1	1	0	12.66	1	1.05	0.95
14	1	0.077	0.08	0	0	1	1	0	12.66	1	1.05	0.95
15	1	0.013	0.01	0	0	1	1	0	12.66	1	1.05	0.95
16	1	0.013	0.02	0	0	1	1	0	12.66	1	1.05	0.95
17	1	0.013	0.02	0	0	1	1	0	12.66	1	1.05	0.95
18	1	0.019	0.04	0	0	1	1	0	12.66	1	1.05	0.95
19	1	0.019	0.04	0	0	1	1	0	12.66	1	1.05	0.95
20	1	0.019	0.04	0	0	1	1	0	12.66	1	1.05	0.95
21	1	0.019	0.04	0	0	1	1	0	12.66	1	1.05	0.95
22	1	0.071	0.04	0	0	1	1	0	12.66	1	1.05	0.95
23	1	0.019	0.05	0	0	1	1	0	12.66	1	1.05	0.95
24	1	0.089	0.20	0	0	1	1	0	12.66	1	1.05	0.95
25	1	0.142	0.20	0	0	1	1	0	12.66	1	1.05	0.95
26	1	0.089	0.025	0	0	1	1	0	12.66	1	1.05	0.95
27	1	0.089	0.025	0	0	1	1	0	12.66	1	1.05	0.95
28	1	0.089	0.02	0	0	1	1	0	12.66	1	1.05	0.95
29	1	0.253	0.07	0	0	1	1	0	12.66	1	1.05	0.95
30	1	0.042	0.60	0	0	1	1	0	12.66	1	1.05	0.95
31	1	0.032	0.07	0	0	1	1	0	12.66	1	1.05	0.95
32	1	0.097	0.10	0	0	1	1	0	12.66	1	1.05	0.95
33	1	0.013	0.04	0	0	1	1	0	12.66	1	1.05	0.95
];												

branch data

fbus	tbus	r	x	b	rateA	rateB	rateC	ratio	angle	status	angmin	angmax

mpc.branch = [

1	2	0.0922	0.0470	0	4.60	4.60	4.60	0	0	1	-360	360
2	3	0.4930	0.2511	0	4.10	4.10	4.10	0	0	1	-360	360
3	4	0.3660	0.1864	0	2.90	2.90	2.90	0	0	1	-360	360
4	5	0.3811	0.1941	0	2.90	2.90	2.90	0	0	1	-360	360
5	6	0.8190	0.7070	0	2.90	2.90	2.90	0	0	1	-360	360
6	7	0.1872	0.6188	0	1.50	1.50	1.50	0	0	1	-360	360
7	8	0.7114	0.2351	0	1.05	1.05	1.05	0	0	1	-360	360
8	9	1.0300	0.7400	0	1.05	1.05	1.05	0	0	1	-360	360
9	10	1.0440	0.7400	0	1.05	1.05	1.05	0	0	1	-360	360
10	11	0.1966	0.0650	0	1.05	1.05	1.05	0	0	1	-360	360
11	12	0.3744	0.1238	0	1.05	1.05	1.05	0	0	1	-360	360
12	13	1.4680	1.1550	0	0.50	0.50	0.50	0	0	1	-360	360
13	14	0.5416	0.7129	0	0.45	0.45	0.45	0	0	1	-360	360
14	15	0.5910	0.5260	0	0.30	0.30	0.30	0	0	1	-360	360
15	16	0.7463	0.5450	0	0.25	0.25	0.25	0	0	1	-360	360
16	17	1.2890	1.7210	0	0.25	0.25	0.25	0	0	1	-360	360
17	18	0.7320	0.5740	0	0.10	0.10	0.10	0	0	1	-360	360
2	19	0.1640	0.1565	0	0.50	0.50	0.50	0	0	1	-360	360
19	20	1.5042	1.3554	0	0.50	0.50	0.50	0	0	1	-360	360
20	21	0.4095	0.4784	0	0.21	0.21	0.21	0	0	1	-360	360
21	22	0.7089	0.9373	0	0.11	0.11	0.11	0	0	1	-360	360
3	23	0.4512	0.3083	0	1.05	1.05	1.05	0	0	1	-360	360
23	24	0.8980	0.7091	0	1.05	1.05	1.05	0	0	1	-360	360
24	25	0.8960	0.7011	0	0.50	0.50	0.50	0	0	1	-360	360
6	26	0.2030	0.1034	0	1.50	1.50	1.50	0	0	1	-360	360
26	27	0.2842	0.1447	0	1.50	1.50	1.50	0	0	1	-360	360
27	28	1.0590	0.9337	0	1.50	1.50	1.50	0	0	1	-360	360
28	29	0.8042	0.7006	0	1.50	1.50	1.50	0	0	1	-360	360
29	30	0.5075	0.2585	0	1.50	1.50	1.50	0	0	1	-360	360
30	31	0.9744	0.9630	0	0.50	0.50	0.50	0	0	1	-360	360
31	32	0.3105	0.3619	0	0.50	0.50	0.50	0	0	1	-360	360
32	33	0.3410	0.5302	0	0.10	0.10	0.10	0	0	1	-360	360
8	21	2.0000	2.0000	0	0.50	0.50	0.50	0	0	1	-360	360
9	15	2.0000	2.0000	0	0.50	0.50	0.50	0	0	1	-360	360
12	22	2.0000	2.0000	0	0.50	0.50	0.50	0	0	1	-360	360
18	33	0.5000	0.5000	0	0.50	0.50	0.50	0	0	1	-360	360
25	29	0.5000	0.5000	0	0.10	0.10	0.10	0	0	1	-360	360

];

Appendix C

The data for 36-bus DN

bus data
bus_i type Pd Qd Gs Bs area Vm Va baseKV zone Vmax Vmin
mpc.bus = [

1	3	0.00	0.00	0	0	1	1	0	11	1	1.05	0.95
2	1	0.10	0.06	0	0	1	1	0	11	1	1.05	0.95
3	1	0.09	0.04	0	0	1	1	0	11	1	1.05	0.95
4	1	0.12	0.08	0	0	1	1	0	11	1	1.05	0.95
5	1	0.06	0.03	0	0	1	1	0	11	1	1.05	0.95
6	1	0.06	0.02	0	0	1	1	0	11	1	1.05	0.95
7	1	0.2	0.30	0	0	1	1	0	11	1	1.05	0.95
8	1	0.2	0.30	0	0	1	1	0	11	1	1.05	0.95
9	1	0.06	0.02	0	0	1	1	0	11	1	1.05	0.95
10	1	0.06	0.02	0	0	1	1	0	11	1	1.05	0.95
11	1	0.05	0.03	0	0	1	1	0	11	1	1.05	0.95
12	1	0.06	0.035	0	0	1	1	0	11	1	1.05	0.95
13	1	0.06	0.035	0	0	1	1	0	11	1	1.05	0.95
14	1	0.12	0.08	0	0	1	1	0	11	1	1.05	0.95
15	1	0.06	0.01	0	0	1	1	0	11	1	1.05	0.95
16	1	0.06	0.02	0	0	1	1	0	11	1	1.05	0.95
17	1	0.06	0.02	0	0	1	1	0	11	1	1.05	0.95
18	1	0.09	0.05	0	0	1	1	0	11	1	1.05	0.95
19	1	0.09	0.05	0	0	1	1	0	11	1	1.05	0.95
20	1	0.09	0.05	0	0	1	1	0	11	1	1.05	0.95
21	1	0.09	0.05	0	0	1	1	0	11	1	1.05	0.95
22	1	0.09	0.05	0	0	1	1	0	11	1	1.05	0.95
23	1	0.09	0.05	0	0	1	1	0	11	1	1.05	0.95
24	1	0.40	0.30	0	0	1	1	0	11	1	1.05	0.95
25	1	0.40	0.30	0	0	1	1	0	11	1	1.05	0.95
26	1	0.06	0.04	0	0	1	1	0	11	1	1.05	0.95
27	1	0.06	0.04	0	0	1	1	0	11	1	1.05	0.95
28	1	0.06	0.03	0	0	1	1	0	11	1	1.05	0.95
29	1	0.12	0.07	0	0	1	1	0	11	1	1.05	0.95
30	1	0.20	0.10	0	0	1	1	0	11	1	1.05	0.95
31	1	0.06	0.09	0	0	1	1	0	11	1	1.05	0.95
32	1	0.20	0.30	0	0	1	1	0	11	1	1.05	0.95
33	1	0.06	0.04	0	0	1	1	0	11	1	1.05	0.95
34	1	0.13	0.09	0	0	1	1	0	11	1	1.05	0.95
35	1	0.13	0.09	0	0	1	1	0	11	1	1.05	0.95
36	1	0.13	0.09	0	0	1	1	0	11	1	1.05	0.95

];

branch data

fbus tbus r x b rateA rateB rateC ratio angle status angmin angmax

mpc.branch = [

1	2	0.0990	0.2189	0	4.60	4.60	4.60	0	0	1	-360	360
2	3	0.7860	0.2124	0	4.10	4.10	4.10	0	0	1	-360	360
3	4	0.0655	0.1770	0	2.90	2.90	2.90	0	0	1	-360	360
4	5	0.1048	0.2832	0	2.90	2.90	2.90	0	0	1	-360	360
5	6	0.1179	0.3186	0	2.90	2.90	2.90	0	0	1	-360	360
6	7	0.1048	0.2832	0	1.50	1.50	1.50	0	0	1	-360	360
7	8	0.0917	0.2478	0	1.05	1.05	1.05	0	0	1	-360	360
8	9	0.1572	0.4248	0	1.05	1.05	1.05	0	0	1	-360	360
9	10	0.1441	0.3894	0	1.05	1.05	1.05	0	0	1	-360	360
10	11	0.0786	0.2124	0	1.05	1.05	1.05	0	0	1	-360	360
11	12	0.1834	0.4956	0	1.05	1.05	1.05	0	0	1	-360	360
12	13	0.1179	0.3186	0	0.50	0.50	0.50	0	0	1	-360	360
13	14	0.0655	0.1770	0	0.45	0.45	0.45	0	0	1	-360	360
14	15	0.1179	0.3186	0	0.30	0.30	0.30	0	0	1	-360	360
15	16	0.1703	0.4602	0	0.25	0.25	0.25	0	0	1	-360	360
16	17	0.1048	0.2832	0	0.25	0.25	0.25	0	0	1	-360	360
17	18	0.1572	0.4248	0	0.10	0.10	0.10	0	0	1	-360	360
2	19	0.4725	0.2505	0	0.50	0.50	0.50	0	0	1	-360	360
19	20	0.7560	0.4008	0	0.50	0.50	0.50	0	0	1	-360	360
20	21	0.4095	0.4784	0	0.21	0.21	0.21	0	0	1	-360	360
21	22	0.9450	0.5010	0	0.11	0.11	0.11	0	0	1	-360	360
3	23	0.5670	0.3006	0	1.05	1.05	1.05	0	0	1	-360	360
23	24	0.8505	0.4509	0	1.05	1.05	1.05	0	0	1	-360	360
24	25	0.6615	0.3507	0	0.50	0.50	0.50	0	0	1	-360	360
6	26	0.5670	0.3006	0	1.50	1.50	1.50	0	0	1	-360	360
26	27	0.4725	0.2505	0	1.50	1.50	1.50	0	0	1	-360	360
27	28	0.6615	0.3507	0	1.50	1.50	1.50	0	0	1	-360	360
28	29	1.0395	0.5511	0	1.50	1.50	1.50	0	0	1	-360	360
29	30	0.2835	0.1503	0	1.50	1.50	1.50	0	0	1	-360	360
30	31	0.4725	0.2505	0	0.50	0.50	0.50	0	0	1	-360	360
31	32	0.7560	0.4008	0	0.50	0.50	0.50	0	0	1	-360	360
32	33	0.5670	0.3006	0	0.10	0.10	0.10	0	0	1	-360	360
33	34	0.9450	0.5010	0	0.50	0.50	0.50	0	0	1	-360	360
33	35	0.9450	0.5010	0	0.50	0.50	0.50	0	0	1	-360	360
33	36	0.9450	0.5010	0	0.50	0.50	0.50	0	0	1	-360	360
34	36	0.9450	0.5010	0	0.50	0.50	0.50	0	0	1	-360	360
35	36	0.9450	0.5010	0	0.10	0.10	0.10	0	0	1	-360	360

];

Appendix D

The new parameters of 36-bus test DN for impacts factors analyse

Table 7.1 Comparison between R and X

Original Parameters				New Parameters			
From Bus i	To bus i+1	Resistance (Ω)	Reactance (Ω)	From Bus i	To bus i+1	Resistance (Ω)	Reactance (Ω)
9	10	0.1441	0.3894	9	10	0.2835	0.1503
10	11	0.0786	0.2124	10	11	0.4725	0.2505
11	12	0.1834	0.4956	11	12	0.756	0.4008
12	13	0.1179	0.3186	12	13	0.567	0.3006
13	14	0.0655	0.177	13	14	0.945	0.501
14	15	0.1179	0.3186	14	15	0.945	0.501
15	16	0.1703	0.4602	15	16	0.945	0.501
16	17	0.1048	0.2832	16	17	0.945	0.501
17	18	0.1572	0.4248	17	18	0.945	0.501
29	30	0.2835	0.1503	29	30	0.1441	0.3894
30	31	0.4725	0.2505	30	31	0.0786	0.2124
31	32	0.756	0.4008	31	32	0.1834	0.4956
32	33	0.567	0.3006	32	33	0.1179	0.3186
33	34	0.945	0.501	33	34	0.0655	0.177
33	35	0.945	0.501	33	35	0.1179	0.3186
33	36	0.945	0.501	33	36	0.1703	0.4602
34	36	0.945	0.501	34	36	0.1048	0.2832
35	36	0.945	0.501	35	36	0.1572	0.4248

Table 7.2 Comparison between different loads

Original Parameters		New Parameters	
Bus NO.	Active load (MkW)	Bus NO.	Active load (MkW)
11	0.05	11	0.2
12	0.06	12	0.24
13	0.06	13	0.24
14	0.12	14	0.48
15	0.06	15	0.24
16	0.06	16	0.24
17	0.06	17	0.24
18	0.09	18	0.36
29	0.12	29	0.03
30	0.2	30	0.05
31	0.06	31	0.015
32	0.2	32	0.05
33	0.06	33	0.015
34	0.13	34	0.0325
35	0.13	35	0.0325
36	0.13	36	0.0325

Table 7.3 Comparison between different network parameters

Original Parameters				New Parameters			
From	To	Resistance	Reactance	From	To	Resistance	Reactance

Bus i	bus i+1	(Ω)	(Ω)	Bus i	bus i+1	(Ω)	(Ω)
9	10	0.1441	0.3894	9	10	0.2835	0.1503
10	11	0.0786	0.2124	10	11	0.4725	0.2505
11	12	0.1834	0.4956	11	12	0.756	0.4008
12	13	0.1179	0.3186	12	13	0.567	0.3006
13	14	0.0655	0.177	13	14	0.945	0.501
14	15	0.1179	0.3186	14	15	0.945	0.501
15	16	0.1703	0.4602	15	16	0.945	0.501
16	17	0.1048	0.2832	16	17	0.945	0.501
17	18	0.1572	0.4248	17	18	0.945	0.501
29	30	0.2835	0.1503	29	30	0.1441	0.3894
30	31	0.4725	0.2505	30	31	0.0786	0.2124
31	32	0.756	0.4008	31	32	0.1834	0.4956
32	33	0.567	0.3006	32	33	0.1179	0.3186
33	34	0.945	0.501	33	34	0.0655	0.177
33	35	0.945	0.501	33	35	0.1179	0.3186
33	36	0.945	0.501	33	36	0.1703	0.4602
34	36	0.945	0.501	34	36	0.1048	0.2832
35	36	0.945	0.501	35	36	0.1572	0.4248

Table 7.4 Comparison between different network loads

Original Parameters		New Parameters	
Bus NO.	Active load (MkW)	Bus NO.	Active load (MkW)
11	0.05	11	0.4
12	0.06	12	0.4
13	0.06	13	0.4
14	0.12	14	0.4
15	0.06	15	0.4
16	0.06	16	0.4
17	0.06	17	0.4
18	0.09	18	0.4

References List:

[1] D.S.Ginley, *Fundamentals of Materials for Energy and Environmental Sustainability*, 1st ed. Cambridge: Cambridge University Press, 2012.

[2] Depart of Energy and Climate Change, "The Smart Grid: the opportunity," *HM GOVERNMENT*, 2009.

[3] Department of Energy and Climate Change, "The UK Low Carbon Transition Plan," *HM GOVERNMENT*, 2009. [Online]. Available: https://www.gov.uk/government/uploads/system/uploads/attachment_data/file/228752/9780108508394.pdf.

[4] Depart of Energy and Climate Change, "UK Solar PV Strategy Part 1," *HM GOVERNMENT*, 2013.

[5] EPSRC, "Whole System Impacts and Socio-economics of wide scale PV integration," 2013.

[6] P. Swift, "Project Progress Report Reporting Period : December 2014 – May 2015 Six Monthly Progress Report Network Equilibrium," no. May, 2015.

[7] J. Watson, I. Scrase, and L. Stapleton, "Transforming the UK Energy System: Policies for the 2020 Renewables Target and Beyond," *Friends of the Earth*, 2010.

[8] DECC, "UK Renewable Energy Roadmap," *Carbon N. Y.*, vol. 5, no. July, pp. 293–298, 2011.

[9] Depart of Energy and Climate Change, "Smarter grids: the opportunity," *HM GOVERNMENT*, 2016. [Online]. Available: https://www.gov.uk/government/organisations/department-of-energy-climate-change.

[10] British Hydropower Association,"Hydro in the UK,"[Online]. Available: http://www.british-hydro.org/index.asp.

[11] F. Report, "Assessing the Costs and Benefits of Electricity Generation Using Alternative Energy Resources on the Outer Continental Shelf Final Report Assessing the Costs and Benefits of Electricity Generation Using Alternative Energy Resources on the Outer Continenta," 2007.

[12] E. Proffitt, "Profiting from Demand Side Response," National Grid, 2016.

[13] L. Macleod, "Overview of National Grid 's Balancing Services,"Nationa Grid, 2013.

[14] P. Swift *et al.*, "Fourth Carbon Budget Review – Technical Report," *Int. Conf. Renew. Energies Power Qual.*, vol. 1, no. July, p. 238, 2013.

[15] S. Faias, J. Sousa, L. Xavier, and P. Ferreira, "Energy Consumption and CO2

Emissions Evaluation for Electric and Internal Combustion Vehicles using a LCA Approach," *Int. Conf. Renew. Energies Power Qual.*, vol. 1, no. 9, pp. 1382–1388, 2014.

[16] C. Cluzel, E. Standen, B. Lane, and J. Anable, "Pathways to high penetration of electric vehicles - Report prepared for Committee on Climate Change," The University of Aberdeen, pp. 1–189, 2013.

[17] D. Rajagopal and D. Zilberman, "Review of Environmental Economic and Policy Aspects of Biofuels," *Polyicy Res. Work. Pap.*, no. September, p. 109, 2007.

[18] T. Trigg, P. Telleen, R. Boyd, and F. Cuenot, "Global EV Outlook: Understanding the Electric Vehicle Landscape to 2020," *Iea*, no. April, pp. 1–41, 2013.

[19] "Overview of the Electric Vehicle Market and the Potential of Charge Points for Demand Response," Services, ICF Consulting, 2016. .

[20] National Grid, "National Electricity Transmission System Seven Year Statement," *Energy*, no. May, p. 110, 2011.

[21] K. De Craemer and B. Claessens, "Combining Market-Based Control with Distribution Grid Constraints when Coordinating Electric Vehicle Charging," *Engineering*, vol. 1, no. 4, pp. 453–465, 2015.

[22] Ofgem, DECC, and Smart Grid Forum, "Smart Grid Vision and Routemap Smart Grid Forum," *Rep. Number URN 14D / 056*, no. February, 2014.

[23] D. S. Kirschen and S. Member, "Demand-Side View of Electricity Markets," *IEEE Trans. Power Syst*, vol. 18, no. 2, pp. 520–527, 2003.

[24] M. Dijk and M. Yarime, "The emergence of hybrid-electric cars: Innovation path creation through co-evolution of supply and demand," *Technol. Forecast. Soc. Change*, vol. 77, no. 8, pp. 1371–1390, 2010.

[25] M. Anderman, "The challenge to fulfill electrical power requirements of advanced vehicles," *J. Power Sources*, vol. 127, no. 1–2, pp. 2–7, 2004.

[26] N. Xuan Bac *et al.*, "A SiC-Based Matrix Converter Topology for Inductive Power Transfer System," *IEEE Trans. Power Electron.*, vol. 29, no. 8, pp. 4029–4038, 2014.

[27] M. Budhia, J. T. Boys, G. A. Covic, and C. Y. Huang, "Development of a single-sided flux magnetic coupler for electric vehicle IPT charging systems," *IEEE Trans. Ind. Electron.*, vol. 60, no. 1, pp. 318–328, 2013.

[28] S. Rajakaruna, A. Ghosh, and F. Shahnia, *Plug In Electric Vehicles in Smart Grids: Integration Techniques*. 2014.

[29] J.Cole, "December 2012 Plug-In Electric Vehicle Sales Report Card," *Inside EV*, 2013.

[Online]. Available: http://insideevs.com/december-2012-plug-in-electric-vehicle-sales-report-card/.

[30] X. Li, L. A. C. Lopes, and S. S. Williamson, "On the suitability of plug-in hybrid electric vehicle (PHEV) charging infrastructures based on wind and solar energy," *2009 IEEE Power Energy Soc. Gen. Meet.*, pp. 1–8, 2009.

[31] M. Valentine-urbschat and W. Bernhart, "Powertrain 2020 – The Future Drives Electric."

[32] P. H. Andersen, J. A. Mathews, and M. Rask, "Integrating private transport into renewable energy policy : The strategy of creating intelligent recharging grids for electric vehicles," vol. 37, pp. 2481–2486, 2009.

[33] D. L. Greene, P. D. Patterson, M. Singh, and J. Li, "Feebates, rebates and gas-guzzler taxes: A study of incentives for increased fuel economy," *Energy Policy*, vol. 33, no. 6, pp. 757–775, 2005.

[34] A. Corrigan, D. Masias, "Batteries for electric and hybrid vehicles. 4th ed.," *New York: McGraw Hill.*, 2011. [Online]. Available: https://www.accessengineeringlibrary.com/browse/lindens-handbook-of-batteries-fourth-edition/p2001c2f299729_3001.

[35] S. Grover, "UK Utility to Install 250 Electric Vehicle Charging Points," 2007. [Online]. Available: http://www.treehugger.com/cars/uk-utility-to-install-250-electric-vehicle-charging-points.html.

[36] C. Jeff, "2014.Top 6 Plug-In Vehicle Adopting Countries.," 2014. [Online]. Available: http://www.hybridcars.com/top-6-plug-in-vehicle-adopting-countries-2014/.

[37] S. Zachary, "Electric vehicle market share in 19 countries. ABB Conversations.," 2013. [Online]. Available: https://www.abb-conversations.com/2014/03/electric-vehicle-market-share-in-19-countries/.

[38] M. Moeini Aghtaie, A. Abbaspour, M. Fotuhi Firuzabad, and P. Dehghanian, "PHEVs centralized/decentralized charging control mechanisms: Requirements and impacts," *45th North Am. Power Symp. NAPS 2013*, 2013.

[39] M. Yilmaz and P. T. Krein, "Review of charging power levels and infrastructure for plug-in electric and hybrid vehicles," *2012 IEEE Int. Electr. Veh. Conf. IEVC 2012*, vol. 28, no. 5, pp. 2151–2169, 2012.

[40] Office of Energy Efficiency & Renewable Energy, "Alternative Fuels Data Center, Developing Infrastructure to Charge Plug-In Electric Vehicles," *U.S. Department of Energy*.

[41] R. Ellis and P. Eng, “Power System Harmonics–A Reference Guide to Causes, Effects and Corrective Measures,” *An Allen-Brandley Ser. Issues Answers*, pp. 1–14, 2001.

[42] P. Owen, “Powering the Nation Household electricity-using habits revealed,” in *Energy Saving trust*, London, 2011.

[43] S. Power, “Energy consumption of typical household appliances,” 2008.

[44] I. Felea and A. Daniel, “Impact Analysis of Unbalanced and Loading Degree on Power Losses Weight in a Distribution Network,” no. 2, pp. 195–200.

[45] F. Statutes, “Report On Electric Vehicle Charging,” no. December, 2012.

[46] K. Clement-Nyns, E. Haesen, and J. Driesen, “The impact of charging plug in hybrid electric vehicles on a residential distribution grid,” *IEEE Trans. Power Syst.*, vol. 25, no. 1, pp. 371–380, 2010.

[47] E. Benedict *et al.*, “Losses in Electric Power Systems,” *Electr. Comput. Eng. Tech. Rep. - Purdue Univ.*, pp. 1–91, 1992.

[48] S. Abe, R. R. Shoults, M. S. Chen, P. Eichenberger, and D. Farris, “Calculation of Energy Losses in a Distribution System,” *IEEE Trans. Power Appar. Syst.*, vol. PAS-99, no. 4, pp. 1347–1356, 1980.

[49] C. Gross, *Powere system analysis. 2 ed.* New York: John Wiley & Sons, 1986.

[50] A. H. Al-badi, A. Elmoudi, I. Metwally, A. Al-wahaibi, H. Al-Ajmi, and M. Al Bulushi, “Losses Reduction In Distribution Transformers,” *Proc. Int. MultiConferences Eng. Comput. Scienists 2011 , IMECS , March 16-18 ,2011, Hong Kong*, vol. II, 2011.

[51] L. Ran, K. S. Smith, Y. Liao, and G. A. Putrus, “Calculation of transformer core losses with nonlinear loads,” *10th Int. Conf. Harmon. Qual. Power. Proc. (Cat. No.02EX630)*, vol. 2, pp. 682–687, 2002.

[52] J. C. Olivares, R. Escarela-Pérez, Y. Liu, J. Driesen, J. M. Cañedo, and P. Moreno, “Reducing losses in distribution transformers,” *IEEE Trans. Power Deliv.*, vol. 18, no. 3, pp. 821–826, 2003.

[53] E. Benedict *et al.*, “Losses in Electric Power Systems,” *Electr. Comput. Eng. Tech. Rep.*, 1992.

[54] M. E. Baran and F. F. Wu, “Network reconfiguration in distribution systems for loss reduction and load balancing,” *Power Deliv. IEEE Trans.*, vol. 4, no. 2, pp. 1401–1407, 1989.

[55] N. Acharya, P. Mahat, and N. Mithulananthan, “An analytical approach for DG allocation in primary distribution network,” *Int. J. Electr. Power Energy Syst.*, vol. 28, no. 10, pp. 669–678, 2006.

[56] D. M. Said and K. M. Nor, “Effects of harmonics on distribution transformers,” *2008 Australas. Univ. Power Eng. Conf.*, no. PECon 08, pp. 1–5, 2008.

[57] F. Report and EPRI-DOE, “Handbook of Energy Storage for Transmission & Distribution Applications,” *Power*, vol. 2, no. December, p. 512, 2003.

[58] Sandia National Laboratories, “Battery Energy Storage : A Preliminary Assessment of National Benefits (The Gateway Benefits Study),” no. December, 1993.

[59] P. C. Butler, “Battery Energy Storage for Utility Applications : Phase I - Opportunities Analysis,”pp. 69, 1994.

[60] J. Eyer, “Energy Storage for the Electricity Grid : Benefits and Market Potential Assessment Guide A Study for the DOE Energy Storage Systems Program,” no. February, 2010.

[61] N. W. Miller, R. S. Zrebiec, G. Hunt, and R. W. Deimerico, “Design and commissioning of a 5 MVA, 2.5 MWh battery energy storage\nsystem,” *Proc. 1996 Transm. Distrib. Conf. Expo.*, no. M, pp. 2–8, 1996.

[62] L. H. Walker, “10-MW GTO Converter for Battery Peaking Service,” vol. 26, no. 8931456, pp. 63–72, 1990.

[63] A. Gabash and P. Li, “Active-reactive optimal power flow in distribution networks with embedded generation and battery storage,” *IEEE Trans. Power Syst.*, vol. 27, no. 4, pp. 2026–2035, 2012.

[64] A. Gabash and P. Li, “Evaluation of reactive power capability by optimal control of wind-vanadium redox battery stations in electricity market,” *Sell*, vol. 1, no. 9, p. 24, 2011.

[65] A. A. Akhil *et al.*, “DOE / EPRI 2013 Electricity Storage Handbook in Collaboration with NRECA,” no. July, 2013.

[66] Beacon Power, “Beacon Power installs first Flywheels at Pennsylvania Energy Storage Plant: Officials cite benefits for improved grid stability and renewable energy expansion at commencement ceremony,” pp. 1–2, 2014.

[67] P. W. Parfomak, “Energy storage for power grids and electric transportation: A technology assessment,” *Energy Storage Technol. Power Grids Electr. Transp*, pp. 1–127, 2012.

[68] C. Polk, R. W. Boom, and Y. M. Eyssa, “Superconductive magnetic energy storage (SMES) external fields and safety considerations,” *IEEE Trans. Magn.*, vol. 28, no. 1, pp. 478–481, 1992.

[69] E. Barbour, “Pumped Hydroelectric Storage (PHS),” pp. 1–11, 2012.

[70] D. Rastler, “Electricity Energy Storage Technology Options,” p. 170, 2010.

[71] S.-I. Inage, “Prospects for Large-Scale Energy Storage in Decarbonised Power Grids,” *Int. Energy Agency*, p. 90, 2009.

[72] H. R. Mirjalili, “Electrical Energy Storage Source Placement in Distribution,” no. June, pp. 15–18, 2015.

[73] D. Elettronica, I. Bioingegneria, and P. Milano, “Optimal Placement of Energy Storage Devices for Loss Reduction in Distribution Networks,” pp. 9–13, 2013.

[74] M. Farrokhifar, S. Grillo, E. Tironi, D. Elettronica, I. Bioingegneria, and P. Milano, “Loss Minimization in Medium Voltage Distribution Grids by Optimal Management of Energy Storage Devices,” no. Mv, pp. 1–5, 2013.

[75] F. H. Biabani, “Increment of Distributed Generation Penetration in Distribution Networks Using Simultaneous Placement of Distributed Generation Resources and Energy Storage Systems,” *Nashriyyah-i Muhandesi-i Barq Va Muhandesi-i Kampyutar-i Iran*, vol. 11, pp. 57 -65, 2013.

[76] A. D. Petropoulos, N. C. Koutsoukis, E. S. Karapidakis, and P. S. Georgilakis, “Optimal mix of wind generation and energy storage systems in power distribution networks,” *MedPower 2014*, pp. 1–6, 2014.

[77] H. Saboori and H. Abdi, “Application of a grid scale energy storage system to reduce distribution network losses,” pp. 1–5, 2013.

[78] A. Oudalov, R. Cherkaoui, and A. Beguin, “Sizing and optimal operation of battery energy storage system for peak shaving application,” *2007 IEEE Lausanne POWERTECH, Proc.*, no. 1, pp. 621–625, 2007.

[79] A. Nourai, V. I. Kogan, and C. M. Schafer, “Load leveling reduces T & D line losses,” *IEEE Trans. Power Deliv.*, vol. 23, no. 4, pp. 2168–2173, 2008.

[80] G. Liu *et al.*, “Advanced Energy Storage Management in Distribution Network,” 2016.

[81] C. Wang, R. Dunn, F. Robinson, B. Lian, W. Yuan, and M. Redfern, “Active-reactive power approaches for optimal placement of charge stations in power systems,” *Int. J. Electr. Power Energy Syst.*, vol. 84, pp. 87–98, 2017.

[82] W.Miller, *Mathematical Optimization Techniques, Numerical Time-Dependent Partial Differential Equations for Scientists and Engineers*, vol. 213.pp1-295, 2010.

[83] K. G. E. Morse P.M., *Methods of operations research*. New York: Wiley & Sons, 1950.

[84] M. R. AlRashidi ,M. E. El-Hawary, “Hybrid Particle Swarm Optimization Approach for Solving the Discrete OPF Problem Considering the Valve Loading Effects.,” *IEEE Trans. Power Syst.*, vol. 22, pp. 2030–2038, 2007.

[85] R. Michael, “Theory, Methods, and Applications,” in *In Applied Linear Programming, Academic Press*, 1978.

[86] K. P. F.Hugo, M.Péter, “Optimal scheduling of a renewable micro-grid in an isolated load area using mixed-integer linear programming,” *Renew. Energy*, vol. 35, no. 1, pp. 151–156, 2010.

[87] X. Wang, C. Q. Tao, and G. J. Tang, “A class of differential quadratic programming problems,” *Appl. Math. Comput.*, vol. 270, pp. 369–377, 2015.

[88] F. Chen, G. H. Huang, Y. R. Fan, and R. F. Liao, “A nonlinear fractional programming approach for environmental–economic power dispatch,” *Int. J. Electr. Power Energy Syst.*, vol. 78, pp. 463–469, 2016.

[89] R. C. Bansal, “Optimization methods for electric power systems: An overview,” *Int. J. Emerg. Electr. power Syst.*, vol. 2, p. 1021,2005.

[90] S. Sivanandam, S. Deepa, *Introduction to Genetic Algorithms*. New York: Springer Berlin Heidelberg, 2008.

[91] K. Chang, “An optimization algorithm-based pinch analysis and GA for an off-grid batteryless photovoltaic-powered reverse osmosis desalination system,” *Renew. Energy*, vol. 91, pp. 960–1481, 2016.

[92] M. M. K. Tabassum, “A Genetic Algorithm Analysis towards Optimization solutions,” *J. Digit*, vol. 4, pp. 124–142, 2014.

[93] T. Ipfc and M. M. Al Khabbaz, “Transmission Power Loss Reduction Using Intelligent,” pp. 423–428, 2014.

[94] S.Joseph and C.D.Balaji, “Transmission Loss Minimization Using Optimization Technique Based On Pson,” *IOSR J. Electr. Electron. Eng.*, vol. 6, no. 1, pp. 01–05, 2013.

[95] K. Bhumkittipich and W. Phuangpornpitak, “Optimal Placement and Sizing of Distributed Generation for Power Loss Reduction Using Particle Swarm Optimization,” *Energy Procedia*, vol. 34, no. July, pp. 307–317, 2013.

[96] N. C. H.Yapici, “Reduction of power loss using reactive power optimization in a real distribution system, ” *International Symposium on Innovations in Intelligent SysTems and Applications*,pp1-4,2015.

[97] D. Zhang, Z. Fu and L. Zhang, “Joint Optimization for Power Loss Reduction in Distribution System,” IEEE Trans. on Power Systems, Vol. 23, no. 1, pp. 161-169, 2008.

[98] S. A. Nagy, I. S. Ibrahim, M. K. Ahmed, A. S. Adail, and S. Soliman, “Network

Reconfiguration for Loss Reduction in Electrical Distribution System Using Genetic Algorithm," vol. 46, no. 1, pp. 78–87, 2013.

[99] S. Agrawal, B. K. Panigrahi, and M. K. Tiwari, "Multiobjective Particle Swarm Algorithm With Fuzzy Clustering for Electrical Power Dispatch," *Evol. Comput. IEEE Trans.*, vol. 12, no. 5, pp. 529–541, 2008.

[100] A. Raskin and S. Saurin, "The Emergence of Hybrid Vehicles," *Alliance Bernstein*, vol. Research, 2006.

[101] J. K. Park,J. Sohn, J., Park, "Optimal capacitor allocation in a distribution system considering operation costs," *IEEE Trans. Power Syst.*, vol. 24, pp. 462–468, 2008.

[102] M. Falaghi, H. Ramezani, M. Haghifam, "Optimal conductor selection for radial distribution systems," pp. 95–103, 2005.

[103] D. Chembe, *Reduction of Power Losses Using Phase Load Balancing Method in Power Networks*. San Francisco, USA,.

[104] J. Voeclcker, "Green Car report," 2012. [Online]. Available: http://www.greencarreporrts.com/news/1078116_july-plug-in-electric-car-sales-volt-steady-leaflethargic-again.

[105] J.Cole,"Green Car Report,"2013.[Online].Available: http://insideevs.com/september-2013-plug-in-electric-vehicle-sales-report-card/.

[106] J.Cole,"Green Car Report,"2013.[Online].Available: http://insideevs.com/june-2013-plug-in-electric-vehicle-sales-report-card/.

[107] R. Kassakian, J. Schmalensee, "The future of the electric grid. MIT Press.," *Mit Study Futur. Electr. Grid*, 2001.

[108] G.Zeiss,"Electrifying Transportation,"2011.[Online].Available: http://geospatial.blogs.com/geospatial/2011/07/electrifying-transportation.htm.

[109] S. G. Naik, D. K. Khatod, and M. P. Sharma, "Optimal allocation of combined DG and capacitor for real power loss minimization in distribution networks," *Int. J. Electr. Power Energy Syst.*, vol. 53, pp. 967–973, 2013.

[110] S. Raskin, A. and Shah, *The Emergence of Hybrid Vehicles, Researchon Strategic Change.* 2006.

[111] I. Abdelhamid, M. Singh, R., Singh, A. Qattawi,"Evaluation of On-Board Photovoltaic Modules Options for Electric Vehicles.," *IEEE J. Photovoltaics*, vol. l.4, pp. 1576–1584, 2014.

[112] P. K. M.Singh, "Designing a multi charge station for Electric Vehicles and its utilization for the grid support," *Power Energy Soc. Gen. Meet.*, pp. 22–26, 2012.

[113] Y. Ota, H. Taniguchi, T. Nakajima, K. M. Liyanage, J. Baba, and A. Yokoyama, "Autonomous distributed V2G (vehicle-to-grid) satisfying scheduled charging," *IEEE Trans. Smart Grid*, vol. 3, no. 1, pp. 559–564, 2012.

[114] J. Timpner and L. Wolf, "Design and evaluation of charging station scheduling strategies for electric vehicles," *IEEE Trans. Intell. Transp. Syst.*, vol. 15, no. 2, pp. 579–588, 2014.

[115] H. Z. F.Xu, Q.Gu, "Tentative analysis of layout of electrical vehicle charging stations," *East China Electr. Power*, vol. 37, pp. 1678–1682, 2009.

[116] Z. Liu, F. Wen, G. Ledwich, and S. Member, "Optimal Planning of Electric-Vehicle Charging Stations in Distribution Systems," vol. 28, no. 1, pp. 102–110, 2013.

[117] W. Yao *et al.*, "A multi-objective collaborative planning strategy for integrated power distribution and electric vehicle charging systems," *IEEE Trans. Power Syst.*, vol. 29, no. 4, pp. 1811–1821, 2014.

[118] Y. Li, L. Li, J. Yong, Y. Yao, and Z. Li, "Layout Planning of Electrical Vehicle Charging Stations," *Electr. Power Syst. Comput. Vol. 99 Ser. Lect. Notes Electr. Eng.*, pp. 661–668, 2011.

[119] S. Ge, L. Feng, and H. Liu, "The planning of electric vehicle charging station based on Grid partition method," *2011 Int. Conf. Electr. Control Eng. ICECE 2011 - Proc.*, pp. 2726–2730, 2011.

[120] N. MacHiels, N. Leemput, F. Geth, J. Van Roy, J. Buscher, and J. Driesen, "Design criteria for electric vehicle fast charge infrastructure based on flemish mobility behavior," *IEEE Trans. Smart Grid*, vol. 5, no. 1, pp. 320–327, 2014.

[121] J. I. Cairo and A. Sumper, "Requirements for EV charge stations with photovoltaic generation and storage," *IEEE PES Innov. Smart Grid Technol. Conf. Eur.*, pp. 1–6, 2012.

[122] H. Ding, Z. Hu, and Y. Song, "Coordinated Control Strategy of Energy Storage System with Electric Vehicle Charging Station," pp. 1–5, 2014.

[123] Y. M. Atwa, S. Member, and S. Member, "Optimal Allocation of ESS in Distribution Systems With a High Penetration of Wind Energy," vol. 25, no. 4, pp. 1815–1822, 2010.

[124] M. Nick, S. Member, R. Cherkaoui, S. Member, M. Paolone, and S. Member, "Optimal Allocation of Dispersed Energy Storage Systems in Active Distribution Networks for Energy Balance and Grid Support," pp. 1–11, 2014.

[125] G. Celli *et al.*, "Optimal Integration of Energy Storage in Distribution Networks," pp.

1–7, 2009.

[126] Y.F.Dong, “Optimal allocation of energy storage system in distribution systems,” *Procedia Eng.*, vol. 15, pp. 346–351, 2011.

[127] C. Wang and M. H. Nehrir, “Analytical Approaches for Optimal Placement of Distributed Generation Sources in Power Systems,” *IEEE Trans. Power Syst.*, vol. 19, no. 4, pp. 2068–2076, 2004.

[128] J.Voelcker, “Plug-in electric car sales for Feb: Volt outsells Prius Prime, Bolt EV, Leaf (final update),” *greencarreports*, 2017. [Online]. Available: http://www.greencarreports.com/news/1109109_plug-in-electric-car-sales-for-feb-volt-outsells-bolt-ev-substantially.

[129] J.Voelcker, “Plug-In Electric Car Sales Triple In 2012 As Buyers, Models Increase,” *greencarreports*, 2013. [Online]. Available: http://www.greencarreports.com/news/1081419_plug-in-electric-car-sales-triple-in-2013-as-buyers-models-increase.

[130] J.Cole, “March 2013 Plug-In Electric Vehicle Sales Report Card,” 2013. [Online]. Available: http://insideevs.com/march-2013-plug-in-electric-vehicle-sales-report-card/.

[131] J.Cole, “December 2013 Plug-In Electric Vehicle Sales Report Card,” 2013. [Online]. Available: http://insideevs.com/december-2013-plug-in-electric-vehicle-sales-report-card/.

[132] Office of Energy Efficiency, “Developing Infrastructure to Charge Plug-In Electric Vehicles,” *U.S. Department of Energy*, 2016. [Online]. Available: http://www.afdc.energy.gov/fuels/electricity_infrastructure.html.

[133] C. Su, C. Lin, and J. Wong, “Optimal Size and Location of Capacitors Placed on a Distribution System,” *Power*, vol. 3, no. 4, pp. 247–256, 2008.

[134] T. K. K. Chen, “Locating Electric Vehicle Charging Stations Parking-Based Assignment Method for Seattle,” *Transp. Res. Rec. J. Transp. Res. Board*, vol. 23, pp. 28–36, 2013.

[135] P. Fan, B. Sainbayar, and S. Ren, “Operation Analysis of Fast Charging Stations With Energy Demand Control of Electric Vehicles,” *IEEE Trans. Smart Grid*, vol. 6, no. 4, pp. 1819–1826, 2015.

[136] Z. Liu, F. Wen, and G. Ledwich, “Optimal planning of electric-vehicle charging stations in distributions systems,”. *IEEE Trans. Power Deliv*, vol. 28, no. 1, pp. 102–110, 2013.

[137] Z. Wang, P. Liu, J. Cui, Y. Xi, and L. Zhang, “Research on quantitative models of

electric vehicle charging stations based on principle of energy equivalence," *Math. Probl. Eng.*, vol. 2013.

[138] G. Wang, Z. Xu, F. Wen, and K. P. Wong, "Traffic-constrained multiobjective planning of electric-vehicle charging stations," *IEEE Trans. Power Deliv.*, vol. 28, no. 4, pp. 2363–2372, 2013.

[139] National Travel Survey, "Travel to work: personal travel factsheet," *Department for Transport*, 2007.

[140] K. Qian, C. Zhou, M. Allan, and Y. Yuan, "Modeling of load demand due to EV battery charging in distribution systems," *IEEE Trans. Power Syst.*, vol. 26, no. 2, pp. 802–810, 2011.